DISSERTATION

DISTRIBUTED RUNOFF SIMULATION OF EXTREME MONSOON RAINSTORMS IN MALAYSIA USING TREX

Submitted by

Jazuri Abdullah

Department of Civil and Environmental Engineering

In partial fulfillment of the requirements

For the Degree of Doctor of Philosophy

Colorado State University

Fort Collins, Colorado

Summer 2013

Doctoral Committee:

Advisor: Pierre Y. Julien

Brian P. Bledsoe
Subhas K.Venayagamoorthy
Ellen E. Wohl

ABSTRACT

DISTRIBUTED RUNOFF SIMULATION OF EXTREME MONSOON RAINSTORMS IN MALAYSIA USING TREX

Malaysia has a monsoon climate and most areas receive more than 2,500 mm of rainfall every year. For the past five years, the frequency and magnitude of floods in Malaysia have been relatively high. Floods have become the most significant type of natural disaster for Malaysia in terms of the population affected, financial losses and adverse socio-economic impact. This study uses the distributed two-dimensional TREX model to simulate infiltration, overland runoff and channel flow during extreme rainfall events. The main objective is to calibrate the distributed hydrological model to simulate monsoon floods. The second objective is to determine the affected flooding area under different rainfall events (i.e., large and extreme rainfall events). Large rainfall events cover return periods ranging from two to one hundred years. Extreme rainfall events include both the PMP and the world's largest rainfall events. The third objective is to examine the effect of rainfall duration on the magnitude of peak flood discharge as a function of watershed size. Finally, determine and produce graphs for the relationships between peak specific-discharge and watershed sizes.

Three different sizes of watersheds are considered: Lui (small – 68 km^2), Semenyih (medium – 236 km^2) and Kota Tinggi (large - 1,635 km^2). Generally, the topography of these watersheds is steep, except for the large watershed. The TREX model calibration and validation have been done using field measurements during several storm events. The performance of the model to find peak discharge, time to peak, and volume has been tested using three metrics: Relative Percentage Difference (RPD), Percentage Bias (PBIAS) and Nash-Sutcliffe Efficiency

Coefficient (NSEC)) comparison. On average, the model performance was *good* for small (RPD – 7%, PBIAS – 14% and NSEC – 0.4) and medium watersheds (RPD – 14%, PBIAS – 28% and NSEC – 0.7). The RPD (4%), PBIAS (2%) and NSEC (0.8) for the large watershed shows that the model performance was *very good*.

The spatial and temporal runoff distribution for overland and channel flows were successfully visualized in 3D. Both small and medium watersheds were not flooded by large events, except in the main channel. The flow depth reached 1.72 m in the valley of the small watershed only during extreme events. It was estimated that about 24% (±10%) and 83% (±5%) of the valley area exceed a flow depth of 1.72 m during PMP and world's largest events, respectively. For the medium watershed, the valley area was covered with water in excess of 4.49 m under the world's largest events. The visualization tool shows that the valley areas are prone to severe flooding (in excess of 4.49 m of flow depth) under this event (±5%). For the large watershed, the low land areas (i.e., along the tributaries and channels) are more likely to be flooded during large and extreme events. The water depths covered more than 2.8 m in these areas.

The maximum estimated discharges (MED) for large rainfall events were highest for rainfall durations of 3 to 5 hours on small watersheds. However, the MED values for medium watersheds were obtained for rainfall durations between 5 and 12 hours. The MED values for extreme rainfall events were highest for rainfall durations between 10 and 13 hours on both watersheds. For the large watershed, the MED values of large and extreme events were obtained for a rainfall duration of 168 hour.

The main conclusions of this study are: (1) rainfall intensity (i.e., hourly data) is one of the main factors that contribute to the magnitude of flooding on small and medium watersheds

(watershed size less than 1,000 km^2). The flooding events on large watersheds (watershed size more than 1,000 km^2) result from longer rainfall durations (i.e., multi-day rainstorms), (2) for all size watersheds, the average magnitude of peak discharge for the PMP and the world's largest events are approximately 5 and 12 times larger than a 100-year rainfall event, (3) the peak specific-discharge (cms/km^2) decreased as the watershed size (km^2) increased, and (4) the runoff coefficient C increased significantly (i.e., a factor of three) from the 100-year rainfall event to the PMP and the world's largest events for all watersheds (C_{PMP},$C_{WGR} > 0.7$).

ACKNOWLEDGEMENTS

First and foremost I would like to thank the Ministry of Higher Education (MOHE), Malaysia and Universiti Teknologi MARA (UiTM), Malaysia for their financial support under the Young Lecturer Scheme.

Secondly, I would like to express my gratitude and appreciation to Dr. Pierre Y. Julien for giving me the opportunity to carry out my PhD dissertation under his supervision. It was a great experience for me to work with him. I had the chance to apply all the technical knowledge that I learned in undergraduate and graduate studies programs and to understand their real world applications.

I would like to extend my gratitude to my committee members in helping me produce this research via their knowledge, especially while taking their classes. They are Dr. Brian P.Bledsoe, Dr. Subhas K. Venayagamoorthy and Dr. Ellen E. Wohl

Thanks go to my colleagues in Malaysia for providing me with the data for the study. Data for the watersheds were provided by: Mohd Rozi Talib (Ex-DSMM), Nor Haslinda Mohamed Yusop and Arshad Mohd Isa from DSMM and Lizawati Turi, Abu Salim Abd. Aziz, Khairul Fadzilah Mohd Omar, Mohd Shawal Abd. Wahid and Azmi Md. Jafri from DID. I also appreciate the assistance of Junaidah Ariffin, Joe Nyuin, Azmi Ibrahim and Norizan Ismail from UiTM and Othman Jaafar from the National University of Malaysia for providing useful information related to the watersheds. Also my colleagues in the United States: James Halgren, An Sang Do, Kim Jae Hoon, Park Kiyoung and Andy Steininger from CSU. Thanks also to Mark Velleux (HydroQual, New Jersey) and John England (U.S. Bureau of Reclamation) for their help in using the TREX model.

Finally, to my lovely wife, Nur Shazwani Muhammad, thanks for your infinite love support and motivation throughout my study. I owe you more than I can describe here. Also to my mother (Zaiton Mat Piah), late father (Abdullah Hadani), mother-in-law (Jamilah Jaafar), father-in-law (Muhammad Mohd Nor), and all my family members for their "*doa*" and moral support.

THANK YOU ALL

TABLE OF CONTENTS

LIST OF TABLES

LIST OF FIGURES

CHAPTER ONE

INTRODUCTION

1.1 MOTIVATION

Malaysia has 1,800 rivers and streams and receives an annual rainfall of approximately 2,500 mm. This makes Malaysia rich in water resources by receiving an abundant amount of water every year. However, there are some water related problems that raise concern among engineers, developers and the public. The problem is not having a proper outlet system for rain runoff. This is due to inappropriate channel designs created from improper methods for predicting peak discharge and volume of water (MSMA 2000). Towards the year 2020, Malaysia will face serious challenges relating to flood and drought management. Rapid urbanization has accelerated the impact on catchment hydrology and geomorphology (Chang et al. 2008). In recent years, rapid urban development within river watersheds has resulted in higher runoff and decreasing river capacity. These, in turn, resulted in an increase in flood frequency and magnitude, as shown in Tables 1.1a and 1.1b.

Modeling and simulating rainfall-runoff relationships is very rare in Malaysia, especially in two-dimensions, with a distributed model and the visualization of the output in two or three-dimensions. Utilization of data from the government of Malaysia, through the Department of Irrigation and Drainage (DID), the Department of Meteorological Malaysia (DMM) and the Department of Surveying and Mapping Malaysia (DSMM), could be very useful for rainfall-runoff modeling.

Table 1.1(a) Flooding in Peninsular Malaysia from 2007 to 2012

YEAR	DATE	STATE	NOTE	SOURCE
2007	Jan. 11 - 14	Johore and Pahang	Heavy continuous rainfall RM 407 Milliom (USD 136 Million) for road, bridge and DID works and 101,508 people were evacuated	Shafie (2009); MMD (2007)
	June 10	Kuala Lumpur	Widespread heavy rain with strong wind	MMD (2007)
	Dec. 5 - 20	Kedah, Negeri Sembilan Kelantan, Pahang, Johore	Widespread heavy rain RM 813 Million (USD 263 Million) and 157,507 people from 38,387 families were evacuated	
2008	April 16	Negeri Sembilan (Seremban)	Sg. Temiang burst its bank after continuous rain Situation was chaotic as traffic became stabdstill and flood victims spent the night at a multipurpose hall	MMD (2008)
	Aug. 27	Kuala Lumpur	Continuous heavy rain for several hours Most of the major roads effected and caused traffic chaos during the afterwork rush hour	
	Sept. 6	Penang (Bayan Baru, Bkt. Mertajam, Seberang Jaya)	Intermittent moderate occasionally heavy rain Two landslides occurred and caused traffic chaos	
	Nov. 27 - Dec. 1	Kelantan Terengganu, Pahang	Continuous heavy rain Over 6,000 people were evacuated to 40 flood evacuation centers	
2009	March 3	Kuala Lumpur	Heavy rain Dozens of vehicles were submerged in water and caused severe traffic congestion	MMD (2009)
	April 19	Kelantan	Severe thunderstorm	
	Aug. 23	Kedah	Continuous heavy rain for several days About 10 houses and main road effected by the floods	
	Nov. 3	Selangor (Selayang)	Heavy rain Landslide - cutting off the road access	
	Nov. 6	Kelantan (Pasir Mas, Tumpat)	Golok River overflowed as a result from the heavy monsoon rain	
	Dec. 4	Pahang (Maran)	Continuous heavy rain for several days About 60 families were evacuated when two rivers overflowed	
	Dec. 26	Selangor (Damansara)	Heavy rain caused severe traffic congestion	
2010	Jan. 1	Negeri Sembilan (Seremban)	Severe thunderstorm (strong winds and heavy rain) Houses damaged	MMD (2010)
	May 18	Selangor (Klang Valley)	Heavy rain lasted for two hours Caused floods, uprooted trees, traffic congested, landslide	
	Nov. 1	Kedah, Perlis, Terengganu, Kelantan	Due to a tropical depression and continuous rain (more than monthly means in Oct. and Nov.) The flood was worst than in 2005 - approximately 45,000 people were evacuated	
	Dec. 8	Selangor (Klang Valley)	Caused by the unusual high volume of rain Traffic choas in Kuala Lumpur	
	Dec. 30	Pahang (Kuantan)	Two days of continuous rain Flood water as high as 1.0 m immersing the town and Kuantan-Jabor main road	

Table 1.1(b) Flooding in Peninsular Malaysia from 2007 to 2012 (continued)

YEAR	DATE	STATE	NOTE	SOURCE
2011	Jan. 4 - 8	Perlis, Kelantan, Terengganu	Continuous heavy rain More than 7,000 people were evacuated and water level more than 1.0 m	Taucan et al. (2011); Utusan (2011a)
	Jan. 31 - Feb. 1	Johore, Pahang, Negeri Sembilan, Melaka	Continuous heavy rain and water depth approximately 2.0 m More than 50,000 people were evacuated and most of the main road effected by flood	Maslih et al. (2011); Ismail (2011)
	March 29	Terengganu (Kuala Terengganu)	Continuously heavy rain Most of the main road were closed and created chaos	Utusan (2011b)
	Apr. 1	Perlis (Kangar)	Approximately 8,000 people were evacuated to the safer places	Abdullah (2011)
	Aug. 28	Kedah (Baling)	Heavy rainfall for 4 hours Water depth more than 0.5 m and approximately 2,000 people were evacuated	Md. Noor (2011)
	Nov. 25	Kelantan, Terengganu, Pahang	More than 4,000 people were evacuated, water depth is more than 0.5 m and created chaos as most of the main roads were closed	Utusan (2011c)
	Dec. 3	Kuala Lumpur	Heavy rainfall Massive traffic jams after working hours and water depth approximately 1.0 m	Mohd and Perimbanayagam (2011)
2012	Jan. 22	Kelantan (Rantau Panjang)	All day rain Water depth more than 1.0 m and took about 1 week to back to normal	Utusan (2012a)
	Feb. 21	Perak (Ipoh)	Heavy rain at 2:00 am and the worst flood in Kg. Manjoi history	Utusan (2012b)
	March 9 - 13	Selangor, Kuala Lumpur	More than 4,000 people were evacuated, some houses swept by high flow and most of the main roads were closed	Jamaluddin and Hassan (2012); Maslih (2012)
	Apr. 20	Perak (Kampar)	More than 1,500 people were evacuated and water depth is more than 3.0 m	Utusan (2012c)
	May 3 - 8	Kuala Lumpur, Selangor	Water depth is more than 2.0 m, approximately 2,500 people were evacuated and caused traffic chaos	Sinyang (2012); Wan Alias (2012)
	Oct. 18	Selangor (Subang Jaya)	Short duration of heavy rain Drainage not design properly	Chan (2012)
	Aug. 8	Penang (Georgetown)	Heavy rainfall for 4 hours duration from 3 am Most of the main roads were closed and caused severe traffic congested	Utusan (2012d)
	Sept. 5	Selangor (Kajang, Serdang)	Heavy rain Water rose up to 1.5 m, submerged houses and vehicle and caused massize jams	Camoens and Wong (2012)
	Nov. 7	Selangor	Continuously rain for about 1 week Approximatle 1,820 people were evacuated	myMetro (2012)
	Nov. 16	Penang (Butterworth)	Heavy rain and drainage system is failure More than 1,000 people were effected and water depth is more than 0.5 m	Utusan (2012e)
	Nov. 26	Kedah (Baling)	Heavy rain for 3 days About 600 houses were flooded	Md. Noor (2012)

1.2 PROBLEM STATEMENT

For the past five years, the frequency and magnitude of floods in Malaysia have been relatively high. Generally, floods happen between November and February each year due to the monsoon climate. The problem is made worse by malfunctioning early warning systems at the flooding areas. These floods have caused massive damage, but they also provide valuable information. This information could help Malaysian researchers and authorities to develop new algorithms, new software and procedures for designing future developments.

The government has been spending large amounts of money on flood mitigation projects in urban and rural areas. Therefore, it is important to correctly predict flow in rivers and flood plains under extreme rainfall events. Most of the past studies are based on idealized experimental laboratory investigations, which are then presented in terms of a regression model to determine runoff. However, a better understanding of the relationship between rapid development and channel stability will allow engineers and developers to make more informed decisions in designing and planning by establishing a new numerical model and guidelines.

1.3 RESEARCH QUESTIONS

The main questions to conduct this study are:

1. There are several hydrological models to study rainfall-runoff relationships. Can any of these models be used to simulate floods from monsoon climates in countries with wide/flat valleys and steep mountain area? The related question is: how well can these models simulate the peak discharge and time to peak under extreme monsoon precipitation?

2. What is the percentage (and uncertainty) of the valley areas flooded under different rainfall events?
3. How does the magnitude of peak flood discharges Q_p vary with the size of watersheds?
4. What is the relationship between peak specific-discharge (Q_p/A_w) and watersheds area (A_w)?

1.4 OBJECTIVES

The overall goal of this study is to simulate large and extreme rainfall events at three different sizes of watersheds (small, medium and large) in Malaysia using a mathematical approach. Large rainfall events cover return periods ranging from two to one hundred years. Extreme rainfall events include the Selangor-PMP (S-PMP), Kota Tinggi PMP (KT-PMP) and the world's largest rainfall events. This study also aims to provide basic knowledge to engineers and developers of the behavior of the watersheds under extreme rainfall events. The main objectives of this study are as follows:

1. Calibrate the distributed hydrological model to simulate monsoon floods;
2. Determine the affected flooding area under different rainfall events;
3. Examine the effect of rainfall duration on the magnitude of peak flood discharge as a function of watershed size; and
4. Determine and produce graphs for the relationship between peak specific-discharge and watershed sizes.

The first objective must be achieved before continuing to the other objectives. The TREX model was developed and tested using data in the United States of America (USA). The model was successful in simulating the relationship of rainfall-runoff as reported by Velleux (2005),

England et al. (2007), and Velleux et al. (2006 and 2008). However, at the time of this study, the model had not been tested in other countries. Expanding on the use of this model may benefit the world of hydrologic modeling through its successful use in this study.

Chapter 2 provides background information about the availability of the different distributed models in hydrological modeling. The uses of stochastic and deterministic models in Malaysia are also given in this chapter. The grid size selection and the evaluation of model performance are discussed towards the end of this chapter. The model description and numerical schemes for the selected model are described and explained in Chapter 3. Chapter 4 presents the calibration and validation to accomplish the specific objective 1. The simulations for large and extreme monsoon rainstorms at different size watersheds are presented in Chapter 5. In this chapter, the distribution of water depth across the watersheds is visualized in pseudo three-dimensions and discussed (Objective 2). The uncertainty analysis is conducted to determine the variability of the magnitude of peak flood discharge (Objective 3) and produce the relationship between peak specific-discharge and watershed size in the graph form (Objective 4). Finally, Chapter 6 summarizes the main conclusions of this study. Eight appendixes are also provided to show the details of any relevant discussions.

CHAPTER TWO

LITERATURE REVIEW

This chapter provides a brief overview of distributed models. There is also a discussion on the hydrological approach used by Malaysian researchers and agencies to forecast and study the relationship between rainfall and runoff. The methods to evaluate the performance of the models are described in the last section of this chapter.

2.1 CRITERIA FOR SELECTING HYDROLOGICAL MODEL

Several well-known general hydrological models are currently in use. The availability of source code is one of the main criteria for model selection. The model must also have the ability to support the distributed parameters and the two-dimensional overland routing approach. Some models use either a semi-distributed or lumped (Figure 2.1a) approach, but these do not consider the spatial variability of the processes, boundary conditions or watershed geometric characteristics. A distributed model (Figure 2.1b) is expected to give better results than semi-distributed models because they do take these missing factors into account (El-Nasr et al. 2005). Two-dimensional overland (Figure 2.2b) routing is more accurate compared to one-dimensional overland (Figure 2.2a) routing because it analyzes more outputs, which provides more information. An additional value to a distributed model is the ability to work with raster (raster consists of a matrix of cells (or pixels) organized into rows and columns (or a grid) where each cell contains a value representing information, such as elevation and water depth (ESRI 2012)) GIS database. The availability of rainfall and flow data is also considered.

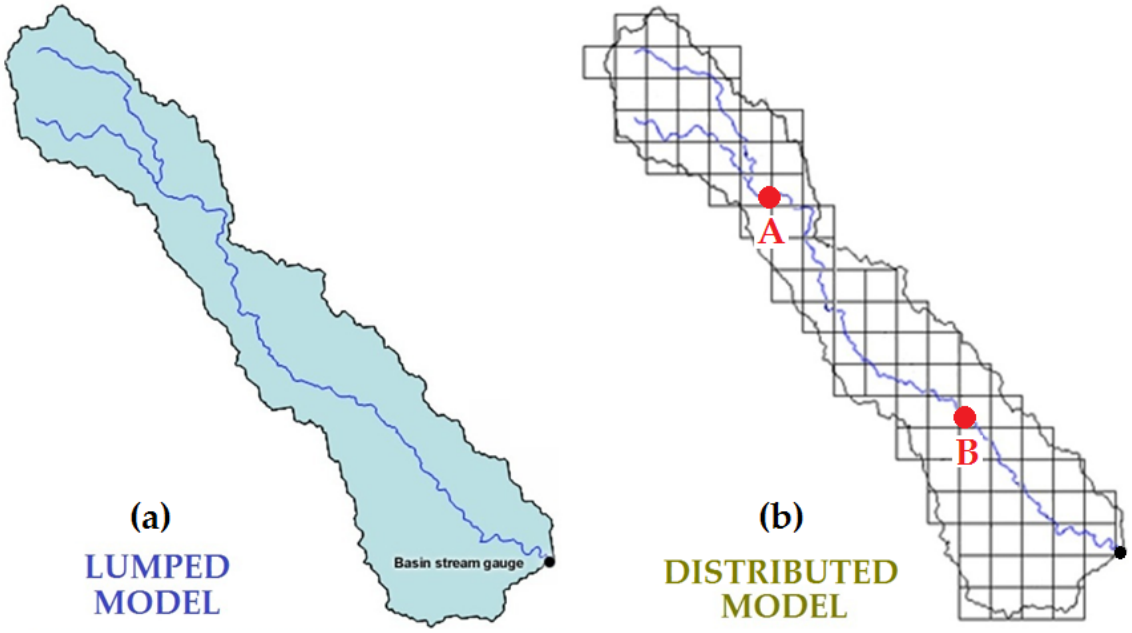

Figure 2.1 Lumped and distributed (COMET 2012)

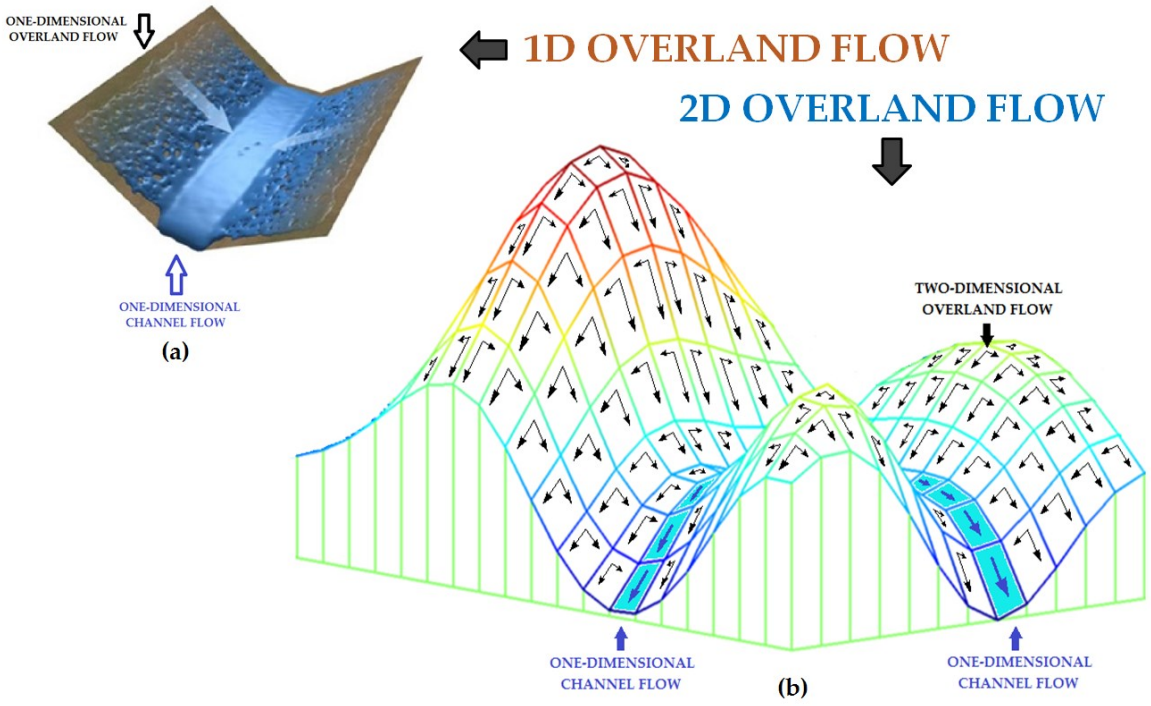

Figure 2.2 Comparison of overland flow (a) 1D overland flow (modified from COMET 2012) and (b) 2D overland flow

2.2 LUMPED VERSUS DISTRIBUTED MODELS

Lumped models (Figure 2.1a) have been used for over fifty years to estimate flow at watershed outlets. However, the simplification of many watershed characteristics may affect the simulation results. The parameters used in lumped models are spatially averaged and made uniform across the watersheds (Johnson and Miller 1997; Shah et al. 1996) and the number of parameters is less (Refsgaard 1997). However, in reality, these input data vary.

A number of questions remain as to how the variability of rainfall and watershed characteristics impact runoff to generate streamflow at the watershed outlet (Woolhiser 1996; Smith and Konstantine 2004; Smith et al. 2004; Carpenter 2004). Nowadays, instead of lumped modeling, distributed modeling (Figure 2.1b) is becoming a more favorable approach in research. This is because most of the models are compatible to work with GIS and the emergence of large data sets and the increased efficiency of powerful computers to simulate and display the results (Smith et al. 2004). Distributed models better represent the spatial variability of factors that control runoff, thus enhancing the predictability of hydrologic processes (Vieux and Vieux 2002; El-Nasr et al. 2005). These models usually use parameters that are directly related to the physical characteristics of the watershed including: topography (i.e., elevation), soil type, channel properties, land use, etc. The climate variability can also be taken into account as reported by Shultz (2006). Results are presented in the form of spatial and temporal characteristics (Vieux and Fekadu 2003; Velleux 2005; Velleux et al. 2008).

Several potential distributed models include: the Institute of Hydrology Distributed Model (IHDM), MIKE-SHE, InfoWorks River Simulation (IWRS), Système Hydrologique Européen Transport (SHETRAN), a real-time distributed hydrological model (Vflo™) and Two-

dimensional Runoff, Erosion and Export (TREX). Discussions of each of these models are given in the following sections.

2.2.1 Institute of Hydrology Distributed Model (IHDM)

IHDM is a physically-based rainfall-runoff model developed at the UK Institute of Hydrology (Beven et al. 1987; Calver and Wood 1995). IHDM started in 1977 and combines a finite difference method of the one-dimensional Saint-Venant equation for overland and channel flows with a conceptual soil water storage model with distributed parameters. Modifications were made to allow the area of overland flow on a hillslope plane to expand and to contract dynamically, flexibility in controlling the evapo-transpiration from surface water and the root zone, and interception and snowmelt calculations. The Institute of Hydrology Report provides detailed descriptions, including changes from the earlier versions of the IHDM model (Beven et al. 1987). The watershed is divided into hillslope areas and channel lengths (Figure 2.2a). The hillslope and channel lengths are represented as square rectangular sloping planes and constant cross-section, respectively. This model was successfully tested by Beven et al. (1987) on the Wye catchment at Plynlimon, mid-Wales. The model has the ability to simulate rainfall-runoff on several watersheds (Rogers et al. 1985; Calver 1988; Beven and Binley 1992; Calver and Cammeraat 1993), including ungaged watersheds (Morris 1980). The availability of the model cannot be found, but the user manual is available (Beven et al. 1987).

2.2.2 MIKE-SHE

MIKE-SHE was introduced by Refsgaard and Storm (1995). The model is a comprehensive, deterministic, distributed, and physically based modeling system. It can be used

for the simulation of hydrological processes occurring in the land phase of the hydrological cycle. It simulates overland and channel water flow, water quality and sediment transport. This model is user-friendly and based on the SHE modeling concept (Abbott et al. 1986a and 1986b). MIKE-SHE is applicable to a wide range of water resources and environmental problems. For surface waters, flow routing is performed using a diffusive wave approximation. The model simulates two-dimensional overland flow and one-dimensional flow in channels. The MIKE-SHE is widely used by a large number of organizations. As the extended version of SHE (Système Hydrologique Européen), a list of applications can be found in Singh (1995). Unfortunately, the MIKE-SHE model source code (and documentation) could not be obtained and is not publicly available. MIKE-SHE is the product of DHI (Danish Hydraulic Institute) and more information about MIKE-SHE can be found at DHI's website (*http://mikebydhi.com/ Products/Water Resources?MIKESHE.aspx*).

2.2.3 InfoWorks River Simulation (IWRS)

IWRS is a hydrodynamic model that solves for full unsteady flow equations. The model originated from the UK. This model can be used to simulate rainfall-runoff relationships either in one- or two-dimensions. The IWRS model has the capabilities to simulate the widest range of flow situations and channel characteristics based on the Saint-Venant equation, which uses the conservation of mass and momentum. The model uses a base flow in the steady state condition to generate the initial conditions for the full, unsteady solution. This steady state run is used to solve most of the instability issues that arise as the model begins because the unsteady model cannot run for a dry condition (Mountz and Crowley 2009). The output from this model can be merged into ArcGIS, which provides the ability to present an integrated view of geo-referenced

characteristics and spatial relationships. It has been shown that the IWRS model has successfully simulated the rainfall-runoff relationship (Carmona and Vargas 2008; Noh 2008; Ma 2008; Sloan 2009; Hassan 2011). The steady state analysis of initial conditions was simulated using direct runoff inputs. The unsteady analysis can be calculated using either a fixed-time step set by the user or an adaptive (variable) time step determined by the program. Unfortunately, this model is not publicly available either. However, the Innovyze Company provides a special price to universities for up to twenty licenses for water distribution, sanitary and storm sewer, and urban drainage systems analysis software with a cost of $1000 per year (*http://www.innovyze.com /education/universities/*). Further information can be found at the Innovyze Company website (*http://www.innovyze.com/ products/infoworks_rs/*).

2.2.4 Système Hydrologique Européen Transport (SHETRAN)

SHETRAN is a physically-based, distributed, deterministic, integrated surface and subsurface modeling system. It is designed to simulate water flow, sediment transport and contaminant transport at the catchment scale (Ewen et al. 2000 and 2002). This model is based on the SHE modeling concept (Abbott et al. 1986a and 1986b) and is designed primarily to model watersheds and channel networks feeding surface and subsurface responses to precipitation to a single outflow reach of the channel. For surface waters, flow routing is performed using the diffusive wave approximation and is two-dimensional for overland flow and one-dimensional in channels. SHETRAN is publicly available and can be downloaded through the School of Civil Engineering and Geosciences, Newcastle University, UK (*http://research.ncl.ac.uk/shetran /index.htm*). However, the main limitation of this model is that

it can only generate a grid size up to 50 m. A larger grid size can be amended to the code by collaborating with the school, as recommended by its author.

2.2.5 A Real-time Distributed Hydrological Model (Vflo™)

Vflo™ is a real-time distributed and physics-based hydrologic model for managing water resources, water quality management and flood warning systems. Digital maps of soils, land use, topography and rainfall rates are used to compute and route rainfall excess through a network formulation based on the Finite Element Method (FEM) computational scheme, as described by Vieux (2001a and 2001b). Runoff production is from infiltration excess and is routed downstream using the kinematic wave analogy. This model represents an important advance in simulating rainfall-runoff using digital data describing Earth's terrain coupled with new technology in radar precipitation detection. Hydrographs can be simulated in real-time and post-analysis can be conducted at any location where there is a channel or an overland flow element. The details of this model have been described in Vieux and Vieux (2002).

Vflo™ is commercial code and can be purchased through VIEUX, INC. There are two types of Vflo™ model: basic and professional. The basic Vflo™ has limitations in terms of number of cells, maximum time to solve the problem, and the output cannot be exported for inundation mapping and animation, and has a limited numbers of rain gages. Further information about this model can be found at *http://www.vieuxinc.com/vflo.html*.

2.2.6 Two-dimensional Runoff, Erosion, and Export (TREX)

TREX is a two-dimensional distributed, physically-based model that can be used to simulate precipitation, overland runoff, channel flow, soil erosion, stream sediment transport and

chemical transport and fate at the watershed scale (Velleux et al. 2008; England et al. 2007; Velleux et al. 2006; Velleux 2005). This framework is based on the CASC2D watershed model (Julien et al. 1995; Johnson et al. 2000; Julien and Rojas 2002). TREX has three main components, which are hydrology, sediment transport and chemical transport and fate. The code has been subjected to extensive testing to ensure accuracy and error-free performance. This model has been applied to different sizes of watersheds, ranging from small to large (Ogden and Julien 2002; Velleux 2005; England 2006; Velleux et al. 2006; Velleux et al. 2008; England et al. 2007).

The hydrological processes simulated are rainfall (England et al. 2007; Velleux 2005; Velleux et al. 2006; Velleux et al. 2008) and snowfall (precipitation), interception, snowmelt (Kang 2005) and surface storage, infiltration and transmission loss, and overland and channel flow. Model state variables are water depth in the overland plane and stream channels. Precipitation can be uniform or distributed in both time and space (Jorgeson 1999; Ogden 1992; Ogden and Julien 1993, 1994 and 2002; Ogden et al. 2000; Richardson et al. 1983) and can also be specified using several grid-based formats to facilitate radar precipitation data use. When spatially distributed precipitation is simulated, areal estimates are interpolated from point gage data using an inverse distance weighting approach. Interception and surface storage are simulated as equivalent depths. Infiltration and transmission loss rates are simulated using the Green and Ampt (1911) relationship. Overland and channel flows are simulated using the diffusive wave approximation in two- and one-dimensions, respectively. TREX model is publicly available and can be downloaded at *http://www.engr.colostate.edu/~pierre/ceold/Projects/TREX%20Web%20Pages/TREX-Home.html*.

These findings and availability of the programs lead to only one model to be used in this research, the TREX model. The criteria for model selection have been summarized and tabulated, as shown in Table 2.1. Detailed descriptions on governing equations and numerical schemes are described and explained in Chapter Three.

Table 2.1 Summary of the criteria for model selection

HYDROLOGICAL MODELING	**CRITERIA**				
	Distributed Model	Compatible with ArcGIS	2D overland routing	Continuous rainfall event	Source code availability
IHDM	**YES**	NO	NO	NO	NO
IWRS	**YES**	**YES**	**YES**	**YES**	NO
SHETRAN	**YES**	NO	**YES**	**YES**	**YES**
MIKE-SHE	**YES**	**YES**	**YES**	**YES**	NO
Vflo^{TM}	**YES**	**YES**	**YES**	**YES**	NO
TREX	**YES**	**YES**	**YES**	**YES**	**YES**

2.3 SELECTION OF THE COMPLEXITY OF THE MODEL

The main discussions in this section are to compare the selection and the application of one-, two- and three-dimensional hydrologic models. Also discussed are the risks of not being able to represent the topography of the watersheds, the difficulty in getting a solution and the application of the hydrological models at difference sizes of watersheds. These are the main concerns in selecting the complexity of the hydrological model (CHM). Figure 2.3 shows the "trade-off diagram" for the CHM (i.e., one-, integrated one-two, two- and three-dimensional hydrological modeling) and size of the watershed.

Generally, the choice of CHM depends on the project objectives (Dooge 1977; McPherson 1978) and scope, the knowledge and skills of the modeler, resources constraints

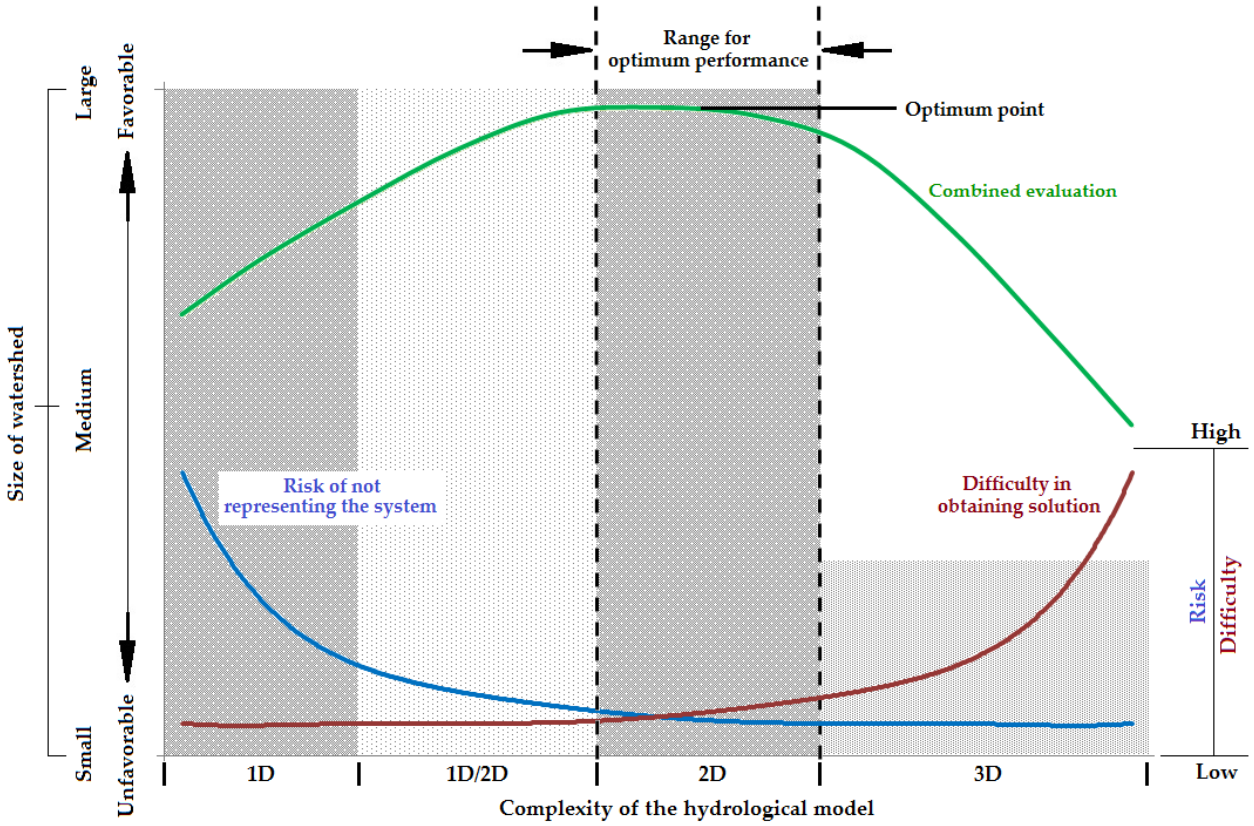

Figure 2.3 "Trade-off diagram" in selecting dimensions of hydrological modeling (modified from Overton and Meadows 1976)

(Overton and Meadows 1976) and time and length scales (Church 2006; Grayson and Blöschl 2000). In addition to these, the optimization and presentation of the final output should be considered as described by Scoging et al. (1993). Choosing a complex hydrological model will represent the characteristics of the watershed better, but it makes obtaining a solution more difficult. Another factor that should also be considered is the size of the watershed. A simpler model was usually selected when a large size watershed was to be modeled. From Figure 2.3, the 1D and 2D models are more favorable to simulate hydrological models for any size of watershed. Conversely, the application of 3D models in hydrological modeling for a variety of watershed sizes is rare (Church 2006; CWCB 2008). The water depth distribution, as a function of time and

length scale, is one of the most important objectives of this study. Therefore, based on Church (2006) and CWCB (2008), a 1D or 2D model is sufficient to simulate this distribution as compared to 3D, which may not be realistic because it currently is very costly. Therefore, the 3D models will not be discussed in this section.

2.3.1 Risk of not presenting the system

In hydrological modeling, the representation of the system should be as accurate as it possibly can be. The representation of the system can be extracted directly from the digital elevation model (DEM). This is the most important data because topography controls runoff and watershed boundaries (Vieux 2004). The shape and timing of the hydrograph have been shown to be a function of size, slope, shape, soil types, storage capacity, land use and climatic variables. When a model is able to reflect the principle of how a watershed functions hydrologically, then the possibility to extrapolate beyond current situations with reliable predictions may be possible (Sivapalan and Young 2004). Rainfall intensity and duration are the major driving forces of the rainfall-runoff process, followed by watershed characteristics that translate the rainfall input into an output hydrograph at any point of the watershed.

2.3.2 Difficulty in obtaining solution

The difficulties in obtaining accurate solutions involve: (1) easy to use and prepare the input data, (2) model accuracy, (3) hydrologic parameters consistency, (4) sensitivity of the output when parameters changes, (5) storage (in computer hard drive space) required for the output, (6) data limitations, and (7) computer time simulation. The availability of data is the most

important in selecting the CHM (Bedient and Huber 2002). In general, the 1D model can predict flow and produce accurate hydrographs when it has been calibrated and validated.

According to Knapp et al. (1991), the basic idea in the selection of models is to adopt the simplest model (i.e., easy to use and apply) that will provide acceptable results. However, the ease of application will also depend upon the individual experience of the modeler, both in the use of the model and the knowledge of the watershed. Generally, the complexity of the model strongly relates to the ease of the application. This means that the simpler models normally require the least effort to apply and least effort in calibration and validation as compared to more complex models (WMO 1975; Abbott 1978; Franchini and Paccicani 1991).

A study conducted by McPherson (1978) regarding the accuracy of the rainfall-runoff model may vary and is mostly inconclusive, and therefore controversial. However, other studies show that most rainfall-runoff models will predict runoff and streamflow with similar accuracy (Papadakis and Preul 1973; Heeps and Mein 1974; Marsalek et al. 1975; WMO 1975; Abbott 1978; Loague and Freeze 1985; Franchini and Pacciani 1991; Melching et al. 1991). The accuracy of the model is determined by availability of the input data and an observed input and output time series at various locations in a watershed (Bedient and Huber 2002). The accuracy of the model can be measured using model performance evaluation techniques as suggested by Legates and McCabe (1999), Krause et al. (2005), and Moriasi et al. (2007). The sensitivity analyses of a model will reveal information on the relative importance of many input parameters as well as uncertainty in the model output (James and Kuch 1998).

Based on these discussions (i.e., sections 2.3.1 and 2.3.2), Figure 2.3 shows that a two-dimensional hydrological model was recommended to study the rainfall-runoff relationship as concluded in the reports by Bates and De Roo (2000), Juza and Barad (2000), Syme (2001),

Wagner and Mueller (2001), Leorpardi et al. (2002), Kelly and Rydlund (2005), Musser and Dyer (2005), Barnard et al. (2007), Schumann et al. (2008), Tayefi et al. (2007), CWCB (2008) and Papanicolaou et al. (2009).

2.4 RAINFALL-RUNOFF MODELING IN MALAYSIA

In Malaysia, the prediction of flood frequency using stochastic models is common. The statistical concept (Suhaila and Jemain 2007 and 2008; Wan-Zin et al. 2009a and 2009b) and artificial neural network (ANN) (Nor et al. 2007; Wardah et al. 2008; Sulaiman et al. 2011) are the preferred methods, as compared to other stochastic models. Deterministic models are still relatively new in Malaysia, even though they have been widely used in many other countries (Ab. Ghani et al. 2009). However, some of the hydrological simulations that have been successfully conducted are briefly discussed.

In Malaysia, models from the United Kingdom (UK), United States of America (USA) and Australia are widely used for rainfall-runoff simulations. Mah et al. (2007, 2010 and 2011), Said et al. (2009) and Ali and Ariffin (2011) used the commercial software InfoWorks River Simulation (IWRS) and Siang et al. (2007) used InfoWorks Collection System (IWCS) from the UK to simulate rainfall-runoff. Hydrological models from the USA such as HEC (Yusop et al. 2007; Razi et al. 2010; Mohammed et al. 2011), L-THIA program (Izham 2010), MIKE (Billa et al. 2004 and 2006; Lim and Cheok 2009) and MAYA 3D (Ghazali and Kamsin 2008) have been used to simulate flood events. Teo et al. (2009) and Toriman et al. (2009) used the 2DSWAMP and XP-SWMM models from Australia to simulate runoff. Except for the L-THIA model, the other models listed are not publicly available. Most hydrological modeling studies in Malaysia were carried out using a one-dimensional approach (except Lim and Cheok 2009 and Teo et al.

2009, which are two-dimensional approaches). While modelers are aware of the advantages of two-dimensional models, the lack of reliable information is another main reason modelers in Malaysia avoid using them.

Commercial software from the UK, namely IWRS and IWCS, has been widely used in simulating hydrological processes. Siang et al. (2007) used the IWCS model in their case study at Tanjong Malim, Perak to draft a comprehensive stormwater management and flood mitigation plan for local authorities. They found that this model has the ability to simulate the interaction between rivers and urban drainage. These results were useful to design the flood mitigation plan based on the impact of variously designed storm events in the study area. Additionally, the study provides local authorities with valuable information to plan for existing and future land use changes. Mah et al. (2007, 2010 and 2011) and Said et al. (2009) used the IWRS model to simulate the impact of runoff on the floodplains and the water quality of the river before and after the floods. They successfully simulated these events and the information is useful to the city council for flood mitigation design and water quality management. Ali and Ariffin (2011) used IWRS to simulate the flood events at the Damansara Catchment (Kg. Melayu Subang – upstream, Taman TTDI Jaya, Batu 3, and Taman Sri Muda) in 2006, 2007 and 2008. The model has the ability to simulate and produce hydrographs that are useful in designing structures such as retention ponds and flood walls, especially in low-lying areas (i.e., Taman TTDI Jaya and Batu 3).

Yusop et al. (2007) used the commercial software HEC-HMS to determine the runoff and hydrograph-characteristic modeling for an oil palm plantation in the Skudai River watershed. From the high index of the model's performance (calibrated and validated models efficiency index of 0.81 and 0.82, respectively), they suggested that the model could be used for filling in

the missing runoff from rainfall data. Razi et al. (2010) used HEC-HMS at the Johor River to estimate flooding. The model has been suggested for use as a tool to estimate peak discharge. This conclusion has been supported because the evaluation of the model's performance is close to unity with observation. The HEC-2 model was adopted by Mohammed et al. (2011) to predict water surface profiles for the Langat River at Selangor and Linggi River at Negeri Sembilan (both tropical rivers). The HEC-2 model was developed by the US Army Corps of Engineers especially to compute water surface profiles. The HEC-2 model successfully predicted the water level at Linggi River, Negeri Sembilan with a small error. However, the model at the Langat River, Selangor did not have a good agreement. According to the authors, the model can still be applied to tropical rivers with a reasonable level of error if the input data are good.

Modeling the effects of mangroves on tsunamis has used commercial software from Australia, namely 2DSWAMP, by Teo et al. (2009). This model was used to investigate the pattern of mangrove tree distribution and diameters that can affect the attenuation of tsunamis at the Merbok Estuary, Kedah. A one-dimensional hydrodynamic model, namely XP-SWMM, was used by Toriman et al. (2009) to simulate flood water of the Damansara River at TTDI, Selangor. The authors studied the time of water filling and volume of flood discharge (m^3/s) over the flood plain. They were successful in producing a Flood Hazard Mapping for Urban Area (FHMUA). Izham et al. (2010) used a free commercial program, L-THIA (Purdue University), to simulate runoff at Pinang River, Pulau Pinang. Lim and Cheok (2009) used MIKE-FLOOD coupled with MIKE-11 and MIKE-21 to simulate flood events at Damansara River, Selangor. In summary, the two-dimensional simulations provide crucial information with regard to the direction and rate of flood propagation, the flood inundation extent, and flood depths and flood durations that cannot be achieved using one-dimensional simulations.

2.5 SIMULATING LARGE AND EXTREME FLOOD EVENTS

Though rare in reality, large and extreme flood simulations are important for both urban and rural areas (Curran et al. 2005). Malaysia receives heavy rainfall for a period of a few hours and development has contributed to an increase in the frequency of flooding in both urban and rural areas (Suhaila and Jemain 2007 and 2008; Wan-Zin et al. 2009a and 2009b). This condition is different than the US, which receives a series of small precipitation (Votteler 2002) that usually results in flooding (Grigg 2003).

Typical parameters that affect the runoff estimation are: time, land covers, soil type and size of watershed, and rainfall. Gravitational, thermodynamics and other natural forces affect the generated runoff and these effects are influenced by time (Shaver et al. 2007). The response time of runoff indicates how quickly the runoff created from the rainfall event drains to the outlet and how quickly the rate of that runoff will change as the rainfall changes. The soil surface and subsurface plays a direct role in determining the volume and rate of runoff from rainfall (Bissonnais et al. 2005). Among soil types, sands, which have less void space and permeability, can be expected to produce less runoff volume than silts and clay (Shaver et al. 2007). The characteristics of the vegetation and impervious surfaces can also affect the volume of resulting runoff and watershed response time (Chow et al. 1988; Singh 1989; Bras 1990).

2.5.1 Watersheds size classification

The temporal and spatial flood magnitude and the response time of the peak discharge are both related to the size of the watershed (Grigg 2003; England et al. 2007). Research conducted on watershed modeling at different areas has used several definitions for classifying the size of

the watershed. These sizes vary greatly. In the next paragraph, the classification for small, medium and large watersheds will be discussed.

Yaolin and Zhijun (2005) claimed that 26.14 km^2 is a small watershed when they conducted a case study on the estimation of the amount of soil erosion at Taipingxi, China. Cheng (1987) did the analysis of storm design on 6.32 km^2 and 97.9 km^2 watersheds in Dashuiken and Fengsulang, respectively. Cui et al. (2011) applied the AHP-PCA method on the 40.5 km^2 watershed at Puwa to evaluate the sustainable development of a small watershed. Li et al. (2009) used the trace technique to estimate the net soil loss on a 4.46 km^2 watershed in Sichuan Hilly, China. Ni et al. (2008) claimed that 187 km^2 is a small watershed in their study to simulate the water and soil erosion at Loess Plateau. Zhou et al. (2005) labeled a 15,300 km^2 watershed as small when they designed the flood management system at Miyun and Guanting.

However, Jinliang et al. (2009) stated that a 14,700 km^2 watershed was medium sized when they conducted a study at the Jiulong River watershed. Liu et al. (2004) defined a medium size watershed as more than 500 km^2. Bitew and Gebremichael (2011) used two medium sized watersheds (299 km^2 and 1,656 km^2) to determine the streamflow using satellite rainfall in regions of the Ethiopian highlands. Feyen et al. (2000) defined 600 km^2 as a medium size watershed.

Frenette and Julien (1987) determined the soil erosion and sediment yields on a large watershed (6,684 km^2) at Quebec, Canada. Molnar (1997) described a large watershed as 560 km^2 for his study area at Hickahala-Senatobia basin in Northwestern Mississippi. Lange et al. (1999) studied a large arid watershed of Nahal Zin, Israel with an area of 1,400 km^2. Güntner and Bronstert (2004) stated that a large watershed for modeling is between 10,000 and 100,000 km^2. Boston et al. (2004) used the Banqiao sub-catchment of the Malianhe watershed in China with an

area of 730 km^2, and termed this as a large watershed in a semi-arid region. Skøien (2003) defined small, medium and large watersheds as 3 to 70 km^2, 70 to 250 km^2 and 250 to 130,000 km^2, respectively.

For this study, the classifications of the watershed size as defined by Singh (1995) will be used. He categorized the area of a watershed that is less than 100 km^2 as small, and more than 1,000 km^2 as large. Watershed areas between these two sizes are defined as medium.

The term peak specific-discharge, which is the ratio between peak discharges to the watershed size, was first used by Julien (2002). He used the term to plot the relationship between peak specific-discharge and watershed size (Figure 2.4). Later, Smith et al. (2005a, 2005b and 2007) and Javier et al. (2007a and 2007b) used similar terms to describe the amount of peak discharge (for observed and simulated) during large flood events. The terms they used are unit discharge, unit specific peaks, peak unit discharge, and unit discharge peaks. However, the graph was first introduced by Creager (1939). He used recorded big flood data in the USA for the years of 1890, 1913, 1921, 1934, and 1939. He believed that the big flood will increase as time goes by if more recorded data were available and used in this analysis. Six years after he wrote this article, Creager et al. (1945) used more data, as suggested in the previous article. They collected the big flood event data in the USA and some other countries from the various sources. Data were recorded between 1501 and 1940. Gupta (2001) described Creager's method in his book.

2.5.2 Large and extreme rainfall events

According to Nathan and Weinmann (1999), there are three categories of rainfall and flood events (Figure 2.5): large, rare and extreme. The large events can be obtained from interpolation techniques with moderate uncertainty and range from one in fifty years to one in

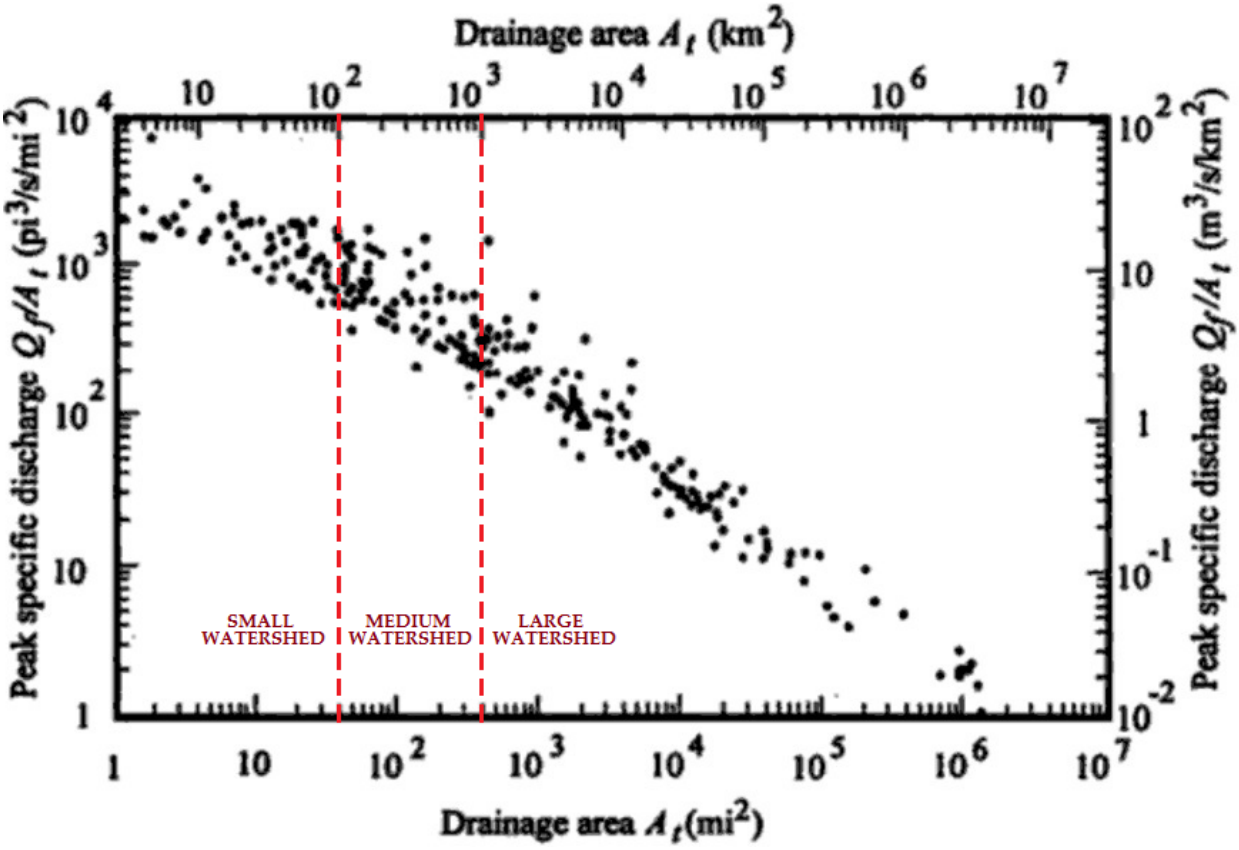

Figure 2.4 Extreme peak specific-discharges vs. drainage area (modified from Julien 2002)

one hundred years Annual Exceedence Probability (AEP). An extrapolation from the known to the unknown, and a pragmatic approach based on theoretical upper limits, is the technique used to obtain information on rare and extreme events, respectively. These events have a value of less than one in 2,000 years AEP for rare events and more than one in 2,000 years for extreme events. The uncertainty for rare events can be from moderate to large, and unquantifiable for extreme events. In this study, levels of one in two years, one in five years, one in ten years and one in twenty year events have been added to the large events category for simulations.

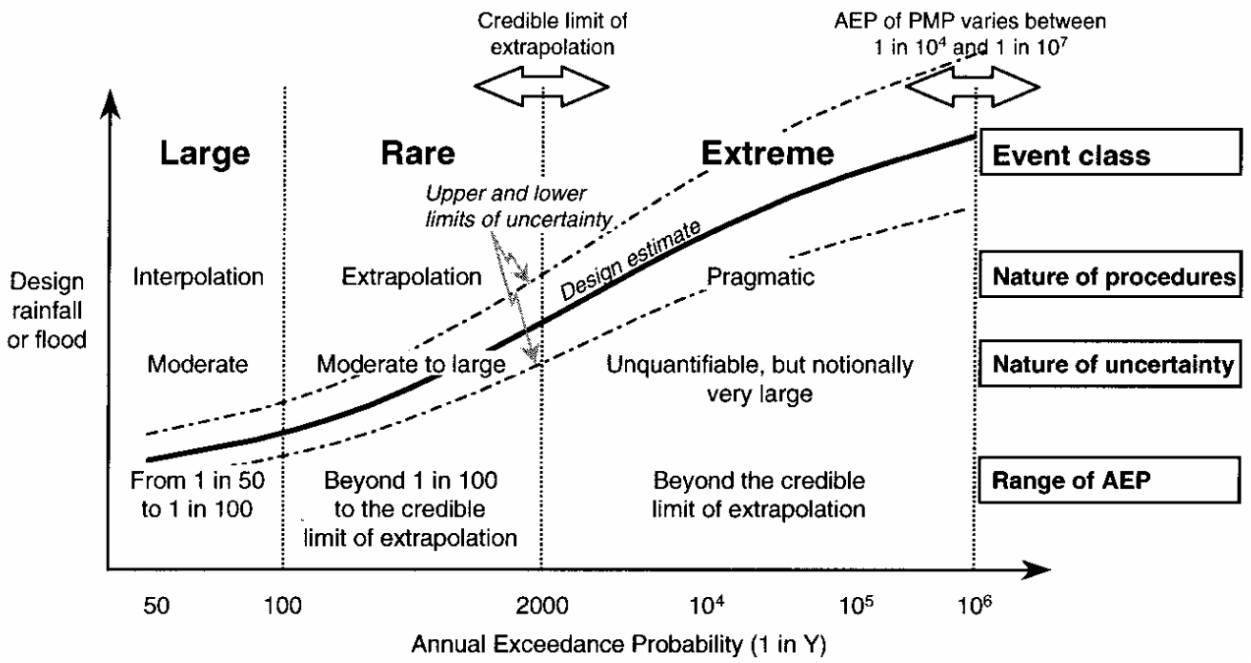

Figure 2.5 Categories in designing rainfall and flooding modeling (adapted from Nathan and Weinmann 1990)

The polynomial approximation as shown in Equation 2.1 has been used to calculate the rainfall intensity for large rainfall events covering return periods ranging from two to one hundred years for Selangor (Table 2.2) and Kota Tinggi (Table 2.3), as suggested in MSMA (2000).

$$\ln(I_t^R) = a + b\ln(t) + c[\ln(t)]^2 + d[\ln(t)]^3 \qquad \text{[Equation 2.1]}$$

Where, I_t^R = the average rainfall intensity (mm/hr) for ARI and duration t

R = average return interval (years)

Table 2.2 Duration of rainfall intensity (mm/hr) for Selangor – small and medium watersheds

RAINFALL DURATION (hrs.)	RETURN PERIOD (year)						RAINFALL DURATION (hrs.)	RETURN PERIOD (year)					
	2	5	10	20	50	100		2	5	10	20	50	100
1	53.6	64.1	72.2	79.8	87.7	94.9	9	10.5	13.1	14.9	16.3	17.9	19.1
2	35.1	42.7	48.2	52.8	58.2	62.3	10	9.5	11.9	13.4	14.8	16.2	17.3
3	26.3	32.4	36.7	40.0	44.2	47.1	11	8.7	10.9	12.2	13.5	14.8	15.8
4	21.0	26.2	29.6	32.3	35.7	38.0	12	8.0	10.0	11.2	12.4	13.6	14.5
5	17.5	21.9	24.8	27.1	30.0	31.9	13	7.4	9.2	10.4	11.5	12.5	13.4
6	15.0	18.9	21.4	23.3	25.8	27.4	14	6.9	8.5	9.6	10.7	11.6	12.4
7	13.1	16.5	18.7	20.4	22.5	24.0	15	6.4	7.9	8.9	9.9	10.8	11.6
8	11.6	14.6	16.6	18.2	20.0	21.3	16	6.0	7.4	8.3	9.3	10.1	10.8

Table 2.3 Duration of rainfall intensity (mm/hr) for Kota Tinggi – large watershed

RAINFALL DURATION (hrs.)	RETURN PERIOD (year)						RAINFALL DURATION (hrs.)	RETURN PERIOD (year)					
	2	5	10	20	50	100		2	5	10	20	50	100
1	67.2	81.4	92.0	107.7	118.4	129.7	12	14.3	19.6	22.7	25.6	30.6	34.1
2	44.5	56.2	63.9	72.4	82.5	90.3	13	13.6	18.7	21.6	24.6	29.2	32.6
3	34.6	44.7	51.1	56.7	66.3	72.7	14	13.0	17.8	20.7	23.7	28.0	31.3
4	28.8	37.8	43.4	47.7	56.6	62.3	15	12.5	17.1	19.9	22.9	26.9	30.1
5	25.0	33.2	38.1	41.7	50.0	55.2	16	12.0	16.4	19.1	22.2	26.0	29.0
6	22.2	29.8	34.3	37.5	45.1	50.0	24 (1-day)	9.5	12.8	14.9	18.7	20.7	23.1
7	20.1	27.2	31.3	34.3	41.4	45.9	48 (2-days)	6.5	8.4	9.8	15.0	14.1	15.6
8	18.5	25.1	28.9	31.8	38.4	42.7	72 (3-days)	5.4	6.6	7.7	14.0	11.3	12.4
9	17.2	23.3	27.0	29.8	35.9	40.0	120 (5-days)	4.4	4.9	5.7	13.8	8.7	9.2
10	16.1	21.9	25.3	28.2	33.9	37.7	168 (7-days)	4.0	4.0	4.7	14.4	7.3	7.6
11	15.1	20.7	23.9	26.8	32.1	35.8							

t = duration (minutes)

a, b, c, d = fitting constants dependent on ARI (Tables 2.4 and 2.5)

Table 2.4 Coefficients for the polynomial approximation for Selangor - small and medium watersheds ($30 \leq t \leq 1000$ min)

ARI (Year)	SELANGOR			
	a	**b**	**c**	**d**
2	4.2095	0.5056	- 0.1551	0.0044
5	5.1943	- 0.0350	- 0.0392	- 0.0034
10	5.5074	- 0.1637	- 0.0116	- 0.0053
20	5.6772	- 0.1562	- 0.0229	- 0.0040
50	6.0934	- 0.3710	0.0239	- 0.0073
100	6.3094	- 0.4087	0.0229	- 0.0068

Table 2.5 Coefficients for the polynomial approximation for Kota Tinggi – large watershed ($30 \leq t \leq 10080$ min)

ARI (Year)	KOTA TINGGI			
	a	**b**	**c**	**d**
2	5.1028	0.2883	- 0.1627	0.0095
5	5.7048	- 0.0635	- 0.0771	0.0036
10	5.8489	- 0.0890	- 0.0705	0.0032
20	4.8420	0.7395	- 0.2579	0.0165
50	6.2257	- 0.1499	- 0.0631	0.0032
100	6.7796	- 0.4104	- 0.0160	0.0005

The coefficients in Tables 2.4 and 2.5 are valid for rainfall durations from 30 to 1,000 minutes (MSMA 2000). The margin of error is likely to be higher for durations shorter than 30 minutes and longer than 1,000 minutes (MSMA 2000). However, for the Kota Tinggi watershed, the rainfall duration needed to extend up to 10,080 minutes (7 days). This is because the maximum estimated discharge for this watershed can only be reached when the duration of

rainfall is longer, as compared to small and medium watersheds (Knighton 1998). The rainfall intensity for extreme rainfall events include the Selangor Probable Maximum Precipitation (S-PMP), Kota Tinggi Probable Maximum Precipitation (KT-PMP) and the world's largest rainfall events (Table 2.6), which were obtained from NAHRIM (2008) and Poon and Hwee (2010) and Jennings (1950), respectively. These tabulated values (Tables 2.2, 2.3 and 2.6) are visualized in Figures 2.6 and 2.7, respectively.

Table 2.6 Rainfall duration and intensity for S-PMP, KT-PMP and the world's largest events

RAINFALL DURATION (hrs.)	**S-PMP (mm/hr)**	**KT-PMP (mm/hr)**	**WORLD'S EVENT (mm/hr)**
1	188	185.7	260.9
2	---	---	186.6
3	100	74.3	153.4
4	---	---	133.4
5	---	---	119.8
6	65.2	58.8	109.7
7	---	---	101.8
8	---	---	95.4
9	---	---	90.2
10	---	---	85.7
11	---	---	81.8
12	43.2	44.0	78.4
13	---	---	75.5
14	---	---	72.8
15	---	---	70.4
16	---	---	68.3
24 (1-day)	25.7	27.3	56.1
48 (2-days)	---	19.3	40.1
72 (3-days)	---	14.8	33.0
120 (5-days)	6.5	10.8	25.8
168 (7-days)	4.9	9.1	21.9

Note: PMP = Probable Maximum Precipitation; S-PMP = Selangor's PMP; KT-PMP = Kota Tinggi PMP

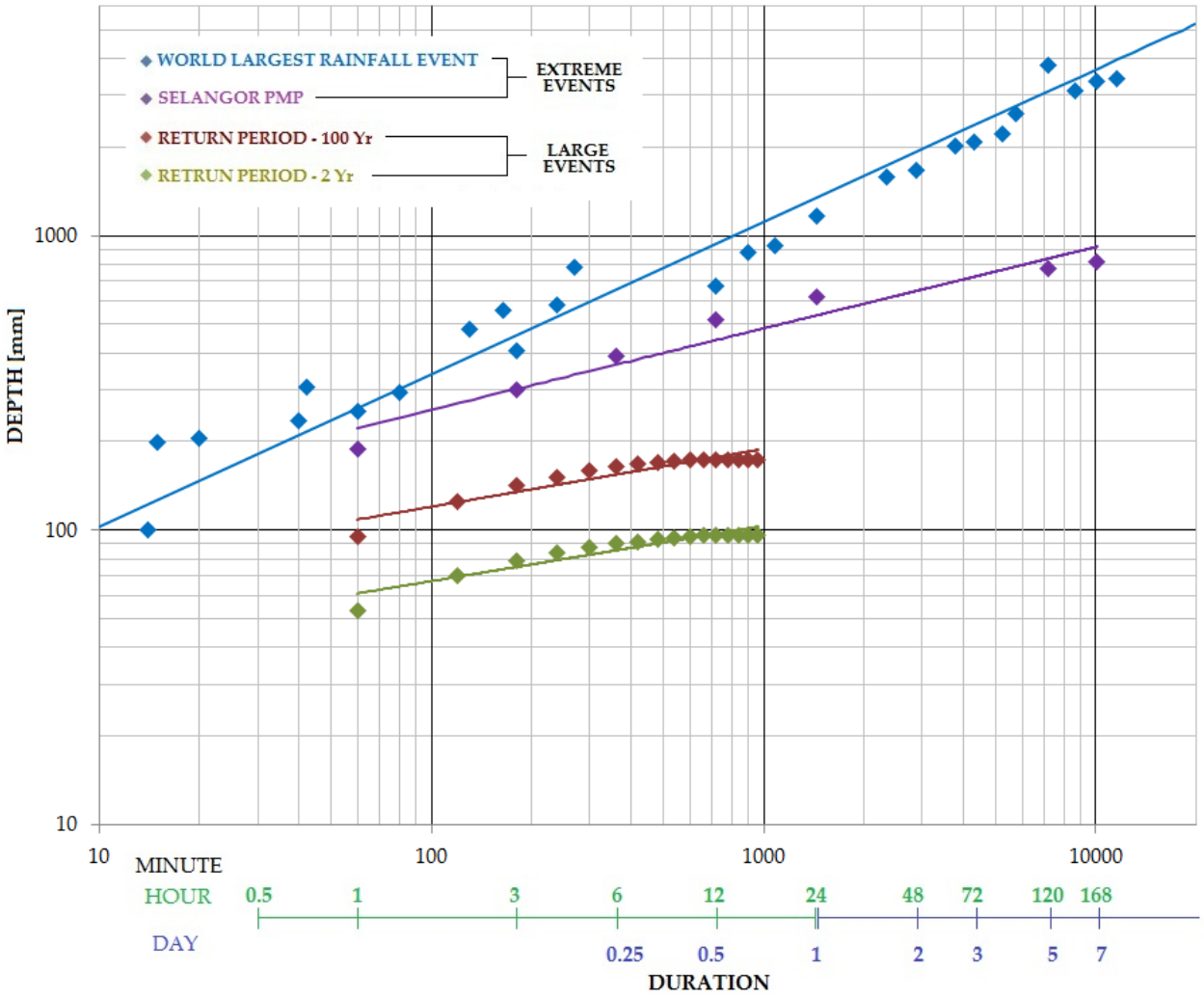

Figure 2.6 Data for simulating large and extreme rainfall events at small and medium watersheds

2.6 SELECTION OF THE GRID SIZE

According to Doe and Harmon (2001), different model outputs can be simulated if the same system is modeled with different grid cell sizes. Several studies, which will be discussed here, have shown that grid size has an influence on both catchment characteristics (as calculated from DEMs) and on modeling results. The simulation results have a significant impact at different spatial resolutions of input data, which is represented by the heterogeneity of landscape (Blöschl et al. 1997). Therefore, there is a need to consider the appropriate spatial resolution in

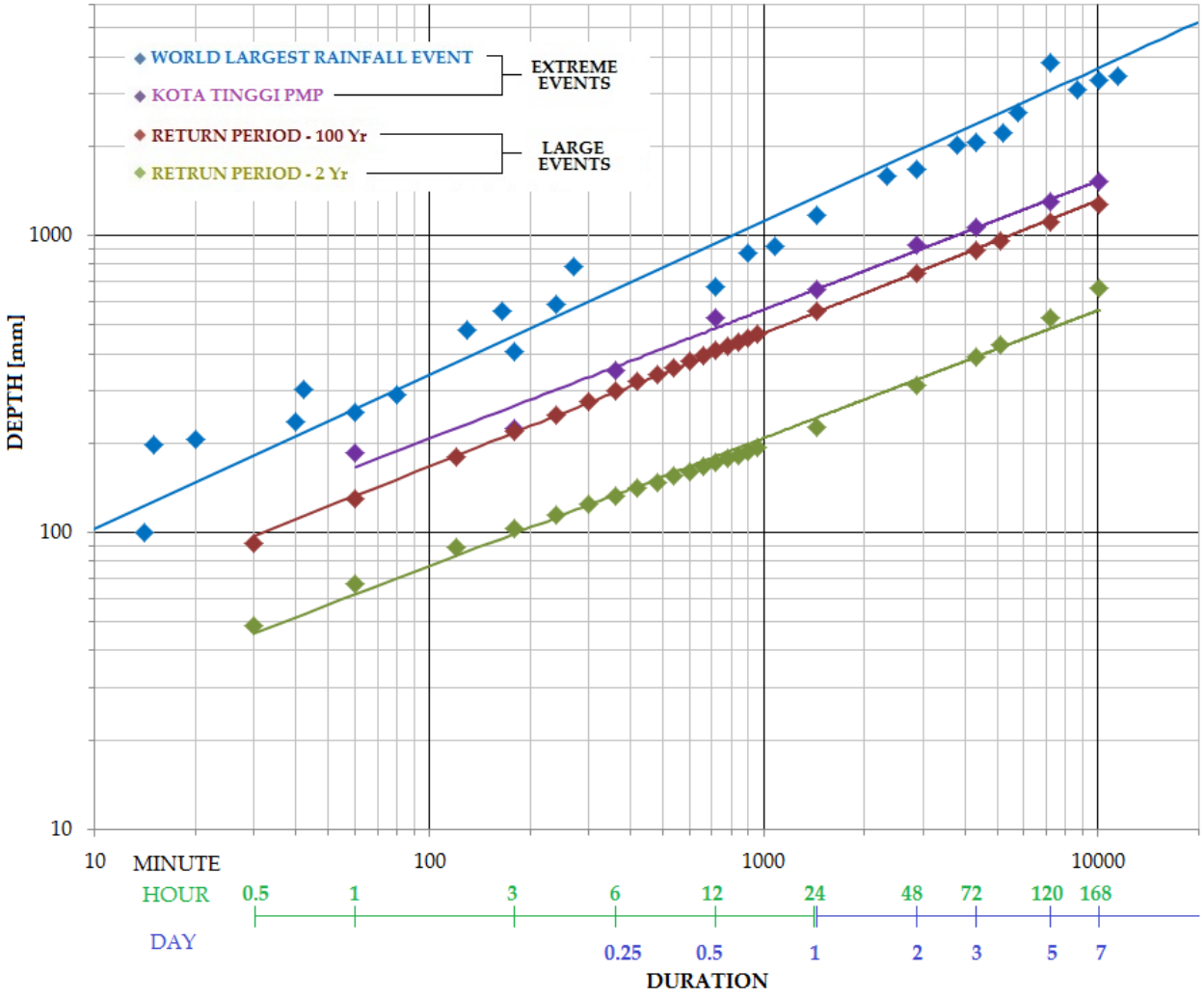

Figure 2.7 Data for simulating large and extreme rainfall events at large watershed

hydrological modeling (Grayson and Blöschl 2000). Generally, increasing the level of discretization could increase the level of accuracy. However, according to Wood et al. (1988) and Mamillapalli et al. (1996), there must be a limit to increasing the level of discretization where the model performance cannot be improved. This section will discuss the recommended grid sizes at different sizes of watersheds. Based on the literature reviewed on this subject, the appropriate grid size will be selected to simulate rainfall-runoff in this study.

Zhang and Montgomery (1994) used TOPMODEL to simulate a hydrologic model at Mettman Ridge (0.3 km^2), Oregon and Tennessee Valley (1.2 km^2), California. They suggested that 10 m grid size would suffice to produce good and reliable results. Fedak (1999) studied the effect of grid size for a 152 km^2 sized watershed. He increased the DEM grid size from 15 to 120 m and the resulting hydrograph generated by TOPMODEL was completely the same. Usul and Paşaoğullari (2004) examined the effect of grid size and map scale on geomorphological basin parameters. They recommended that for a one km^2 watershed (Tarasçi watershed) the grid size should be between 2 and 25 m. Whereas for 10.6 km^2 (Ciftlikozu watershed) and 98 km^2 (Cicek watershed) size of watersheds, appropriate grids ranged between 5 and 30 m and between 10 and 50 m, respectively.

Valeo and Moin (2000) studied the impact of grid size on calibrated parameters for a small catchment in southern Ontario (8 km^2). They found that a coarser grid size increased the topographic index and, as a result, the calibrated transmissivities become larger. These authors recommend an optimal grid size of 50 m if simple hydrologic studies are to be conducted. The effect of different grid sizes on runoff and soil moisture in central New York has been investigated by Kuo et al. (1999). Grid sizes ranging between 10 and 600 m were used. Three different sizes of basins, ranging between 6.5 to 23.6 km^2, were also used. They found that when the simulation was conducted in wet seasons, discharges were not affected by the grid size. However, grid size comparison did show differences in simulated discharges when the same exercises were conducted in dry seasons.

Zhao et al. (2009) studied the impacts of DEM and land use grid size at Xitiaoxi catchment in Southern China (2,200 km^2) on simulated discharge. Four different grid sizes ranging between 100 to 1,000 m were used. They found that at a 1,000 m grid size, the input data

(i.e., DEM and land use) and the model efficiencies did not lead to significant error to the simulated discharge. Bormann (2006) selected the Dill catchment (693 km^2) in Germany to study the impact of spatial data resolution in simulating catchment water balance and model performance. The DEM, soil maps and land use were reclassified from 25 m to various numbers of spatial resolutions between 50 to 2,000 m. The error was small (i.e., 0-3% for annual stream flow) when these input data were reclassified from 25 m up to 500 m. However, when the spatial resolution for these input data increased from 500 m up to 2,000 m, the error becomes significant, which was about twelve percent for annual stream flow.

Shrestha et al. (2002 and 2006) introduced a method to determine grid size, the IC-ratio, which is the ratio of the input data (e.g., DEM, soil types and land use) grid size to the watershed size. They suggested that IC-ratios between 1:6 and 1:20 are considered to be optimal for performance of the model. That means, if the IC-ratio is less than 1:6, the performance of the model can be improved, while at an IC-ratio of more than 1:20, the improvement of the model performance is very small (i.e., negligible). Hessel (2005) applied the LImburg Soil Erosion Model (LISEM) at the Danangou catchment (3.5 km^2) area. He studied the effect of grid size to the simulated discharge and recommended that for this catchment, the grid size should not be larger than 20 m. Vázques et al. (2002) studied the effect of grid size on effective parameters and model performance at the Gete watershed in Brussels (586 km^2). They reported that 600 m grid size for the watershed was most appropriate, as compared to 300 and 1,200 m. A wide range of DEM resolutions up to 3,000 m were by Wu et al. (2007) at two different watersheds: GoodwinCreek (GCW) (21.3 km^2) and Peacheater Creek (PCW) (64 km^2). The efficiency of the model was equivalent when the grid size increased from 100 to 1,000 m for both watersheds. England (2006) and England et al. (2007) used a grid size of 960 m to simulate extreme events

on a large watershed (12,000 km^2) using the TREX model. The model successfully showed the effect of extreme storm events for dam safety purposes. Molnar (1997) and Molnar and Julien (2000) used CASC2D to study the grid-size effects on surface runoff. The Hickahala-Senatobia watershed (560 km^2) was used. The square grid sizes ranging from 127 to 914 m were tested. The authors conclude that coarser grid sizes could be used for this watershed without sacrificing important information affecting surface runoff.

Table 2.7 shows a summary of suggested grid sizes by various authors. As previously stated, the size of the watershed for this study is classified according to Singh (1995). In conclusion, from looking at these various studies and grid sizes, the following grid sizes are acceptable for small, medium, and large watersheds, respectively: 10 to 100 m, 15 to 120 m, and 100 to 1,000 m. Therefore, this study will use a 90 m grid size at small (Lui) and medium (Semenyih) watersheds, and a 230 m grid size at the large (Kota Tinggi) watershed.

2.7 TIME-FRAME-SERIES ANIMATION (TFSA)

Visualizing simulated results through Geospatial data has been a cartographic concern for centuries. With technological advancement came animation. The main purpose of animation is to visualize geospatial data by making it visual, and moving, and not just plain data like tables of facts and figures or mathematical equations (Dorling 1992; Sánchez 2002). Dransch (2000) added that the importance of animation is that it is a visual aid for critical thinking, helps to verify the hypothesis, and makes sharing and delivering information between researchers and the public easier. There are three different types of animations that have been explained by Dorling (1992): space, time, and 3D animations.

Table 2.7 Summary of the grid size suggested by various authors

WATERSHEDS	AREA (km^2)	SUGGESTED GRID SIZE (m)	AUTHOR(S)
SMALL WATERSHED (less than 100 km^2)			
Mettman Ridge	0.3	10	Zhang and Montgomery (1994)
Oregon and Tennessee Valley	1.2	10	
Tarasçi	1	2 - 25	Usul and Paşaoğullari (2004)
Ciftlikozu	10.6	5 – 30	
Cicek	98	10 – 50	
Ontario	8	50	Valeo and Moin (2000)
Central New York, New York	6.5 – 23.6	Do not effected	Kuo et al. (1999)
Danangou, China	3.5	20	Hessel (2005)
Goodwin Creek, Mississippi	21.3	100 – 1,000	Wu et al. (2007)
Peacheater Creek, Illinois	64	100 – 1,000	
MEDIUM WATERSHED (between 100 km^2 and 1,000 km^2)			
Back Creek, Virginia	152	15 – 120	Fedak (1999)
Hickahala-Senatobia	560	914	Molnar (1997); Molnar and Julien (2000)
Dill, Germany	693	25 – 500	Bormann (2006)
Gete, Brussels	586	600	Vásques et al. (2002)
LARGE WATERSHED (more than 1,000 km^2)			
Arkansas River	12,000	960	England (2006); England et al. (2007)
Suiping, China	2,093	IC-Ratio between 1:6 – 1:20	Shrestha et al. (2002 and 2006) IC-Ratio (grid size to watershed area)
Wangjiaba, China	29,844		
Bengbu, China	132,350		
Xitiaoxi, China	2,200	Up to 1,000	Zhao et al. (2009)

Note: The classification of the watershed size is adopted from Singh (1995)

This study integrates the Geographical Information System (ArcGIS 9.3) to create a 3D animation. The ArcGIS 9.3 software is widely used in hydrology to generate 3D animation and has successfully helped visualize and enhance the output in a number of previous studies (Rahman et al. 2001; Drogue et al. 2002; Wang et al. 2007; Daxikar et al. 2008; Merwade et al. 2008; Guo et al. 2009; Jiang et al. 2010; Chan and Mori 2011; Hossain et al. 2011; Li et al. 2011).

This study will use frame series animation. According to Peterson (1995), frame-series animation is a product of a group of images that display on-top after one-to-another. There are several factors that must be considered when creating the TFSA. Gersmehl (1990) and Acevedo and Masuoka (1997) suggested five such factors. First is the number of images, because this determines the detail of the animation. With a large number of images, the animation can be shown in excellent quality. However, the size of the animation file is then huge and time consuming. Second is the starting and ending time; this is important because the animation should capture only the most significant events. This factor can be influenced by the duration of the visualization. Third, the number of intervals between images must be defined because it will affect the duration and display time. Fourth, the animation display speed must be determined, which depends on several factors such as human visual perception and the purpose of creating the animation. Last, the user must choose the medium to display the animation, such as a computer screen or recorded onto CD/DVD or on the Internet as mentioned by Dykes (1997) and Cartwright (1997).

2.8 MODEL PERFORMANCE EVALUATION

During model calibration and validation, agreements between observed and simulated values will be evaluated using graphical and statistical methods. The graphical method is the first and simplest overview. It is done by making comparisons between observed and simulated peak discharge, time to peak, and rising and falling limb, as suggested by Green and Stephenson (1986), ASCE (1993) and Legates and McCabe (1999). However, the graphical method can be very subjective, especially when the numbers between observed and simulated are similar but not identical (Green and Stephenson 1986). The second method uses statistical quantitative measures of the agreement between observed and simulated peak discharge, time to peak and total volume. The statistical method for this study will use three criteria: Relative Percentage Difference (RPD), Percent BIAS (PBIAS) and Nash-Sutcliffe Efficiency Coefficient (NSEC).

2.8.1 Relative Percentage Difference (RPD)

The RPD method is the simplest statistical method among others used to calculate the differences between observed and simulated peak discharge, total volume and time to peak (Singh et al. 2005; Fernandez et al. 2005). The RPD value can be calculated using Equation 2.2.

$$\text{RPD} = \frac{q_{\text{sim.}} - q_{\text{obs.}}}{q_{\text{obs.}}} \times 100 \qquad \text{[Equation 2.2]}$$

Where: $q_{\text{sim.}}$ = simulated discharge value [L^3/T]

$q_{\text{obs.}}$ = observed discharge value [L^3/T]

The calculated RPD value can be either negative or positive. A negative sign indicates that the model underestimates the peak discharge, total volume and time to peak values, and

positive indicates the opposite. According to Donigian et al. (1983), the performance of the model can be classified as *very good*, *good* or *satisfactory*, depending on the calculated |RPD| values. The calculated |RPD| is *very good* when the difference between observed and simulated values is less than 10%, *good* when |RPD| is between 10% and 15% and *satisfactory* when |RPD| is between 15% and 25%.

2.8.2 Percent BIAS (PBIAS)

The PBIAS method is a statistical error analysis that measures the average tendency of the simulated results to underestimate or overestimate the observed data (Gupta et al. 1999). The value of the PBIAS can be calculated using Equation 2.3.

$$\text{PBIAS} = \frac{\sum_{i=1}^{N}\left(q_i^{obs} - q_i^{sim}\right)}{\sum_{i=1}^{N} q_i^{obs}} \times 100\% \qquad \text{[Equation 2.3]}$$

Where: N = number of data for simulated/observed [-]

q_i^{sim} = simulated discharge value [L^3/T]

q_i^{obs} = observed discharge value [L^3/T]

The value of the PBIAS can be either negative or positive. If the PBIAS values are approximately equal to zero (≈ 0.0), the observed and simulated peak discharge, total volume and time to peak are the same. However, if PBIAS is negative, then the simulated volume of water value is over-estimated and under-estimated for a positive value.

2.8.3 Nash-Sutcliffe Efficiency Coefficient (NSEC)

This method was introduced by Nash and Sutcliffe (1970). This method is recommended by Leavesley et al. (1983), Wilcox et al. (1990), Sevat and Dezette (1991), Gupta et al. (1999), ASCE (1993) and Legates and McCabe (1999) to be used because it provides extensive information on reported values. It is computed by taking the ratio of the mean square error between observed and simulated values to the variance of the observed data, as shown in Equation 2.4.

$$\mathrm{NSEC} = 1 - \frac{\sum_{i=1}^{N}\left(q_i^{obs} - q_i^{sim}\right)^2}{\sum_{i=1}^{N}\left(q_i^{obs} - q^{mean}\right)^2} \qquad \text{[Equation 2.4]}$$

Where: N = number of data for simulated/observed [-]

q_i^{sim} = simulated discharge value [L^3/T]

q_i^{obs} = observed discharge value [L^3/T]

q^{mean} = mean value from observed data [L^3/T]

The optimal value is 1.0. The NSEC value should be larger than 0.0 to indicate that observed and simulated data have the minimal acceptable criteria. In this study, the classifications defined by Moriasi et al. (2007) are used. They classified the model performance as *very good*, *good*, *satisfactory* and *unsatisfactory* for the calculated NSEC value of more than 0.75, between 0.65 and 0.75, between 0.36 and 0.65 and less than 0.36, respectively. A negative value indicates that the mean observed value is better than the simulated value.

SUMMARY

Estimating the discharge for large (return period) and extreme events (i.e., PMP) in the channel using stochastic models is common in Malaysia as compared to computer models (i.e., physically-based model) (Ab. Ghani et al. 2009). There are several criteria in selecting a proper hydrological model. These criteria are to have a fully-distributed physically-based model, that is compatible with GIS, use two-dimensional overland routing, has continuous or discontinuous hydrology events, and the availability of model code (i.e., publicly available or commercial code). In this study, the fully-distributed physically-based model was chosen to be the main criteria among others. Six potential hydrological models were chosen and compared based on this criterion. From these comparisons, the TREX model was selected to simulate large and extreme events. Three different sized watersheds were selected to simulate these events. The sizes are small (less than 100 km^2), medium (between 100 and 1,000 km^2) and large (more than 1,000 km^2), based on Singh (1995). In this study the large event consists of return periods ranging from 2 to 100 years. These values were obtained from MSMA (2000). The extreme events consist of PMP and world's largest rainfalls. The PMP and world's largest rainfall values were obtained from NAHRIM (2008), Poon and Hwee (2010), and Jennings (1950). The performance of the TREX model will be evaluated using graphical and statistical methods. The graphical method will focus on time to peak, peak discharge and rising and falling limbs. Three different statistical methods, RPD, NSEC and PBIAS, will be used as the quantitative measurement between observed and simulated peak discharge, time to peak and total volume.

CHAPTER THREE

HYDROLOGICAL PROCESSES IN THE TREX MODEL

This chapter will describe the hydrological processes and numerical schemes in the TREX model. The governing equations, such as mass and momentum equations, will be described in section 3.1. The description of the numerical scheme to simulate the hydrological processes is explained in section 3.2.

3.1 GOVERNING EQUATIONS IN THE TREX MODEL

There are four main processes in the TREX hydrological sub-model: (1) precipitation and interception, (2) infiltration and transmission losses, (3) depression storage and (4) overland and channel flow as shown in Figure 3.1.

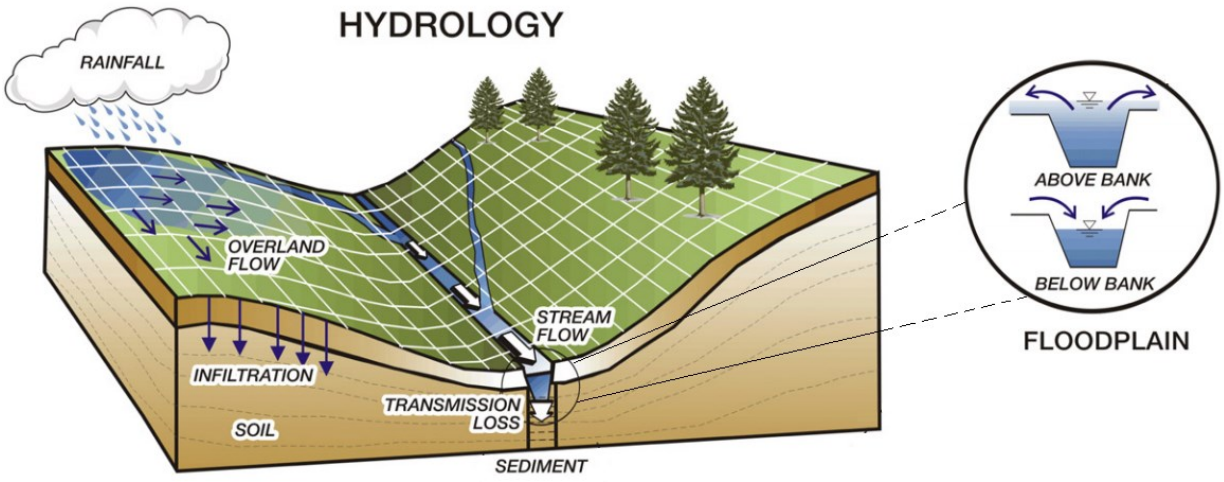

Figure 3.1 Overview of hydrological processes in TREX model

3.1.1 Precipitation and Interception

Precipitation is the beginning of the hydrological cycle. The gross volume of water reaching the near surface can be described in a mathematical model, as shown in Equation 3.1.

$$\frac{dV_g}{dt} = i_g A_s \qquad \text{[Equation 3.1]}$$

Where: V_g = gross precipitation [L^3]

t = time [T]

i_g = gross precipitation rate [LT^{-1}]

A_s = surface area over which precipitation occurs [L^2]

The presence of forests or any other vegetation cover over an area of land influences the distribution pattern of precipitation. Some of the precipitation is intercepted and retained by the leaves and other parts of the tree, and then eventually returns to the atmosphere in the form of evaporation. The TREX model factors interception in volume. Linsley et al. (1982) showed that the interception volume could be calculated using Equations 3.2 and 3.3.

$$V_i = (S_i + Et_R)A_s \qquad \text{[Equation 3.2]}$$

$$V_n = \begin{cases} V_g - V_i & \text{for: } V_g > V_i \\ 0 & \text{for: } V_g \leq V_i \end{cases} \qquad \text{[Equation 3.3]}$$

Where: V_i = interception volume [L^3]

S_i = interception capacity of projected canopy per unit area [L^3L^{-2}]

E = evaporation rate [LT^{-1}]

t_R = precipitation event duration [T]

V_n = net precipitation volume reaching the surface [L^3]

Note that for single storm events, the volume of evaporation, E [LT^{-1}] in Equation 3.2 can be neglected. Net precipitation volume also can be shown as a net precipitation rate by rearranging Equation 3.1 and substituting Equations 3.2 and 3.3 to end with Equation 3.4.

$$i_n = \frac{1}{A_s}\frac{dV_n}{dt} \qquad \text{[Equation 3.4]}$$

Where: i_n = net precipitation rate at the surface [LT^{-1}]

3.1.2 Infiltration and Transmission Losses

Green and Ampt (1911) first analyzed the process of infiltration. Later, Li et al. (1976), Smith and Parlange (1978) and many others provided improved understanding and descriptions about this method. In the TREX model, infiltration rate is calculated using Equation 3.5, as introduced by Green and Ampt (1911).

$$f = K_h\left[1 + \frac{H_c(1 - S_e)\theta_e}{F}\right] \qquad \text{[Equation 3.5]}$$

Where: f = infiltration rate [LT^{-1}]

K_h = effective hydraulic conductivity [LT^{-1}]

H_c = capillary pressure (suction) head at the wetting front [L]

S_e = effective soil saturation [-]

θ_e = effective soil porosity ($\varphi - \theta_r$) [-]

φ = total soil porosity [-]

θ_r = residual soil moisture content [-]

F = cumulative infiltrated water depth [L]

Transmission loss is the process by which water from the river may be lost as the effect of seepage to groundwater, overbank flow that goes into floodplains, wetlands and billabongs and never returns to the river. The rate of transmission may be affected by several factors, particularly hydraulic conductivity. The Green and Ampt (1911) method has been applied to calculate transmission losses (Equation 3.6).

$$t_l = K_h \left[1 + \frac{(H_w + H_c)(1 - S_e)\theta_e}{T}\right] \qquad \text{[Equation 3.6]}$$

Where: t_l = transmission loss rate [LT^{-1}]

H_w = hydrostatic pressure head (depth of water in channel) [L]

T = cumulative depth of water transported by transmission loss [L]

Note here that for single storm events, the recovery of infiltration capacity by evapotranspiration and percolation can be neglected. Similarly, the recovery of transmission loss capacity by evaporation or other processes can be neglected for single storm events.

3.1.3 Depression storage

Precipitation retained in small surface depressions is called depression storage (Linsley et al. 1982). Water in depression storage may be conceptualized as a volume, or when normalized by surface area, a depth. When the water depth is below the depression storage threshold, overland flow is zero. Note that water in depression storage is still subject to infiltration and

evaporation. Similar to depression storage in overland areas, water in channels may be stored in depressions in the stream bed, which are caused when channel water depth falls below some critical level, flow is zero, and the water surface has discontinuities but individual pools of water remain. This mechanism is termed dead storage. Note that water in dead storage is still subjected to transmission loss and evaporation.

For single storm events, recovery of depression storage volume by evaporation can be neglected. Similarly, the recovery of a dead storage volume by evaporation can also be neglected for single storm events.

3.1.4 Overland and Channel Flow

Overland flow occurs when the water depth of the overland plane exceeds the depression storage threshold. Overland flow is governed by the conservation of mass (continuity) and conservation of momentum. The two-dimensional (vertically integrated) continuity equation for gradually-varied flow over a plane in rectangular (x, y) coordinates is shown in Equation 3.7 (Julien et al. 1995; Julien 2002):

$$\frac{\partial h}{\partial t} + \frac{\partial q_x}{\partial x} + \frac{\partial q_y}{\partial y} = i_n - f + \dot{W} = i_e \qquad \text{[Equation 3.7]}$$

Where: h = surface water depth [L]

q_x, q_y = unit discharge in the x- or y-direction = Q_x/B_x , Q_y/B_y [L^2/T]

Q_x, Q_y = flow in x- or y-direction [L^3/T]

B_x, B_y = flow width in x- or y-direction [L]

$\dot{W}$ = discharge from / to a point source / sink [L/T]

i_e = excess precipitation [L/T]

The application of momentum equations (Saint-Venant equations) for x- and y-directions may be derived by relating the net forces per unit mass to flow acceleration (Julien et al. 1995; Julien 2002). The small terms: local and convective acceleration components, of full Saint-Venant equations may be neglected (Cunge et al. 1980), resulting in the diffusive wave approximation for x- and y-directions (Equation 3.8).

$$S_{fx} = S_{ox} - \frac{\partial h}{\partial x} \quad \text{and} \quad S_{fy} = S_{oy} - \frac{\partial h}{\partial y} \qquad \text{[Equation 3.8]}$$

Where: S_{fx} , S_{fy} = friction slope (energy grade line) in the x- or y-direction [-]

S_{ox} , S_{oy} = ground surface slope in the x- or y-direction [-]

Five hydraulic variables must be defined in terms of depth-discharge relationship (Julien et al. 1995; Julien 2002) (Equations 3.9 and 3.10) to describe the flow resistance before the overland flow equations can be solved. Turbulent flow is assumed and resistance is described using Equations 3.9 and 3.10.

$$q_x = \alpha_x h^{\beta} \quad \text{and} \quad q_y = \alpha_y h^{\beta} \qquad \text{[Equation 3.9]}$$

$$\alpha_x = \frac{{S_{fx}}^{1/2}}{n} \quad \text{and} \quad \alpha_y = \frac{{S_{fy}}^{1/2}}{n} \qquad \text{[Equation 3.10]}$$

Where: α_x , α_y = resistance coefficient for flow in the x- or y-direction [$L^{1/3}/T$]

β = resistance exponent $(= 5/3)$ [-]

n = Manning roughness coefficient [$T/L^{1/3}$]

One-dimensional channel flow (along the channel in the down-gradient direction which laterally and vertically integrated) is also governed by conservation of mass (continuity) and momentum. The method suggested by Julien et al. (1995) and Julien (2002) is applied for gradually-varied flow as shown Equation 3.11.

$$\frac{\partial A_c}{\partial t} + \frac{\partial Q}{\partial x} = q_l + \widehat{W} \qquad \text{[Equation 3.11]}$$

Where: A_c = cross sectional area of flow [L^2]

Q = total discharge [L^3/T]

q_l = lateral flow into or out of the channel [L^2/T]

$\widehat{W}$ = unit discharge from / to a point sink / source [L^2/T]

To solve the channel flow equations from the momentum equation (by neglecting the local and convective terms), the diffusive wave approximation may be used for the friction slope (Equation 3.8 – only in x-direction). The Manning relationship (Equation 3.12) is used with the channel flow equations for mass and momentum (Julien et al. 1995; Julien 2002).

$$Q = \frac{1}{n} A_c {R_h}^{2/3} {S_f}^{1/2} \qquad \text{[Equation 3.12]}$$

Where: R_h = hydraulic radius of flow ($= A_c/P$) [L]

P = wetted perimeter of channel flow [L]

3.2 NUMERICAL SCHEME IN THE TREX MODEL

Figure 3.2 shows the visualization of the grid concept that was used in the TREX model to simulate the rainfall-runoff. The square grid size (i.e., W x W in meter) was assigned for the entire watershed area. The hydrologic model parameters (e.g., roughness coefficient and hydraulic conductivity) and the characteristic of the watershed (i.e., land use, soil type, geometry of rivers and topography) are assigned to a central nodal point and are assumed to be uniform throughout the cell area. The explicit Euler method (Chapra and Canale 1985) is used to compute the mass balances for each time step by counting all materials that enters, accumulates within or leaves a grid cell through precipitation excess, interception, infiltration, transmission losses and storage.

This section will mainly describe in detail the numerical scheme or discretization method that was used in the TREX model. The description of this scheme will begin with rainfall distribution, the infiltration process, and finally, overland flow and in channels.

3.2.1 Rainfall

In this study, rainfall is determined using rain gage data. The rainfall intensity is calculated for every cell at each time step. If rainfall is determined using one rain gage, the TREX model will simulate the event as a uniform rainfall across the watershed. An interpolation scheme, inverse distance weighted (IDW) approximation, is used when there are more than one rain gage data. The IDW approximation equation is shown in Equation 3.13, which is the simplest form and was introduced by Shepard (1968). This approximation is the most common method to determine the distribution of rainfall (Watson and Philip 1985; Smith 1993; Keckler 1995; Sharif et al. 2010).

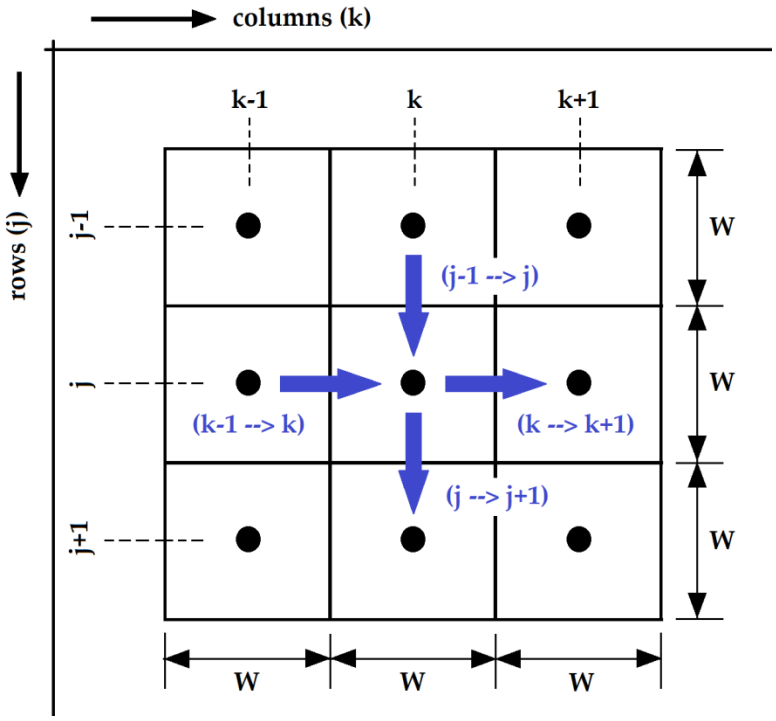

Figure 3.2 A two-dimensional model grid mesh (adapted from Julien and Saghafian 1991)

$$i^t(j,k) = \left(\sum_{NRG=1}^{NRG} \frac{i^t_{NRG}(j,k)}{d^p}\right)\left(\sum_{NRG=1}^{NRG} \frac{1}{d^p}\right)^{-1} \qquad \text{[Equation 3.13]}$$

Where: NRG = number of rain gage

$i^t_{NRG}(j,k)$ = rainfall intensity recorded by the n-th gage located at (j,k) at time t

d = distance from the rain gage to be calculated (j_i, k_i) to cell (j,k)

p = an arbitrary positive real number or power parameter (typically is 2)

3.2.2 Infiltration

Infiltration modeling in the TREX model begins when there is rainfall generated at the watershed. Rainfall intensity is compared to the infiltration capacity of the soil to determine whether there is runoff or not. When the infiltration rate is high, as compared to rainfall intensity,

then water will accumulate as groundwater. However, if the rainfall intensity is high and/or duration of rainfall is long, the soil becomes fully saturated after a certain period of rainfall. As a result, overland flow will begin. The TREX model determines the infiltration for each cell at the middle of the given time step. The value is calculated using the Green and Ampt (1911) method, as suggested by Saghafian (1992). Equation 3.14 is the formula to calculate the infiltration process in the TREX model.

$$f^{t+\Delta t} = K_h \left[1 + \frac{H_c(1 - S_e)\theta_e}{F + \frac{\Delta t}{2} f^{t+\Delta t}} \right] \qquad \text{[Equation 3.14]}$$

Where: $f^{t+\Delta t}$ = infiltration rate [LT^{-1}]

K_h = effective hydraulic conductivity [LT^{-1}]

H_c = capillary pressure (suction) head at the wetting front [L]

S_e = effective soil saturation [-]

θ_e = effective soil porosity $(\varphi - \theta_r)$ [-]

φ = total soil porosity [-]

θ_r = residual soil moisture content [-]

F = cumulative infiltrated water depth [L]

This method indicates that the Green and Ampt (1911) equation is implicit with respect to time. A time explicit solution, as suggested by Li et al. (1976), is used (Equation 3.15).

$$\Delta F = -\frac{(2F - K_h \Delta t)}{2} + \frac{(2F - K_h \Delta t)^2 + 8K_h \Delta t(\delta + F)^{1/2}}{2} \qquad \text{[Equation 3.15]}$$

Substituting Equation 3.15 into Equation 3.14 and then simplifying yields Equation 3.16. This equation is used to numerically solve the infiltration process in the TREX hydrological modeling.

$$f^{t+\Delta t} = \frac{1}{2\,\Delta t}\{(K_h\,\Delta t - 2F^t) + [(K_h\Delta t - 2F^t)^2 + 8(K_h F^t + K_h H_c(1 - S_e)\theta_e)\Delta t]^{1/2}\} \qquad \text{[Equation 3.16]}$$

3.2.3 Overland and channel flows

A 2D explicit difference formulation was selected to model overland flow and enable better representation of the flow paths (Marks and Bates 2000; Ogden 2000; Downer et al. 2002; Ogden and Julien 2002; Horrit et al. 2006). In general, each grid cell is assumed to be a homogeneous unit with one representative value of any hydraulic and hydrologic parameters, such as hydraulic conductivity, roughness and elevation. The Saint-Venant equation of continuity and momentum describe the physics of gradually-varied flow. In this case, it is assumed that the fluid is incompressible. The two-dimensional continuity equation in partial differential form is shown in Equation 3.17.

$$\frac{\partial h}{\partial t} + \frac{\partial q_x}{\partial x} + \frac{\partial q_y}{\partial y} = i_e \qquad \text{[Equation 3.17]}$$

Where: i_e = excess rainfall equal to $(i - f)$ [LT^{-1}]

i = rainfall intensity [LT^{-1}]

f = infiltration from Green-Ampt (1911) [LT^{-1}]

Discretization of Equation 3.17 with first-order approximation for element (j, k) leads to the Equation 3.18.

$$h^{t+\Delta t}(j,k) = h^{t}(j,k) + i_e \Delta t - \left[\frac{q_x^t(k \rightarrow k+1) - q_x^t(k-1 \rightarrow k)}{W} + \frac{q_y^t(j \rightarrow j+1) - q_y^t(j-1 \rightarrow j)}{W} \right] \Delta t \qquad \text{[Equation 3.18]}$$

Where:

$h^{t+\Delta t}(j,k)$	=	flow depth at cell (j, k) at time $t + \Delta t$ [L]
$h^{t}(j,k)$	=	flow depth at cell (j, k) at time t [L]
Δt	=	time step [T]
i_e	=	excess rainfall [LT^{-1}]
$q_x^t(k \rightarrow k+1)$	=	unit flow rate in x-direction at time t from (j, k) to $(j, k+1)$ [L^2T^{-1}]
$q_x^t(k-1 \rightarrow k)$	=	unit flow rate in x-direction at time t from $(j, k-1)$ to (j, k) [L^2T^{-1}]
$q_y^t(j \rightarrow j+1)$	=	unit flow rate in y-direction at time t from (j, k) to $(j+1, k)$ [L^2T^{-1}]
$q_y^t(j-1 \rightarrow j)$	=	unit flow rate in y-direction at time t from $(j-1, k)$ to (j, k) [L^2T^{-1}]
W	=	grid size [L]

The unknown value in Equation 3.18, i.e., the unit flow rate in x- and y-direction, is obtained using Manning's equation, which is given in Equation 3.19. These values are calculated using momentum equations that may be derived by relating the forces per unit mass to flow acceleration (Julien et al. 1995; Julien 2002). Often, the full Saint-Venant equation is necessary in hydrological modeling. The simplification of the full Saint-Venant equation can be accomplished by neglecting the local and convective acceleration of momentum terms because

they have small effects (Cunge et al. 1980; Daluz Vieira 1983; Moussa and Bocquillon 1996 and 2000). By neglecting these terms, a simpler form of the Saint-Venant equation is produced, known as the diffusive wave equation (Equations 3.21a (x-direction) and 3.21b (y-direction)). The diffusive wave equation can be considered a higher order approximation than the kinematic wave approximation (Katapodes 1982; Daluz Vieira 1983; Ferrick 1985; Ponce 1990). The numerical schemes for these equations are discretized and lead to Equations 3.19a and 3.19b, respectively.

$$q_x = \propto_x h^{\beta} \qquad \text{[Equation 3.19(a)]}$$

$$q_y = \propto_y h^{\beta} \qquad \text{[Equation 3.19(b)]}$$

Where: $\propto_x , \propto_y$ = resistance coefficient for flow in x- and y-direction [$L^{1/3}T^{-1}$]

β = resistant exponent (= 5/3) [-]

The resistance coefficients for flow in x- and y-direction are calculated from Equation 3.20.

$$\propto_x = \frac{\left(S_{f_x}^t\right)^{\frac{1}{2}}}{n} \quad \text{and} \quad \propto_x = \frac{\left(S_{f_x}^t\right)^{\frac{1}{2}}}{n} \qquad \text{[Equation 3.20]}$$

Where: $S_{f_x}^t \ and \ S_{f_y}^t$ = friction slope in x- and y-direction [-]

n = Manning's n coefficient in the overland [$TL^{-1/3}$]

The direction of unit flow rate for any given time and location is strongly dependent on its relation to the friction slope, S_f. This relationship is shown in Equations 3.21a and 3.21b for x- and y-direction, respectively.

$$S_{f_x}^t(k-1 \rightarrow k) \cong S_{o_x}(k-1 \rightarrow k) - \left[\frac{h^t(j,k) - h^t(j,k-1)}{W}\right] \qquad \text{[Equation 3.21(a)]}$$

$$S_{f_y}^t(j-1 \rightarrow j) \cong S_{o_y}(j-1 \rightarrow j) - \left[\frac{h^t(j,k) - h^t(j-1,k)}{W}\right] \qquad \text{[Equation 3.21(b)]}$$

Where: $h^t(j,k)$ = flow depth at cell (j,k) at time t [L]

$h^t(j,k-1)$ = flow depth at cell $(j,k-1)$ at time t [L]

The bed slope, S_o, which is expressed in terms of the cell elevation in x- and y-direction, is calculated using the numerical scheme as shown in Equations 3.22a and 3.22b, respectively.

$$S_{o_x}(k-1 \rightarrow k) = \frac{E(j,k-1) - E(j,k)}{W} \qquad \text{[Equation 3.22(a)]}$$

$$S_{o_y}(j-1 \rightarrow j) = \frac{E(j-1,k) - E(j,k)}{W} \qquad \text{[Equation 3.22(b)]}$$

Where: $E(j,k-1)$ = elevation at cell $(j,k-1)$ [L]

$E(j,k)$ = elevation at cell (j,k) [L]

$E(j-1,k)$ = elevation at cell $(j-1,k)$ [L]

Starting with Equation 3.18 and taking from Equations 3.19 through 3.22, then substituting these into Equation 3.17, the specific discharge, q [L^2T^{-1}], in x- and y-direction is calculated using numerical schemes as shown in Equations 3.23(a) and 3.23(b), respectively. The

width of the channel is constant throughout the simulation. The discharge, Q [L^3T^{-1}], is calculated by multiplying the specific discharge (Equation 3.23) and width of the channel. This is the value that was recorded by the TREX model at any point selected by the user.

$$q_x^t(k-1 \rightarrow k) = \frac{1}{n(j,k-1)}[h^t(j,k-1)]^{5/3}\left[S_{f_x}^t(k-1 \rightarrow k)\right]^{1/2} \qquad \text{[Equation 3.23(a)]}$$

$$q_y^t(k-1 \rightarrow k) = \frac{1}{n(j,k-1)}[h^t(j,k-1)]^{5/3}\left[S_{f_y}^t(k-1 \rightarrow k)\right]^{1/2} \qquad \text{[Equation 3.23(b)]}$$

The process of flow exchange between overland (i.e., floodplain) and channel is complex to solve numerically; for this reason, the one-dimensional diffusive wave equation is applied for the channel flow. This method has been well established by Woolhiser and Liggett (1967), Ponce et al. (1978), Morris and Woolhiser (1980), Fread (1985), Julien and Saghafian (1991), Moussa and Bocquillon (1996), Knight and Shiono (1996) and Ogden and Julien (2002). The numerical scheme to calculate the discharge is similar to that used for overland flow. However, the direction of the flow is only in the x-direction. Therefore, the formulation and numerical schemes in the y-direction can be neglected in these processes. The Manning's roughness is specifically used for the bed channel as required in Equation 3.20.

The channel network defined in the TREX model is made up of links that are numbered by the user or automatically by the computer. Each channel consists of several numbers of nodes (the minimum nodes is three). The properties of the channel such as side slope, bed roughness (Manning's n value), sinuosity, initial water depth and width of the channel are applied to each node. The model has the ability to calculate either rectangular and/or trapezoidal shapes by providing the value of the side slope. The tributaries and channel are assumed to be located at the middle of the grid cell, as shown in Figure 3.3.

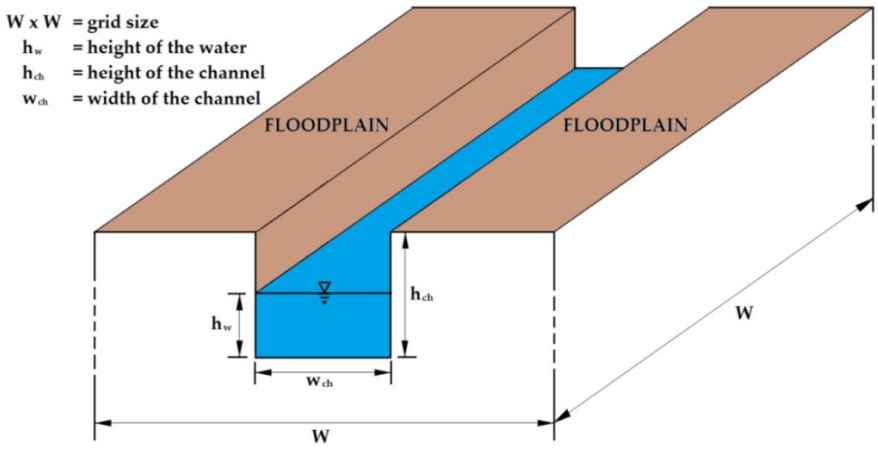

Figure 3.3Channel cross section

The integration of water flow between overland (floodplain) and channel can be shown as two phases. These phases are (1) falling limb of the hydrograph (Figure 3.4a) and (2) rising limb of the hydrograph (Figure 3.4b). Figure 3.4a indicates that the flow depth in a channel (h_w) is less than the height of its bank (h_{ch}). At this phase, overland flows go directly into the channel. The calculation of specific discharge is a one-dimensional (x-direction) diffusive ware approximation. However, when the flow depth in a channel (h_w) is higher than the height of its bank (h_{ch}), water will be transferred to both sides of the floodplains. At this point, the numerical approach is transformed to a two-dimensional (in x- and y-direction) diffusive wave approximation (Figure 3.4b).

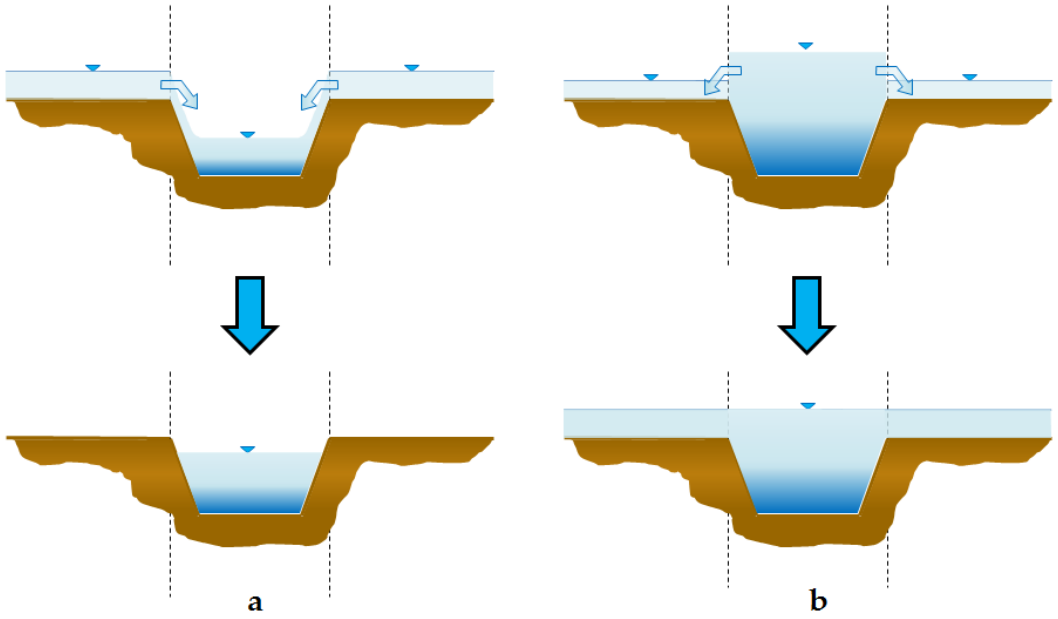

Figure 3.4 Integrated overland and channel flow during (a) the falling limb of the hydrograph and (b) the rising limb of the hydrograph (modified from Velleux et al. 2006)

SUMMARY

The TREX model uses a finite difference scheme to calculate the dynamic mass balances for each variable state. Each grid cell is assumed to be a homogeneous unit with one representative value of any hydraulic and hydrologic parameters, such as hydraulic conductivity, roughness and elevation. In this study, rainfall is determined using rain gage data. The rainfall intensity is calculated for every cell at each time step. If rainfall is determined using one rain gage, the TREX model will simulate it as uniform rainfall across the watershed. An interpolation scheme, an inverse distance weighted (IDW) approximation, is used when there are more than one rain gage data. The infiltration process is calculated using the Green and Ampt (1911) method. Diffusive wave approximation is used to solve for overland and channel flow. A two-dimensional explicit difference formulation is selected to model overland flow and enable a better representation of the flow paths.

CHAPTER FOUR

CALIBRATION AND VALIDATION

Chapter four has been organized into four sections. Sections 4.1 and 4.2 will discuss the study areas and the preparation of the input data. Preparation of the input data includes: digital elevation model (DEM), links (rivers) and nodes, soil type, land use, channel properties, initial water in channels, and in soil and storage depth. In section 4.3, calibration, validation and the performance of the model was evaluated. Discussion of the comparison on the uses of different grid size (only in small watershed) is in section 4.4.

4.1 STUDY AREAS

Malaysia has land borders with Thailand in West Malaysia, and Indonesia and Brunei in East Malaysia (Figure 4.1). These two parts of Malaysia, separated from each other by the South China Sea, share a largely similar landscape in that both Peninsular and East Malaysia feature coastal plains rising to hills and mountains. The study areas are located in Peninsular Malaysia (Figure 4.1 – red color). Three study areas were purposely selected to represent small, medium and large watersheds. There are Lui and Semenyih, which are located in the state of Selangor (Figure 4.2), and Kota Tinggi, which is located in Johor (Figure 4.3). The Lui, Semenyih, and Kota Tinggi watersheds cover 68, 236 and 1,635 km^2, respectively. These study areas have been classified as small, medium and large watersheds, respectively. Influenced by the Southwest and Northeast monsoons, the small and medium watersheds fall into the West Coast rainfall region, where June and July are the driest months and November is the wettest.

The small watershed (Lui) is located north of the medium watershed (Figure 4.2b). The watershed has land surface elevations ranging from 80 to 1,200 m above sea level (a.s.l). Approximately 87% of the area is mountainous, and valleys cover 13% of the watershed area. The flow depth in the Lui watershed ranges from 0.23 m to 0.99 m. The top width of the main channel is constant at 16 m along the river. An average channel bed slope was 0.04. The maximum discharge in the main channel ranged from 0.74 to 17.17 cms during normal flow. The topography of the medium watershed ranged from 40 m a.s.l at the outlet and 1,100 m a.s.l at the upstream end of the watershed. The average terrain slope was about 45% and ranges between 4% and 85%, with very steep mountains overhanging flat and wide valleys. This study area was covered approximately 68% by mountains and the remaining area is valleys. The average normal depth of the main channel in Sungai Semenyih ranges between 0.8 m and 2.49 m. The large watershed is located in the district of Johor (Figure 4.3). Mountains cover about 20% of the watershed, with an elevation of more than 600 m. The lowest elevation is 4 m at the downstream-end of the watershed. The watershed receives annual rainfall of 2,500 mm and the temperature of the watershed ranges between 21^{o}C to 32^{o}C.

Figure 4.1 Locations of Selangor and Johor on Malaysia's map

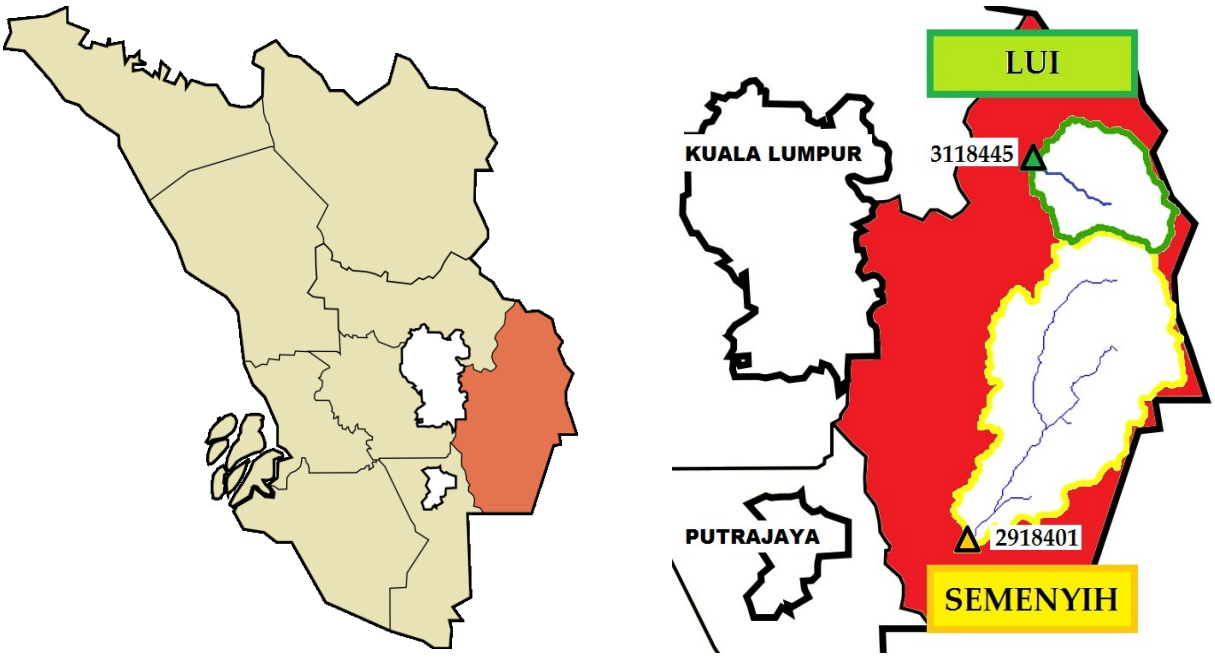

(a) Hulu Langat district on Selangor's map

(b) Lui (small) and Semenyih (medium) watersheds on Hulu Langat district

Figure 4.2 Location of the small and medium watersheds on Malaysia's map

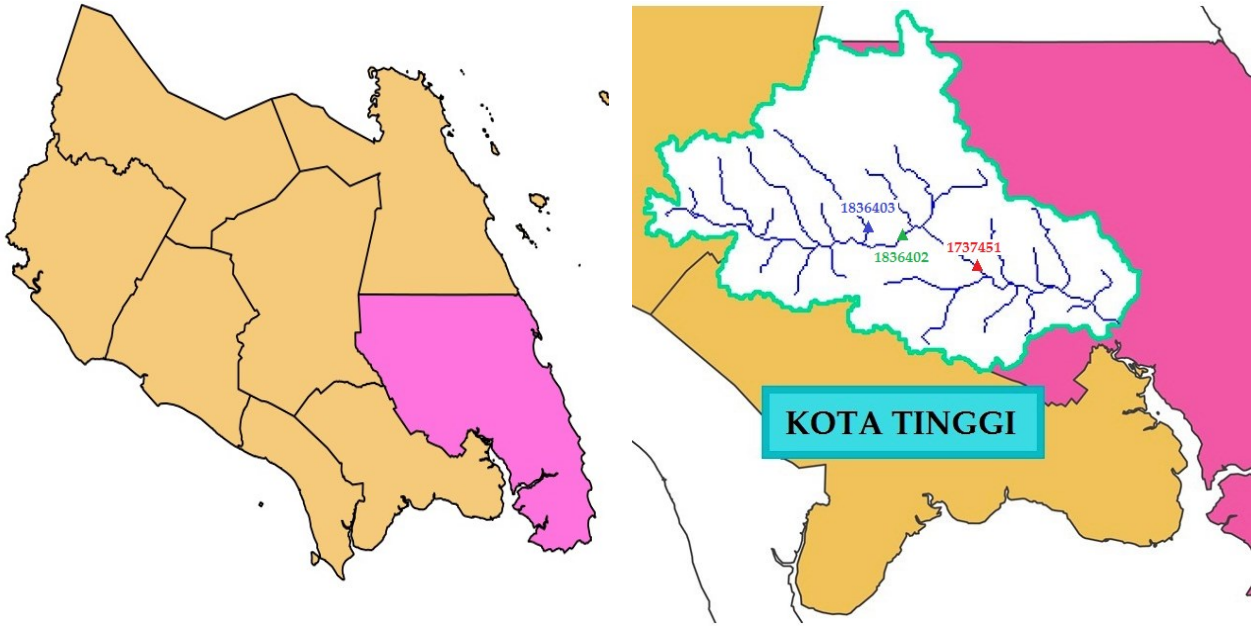

(a) Kota Tinggi district on Johor's map

(b) Kota Tinggi watershed on Kota Tinggi district

Figure 4.3 Location of the large watershed on Malaysia's map

4.2 MODEL PARAMETERIZATION

The TREX model was used to simulate infiltration, overland runoff, and channel flow during extreme rainfall events. Input data were prepared using ArcGIS 9.3 and converted into text files. To resolve surface topography, the watersheds were discretized at a 90 by 90 m grid size for small and medium watersheds, and a 230 by 230 m grid size for large watersheds. Detailed discussion on the selection of these grid sizes can be found in section 2.6 and in Appendix D. There is a possibility that by reducing the grid size will give better simulated result, i.e., runoff and discharge. However, there must be a limit to increase the level of discretization where the model performance cannot be improved (Wood et al. 1988; Mamillapalli et al. 1996). The study conducted by Shrestha et al. (2002 and 2006) confirmed the previous statement for various watershed sizes from 2,000 km^2. From these studies, they concluded that the minimum and maximum ratio between grid size and watershed area are 1:20 and 1:6, respectively. In this study, for a large watershed, the appropriate grid size according to Shrestha et al. (2002 and 2006) is between 80 and 270 m. Therefore, a 230 m grid size was chosen for the large watershed, which is well within the range suggested by Shrestha et al. (2002 and 2006). Considering the time to prepare the input data, simulation time and post-processing the result, a grid analysis for the large watershed was not feasible in this study.

The DEM (Figures 4.4a and 4.5a) data for the small and medium watersheds were bought from the Department of Surveying and Mapping Malaysia (DSMM) and resampled from 20 m to 90 m resolution. The grid size was used to delineate these watersheds. The resultant rectangular raster grid has 122 columns and 109 rows for the small watershed and 265 rows and 197 columns for the medium watershed. That means the total number of grid cells for the small and medium watersheds are 13,298 and 52,205, respectively. Within these raster grids, the watershed

areas are defined by 8,426 and 29,139 grids for small and medium, respectively. For the large watershed, the DEM (Figure 4.6a) was downloaded from the ASTER GDEM website (www.gdem.aster.ersdac.or.jp/search.jsp) with a 90 m resolution. The total active grid size is 31,000 grids from 62,000 total grids, resulting from 292 rows and 292 columns.

The DEM were also used to delineate the channel network within the watersheds. For the small watershed, there is only one link and consists of 66 nodes, making the length of the river approximately 6 km. The land use and soil types are shown in Figures 4.4b and 4.4c, respectively. The defined channel network in the medium watershed comprised 7 links totaling 399 nodes, defining a total river length of approximately 36 km. The land use and soil types at medium the watershed are shown in Figures 4.5b and 4.5c. The land use and soil type at small and medium watersheds were obtained from Jaafar (2007). The total river length at the large watershed is 250 km (1,081 nodes and 42 links). The input data for land use and soil types at this watershed are shown in Figures 4.6a and 4.6b, respectively. These data were obtained from Shafie (2009) and Google Maps. These photos were digitized in ArcGIS 9.3 and converted to raster. Finally, these raster data were converted to ASCII files as input in the TREX model.

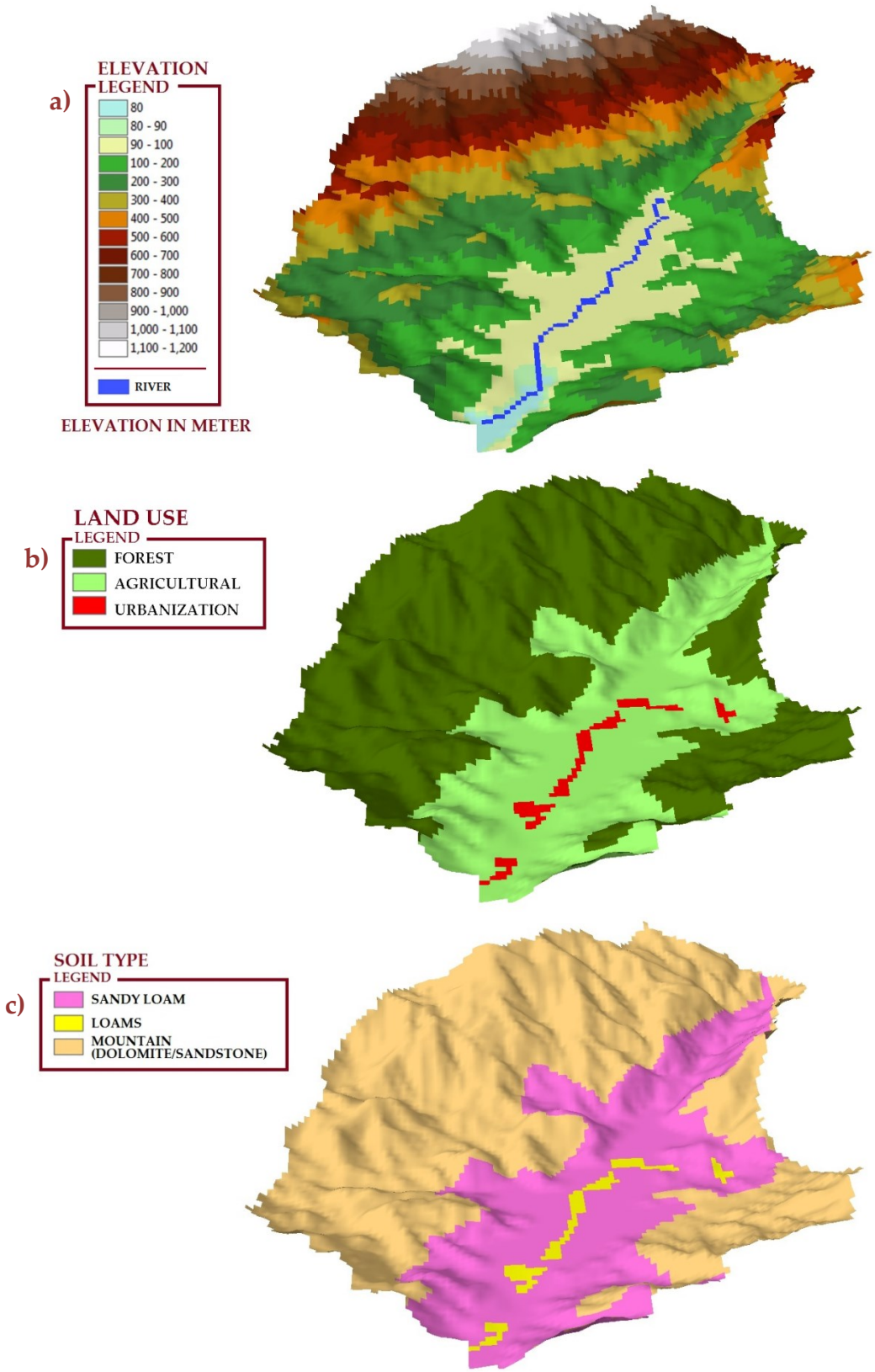

Figure 4.4 Input data for the small watershed (a) DEM, (b) land use and (c) soil type

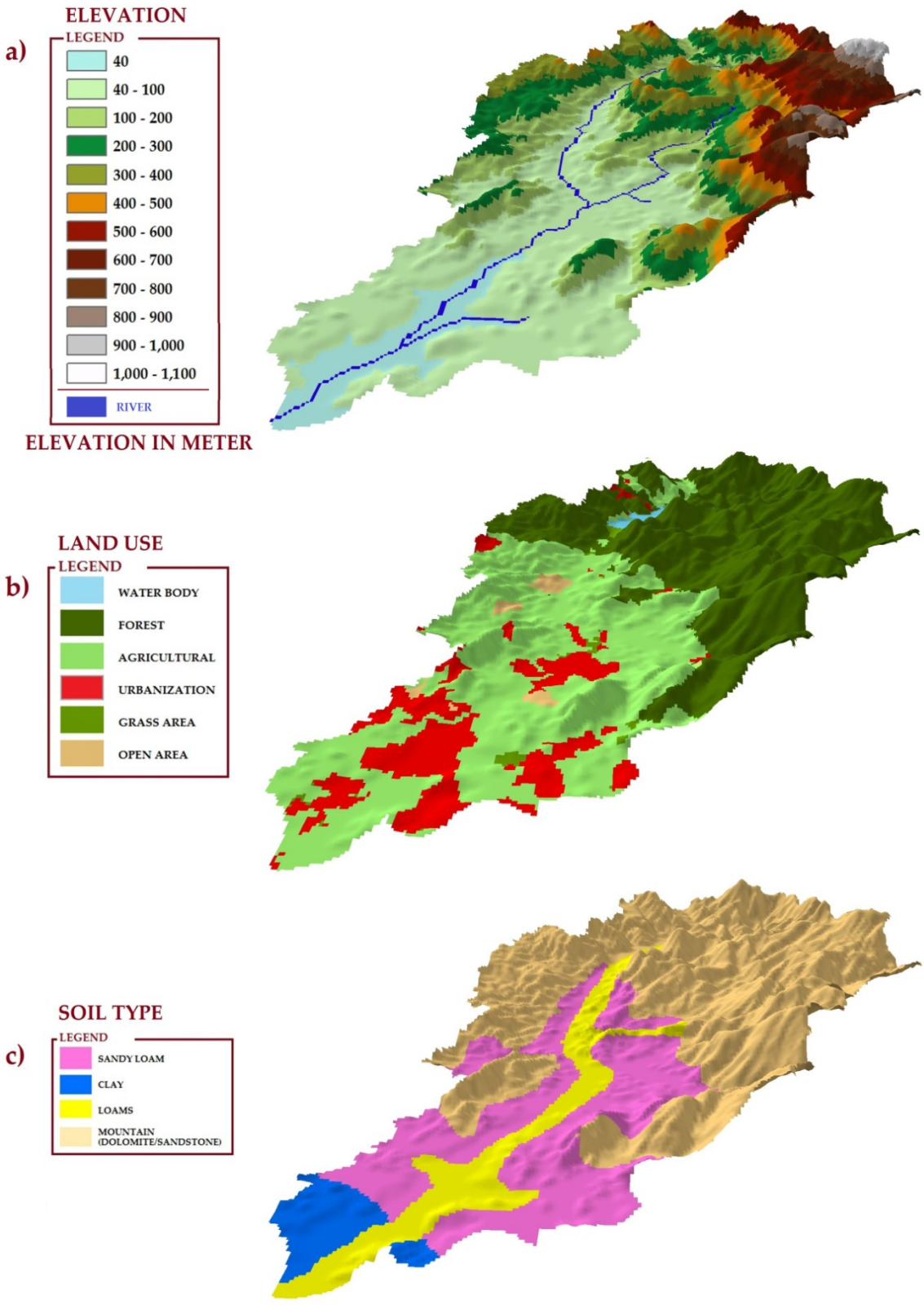

Figure 4.5 Input data for the medium watershed (a) DEM, (b) land use and (c) soil type

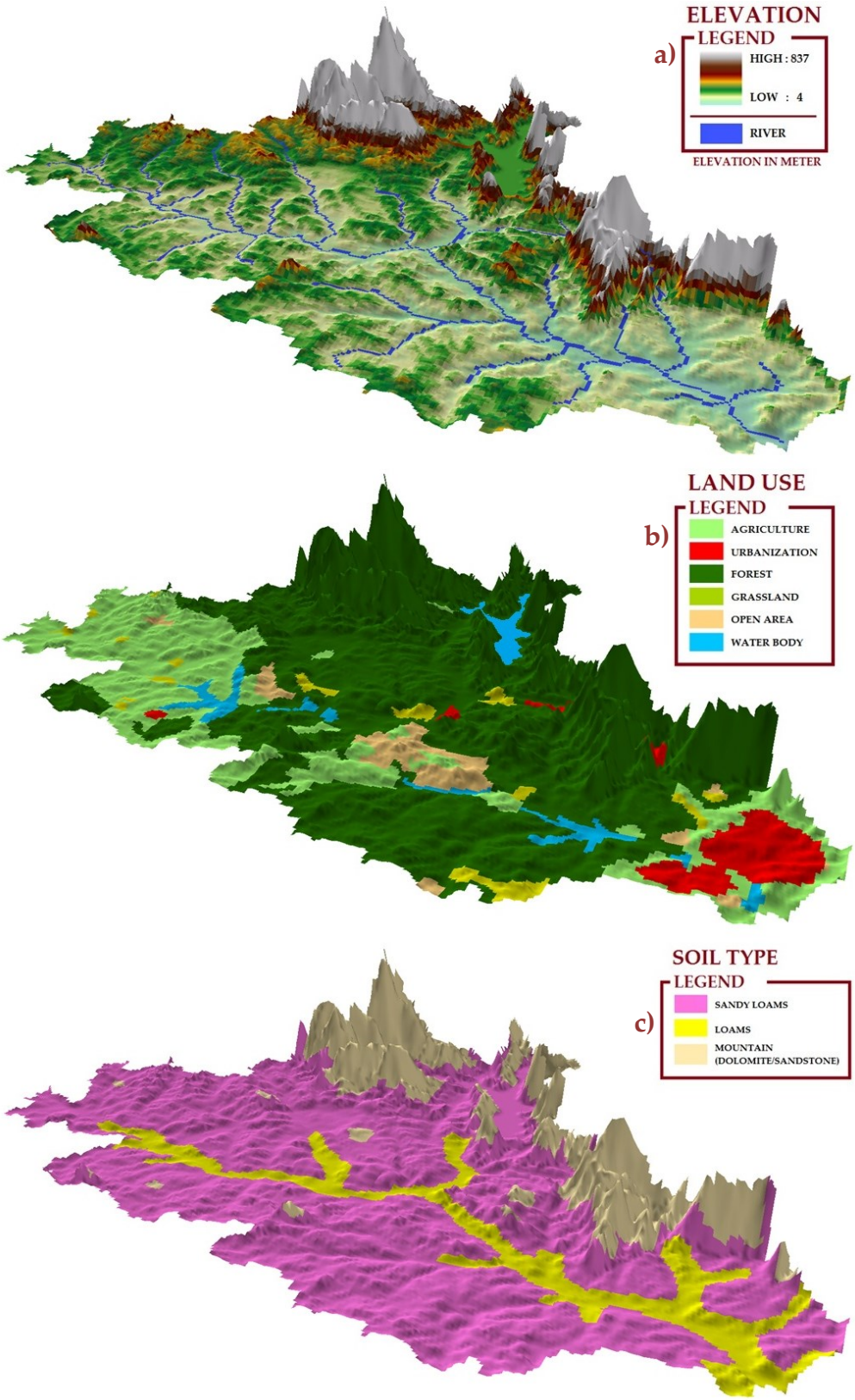

Figure 4.6 Input data for the large watershed (a) DEM, (b) land use and (c) soil type

Model parameters to be calibrated are shown in Table 4.1. Sensitivity analysis (Appendix B) shows that the K_h and Manning's n are the most sensitive parameters during calibration. Other model parameters are less important determinants of overall model performance because significant changes in values have minimum impact to the peak discharge. Parameters for forcing functions and boundary conditions have an impact to the model performance. However, the calibration process for these parameters was not necessary. There were no reported values for hydraulic conductivity and Manning's n, for these watersheds. Therefore, hydraulic conductivities were determined from soil type as described by Rawls et al. (1993). The Manning's n values for bed channel were obtained from Zakaria et al. (2010) for small and medium watersheds. The ranging values of calibrated parameters for small, medium and large watersheds are summarized in Table 4.1. These values were adjusted during calibration to achieve very good agreement between observed and simulated discharges. The antecedent moisture condition for the watershed was assumed to be fully dry at the beginning of the simulation.

4.3 CALIBRATION AND VALIDATION OF THE TREX MODEL

Calibrations for the small and medium watersheds were done using recorded data at stations 3118445 and 2918401, respectively. The simulations were done for 48 hours to provide enough base flow in the channel before the storm events. However, for large watershed, three flow gages were used during calibration and validation processes. The locations of each station were shown in Figure 4.2b for small and medium watersheds and Figure 4.3b for large watershed.

Table 4.1 Summary of model parameter values for small, medium and large watersheds

Parameter	Value	Application
Interception depth (mm)	2.0	Agriculture
	0.05	Urban / Commercial
	5.0	Forest
	1.0	Grass area
	1.0	Open area
Soil moisture deficit (-)	0.29	Sandy loams
		Loams
		Clay
		Mountain – limestone
Capillary suction head (m)	0.14	Sandy loams
	0.22	Loams
	0.33	Clay
	0.17	Mountain – limestone
Hydraulic conductivity K_h (m/s)	$3.5 \times 10^{-10} – 3.5 \times 10^{-7}$	Sandy loams
	$3.7 \times 10^{-10} – 3.7 \times 10^{-7}$	Loams
	$7.7 \times 10^{-10} – 1.3 \times 10^{-8}$	Clay
	$3.5 \times 10^{-11} – 3.2 \times 10^{-6}$	Mountain – limestone
Manning's n	0.05 – 0.35	Agriculture
	0.01 – 0.10	Urban / Commercial
	0.18 – 0.65	Forest
	0.05 – 0.35	Grass area
	0.05 – 0.35	Open area

During the validation processes, the rainfall-runoff relationship was simulated using calibrated parameters (K_h and n) without any changes. The calibration and validation procedure focused on the accuracy of simulated peak discharge and time to peak at the main outlet (i.e., at the point-end-downstream of the link). The total volume was also considered but it will not be discussed in detail because this parameter is less important in flood analysis. The results and discussions are divided into three subsections which are 4.3.1 for the small watershed (Lui), 4.3.2 for the medium watershed (Semenyih) and 4.3.3 for the large watershed (Kota Tinggi).

4.3.1 Small watershed (Lui)

The largest storm on April 10, 2009 was used to calibrate the model. There was no rainfall for several days before this event. Two years of recorded data from 2009 to 2010 were used independently for validation purposes. The availability of the data obtained from Department of Irrigation and Drainage (DID), particularly the duration of the recorded data and missing values, are limitations in this study. Graphs of observed and simulated discharge for this event are presented in Figure 4.7a. Several storm events ranging from small to large events were selected to validate the model parameters. The calibrated and validated hydrograph are shown in Figures 4.7a and Figure 4.7b, 4.7c and 4.7d, respectively.

Graphical method

The graphical methods provide visual comparison between observed and simulated peak discharge, time to peak and rising and falling limb. The calibrated hydrograph (Figure 4.7a) shows fairly good model performance on estimating the peak discharge, time to peak and estimating the rising and falling limb. However, the validated hydrographs (Figures 4.7b – 4.7d) show better performance for estimating the same three parameters. The model estimated higher total volume than the observed. The uniformity of rainfall across the watershed was not a good representation of the true event. The spatial distribution of the rainfall was concentrated at some location. However, the input data (DEM, land use, soil type, hydrologic, hydrology, etc.) and calibrated and validated model parameters can produce hydrographs that are comparable to the observed data. Figures 4.8 and 4.9 show the observed and simulated values are plotted for peak discharge and time to peak, respectively. The 45 degree line (1:1 line) indicates that observed and simulated values estimated by the model are accurate. It was found that most of the

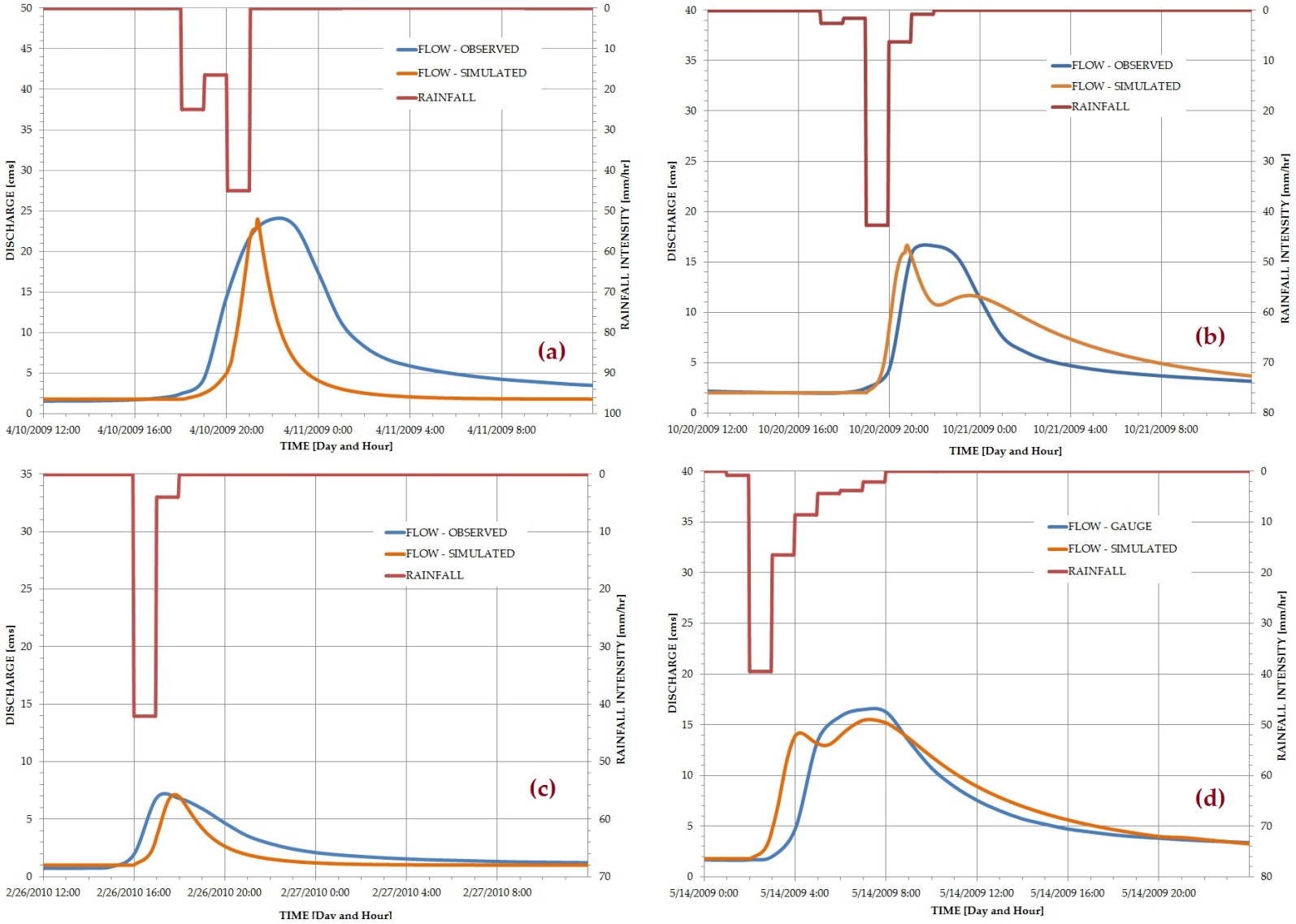

Figure 4.7 Hydrologic calibration (a) and validation (b, c and d) for the small watershed (Lui)

simulated peak discharge values (Figure 4.8) are distributed along the 1:1 line except for a few events (Nov. 13, 2010, Jan. 3, 2009 and May 14, 2009). Comparison between observed and simulated time to peak, as shown in Figure 4.9, found that the model performed fairly well. Most of the simulated times to peaks were simulated to be earlier than the observed time, except for the rainfall events on May 14, 2009 and February 26, 2010, which were delayed by about 30 minutes. On average, the model simulated time to peak at 1.5 hours earlier than the observed value. In general, the overall performance of this model for the calibration and validation were good.

Statistical methods

Model performance evaluation was continued by applying statistical analyses, namely the Relative Percentage Difference (RPD), Percent BIAS (PBIAS) and Nash-Sutcliffe Efficiency Coefficient (NSEC). These values were calculated using Equations 2.2, 2.3 and 2.4 as described in subsections 2.8.1, 2.8.2 and 2.8.3, respectively. The calculated RPD, PBIAS and NSEC values are classified based on the criteria given in Table 4.2. Table 4.3 shows the values of statistical tests between observed and simulated peak discharge, total volume and time to peak during calibration and validation periods. Most of the peak discharge, total volume and time to peak values indicate that the model shows excellent performances specified by RPD values of less than 10%, except for a few events. Even though the calibrated total volume is underestimated by 50%, the validated total volume can be classified as good when an average RPD value is underestimated by 10%. NSEC values for the peak discharge calibration and validation ranged from *unsatisfactory* (-0.5) to *very good* (0.81). The unsatisfactory events are on December 26, 2009 and July 1, 2010 with NSEC values of 0.07 and -0.5, respectively. Statistical tests indicated

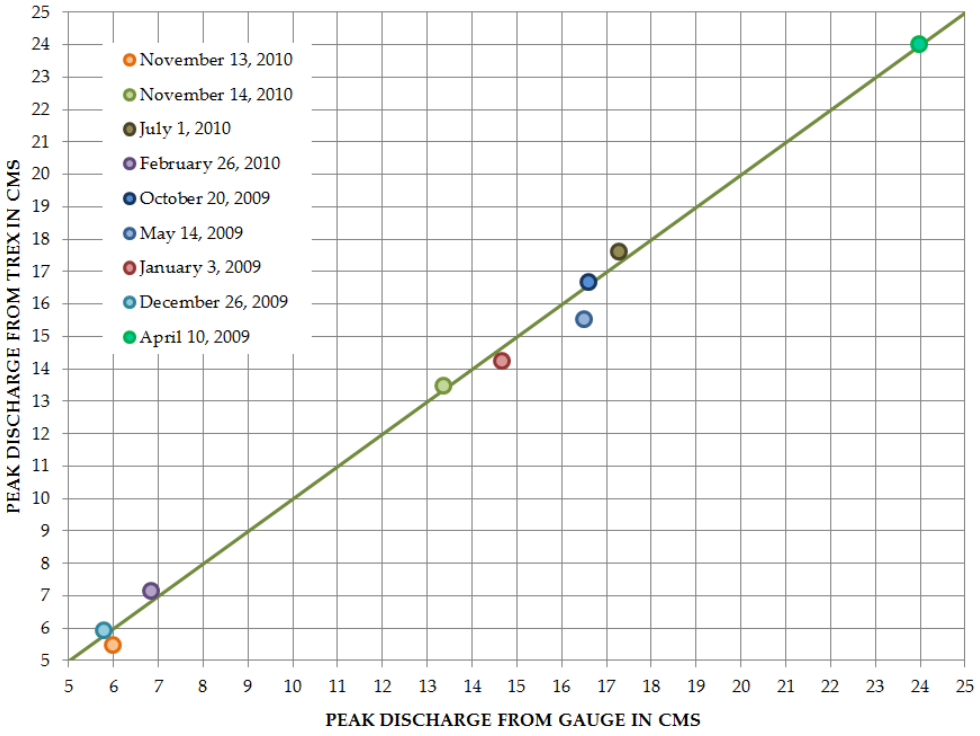

Figure 4.8 Peak discharge for the model calibration and validation events on the small watershed (Lui)

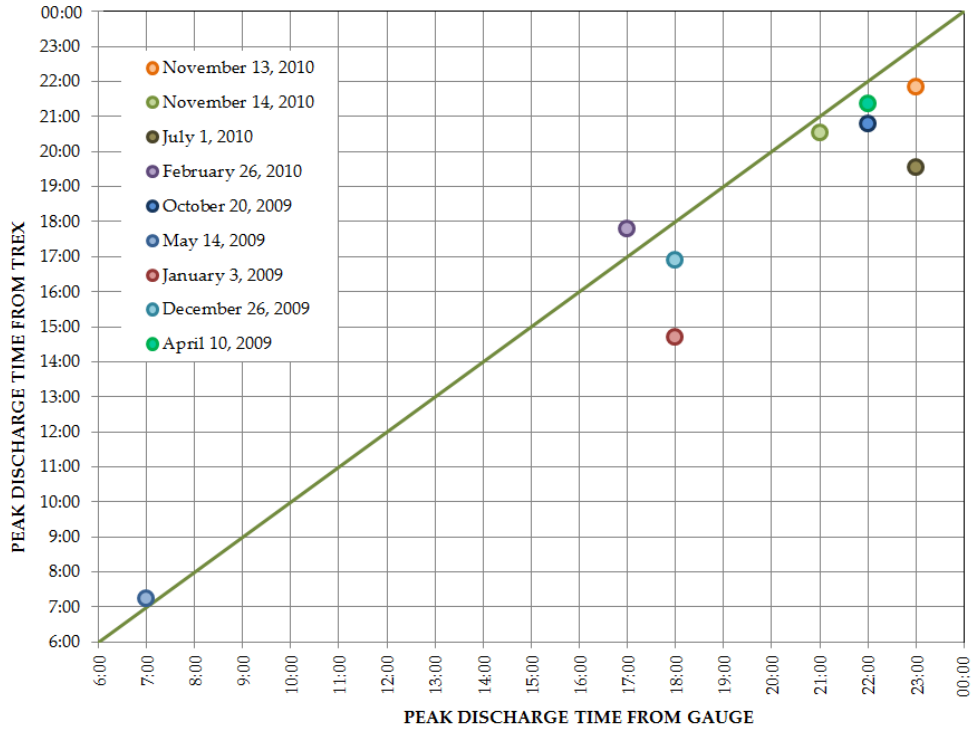

Figure 4.9 Time to peak for the model calibration and validation events on the small watershed (Lui)

that the average PBIAS of total volume during calibration and validation is underestimated by about 14%. The high values of PBIAS during the calibration process (April 10, 2009) and validation process (July 1, 2010) reflected that the model underestimates total volumes beyond the level of acceptance. However, considering the overall statistics, it can be said that the model simulations were good.

Rainfall events recorded in the wettest months (i.e., October, November and December) were selected for the validation process and model performance evaluation. These scenarios were selected in order to observe the capabilities of the model to simulate high rainfall volumes under Malaysia's climate.

4.3.2 Medium watershed (Semenyih)

In this study, data from station 2918401 were used for calibration and validation purposes. The gaging station is located at the downstream end of the medium watershed. The observed and simulated values for the calibrated model are shown in Figure 4.10a. The storm event on April 13, 2003 was used to calibrate the model. There was no rainfall for several days before this event. The calibrated model parameters were then applied for several other rainfall events for validation purposes. Storm events from 2002 to 2009 were used in the validation process. Comparisons between observed and simulated graph discharges for these events are presented in Figures 4.10b – 4.10d.

Table 4.2 General performance ratings to classify the performance of the model

PERFORMANCE RATING	RPD and PBIAS	NSEC
Very Good	RPD, PBIAS $\leq \pm$ 10%	0.75 $\leq$ NSEC < 1.00
Good	$\pm$ 10% < RPD, PBIAS $\leq \pm$ 15%	0.65 $\leq$ NSEC < 0.75
Fair / Satisfactory	$\pm$ 15% < RPD, PBIAS $\leq \pm$ 25%	0.36 $\leq$ NSEC < 0.65

Table 4.3 Summary of the evaluation of hydrologic model performance for the small watershed (Lui)

CALIBRATION											
Date of event	**Total volume (x 1,000 m^3)**			**Peak flow (cms)**			**Time to peak (24 hours)**			**Model's performance**	
	Obs.	**Sim.**	**RPD (%)**	**Obs.**	**Sim.**	**RPD (%)**	**Obs.**	**Sim.**	**RPD (%)**	**NSEC**	**PBIAS**
04/10/09	652	313	- 51.9	23.99	24.01	0.1	22:00	21:11	- 3.7	0.4	50.6
VALIDATION											
11/14/10	520	577	10.9	13.36	13.67	2.3	21:00	20:36	- 1.9	0.5	29.3
12/26/09	216	204	- 5.6	5.80	5.97	3.0	18:00	16:51	- 6.4	0.1	9.1
10/20/09	470	495	5.3	16.60	17.00	2.4	22:00	20:35	- 6.4	0.8	- 11.4
05/14/09	592	573	- 3.2	16.51	13.74	- 16.8	07:00	07:18	4.2	0.8	- 11.1
01/03/09	526	442	- 16.0	14.67	13.37	-8.8	18:00	14:42	- 18.3	0.7	- 7.6
01/07/10	506	522	3.1	17.28	17.76	2.8	23:00	19:36	- 14.8	-0.5	44.7
11/13/10	227	205	- 10.0	5.99	4.25	- 29.1	23:00	22:00	- 4.3	0.7	4.4
02/26/10	203	141	- 30.6	6.86	7.58	10.4	17:00	17:39	3.7	0.7	21.4

Note: Obs. = Observed; Sim. = Simulated; RPD = Relative Percentage Different; NSEC = Nash-Sutcliffe Efficiency Coefficient; PBIAS = Percent BIAS

Graphical method

The simulated model generally followed the shape of observed values perfectly during calibration and validation, as seen in Figure 4.10. The calibrated model parameters produced an excellent hydrograph, as shown in Figure 4.10a. The model accurately estimated the peak discharge, time to peak, and rising and falling limb. The calibrated model parameters were further validated using several independent storm events. The hydrographs of these validations are shown in Figures 4.10b - 4.10d. From this method, the validation of the model was performed very good, same as during the calibration process. The estimated total volume was higher than the observed data. The model requires more time to drain the water after the rainfall events, which causes higher total volume. Figures 4.11 and 4.12 show the observed and simulated values plotted for peak discharge and time to peak, respectively. The 45 degrees line (1:1 line) indicates that observed and simulated values were accurately estimated by the model. The simulated peak discharge values (Figure 4.11) are well distributed along the 1:1 line. The performance of the model has been classified as very good even though the comparison of observed and simulated time to peak graph (Figure 4.12) shows a short delay from the observed by about half an hour.

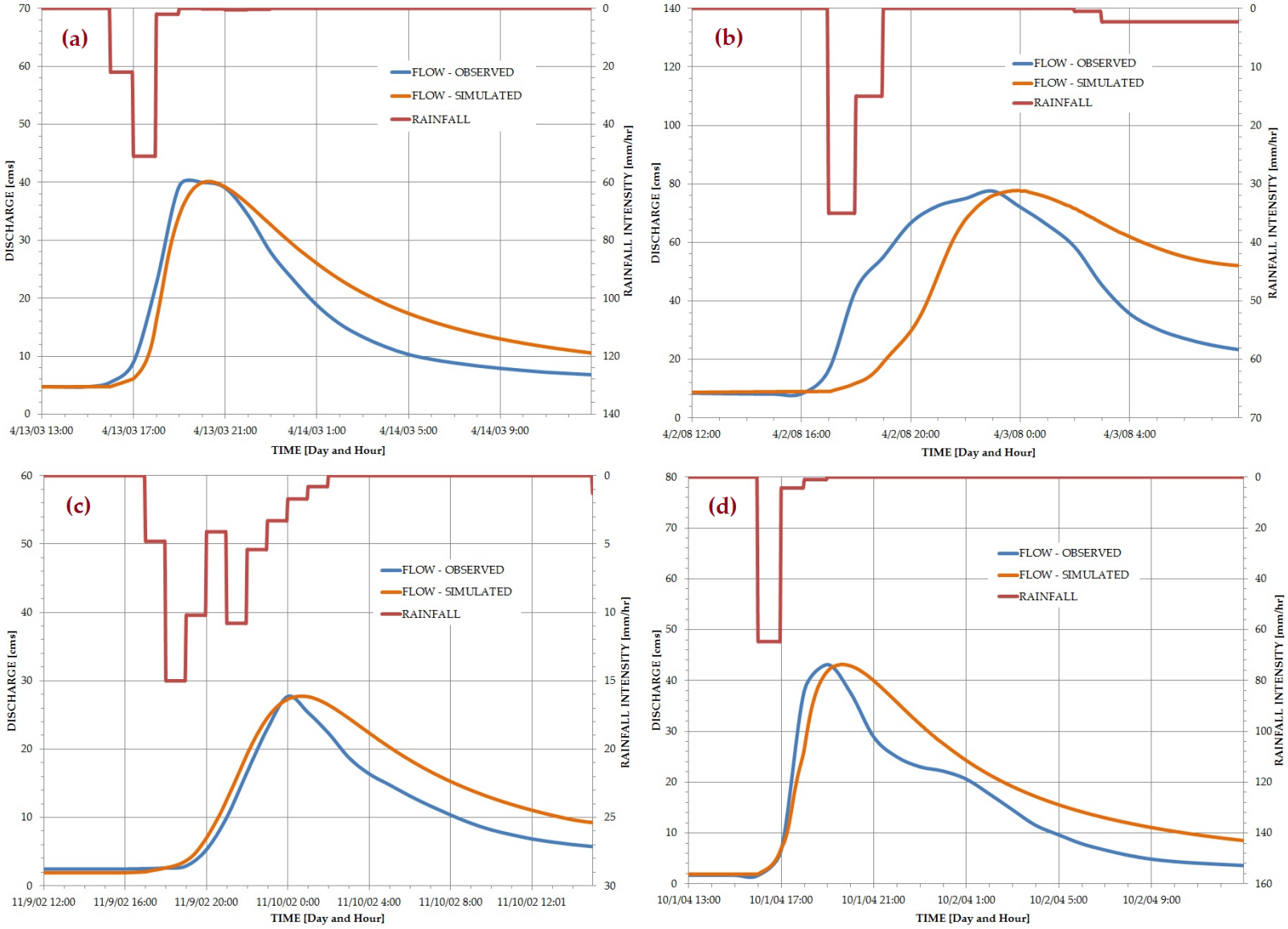

Figure 4.10 Hydrologic calibration (a) and validation (b, c and d) for the medium watershed (Semenyih)

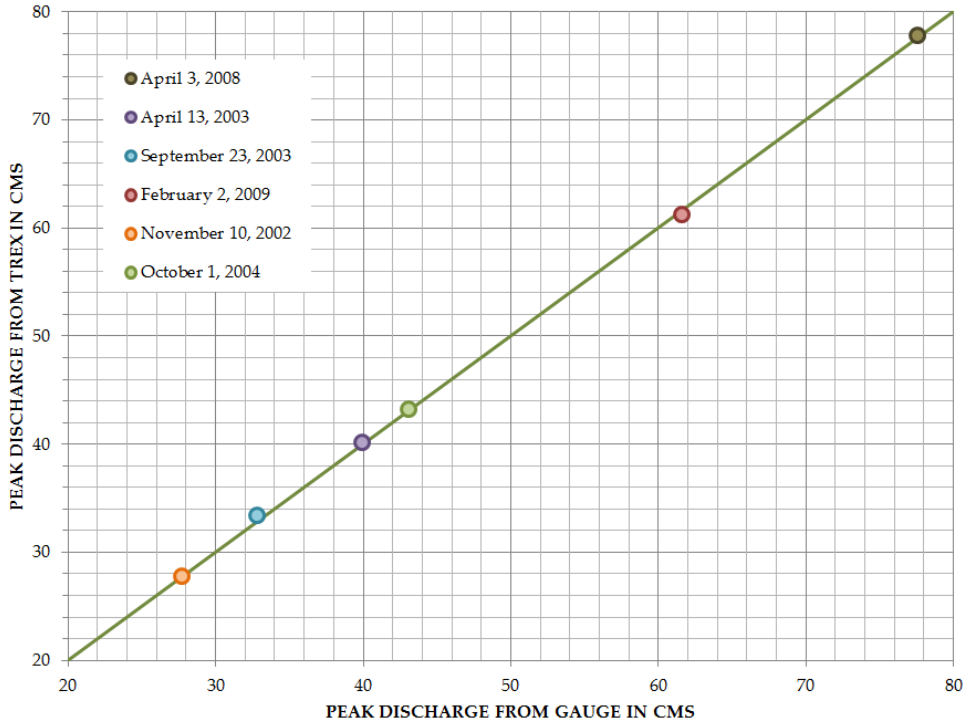

Figure 4.11 Peak discharge for the model calibration and validation event on medium watershed (Semenyih)

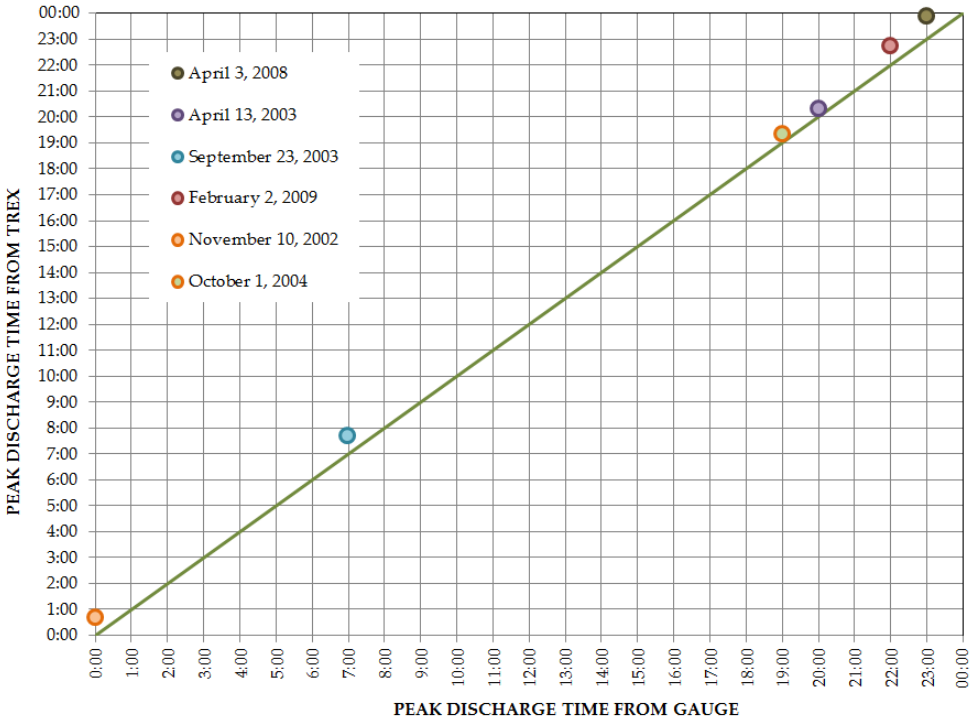

Figure 4.12 Time to peak for the model calibration and validation event on medium watershed (Semenyih)

Statistical methods

Statistical methods, namely RPD, PBIAS and NSEC, were used to assess the model's quantitative accuracy. These values were calculated using Equations 2.2, 2.3 and 2.4 and tabulated in Table 4.4. Table 4.2 was used to classify the rating of the model's performance. The RPD method showed *very good* agreement between observed and simulated for peak discharge and time to peak. The average RPD value for peak discharge and time to peak is overestimated by 0.3% and 4%, respectively. However, the RPD values for total volume for all simulations are classified as *fair*. Except for the simulation event on April 3, 2008, all of the simulated total volume values are overestimated by an average value of 35%. Longer time required by the model to drain the water in the main channel, which causes large discrepancies between the simulated and observed total volumes. The excepted event was considered *very good* with an overestimation of 3.9%. The PBIAS values were calculated for total volume and the model shows overestimation ranging from 7.6% to 31.7%. Different methods were used in RPD and PBIAS to calculate the volume. The RPD method calculates the total volume under the hydrograph and compares the difference between simulated and observed. The same comparison was applied using PBIAS method except that the volume is calculated hourly. Reasonable coefficients using NSEC ranged from 0.4 to 1.0 for model calibration and validation were obtained, except for the event on September 23, 2003, which had an NSEC value of 0.1. On average, the model overestimated the total volume by 58%. A lower NSEC value was obtained due to the fact that the model estimated larger total volumes. It can also be concluded that when the PBIAS value is near to zero, the NSEC value will be close to 1.0. The inaccuracy of the results is due to differences in topography of the watershed such as channel, soil, and land use characterized by the model.

Table 4.4 Summary of the evaluation of hydrologic model performance for the medium watershed (Semenyih)

Date of event	Total volume (x 1,000 m^3)			Peak flow (cms)			Time to peak (24 hours)			Model's performance	
	Obs.	Sim.	RPD (%)	Obs.	Sim.	RPD (%)	Obs.	Sim.	RPD (%)	NSEC	PBIAS
CALIBRATION											
04/13/03	1,375	1,638	19.1	39.98	40.15	0.4	20:00	20:18	1.5	0.8	- 19.3
VALIDATION											
04/03/08	2,939	3,052	3.9	77.58	77.77	0.2	23:00	23:54	3.9	1.0	- 7.6
09/23/03	590	950	61.2	32.83	33.37	1.6	07:00	07:42	10.0	0.1	- 57.7
02/02/09	1,924	2,530	31.5	61.59	61.23	- 0.6	22:00	22:45	3.4	0.4	- 31.7
11/10/02	947	1,277	34.9	27.71	27.74	0.1	00:00	00:42	41.0	0.8	- 25.9
10/01/04	1,236	1,590	28.7	43.12	43.18	0.1	19:00	19:21	1.8	0.8	- 28.9

Note: Obs. = Observed; Sim. = Simulated; RPD = Relative Percentage Different; NSEC = Nash-Sutcliffe Efficiency Coefficient; PBIAS = Percent BIAS

4.3.3 Large watershed

The hydrologic parameters of the model were calibrated to fit the observed daily flow data from DID flow gage stations (Figure 4.3b) at the large watershed during 2010. This year was chosen because it is recent and a good representation of the current climate and land use. These flow gages were used to calibrate and validate the hydrologic parameters at the upstream part of the watershed. The stage data were also used to validate hydrologic parameters at the downstream for flood in December 2006 and January 2007. These data were obtained from Shafie (2009).

The storm event on November 23 – December 4, 2010 was used to calibrate the model (Figure 4.13). The hydrograph indicates that the model performance is very good in estimating the peak discharge and time to peak during this storm event. There were several river tributaries located near station 1836402, which give different travel time and therefore causes the discrepancies of peak discharge. The calibrated model parameters were then applied independently to several other rainfall events for validation purposes. Storm events in December 2006, January 2007 and 2010 were used in the validation process. The comparisons between observed and simulated graph discharges and stage for these events are presented in Figures 4.14 and 4.15, respectively.

Graphical method

Longer simulations were done, i.e., 14 days, as compared to small and medium watersheds (i.e., two days) because the large watershed's flow requires longer travel time from upstream to downstream. As a result, more time is required to reach the peak of the hydrograph. This is important because the assumption is that for large watersheds, the time to peak and peak

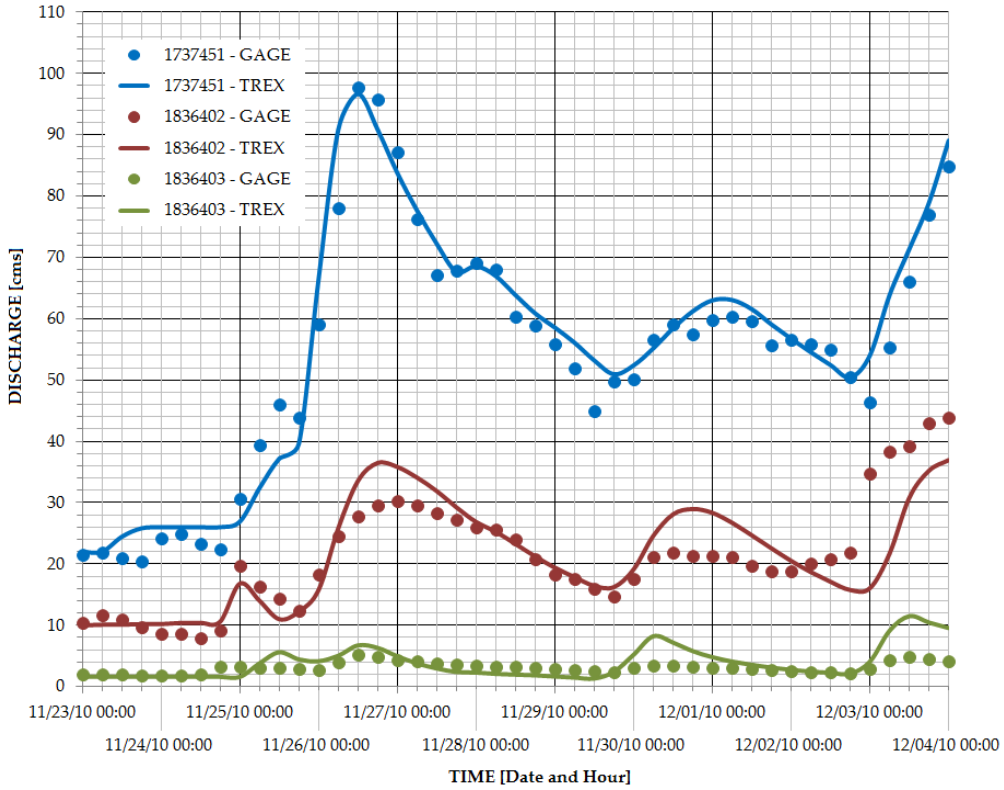

Figure 4.13 Hydrologic calibrations for the large watershed

discharge can be reached within few days after the rainfall events. Graphical results during calibration and validation are shown in Figure 4.13 (validation using discharge data) and Figures 4.14 and 4.15 (validation using flood stage in December 2006 and January 2007). The model shows good and very good performance in estimating peak discharge and peak stage, respectively, during these processes. The model did very well in estimating the rising and falling limb of the hydrograph (Figures 4.13 and 4.14) and stage (Figure 4.15).

Figures 4.16 and 4.17 show the observed and simulated values are plotted for peak discharge and time to peak, respectively. The simulated peak discharge values (Figure 4.16) are very well distributed along the 1:1 line. However, 35% of the simulated data show that there was a 6-hour delay in estimating the time to peak (Figure 4.17).

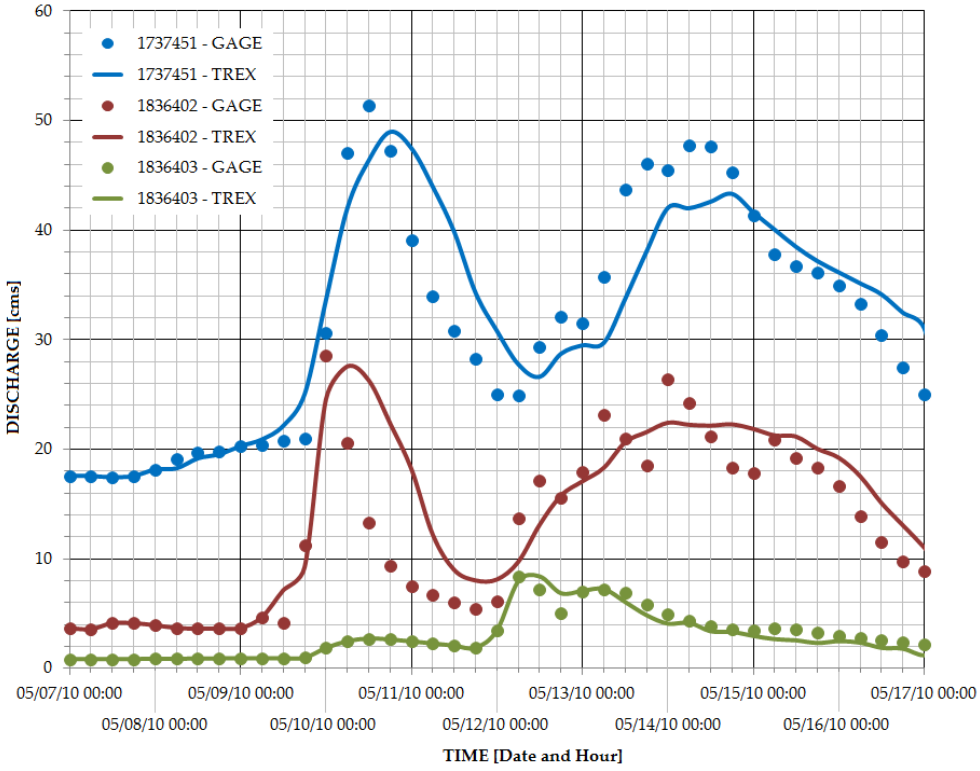

Figure 4.14 Hydrologic validations for the large watershed using discharge

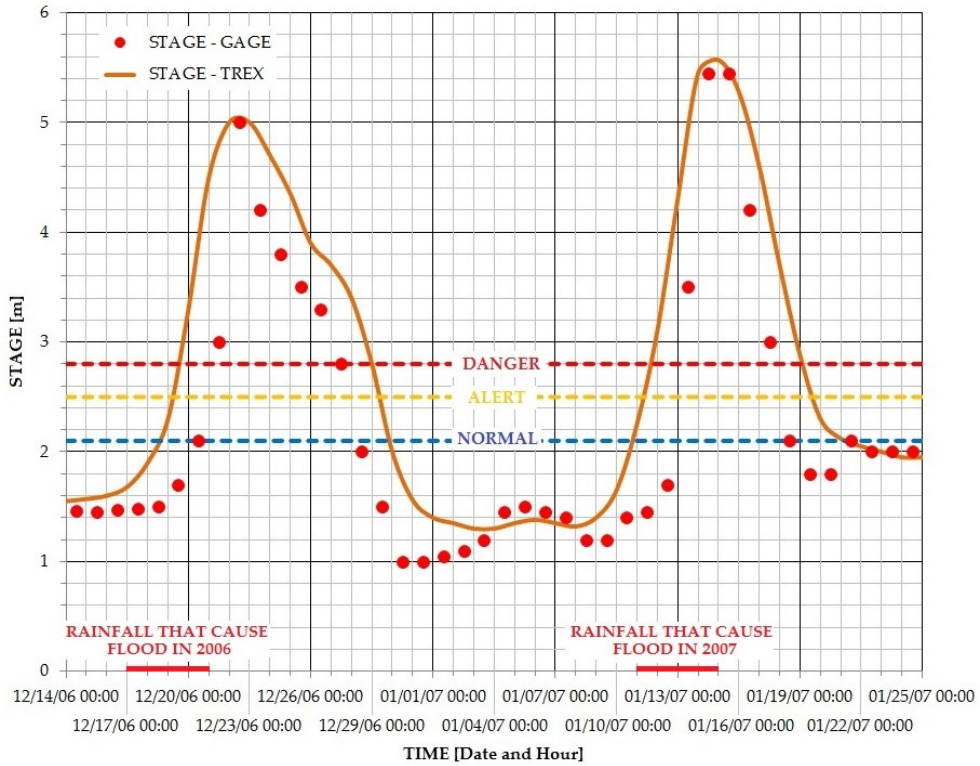

Figure 4.15 Hydrologic validations for the large watershed using stage

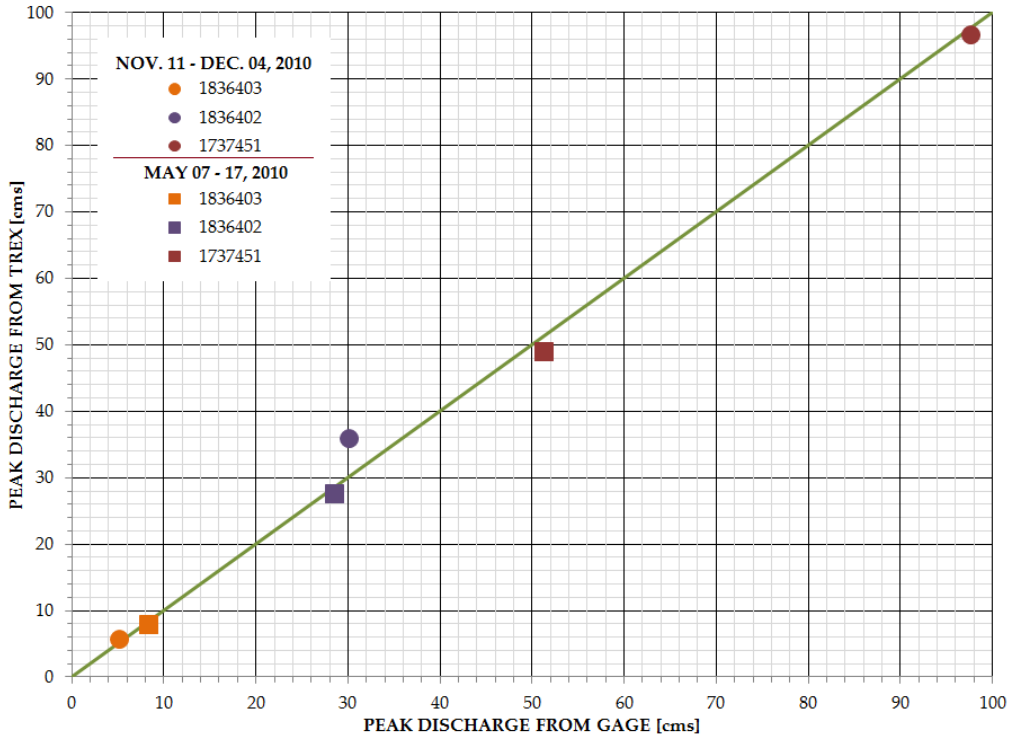

Figure 4.16 Peak discharge for the model calibration and validation event at large watershed (Kota Tinggi)

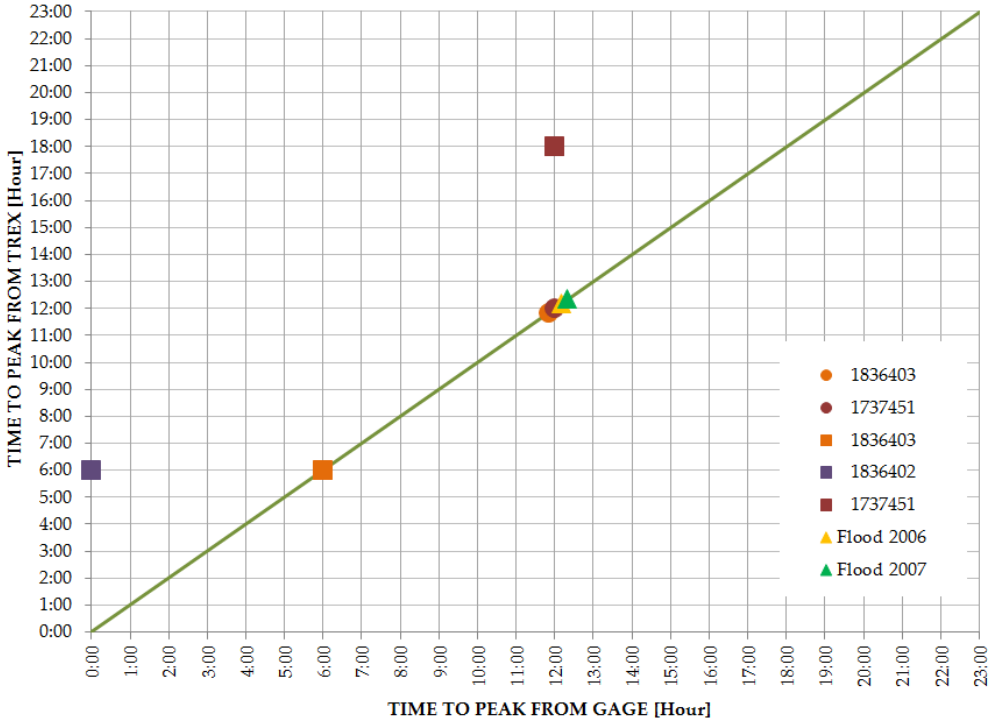

Figure 4.17 Time to peak for the model calibration and validation event at large watershed (Kota Tinggi)

Statistical methods

Equations 2.2, 2.3 and 2.4 as described in sections 2.8.1, 2.8.2 and 2.8.3 were used to calculate the accuracy of the model's performance. These equations are referred to as the statistical methods RPD, PBIAS and NSEC, respectively. Table 4.5 shows the calculated values using these equations. The classifications of the model performance are rated as shown in Table 4.2. During the calibration storm event (i.e., November 11 – December 4, 2010), on average, the RPD values indicated that the model performance is very good in estimating the peak flow (9.7%), time to peak (8%) and total volume (0.6%). The NSEC (0.8) and PBIAS (overestimated by 0.6%) values suggest that the model was very good in estimating hourly flow and volume. The model was validated using storm event on May 7 -17, 2010 and flood in December 2006 and January 2007. The first statistical method, RPD, shows *very good* agreement between observed and simulated total volume and peak flow. The RPD value shows that the total volume and peak discharge is underestimated by about 1.5% and overestimated by about 2.7%, respectively. However, the model was classified as *good* in estimating the time to peak with an average RPD value of about 9.3% (about 3 hours delay on average). The difference of the maximum stage between observed and simulated was used, instead of discharge and volume as storm events in Nov. 11 – Dec. 4, 2010 and May 7 – 17, 2010 in validation purpose. These stage data were obtained from Shafie (2009) for flooding in 2006 and 2007. The RPD value indicated that the model performed *very good* in estimating the maximum stage and time to reach maximum stage. The NSEC and PBIAS methods were used to define the performance of the TREX model for both peak discharge and total volume, respectively. Both methods indicated that the model is *very good* in estimating the peak discharge and total volume, with average overestimation of about 0.8 and 1.5%, respectively.

Table 4.5 Summary of the evaluation of hydrologic model performance for the large watershed (Kota Tinggi)

CALIBRATION											
Date of Event	**Total volume (x 1,000 m^3)**			**Peak flow (cms)**			**Time to peak (24 hours)**			**Model's performance**	
Station	**Obs.**	**Sim.**	**RPD**	**Obs.**	**Sim.**	**RPD**	**Obs.**	**Sim.**	**RPD**	**NSEC**	**PBIAS**
11/11/10 – 12/04/10											
1836403	2,947	2,944	-0.1	5.14	5.73	11.5	12:00	12:00	0.0	0.8	0.1
1836402	20,179	19,954	-1.1	30.18	30.18	18.7	00:00	18:00	25.0	0.6	1.1
1737451	51,411	52,900	2.9	97.68	97.67	-1.0	12:00	12:00	0.0	1.0	-2.9
VALIDATION											
05/07/10 – 05/17/10											
1836403	2,798	2,634	-5.9	8.34	7.94	-4.8	06:00	06:00	0.0	0.9	5.9
1836402	11,602	13,010	12.1	28.56	27.56	-3.5	00:00	06:00	25.0	0.9	-12.1
1737451	29,463	29,806	1.2	51.36	48.96	-4.7	12:00	18:00	25.0	1.0	-1.2
	Total volume (x 1,000 m^3)			**Maximum stage (m)**			**Time to become Maximum stage (24 hours)**			**Model's performance**	
	Obs.	**Sim.**	**RPD**	**Obs.**	**Sim.**	**RPD**	**Obs.**	**Sim.**	**RPD**	**NSEC**	**PBIAS**
Flood in Dec. 2006	---	---	---	5.0	5.0	0.0	12:00	12:00	0.0	0.5	---
Flood in Jan. 2007	---	---	---	5.45	5.57	2.2	12:00	12:00	0.0	0.7	---

Note: Obs. = Observed; Sim. = Simulated; RPD = Relative Percentage Different; NSEC = Nash-Sutcliffe Efficiency Coefficient; PBIAS = Percent BIAS

There are several factors that contributed on the discrepancies of the volume between simulated and observed data. In this study, the hydrologic and hydraulic parameters are the main causes of discrepancies. For the large watershed, the subsurface flow is one of the main contributions to the total discharge at the main outlet, as compared to the small and medium watersheds. TREX model does not take into account the subsurface flow; which contributed to the discrepancies of the water volume. However, in this study, the volume was assumed to be less significant as compared to the peak discharge and time to peak. Other than these parameters, grid size also contributed to the discrepancies of the volume. But because of the time and computational constrains, the grid sizes of 90 m and 230 m are assumed to be best for small and medium, and large watersheds

SUMMARY

The calibration and validation of the hydrologic parameters on small, medium and large watersheds were shown and discussed. A series of sensitivity analysis experiments were performed to determine the most sensitive hydrologic parameters (Appendix B). Hydraulics conductivity K_h and Manning's n (Table 4.1) were the parameters calibrated and validated. Two methods: graphical and statistical, were used in assessing the performance of the TREX model. The graphical method is the simplest overview by making the comparison between observed and simulated results of peak discharge, time to peak and rising and falling limb. The 45 degrees line (1:1 line) was introduced to indicate that observed and simulated values for peak discharge and time to peak were accurately estimated by the model. The graphical method shows that the model performed *good* for the small watershed and *very good* at the medium and large watersheds. Statistical methods: RPD, NSEC and PBIAS were used, as suggested by many

researchers, to give more assurance on the model's performance. The RPD method was used to evaluate the total volume (volume under the hydrograph), peak discharge and time to peak. The NSEC and PBIAS methods were used to evaluate the peak discharge and total volume (hourly), respectively. Table 4.6 shows the classification summary for the graphical and statistical methods on small, medium and large watersheds.

Table 4.6 Summary of the TREX model evaluation performance using graphical and statistical methods on small, medium and large watersheds

METHODS	**WATERSHED**		
	SMALL (Lui)	**MEDIUM (Semenyih)**	**LARGE (Kota Tinggi)**
GRAPHICAL METHOD	Good	Very good	Very Good
	STATISTICAL METHOD		
RPD	Very good (- 6.9)	Good (+ 13.5)	Very good (+ 3.7)
PBIAS	Underestimate volume (14%)	Overestimate volume (28%)	Overestimate volume (1.5%)
NSEC	Satisfactory (0.4)	Good (0.7)	Very good (0.8)
OVERALL	**GOOD**	**VERY GOOD**	**VERY GOOD**

Note: RPD = Relative Percentage Difference; PBIAS = Percent BIAS; NSEC = Nash-Sutcliffe Efficiency Coefficient

CHAPTER FIVE

SIMULATION OF LARGE AND EXTREME RAINFALL EVENTS

The model parameters, i.e., hydraulic conductivity and roughness (channel bed and overland), were calibrated and validated for small, medium and large watersheds. The TREX model performance is good (on a small watershed) and very good (on a medium and large watershed) as discussed in Chapter 4. The results of the simulations for large and extreme rainfall events at small, medium and large watersheds are presented in this chapter. These rainfall events are discussed separately in sections 5.1 and 5.2, respectively. Each section covers the three watershed sizes. The discussion will be aided by 3D graphic visualization of spatial and temporal distribution of water depth overland and in the channel. The main concern of this chapter is the evaluation of spatial and temporal distribution of runoff and flooding areas in the form of water depths for a return period of 100-years, Selangor PMP (S-PMP), Kota Tinggi PMP (KT-PMP) and the world's largest rainfall events. Section 5.3 contains a discussion of the relationship between rainfall duration, peak specific-discharge and watershed area.

5.1 SIMULATION OF THE LARGE RAINFALL EVENTS

Rainfall data in Tables 2.2 (for the small and medium watersheds) and 2.3 (for the large watershed) were used to simulate large rainfall events. The duration of rainfall for return periods is between 1 and 16 hours for the small and medium watersheds. However, for the large watershed, the rainfall durations have been extended up to seven days.

S-PMP rainfall data, which were applied at the small and medium watersheds, are limited to 1, 3, 6, and 12 hour durations (Table 2.6). The peak discharge for each simulated large event

was plotted and tabulated. The Normal Discharge (ND), Alert Discharge (AD) and Danger Discharge (DD) zones were plotted in each graph also. These values were obtained from the Department of Irrigation and Drainage (DID) website.

Small watershed (Lui)

Figure 5.1 is a semi-log graph that shows the Maximum Estimated Discharge (MED) at specific rainfall duration (every hour) for each large event. These values were estimated by the TREX model at the downstream end of the main channel. This graph was plotted from tabulated data in Table A1. The ND, AD and DD zones obtained from DID are 6.5, 16.6 and 47.9 cms, respectively. These zones can be translated into water depth (meter) in the main channel at the downstream end (station 3118445) as ND < 1.72 m, 1.72 m ≤ AD ≤ 2.72 m, and DD > 2.72 m, respectively. The simulation period for these extreme events was 48 hours.

Other than the 2- and 5-year return period events, the MED of the large events were estimated to be bigger than the DD zone. These MEDs values were reached when the duration of the events was between 2 and 5 hours. The MED value for a 100-year return period is 91 cms at a rainfall intensity of 38 mm/hr for four hours total rainfall depth of 152 mm. Even though all the MED value during this event (100-year) is above the DD zone, the 3D visualization shows that there is no flooding in the valley, except in the main channel (Figure 5.2). The 91 cms of the MED value is visualized in the form of water depths, as shown in Figure 5.2c.

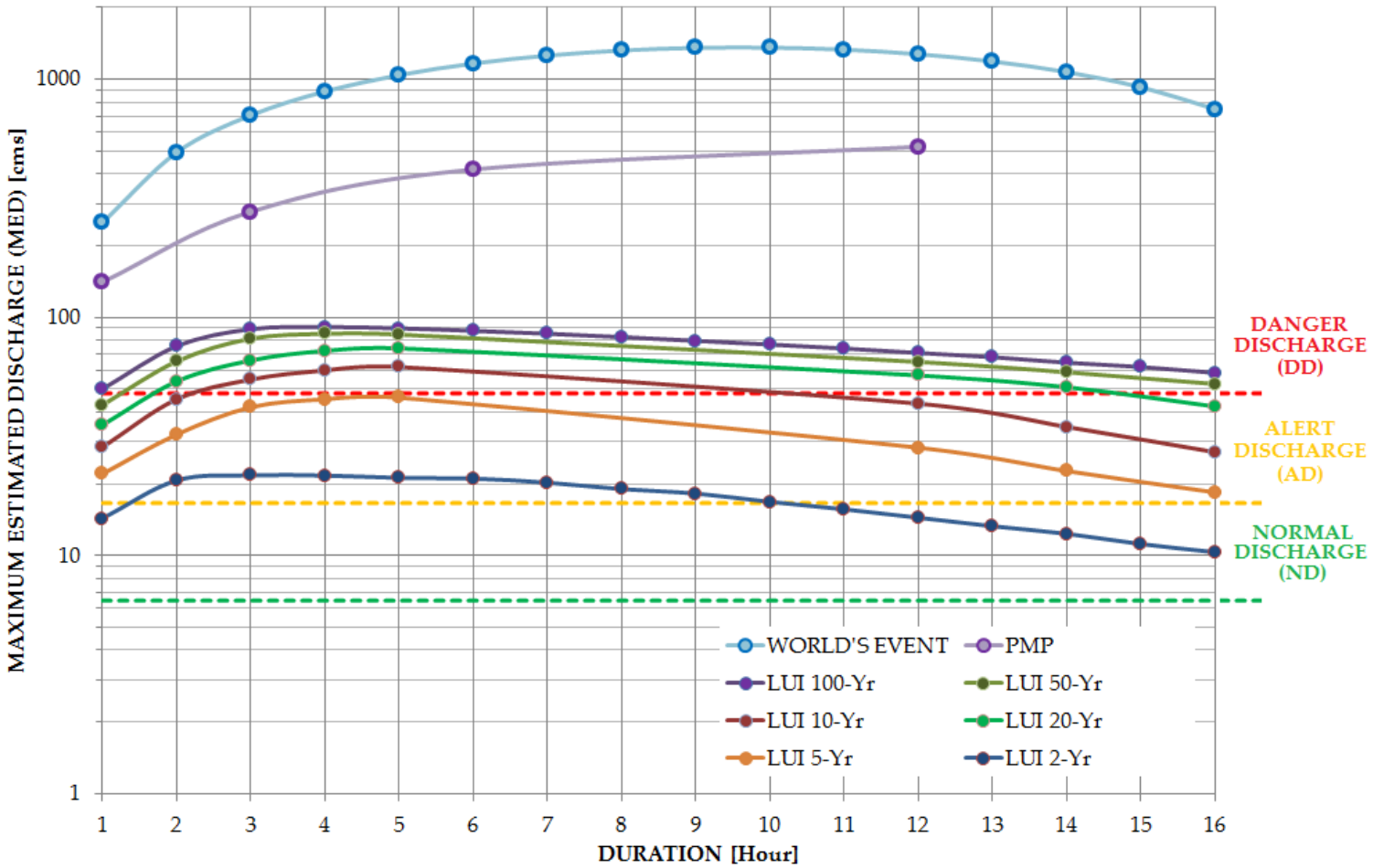

Figure 5.1 Maximum estimated discharges (MED) for the small watershed (Lui)

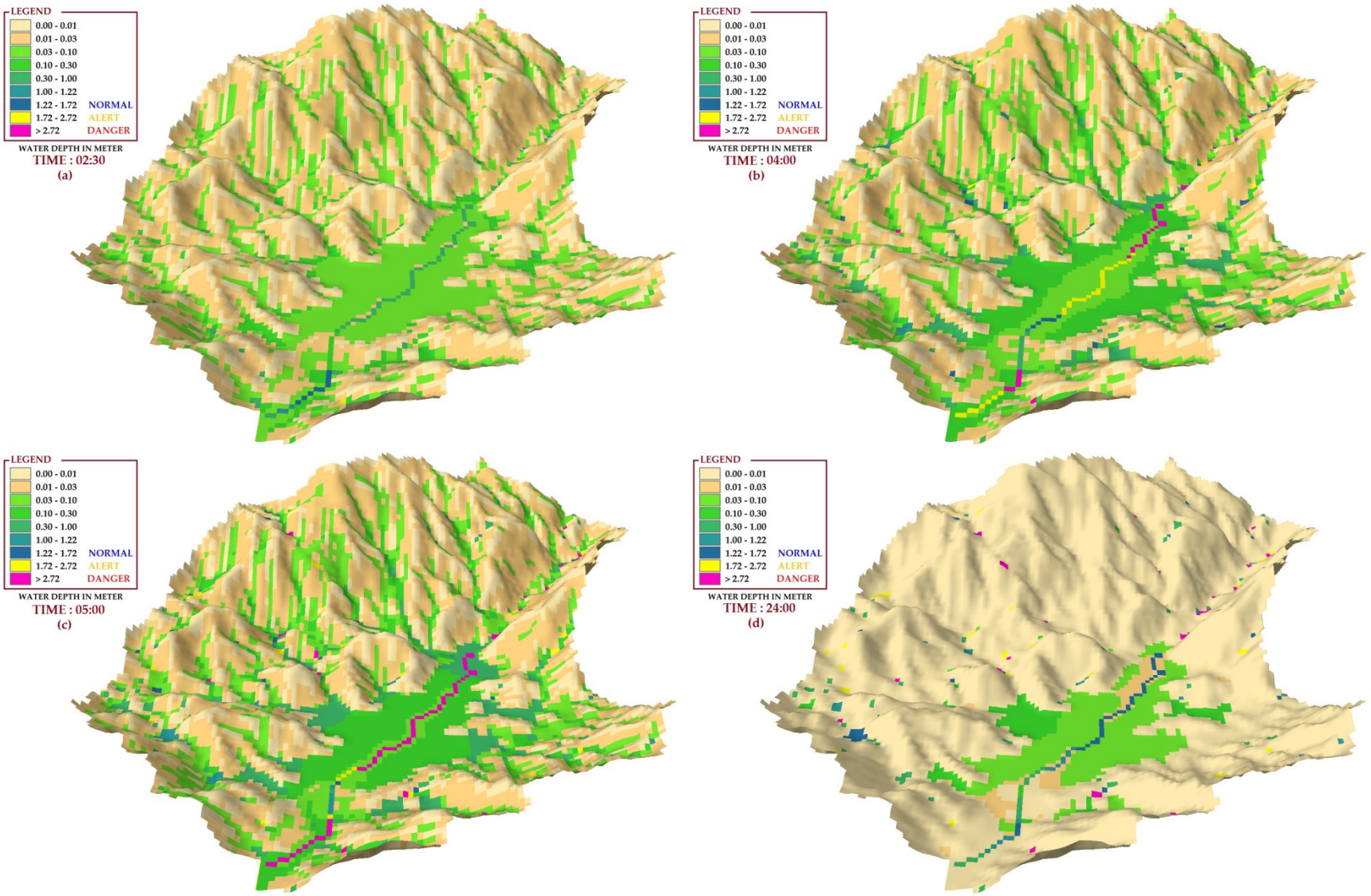

Figure 5.2 Three-dimensional visualizations for a 100-year return period event for the small watershed (Lui)

Medium watershed (Semenyih)

The MED values during large and extreme events at the medium watershed were plotted in semi-log graph as shown in Figure 5.3. The discharges were measured at the downstream-end of this watershed. The results are summarized in Table A2. The ND, AD and DD zones obtained from DID are 22, 96 and 195 cms, respectively. These zones (ND, AD and DD) can be translated into water depth in meters as ND $\leq$ 4.49 m, 4.49 m $<$ AD $\leq$ 6.09 m, and DD $>$ 6.09 m, respectively. All MED values are simulated within 48 hours of the beginning of rainfall.

All large rainfall events exceeded the DD zone except for the two and five year period, as shown in Figure 5.3. The highest MED values for two, five, and ten year return period events were estimated at five hours of rainfall duration with rainfall intensity of 18, 22 and 25 mm/hr, respectively. The MED values of these events are 147, 164 and 206 cms, respectively. However, for 20, 50 and 100-year return period event, the highest MED values were estimated at 12 hours of rainfall duration. Among these events, the highest MED value is 256 cms, which was estimated during a 100-year return period event. The water depth across the watershed for this event was visualized in 3D as shown in Figure 5.4. Figure 5.4a is the scenario at the beginning of the event. Figures 5.4b and 5.4d are the water depths at the rising (water start to accumulate in the main channel) and falling (water start to leave the main channel) limb, as shown in Figure A2 (in Appendix A). The MED value of 256 cms is shown in Figure 5.4c, which is the peak of the hydrograph for a 100-year return period event as shown in Figure A2 (blue line). The valley areas are safe from flood except in the main channel. Approximately 13% and 42% of the main channel was estimated to be in the AD and DD zone, respectively. The remainder of the main channel was in the ND zone.

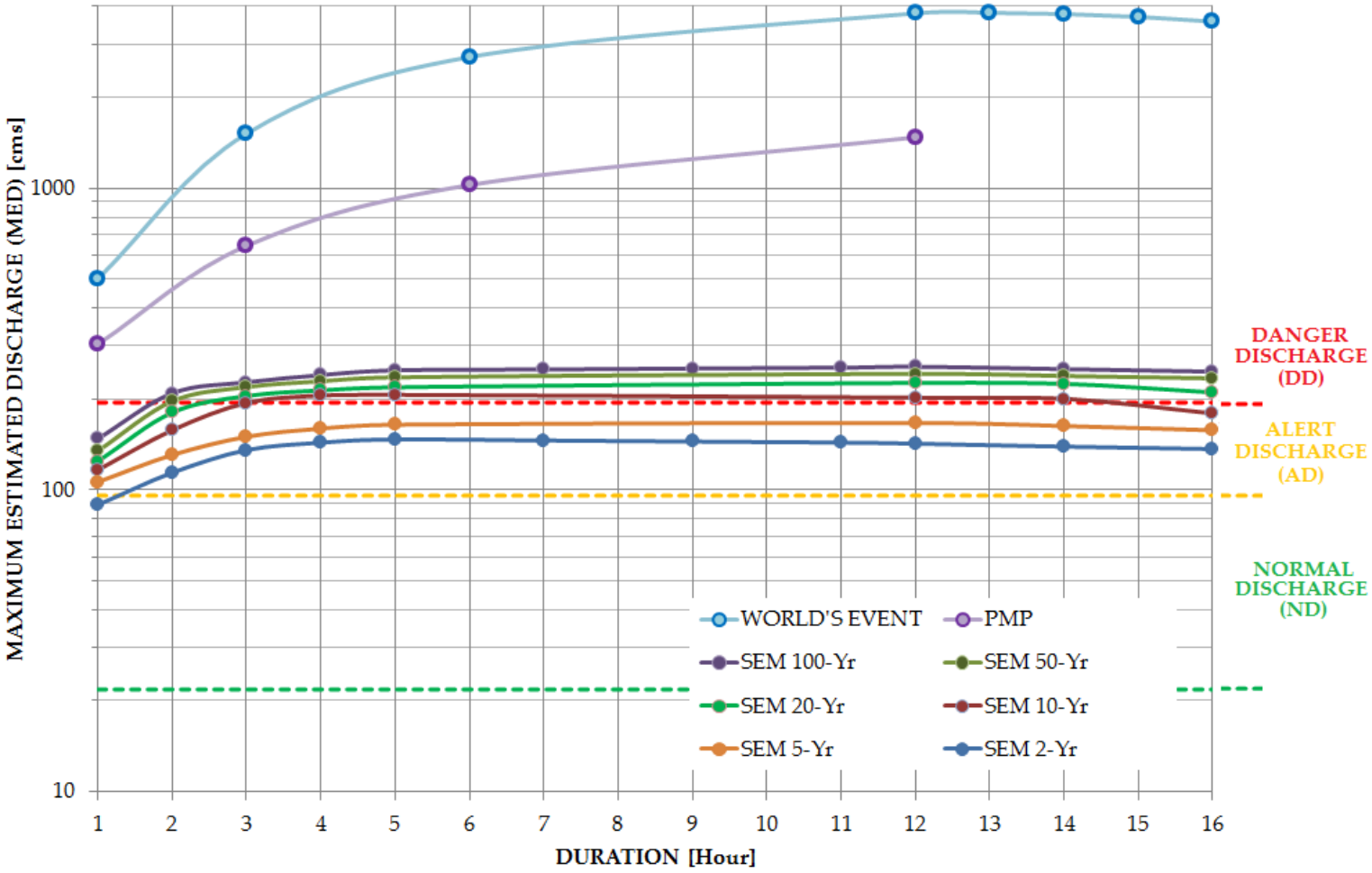

Figure 5.3 Maximum estimated discharge (MED) for the medium watershed (Semenyih)

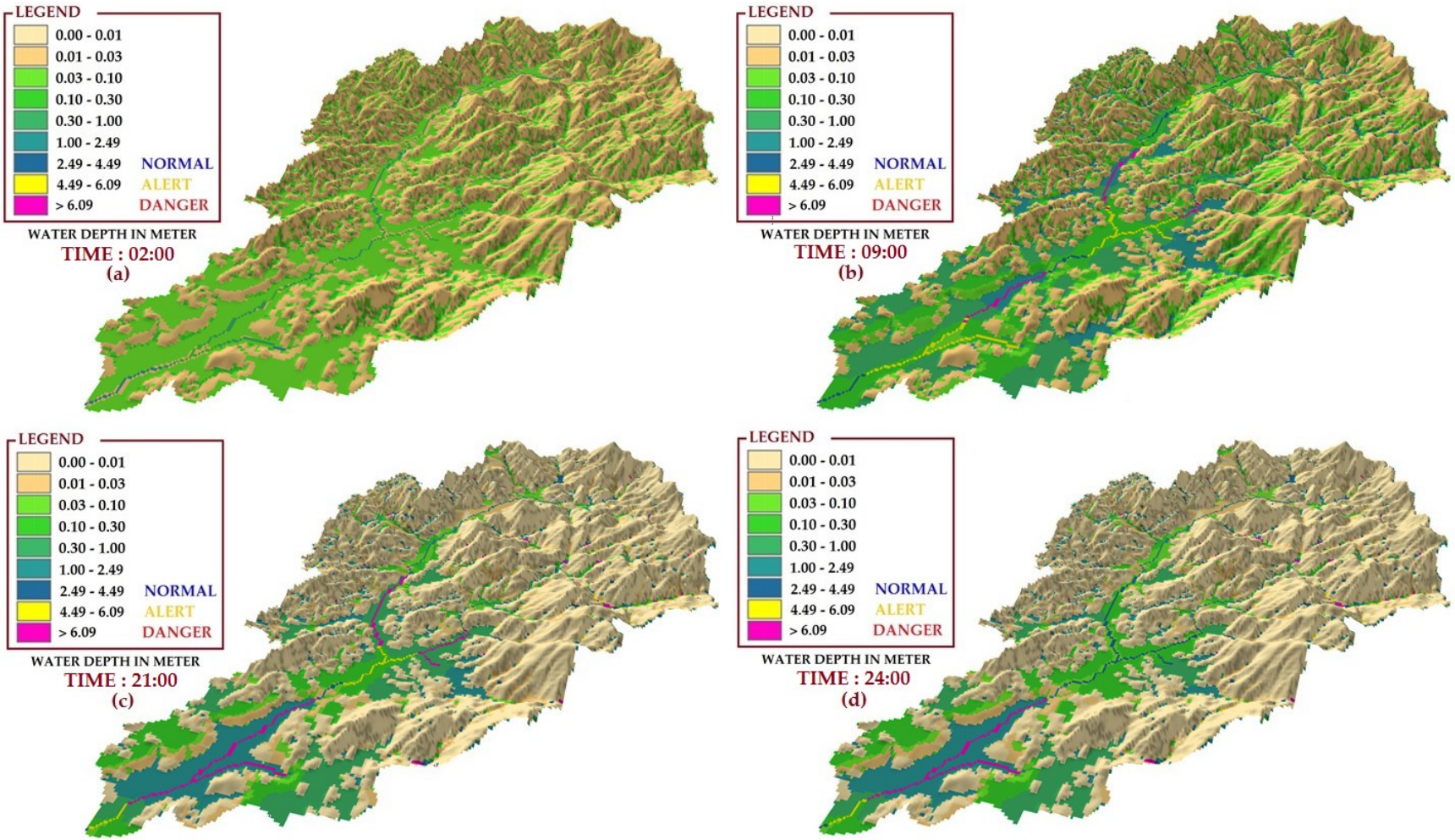

Figure 5.4 Three-dimensional visualizations for a 100-year return period rainfall event for the medium watershed (Semenyih)

Large watershed (Kota Tinggi)

Figure 5.5 shows the MED at the large watershed. Unfortunately, flow gage and stage data were unavailable at the main outlet in this watershed. However, there are three flow gages (which located at the upstream of the large watershed) that have been calibrated and validated as discussed in Chapter 4. The simulated discharge by the model at the main outlet is assumed to be very good. According to DID website, the normal, alert and danger stages are 2.1, 2.5 and 2.8 m, respectively.

Figure 5.6 shows the water depth distribution across the watershed for 7 days of rainfall duration and 7.6 mm/hr of rainfall intensity. The maximum estimated stage value for this event is 5.2 m. The snapshots of this event at the rising limb, peak stage and the falling limb are shown in Figures 5.6a - 5.6c, respectively. Figure 5.6a shows that the water depth in the main channel reached the DS line (i.e., 2.8 m) after 60 hours of rainfall. There are few areas where overtopping occurs (refer to Figure 5.6a), which were identified as low-land areas. The drastic change in slope, i.e., from high to low land areas, affected the velocity of flow. When the rainfall duration of a 100-year event increased up to seven days, all floodplain areas along the channel were flooding (Figure 5.6b). The topography of these areas consists of small valleys that are likely to be flooded. Longer times (i.e., more than 14 days) are needed to drain-out the flood because of the large size of the watershed, as shown in Figure 5.6c. A large-sized watershed requires more time to be drained compared to small and medium watersheds. Having several tributaries with different bed slopes also contributed to this cause. Therefore, the hydrograph's rising limb did not increase as rapidly as at the small and medium watersheds.

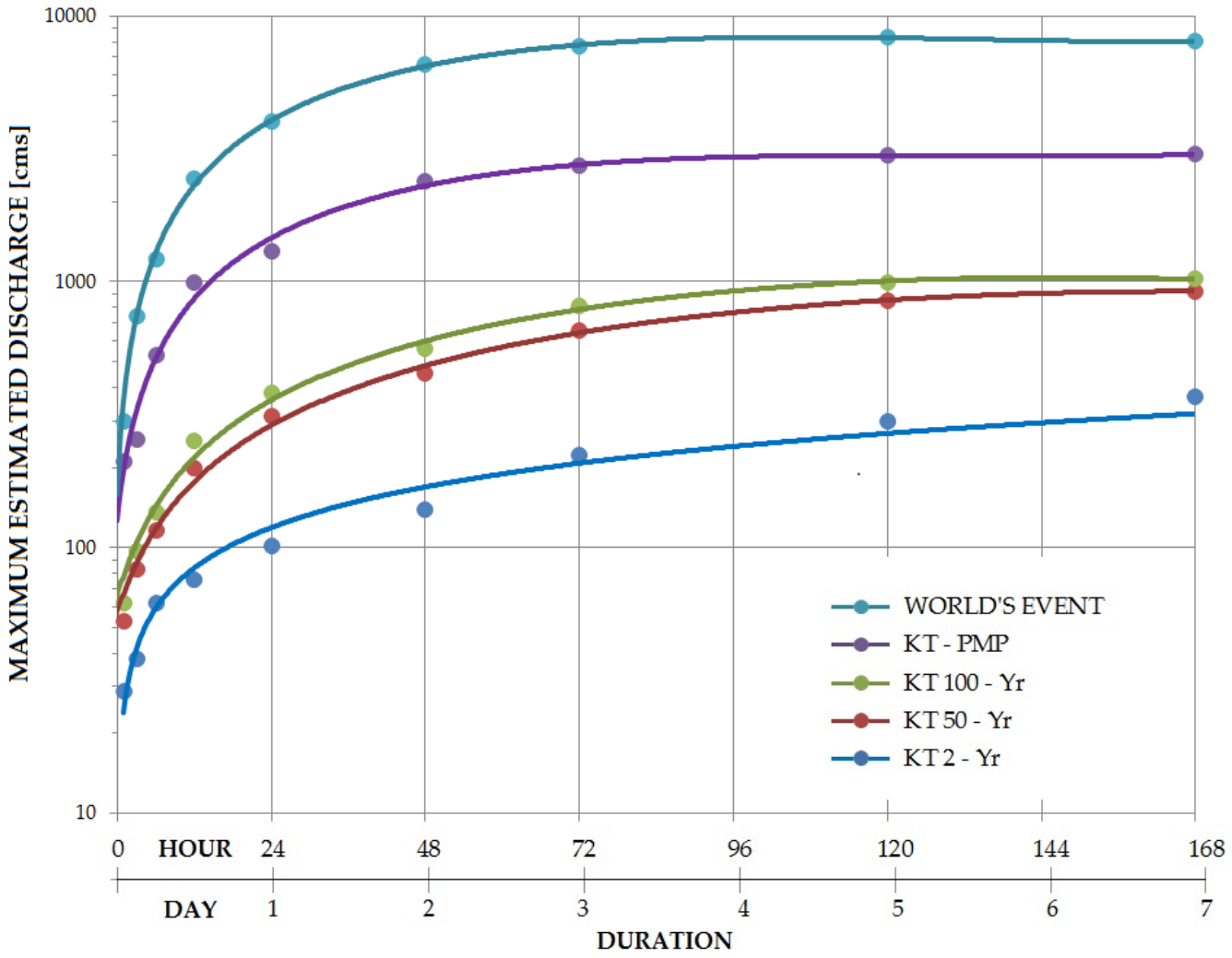

Figure 5.5 Maximum estimated discharge (MED) for the large watershed (Kota Tinggi)

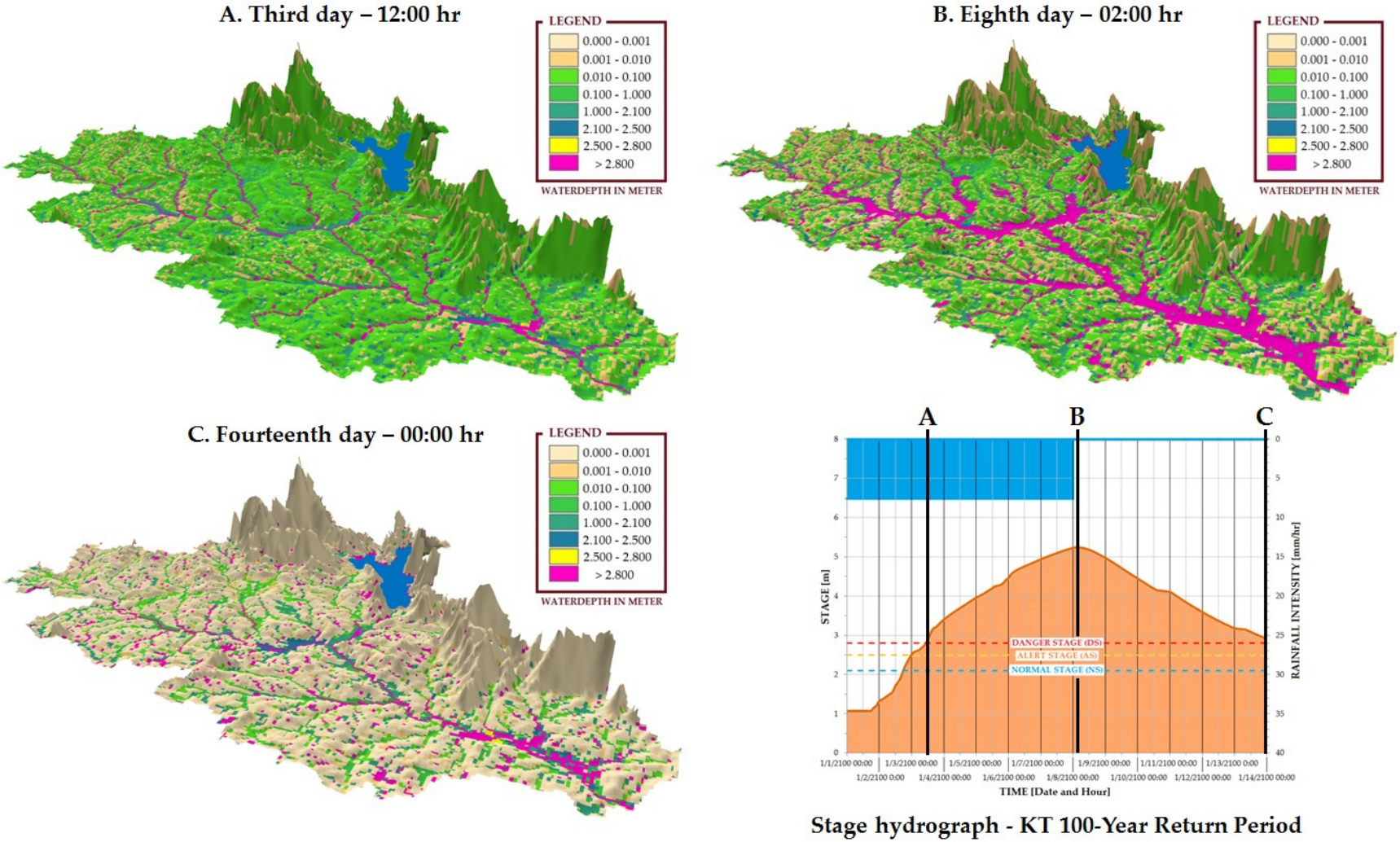

Figure 5.6 Three-dimensional visualizations for a 100-year return period rainfall event for the large watershed (Kota Tinggi)

5.2 SIMULATION OF THE EXTREME RAINFALL EVENTS

The simulation of the extreme event included the PMP and the world's largest recorded rainfall event, as tabulated and plotted in section 2.5.2. Temporal and spatial distribution of water depth at the three different size watersheds is the main concern in this section. In this section, the Maximum Estimated Discharge (MED) is used for small and medium watersheds, whereas the Maximum Estimated Stage (MES) is used for the large watershed.

Small watershed (Lui)

Different trends were observed for the S-PMP events. The simulated S-PMP events showed increasing MED values from 141 cms to 520 cms (Figure 5.1). These values were estimated at rainfall duration between one to 12-hours. The highest MED value for the S-PMP events was 520 cms at 12-hours rainfall duration with an intensity of 43 mm/hr. Figure 5.7 shows the water depth across the watershed for this event. Figure 5.7a shows the water depth across the watershed after one hour of S-PMP event. Figures 5.7b and 5.7d are water depth of the watershed at the rising and falling limb of hydrograph, respectively (Figure A1 – red line). The MED of 520 cms is visualized in Figure 5.7c. The valleys are prone to flooding by 18% and 6% of the AD and DD zone, respectively. The upstream and downstream of the channel were flooding within the AD zone.

The world's largest rainfall events were simulated using various rainfall intensity and duration ranging from one to 16 hours. The trends of the MED values for the world's largest events are shown in Figure 5.1. The simulated MED increased from 250 to 1,100 cms for rainfall durations of one to seven hours. Then, the trends remain stable at approximately 1,300 cms up to eleven hours of rainfall duration before decreasing to 750 cms (Figure 5.1). The highest MED

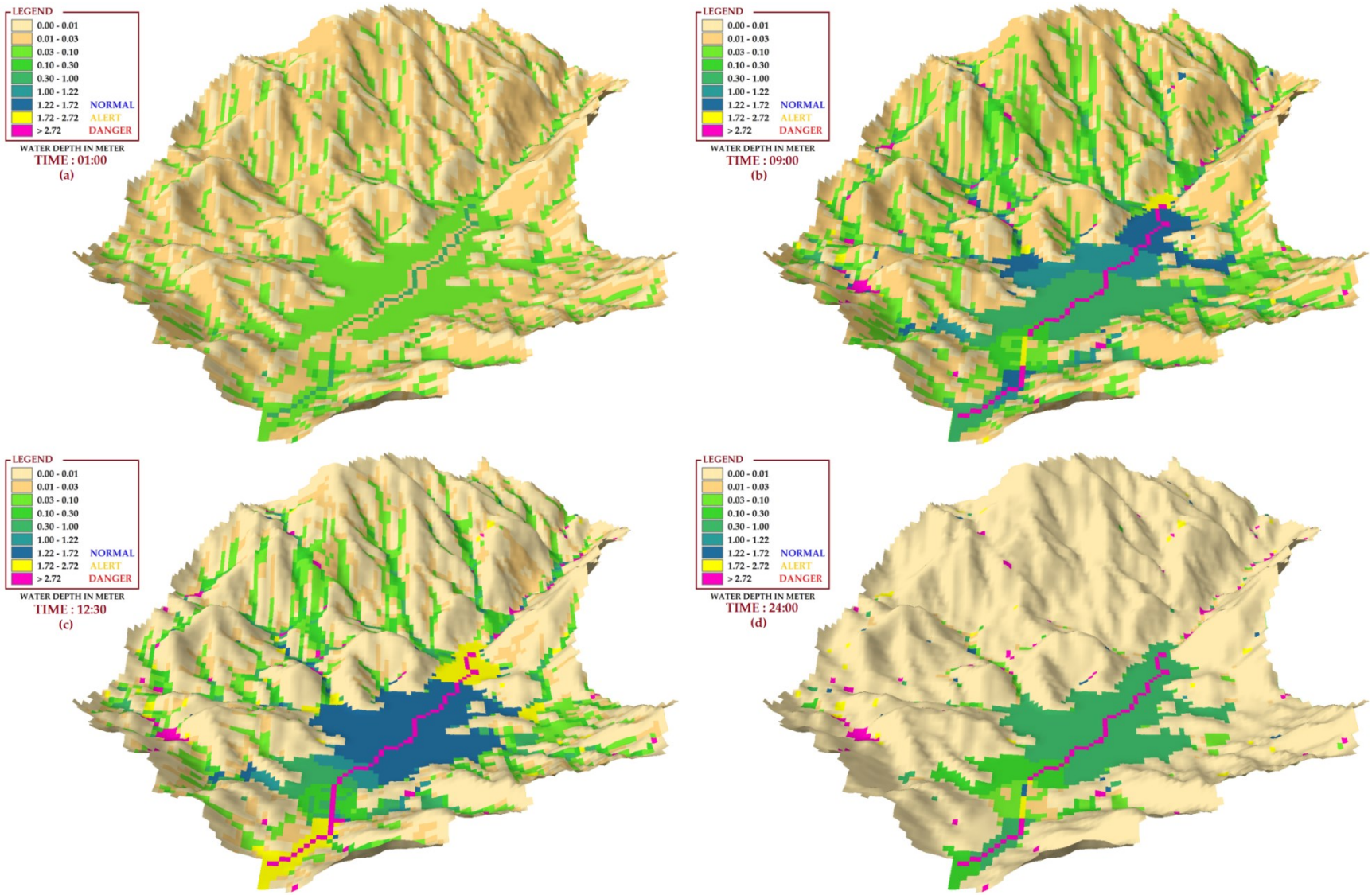

Figure 5.7 Three-dimensional visualizations using S-PMP rainfall event for the small watershed (Lui)

value for this event was 1,358 cms, which was estimated after ten hours of rain with an intensity of 86 mm/hr.

The temporal and spatial distribution of water depths for this event was visualized in 3D, as shown in Figure 5.8. One hour after the rainfall event, the watershed was covered with water at depths between 0.1 m to 0.3 m (Figure 5.8a). The valley was covered by 50% of water at more than 1.72 m (AD zone) approximately six hours after the rainfall event (Figure 5.8b). After eleven hours, about 83% of the valley was covered with more than 1.72 m of water (Figure 5.8c). The downstream of the watershed was fully flooded due to the decreasing valley width (see Figure 4.4a).

Medium watershed (Semenyih)

During the S-PMP events, the MED values increased as the rainfall duration increased (Figure 5.3). The highest MED value during this event was 1,474 cms, with an intensity of 43 mm/hr and 12 hours of rainfall duration (Table A2). Figure 5.9 shows the water depth across the watershed for this event. Figures 5.9a, 5.9b, and 5.9d show the water depths at the beginning and at the rising and falling limbs of the S-PMP event. The water depths for the peak discharge are shown in Figure 5.9c. Looking at the 3D visualization, the valleys appear safe from water depths of more than 4.49 m (AD zone). However, water depth was observed to be more than 6.09 m (approximately 4%) in the mountain area. Approximately 80% of the main channel had water depths of more than 4.49 m (AD zone). If the rainfall intensity or duration is increased, the valleys are even more likely to be in AD zone.

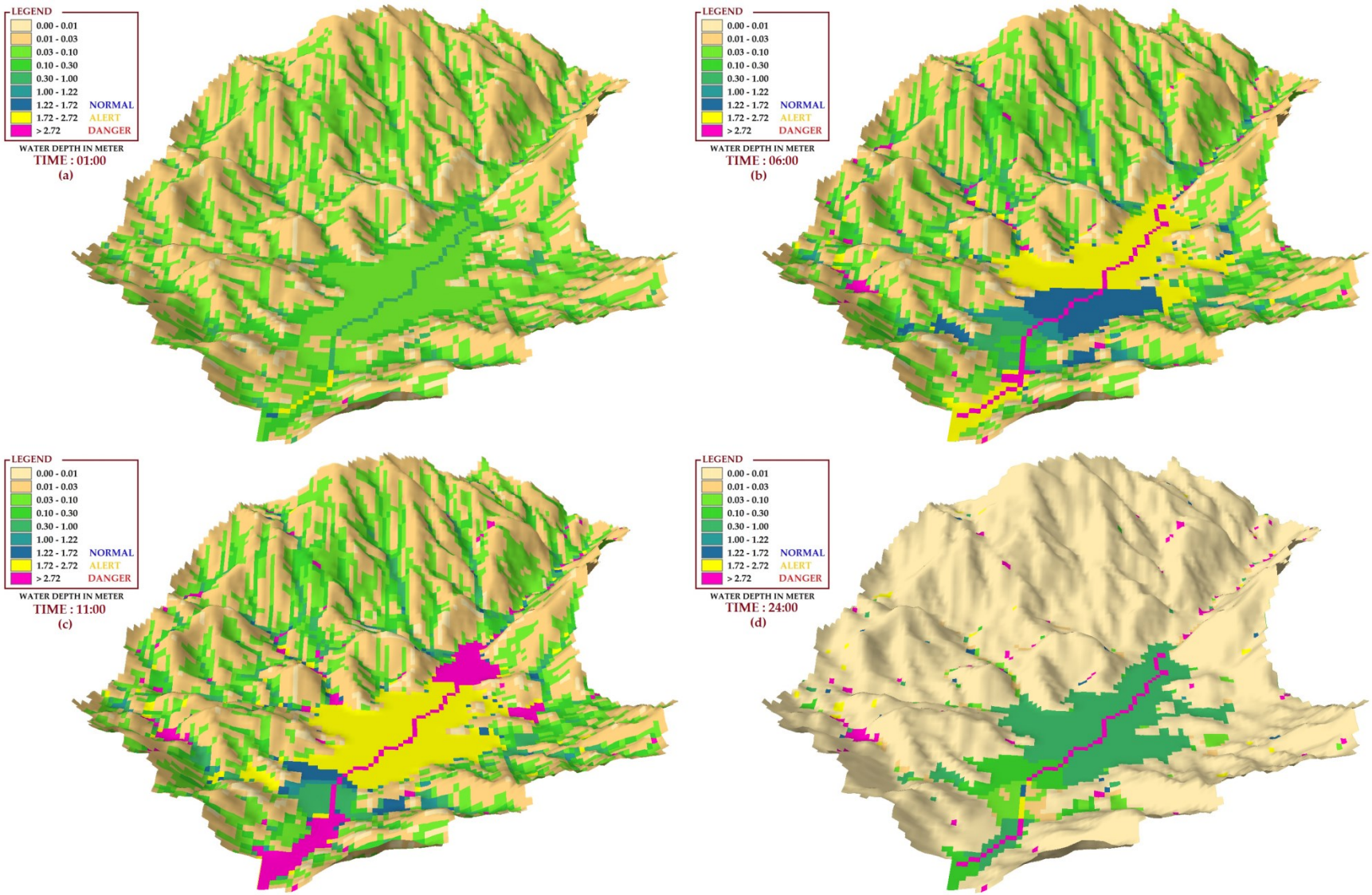

Figure 5.8 Three-dimensional visualizations using the world's largest rainfall event for the small watershed (Lui)

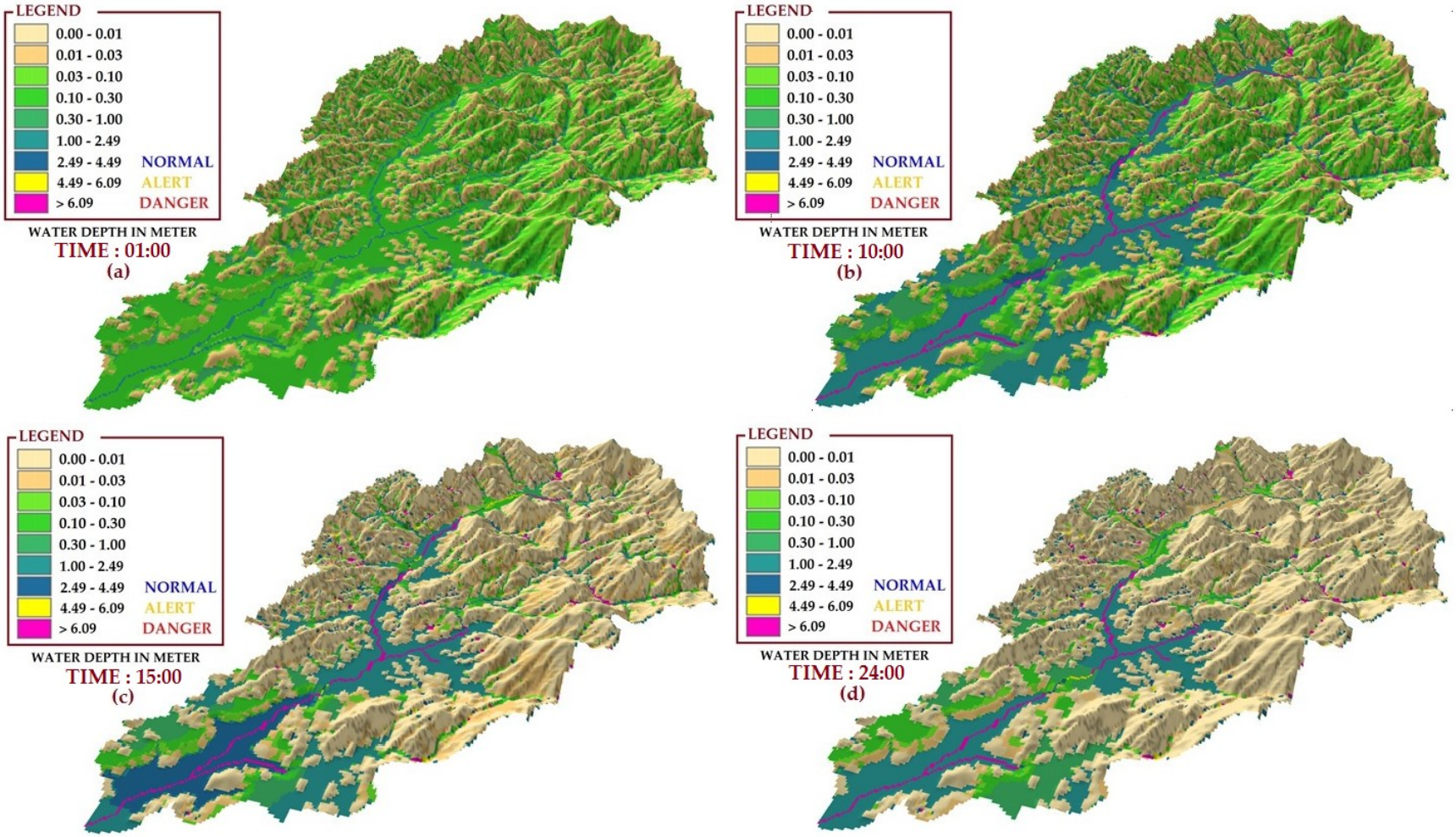

Figure 5.9 Three-dimensional visualizations using S-PMP rainfall event for the medium watershed (Semenyih)

The total rainfalls during the world's largest events are approximately 50% increased from the S-PMP events (Table A2). As a result, the MED values during the world's largest events will be greater than S-PMP events as well. Simulations where rainfall intensity was decreased and rainfall duration was increased showed that MED increased until 12 hours of rainfall. After that, the MED decreased. The highest MED value for the world's largest event was estimated at 3,793 cms, with duration of rainfall at 12 hours and rainfall intensity is 78 mm/hr. The water depth for this event is visualized in Figure 5.10. The runoff starts to raise the water depth from ND to AD at the upstream of the valleys after approximately 10 hours with 78 mm/hr of rainfall intensity (Figure 5.10b). Then it starts to spread out downstream in the valleys, as shown in Figure 5.10c. The percentage of water depth in AD and DD zone is 83% and 16%, respectively. The distribution of water depth of 4.49 m (AD zone) from upstream to downstream of the valleys is very fast, approximately four to five hours. The soil type and land use at the valley area are the main contributions for this condition, other than high rainfall intensity. From Figure 4.5, most of the valley is covered by impervious surface (i.e., urbanization) and far-downstream the soil type is clay. Therefore, infiltration was very small and the soil which becomes fully saturated very fast.

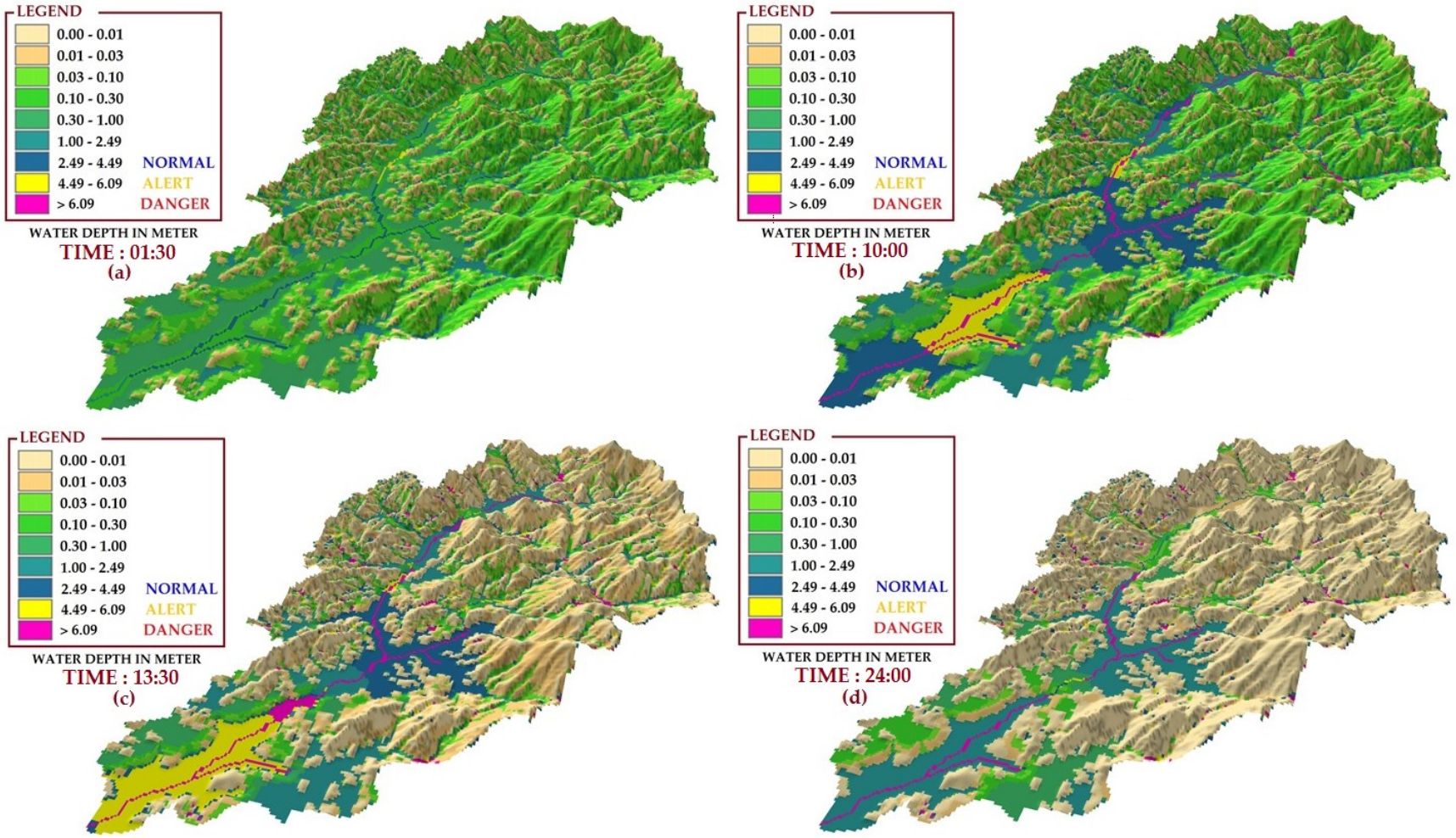

Figure 5.10 Three-dimensional visualizations using the world's largest rainfall event for the medium watershed (Semenyih)

Large watershed (Kota Tinggi)

The rainfall duration and intensity for the extreme event at the large watershed are shown in Table 2.6. The maximum estimated stage (MES) for this event was estimated with rainfall durations of seven and five days for KT-PMP and the world's largest event, respectively. To make an easier comparison between large and extreme events, the seven days of rainfall duration for world's largest event is considered. The seven days of rainfall duration was considered to be comparable events because the difference of MES between 5 and 7 days was less than five percent.

Figure 5.11 shows the distribution of water depth after seven days of rainfall for the KT-PMP event. As mentioned in the previous paragraph, by adding about 1.5 to 7.6 mm/hr of rainfall intensity to the 100-year rainfall event, the main channel response to the DS is very fast. It took only 34 hours after a seven-day rainfall KT-PMP event to achieve the depth of more than 2.8 m in the main channel (Figure 5.11a). The difference in rainfall intensity between the 100-year return period event and the KT-PMP event is not as high as S-PMP (i.e., small and medium watersheds). However, analysis of the 100-year event showed that low rainfall intensity was enough to make the watershed become fully saturated. As a result, small additional rainfall intensity from KT-PMP created a very large amount of total runoff. The highest MES value for this event was 8.7 m, which occurred approximately one hour after the rainfall of the KT-PMP event ended (Figure 5.11b). The floodplains along the main channel and tributaries were flooded with water depth of more than 2.8 m. These areas had the lowest elevation in the watershed (see Figure 4.6a). Seven days after the KT-PMP event (Figure 5.11c), upstream of the main outlet, the water depth remained over 2.8 m. The topography of this area is nearly flat and wider than upstream; therefore, more time is required to drain the flood.

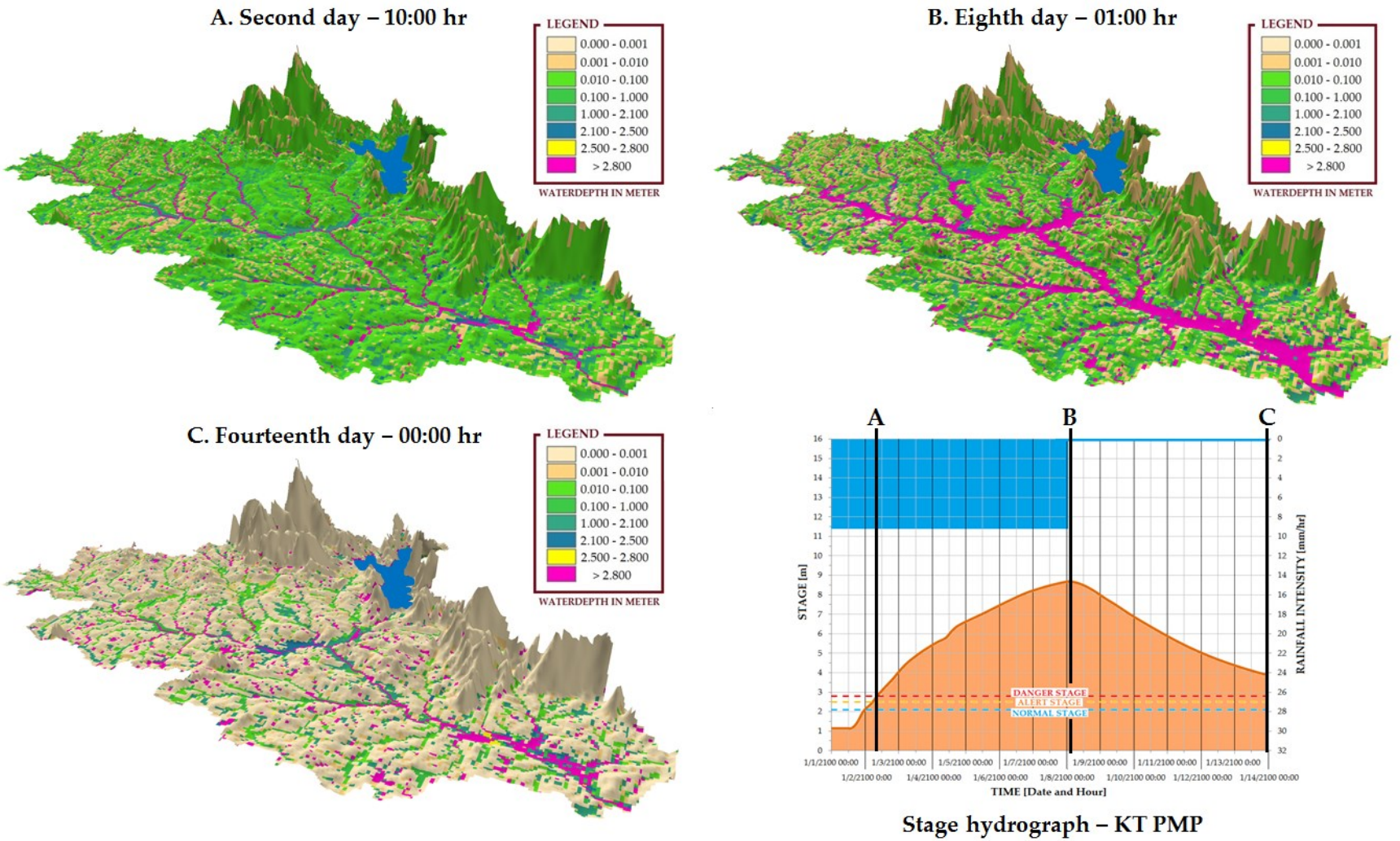

Figure 5.11 Three-dimensional visualizations using KT-PMP rainfall event for the large watershed (Kota Tinggi)

The stage hydrograph, with temporal and spatial distribution of water depth for the world's largest rainfall event, is shown in Figure 5.12. The response time for the water depths in the tributaries and channel to increase to more than 2.8 m is faster than the KT-PMP event. The water depths were in the DS zone approximately 18 hours after the rainfall event (see stage hydrograph in Figure 5.12). At this time, the soil was fully saturated. Figure 5.12a shows that after the second day of the event, the water has overtopped to the floodplain. The MES value for this event was 14.4 m (Figure 5.12b). The stage hydrograph also indicated that if the rainfall intensity is slightly higher for the event, then the equilibrium condition could be reached. At this point, the watershed becomes impervious. This would require more than seven days for water depths to decrease back to the NS zone after the world's largest rainfall event (Figure 5.12c). This time duration is similar to estimates of large and KT-PMP events.

The relationship between the magnitude of the highest maximum discharge value and rainfall events is interesting. The ratio between the highest maximum discharge values for each rainfall events was calculated and tabulated in Table 5.1. The magnitudes at small and medium watersheds were calculated to be from 6 to 15 times bigger than the 100-year rainfall event for S-PMP and the world's largest rainfall events, respectively. However, these magnitudes are smaller at the large watershed. Here, the calculated magnitude was 3 and 8 times bigger for the same comparison. The difference of these magnitudes was mainly influenced by the size of the watershed, land use, and soil type (Appendix F). The properties of the soil and its land use (hydraulic conductivity and roughness) are different at each watershed in this study. A detailed explanation of how these values can affect the discharge is in Appendix B.

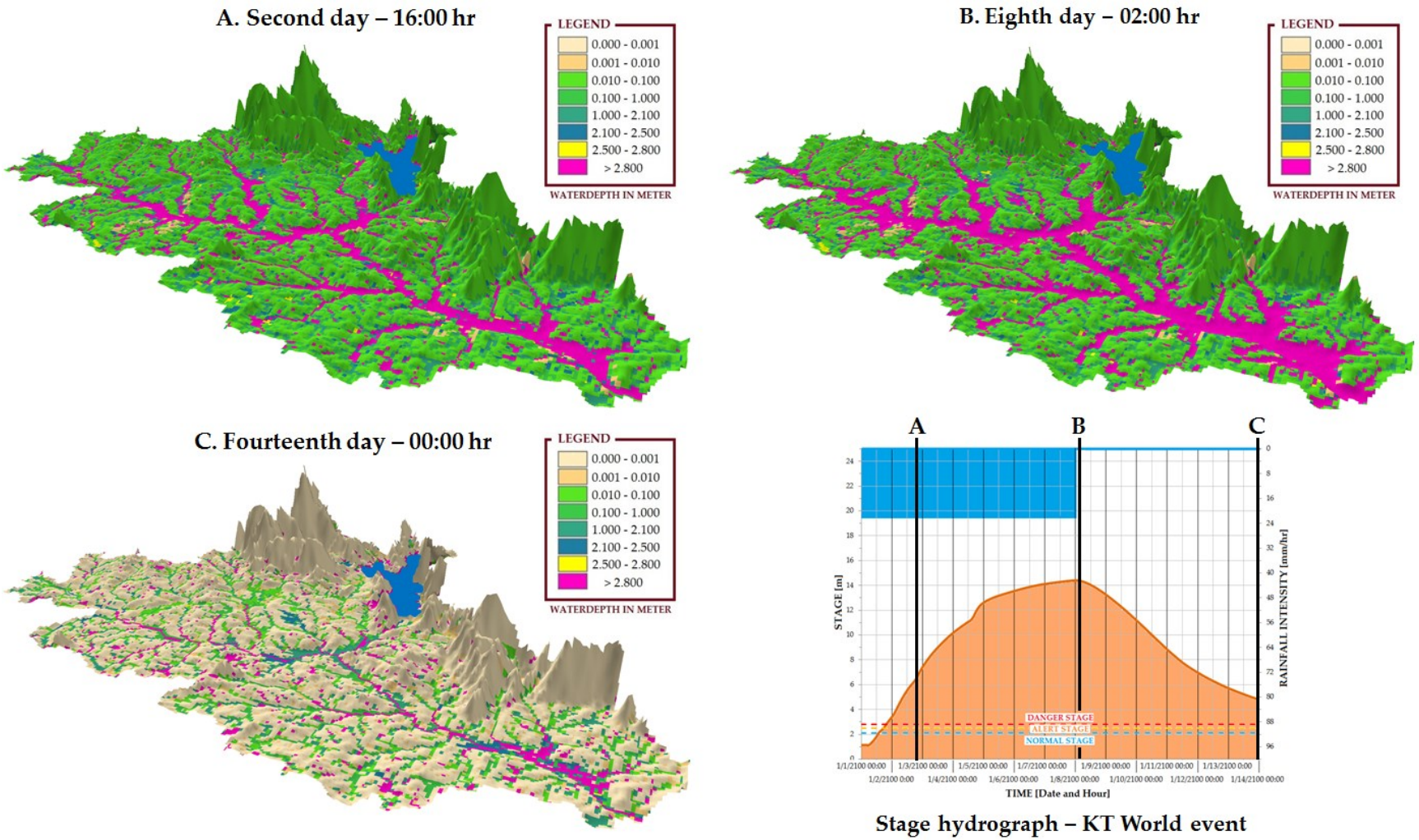

Figure 5.12 Three-dimensional visualizations using the world's largest rainfall event for the large watershed (Kota Tinggi)

Table 5.1 The magnitude of the highest MED values from one rainfall event to another

WATERSHED SIZE	MAXIMUM DISCHARGE, Q_p (cms)				
	100-year	PMP	Ratio [PMP / 100-year]	World	Ratio [World / 100-year]
SMALL (68 km^2)	91	520	6	1358	15
MEDIUM (236 km^2)	256	1474	6	3793	15
LARGE (1,635 km^2)	1023	3016	3	8332	8

5.3 RELATIONSHIP BETWEEN RAINFALL DURATION, PEAK SPECIFIC-DISCHARGE AND WATERSHED AREA

Figure 5.13 is a log-log graph that shows the relationship of the rainfall duration for highest maximum estimated discharge (MED) value estimated by the model for each large and extreme event as a function of watershed size. The highest MED value was selected and the duration of the rainfall at that particular event was determined. For instance, for a 100-year return period event at the small watershed, the highest estimated MED value was 91 cms when the duration of rainfall is four hours (Table A2 – Appendix A). For the large rainfall events (Figure 5.13 - green color), the duration of rainfall to reach the highest MED values for large rainfall events at small and medium watersheds vary. The rainfall duration between 3 and 5 hours was estimated by the model at a small watershed. For medium watershed, the rainfall duration is longer, i.e., between 5 and 12 hours. However, for the large watershed, the rainfall duration were simulated for 7 days to reach the highest MED for all large rainfall events. Similar to a large event, the duration of rainfall for the model to estimate highest MED is not the same as at the small, medium and large watersheds. The TREX model estimated the MED values for small and medium watersheds with the duration of rainfall between 10 and 13 hours (Figure 5.13 – yellow and red dots). However, for the large watershed, the duration of rainfall was longer. The

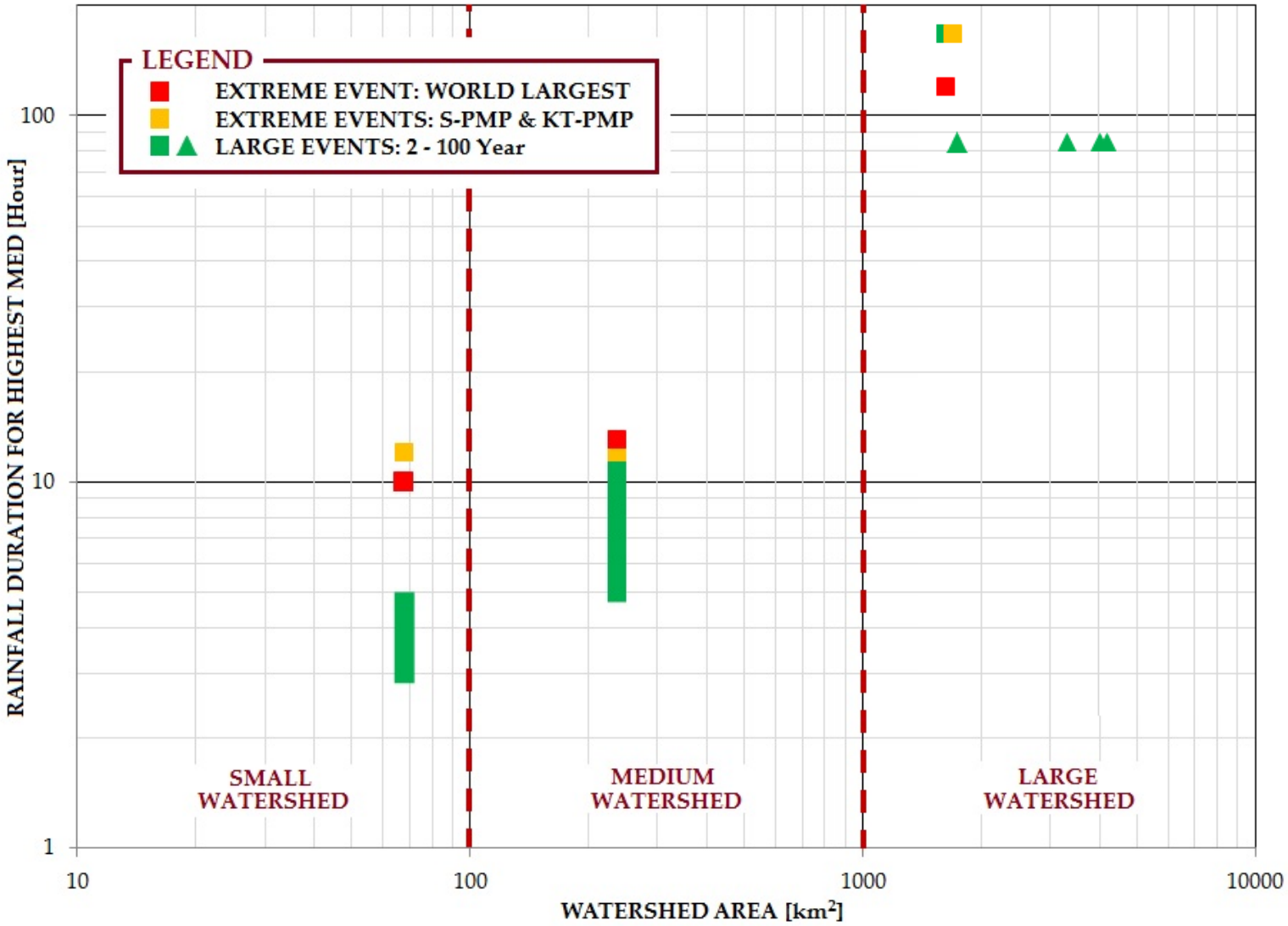

Figure 5.13 The relationship between duration of rainfall of the highest MED value and the watershed area

rainfall duration to get the highest MED value was 168 and 150 hours for the KT-PMP and world's largest rainfall events, respectively.

The topography of the small and medium watersheds is approximately similar, i.e., more than 50% of the watershed is mountainous (Figure 4.4a and 4.5a for the small and medium watershed, respectively). Conversely, more than 50% of the large watershed is a low land area (Figure 4.6a). The topography difference between these watersheds affected the time to reach MED for each simulated event. At the large watershed, the low land area is covered by forest and some places are swampy (Appendix F - Figure F3). Generally, tropical rain forest is dense and their tree trunks are big, which causes the travel time from far-upstream to the downstream end to increase.

During extreme rainfall events, the intensity of rainfall is very high compared to large rainfall events. Therefore, more water was added to the watershed and soils become fully saturated in a very short time. As a result, more overland flow was generated because the rainfall exceeded infiltration rates. Increasing rainfall intensity by a factor of 2.0 (for small and medium watersheds) and 1.6 (for large watershed) from the 100-year return period to PMP event and from PMP to the world's largest event creates rainfall beyond the normal conditions. That means, by increasing the intensity of rainfall, the discharge in the main channel and overland will be much different than during normal events. During normal events, the flow in the main channel is controlled by the channel itself. However, as the rainfall intensity and duration are far beyond the normal conditions, the flow conveyance and distribution is controlled by the rainfall event. The channel and overland surface roughness decrease as the flow depth and volume increase. As a result, the MED values are significantly increased.

The relationship between rainfall duration and intensity as a function of watershed size is interesting as well. The MED at the small and medium watersheds was obtained at rainfall durations between 3 to 13 hours (Table 5.2). This means, the MED values are influenced by rainfall intensity. However, at the large watershed, the duration of rainfall to obtain MED values are longer than the other two watersheds. Except for the world's largest event, the MED values are estimated at 168 hours of rainfall duration (Table 5.2). The MED value for the world's largest event is estimated when the duration of rainfall was at 150 hours. To make this discussion easier, the rainfall duration of this event was assumed to be 168 hours, the same as other events for the large watershed, because the difference of MED values for 150 and 168 hours duration was less than 5%. Therefore, for the large watershed, the duration of rainfall is more important than the rainfall intensity in order to determine the MED value

Figures 5.14 and 5.15 show the relationship between peak specific-discharge and watershed area. The plotted values were calculated by dividing the highest MED for each specific event with the watershed area as tabulated in Table 5.2. The graph has been modified from Creager et al. (1945) and Julien (2002) in order to fit the results of this study. This graph was introduced by Creager et al. (1945) by plotting the highest floods observed from the USA and some big floods from other countries such as China, India and Brazil. These data were tabulated in Appendix G. Additional information, as shown in Table 5.3, was obtained from USNRC (1980), Fontaine (1992), Eberle et al. (2002), REDAC (2006), England et al. (2007), and USACE (2008), Moussa and Bocquillon (2009) and Sharif et al. (2010) to support the findings from this study.

Table 5.2 Duration of rainfall contributed to highest MED value and peak specific-discharges

Rainfall Events		Watershed size (in km^2)								
		Small (68)			Medium (236)			Large (1,635)		
		Highest MED (cms)	Rainfall Duration (hrs)	Peak Specific-Discharge (cms/km^2)	Highest MED (cms)	Rainfall Duration (hrs)	Peak Specific-Discharge (cms/km^2)	Highest MED (cms)	Rainfall Duration (hrs)	Peak Specific-Discharge (cms/km^2)
Large Events	2-year	22	3	0.32	147	5	0.62	368	168	0.23
	5-year	46	5	0.68	167	12	0.71	---	---	---
	10-year	62	5	0.91	206	5	0.87	---	---	---
	20-year	74	5	1.09	226	12	0.96	---	---	---
	50-year	85	4	1.25	242	12	1.03	920	168	0.56
	100-year	91	4	1.34	256	12	1.08	1,023	168	0.63
Extreme Events	PMP	520	12	7.65	1,474	12	6.25	3,016	168	1.84
	World	1,358	10	19.97	3,793	13	16.07	8,332	120	5.10

Table 5.3 Peak specific-discharge data from other researchers

Rainfall event		**Jeniang** [1] (Area = 1,740 km^2)		**Jambatan** [1] (Area = 3,330 km^2)		**Ladang** [1] (Area = 4,010 km^2)		**River Estuary** [1] (Area = 4,210 km^2)	
		Highest MED (cms)	Peak Specific-Discharge (cms.km^{-2})	Highest MED (cms)	Peak Specific-Discharge (cms.km^{-2})	Highest MED (cms)	Peak Specific-Discharge (cms.km^{-2})	Highest MED (cms)	Peak Specific-Discharge (cms.km^{-2})
Large events	50-year	667	0.38	1,386	0.42	1,768	0.44	1,910	0.45
	100-year	767	0.44	1,579	0.47	2,000	0.50	2,100	0.50
100-Yr / PMP		**England et al. (2008)** [2] (Area = 12,000 km^2)		**USNRC (1980)** [3] (Area = 23,491 km^2)		(Area = 267,805 km^2)		**USACE (2008)** [4] (Area = 3,224,535 km^2)	
		2,830	0.24	7,985	0.34	24,069	0.09	85,801	0.03
		Moussa and Bocquillon (2009) [5] (Area = 27,088 km^2)		**Sharif et al. (2010)** [6] (Area = 1,630 km^2)		**Fontaine (1992)** [7] (Area = 690 km^2)		**Eberle et al. (2002)** [8] (Area = 27,088 km^2)	
		2,440	3.25	2,829	1.7	406	0.6	4,020	0.14

Note: The source for [1] is from REDAC (2006)

The plotted data can be classified into three regions: large events cover return periods between two to 100-years, PMP, and world's largest rainfall event. These regions were classified using 50% lower and upper limits from the minimum and maximum of the highest MED values in each region. The first region is represented in green. The region has a minimum limit to ensure that the design discharge is not under estimated. This is important so that any hydrologic design system, for example drainage or widening and deepening of a river could contain high discharge. The second region is represented in orange. The highest MED values resulted from S-PMP (small and medium watersheds) and KT-PMP (large watershed) events were used as benchmarks to produce this region. Additional data from USNRC (1980), Fontaine (1992), Eberle et al. (2002), REDAC (2006), England et al. (2007), and USACE (2008), Moussa and Bocquillon (2009) and Sharif et al. (2010) were used to support the outline of this region. Finally, the world's largest event, which is classified as extreme event, is presented in red. According to Nathan and Weinmann (1990), this event has the annual exceedence probability of at least 1 in 2,000 years (Figure 2.5).The upper bound is introduced to limit the design discharge. If the design discharge is beyond this region, the cost (time and money) of the construction will be high.

The variability of the peak specific discharge decreases for the extreme events (i.e., PMP and world's largest rainfall events). At this point, the hydrologic parameters do not play any role because the soils become fully saturated and the roughness is small. The coverage for all regions decreases as size of watershed increases. The peak specific-discharge decreased trivially as the watershed size increased up to 1 x 10^3 km^2. For one-log-cycle of watershed size, the peak specific-discharge decreased about one-third-log-cycle. However, beyond this watershed size (1 x 10^3 km^2), the value of peak specific-discharge is decreased significantly. The peak specific-

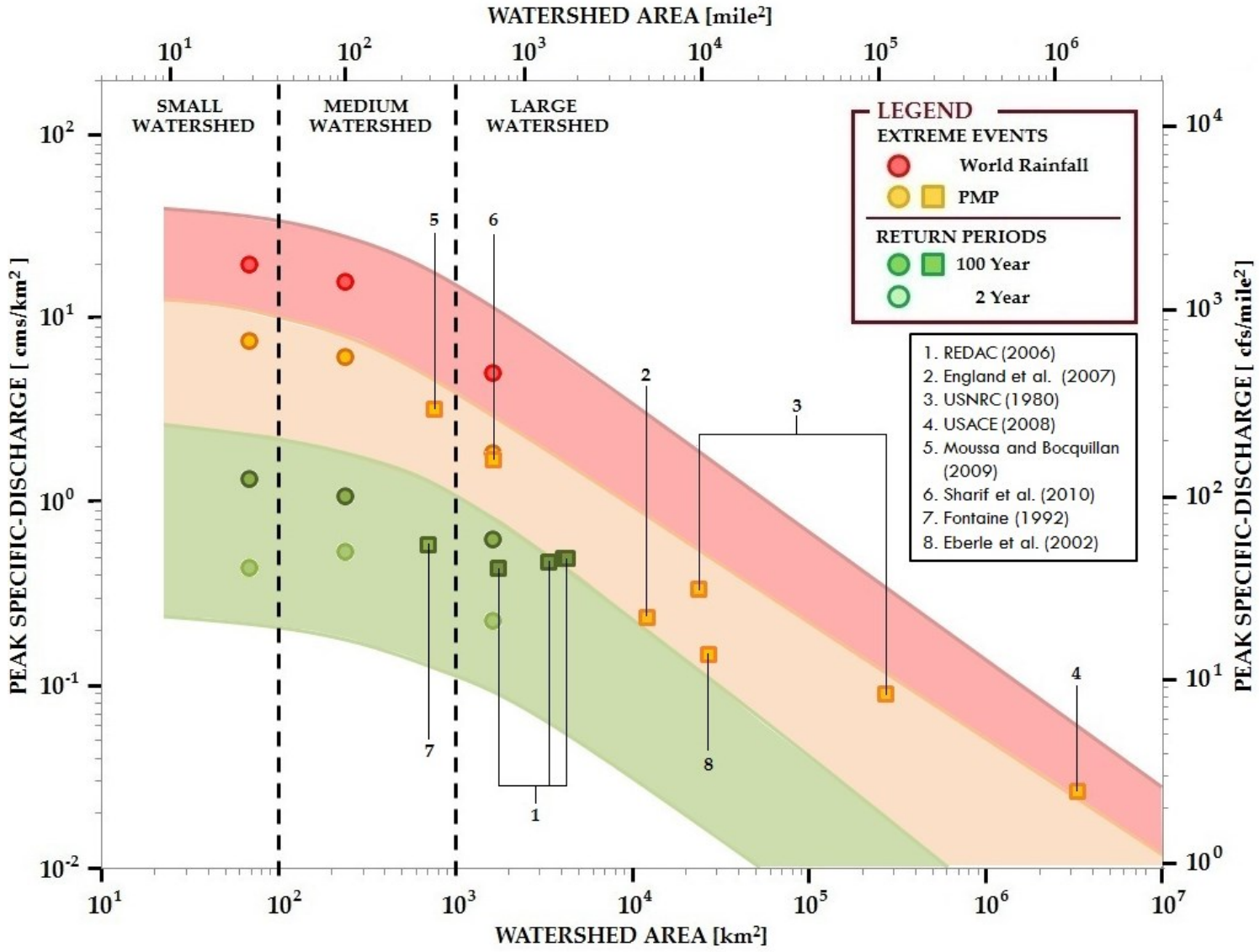

Figure 5.14 Large and extreme peak specific-discharges as a function of watershed area

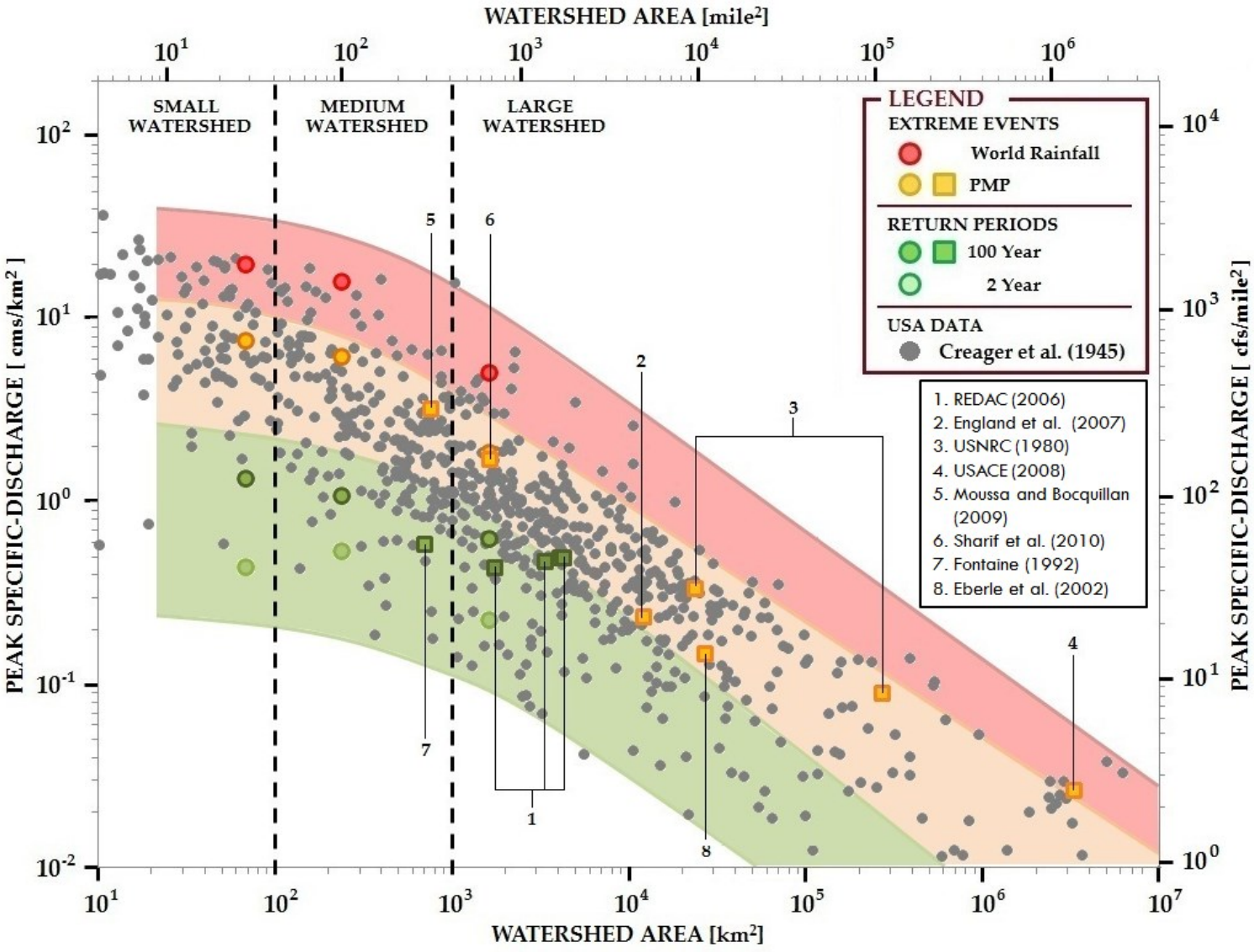

Figure 5.15 Large and extreme peak specific-discharges as a function of watershed area with Creager et al. (1945) flood data.

discharge decreased more than a half-log-cycle. The distributions of these regions are related to the magnitude (or ratio) as shown in Table 5.1. As shown in this table, the magnitude (or ratio) of the highest MED values for the extreme events to the large event (100-year return period) is about the same. The average magnitude is 5 and 12 times bigger for the respective events.

Currently, relationships between rainfall duration, peak specific-discharge and watershed size are not well explained, published or used by other researchers or engineers. This study has provided a graph that gives good approximate values for estimating discharge at small, medium and large watersheds, provided that the characteristics of the watersheds (small, medium and large) to be studied are similar or the same as in this study. This information can also be a good reference and benchmark when conducting large and extreme rainfall event analyses.

5.4 SENSITIVITY ANALYSIS OF THE LARGE AND EXTREME DISCHARGES

Sensitivity analysis was conducted to describe the entire set of possible discharges and runoff coefficients, C, based on several combinations of upper, lower limits and calibrated/validated values. From the sensitivity analysis, the uncertainty of the water depth distribution across three watersheds during these rainfall events (i.e., large and extreme events) will also be highlighted. The upper and lower limits for each parameter are presented in Tables 5.4, 5.5 and 5.6 for the small, medium and large watershed, respectively. There are several sources that contributed to the uncertainty of discharge, which includes the measurement error in rainfall and discharge and the estimation of hydrological and hydraulic parameters in the hydrologic model. However, in this study, the uncertainty analysis for discharge was evaluated using only hydrological and hydraulic parameters. The measurements of rainfall and flow are assumed to be error free in this study. The hydrological and hydraulic parameters for TREX model include the hydraulic conductivity, K_h, soil moisture deficit, hydraulic suction head, H_c,

slope (overland, S_{ov}, and channel, S_{ch}), roughness (Manning's n for overland, n_{ov}, and channel, n_{ch}). These parameters were known to be the most sensitive parameters as discussed in Appendix B. The K_h and Manning's n vary widely between soil classes and land covers, respectively. The variation of the Manning's n depends on the type and condition of vegetative cover, as well as the flow condition (laminar or turbulent). Upper and lower K_h and Manning's n values were assumed to be 50% larger and lower than the calibrated value. To simplify the analysis, only the variation of the overland roughness was explored.

The Logic Tree Analysis (LTA) approach as described by Mishra (2009) was used. The author suggests that this approach is particularly useful for uncertainty propagation when parameter uncertainty is described using a limited number of possibilities (e.g., upper and lower limit, and calibrated and validated parameters values). The LTA is ordered such that the sum of the possibilities is unity (i.e., 1.0) when the combination of upper and lower limits were used. The upper (UP) and lower limits (LL) were selected using the ±50% of calibrated and validated values. These limits correspond to the maximum and minimum permissible values of hydrology and hydraulic parameters (will be referred to as the model parameters in the following paragraph) in hydrological model as suggested by Liong et al. (1989). The model parameters depend on the soil types and topography of the watersheds. The assumption is that these model parameters do not change much as compared to the land use, unless there is a significant work in replacing the existing soil type on the watershed area. The ±50% limits were chosen to depict the plausible and realistic range of parameter uncertainty for the key inputs to assess variability in the system outputs. However, in this study, there are some of the model parameters exceed the Liong's limit. In this case, the exceeding values are used and assumed to be valid.

Table 5.4 Parameter bound for uncertainty analysis at small watershed: hydraulic conductivity and Manning's n

PARAMETER	LOWER LIMIT	UPPER LIMIT	APPLICATION
Hydraulic Conductivity, K_h (m/s)	1.31×10^{-7}	3.405×10^{-7}	Sandy loams
	1.14×10^{-7}	3.930×10^{-7}	Loams
	4.34×10^{-7}	1.301×10^{-6}	Mountain - limestone
Manning's n	0.085	0.255	Agricultural
	0.025	0.075	Urban / Commercial
	0.200	0.600	Forest

Table 5.5 Parameter bound for uncertainty analysis at medium watershed: hydraulic conductivity and Manning's n

PARAMETER	LOWER LIMIT	UPPER LIMIT	APPLICATION
Hydraulic Conductivity, K_h (m/s)	5.60×10^{-9}	1.68×10^{-8}	Sandy loams
	6.35×10^{-9}	1.91×10^{-8}	Loams
	1.53×10^{-9}	4.59×10^{-9}	Clay
	5.90×10^{-11}	1.77×10^{-10}	Mountain - limestone
Manning's n	0.050	0.150	Agriculture
	0.025	0.075	Urban / Commercial
	0.100	0.300	Forest
	0.050	0.200	Grass area
	0.050	0.150	Open area

Table 5.6 Parameter bound for uncertainty analysis at large watershed: hydraulic conductivity and Manning's n

PARAMETER	LOWER LIMIT	UPPER LIMIT	APPLICATION
Hydraulic Conductivity, K_h (m/s)	3.56×10^{-10}	1.07×10^{-9}	Sandy loams
	3.64×10^{-10}	1.09×10^{-9}	Loams
	3.59×10^{-11}	1.08×10^{-10}	Mountain - limestone
Manning's n	0.15	0.45	Agriculture
	0.01	0.03	Urban / Commercial
	0.30	0.90	Forest
	0.15	0.45	Grass area
	0.15	0.45	Open area

The watershed runoff coefficients, C, at each watershed were calculated using the Rational Method (RM) shown in Equation 5.1.

$$C = \frac{Q_p}{iA} \qquad \text{[Equation 5.1]}$$

Where: C = runoff coefficient [-]

Q_p = peak discharge [L^3T^{-1}]

i = rainfall intensity [LT^{-1}]

A = watershed area [L^2]

This method was use with the assumptions that (1) the peak flow is reach when the entire watershed is contributing to the runoff, (2) the rainfall intensity is assumed to be uniform across the watershed and over a time duration, and (3) the peak discharge recurrence interval simulated is equal to the rainfall intensity recurrence interval (i.e., the 100-year rainfall intensity is assumed to produce 100-year flood discharge and so forth).

The simulated peak discharges obtained using combination parameters from Tables 5.4, 5.5 and 5.6 are tabulated in Tables H1- H3 (Appendix H) for the small, medium and large watershed, respectively. Figures 5.16 - 5.18 show the box plot of the peak discharges for return period events from two to 100-year and extreme events, i.e. PMP and world's largest rainfall events. The calibrated/validated (CV) values are presented with white box. The distribution of the peak discharges are presented in the forms of box-plot, red-dotted, and line.

Tables H1 - H3 show discharges and runoff coefficients for different combinations of hydrologic parameters at the small, medium and large watersheds, respectively. The peak discharges, as tabulated in these tables, indicated that the possible peak discharge value at small

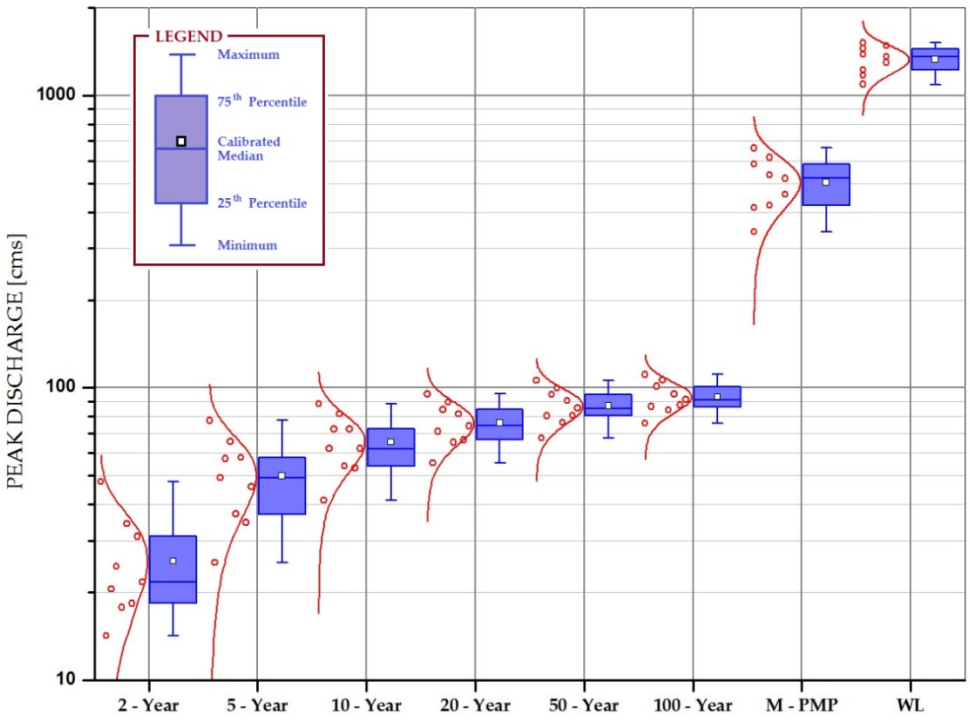

Figure 5.16 Box-plot for hydrological uncertainty at small watershed (Lui)

and medium watersheds are normally distributed for large events (Figures 5.16 and 5.17). Conversely, the distribution of peak discharges at the large watershed is clustered into three (Figure 5.18). These three clusters can be defined as minimum, mean and maximum. The same trend also can be found for extreme events. This trend indicates that during extreme events, the K_h and Manning's n does not affect the discharge. This happens because after a certain period of rainfall, soil becomes fully saturated and roughness becomes smooth very fast as compared to during large events (except at the large watershed). All rainfall becomes runoff and flows directly to tributaries and the main channel. The runoff coefficient, C, value for the calibrated hydrologic parameters is between 0.1 and 0.3 for large events at all watersheds (see Figures H1 – H3 in an Appendix H). However, the coefficient drastically increased for extreme event at all watersheds, which was between 0.6 and 0.9. From these values, it can be said that Manning's n is

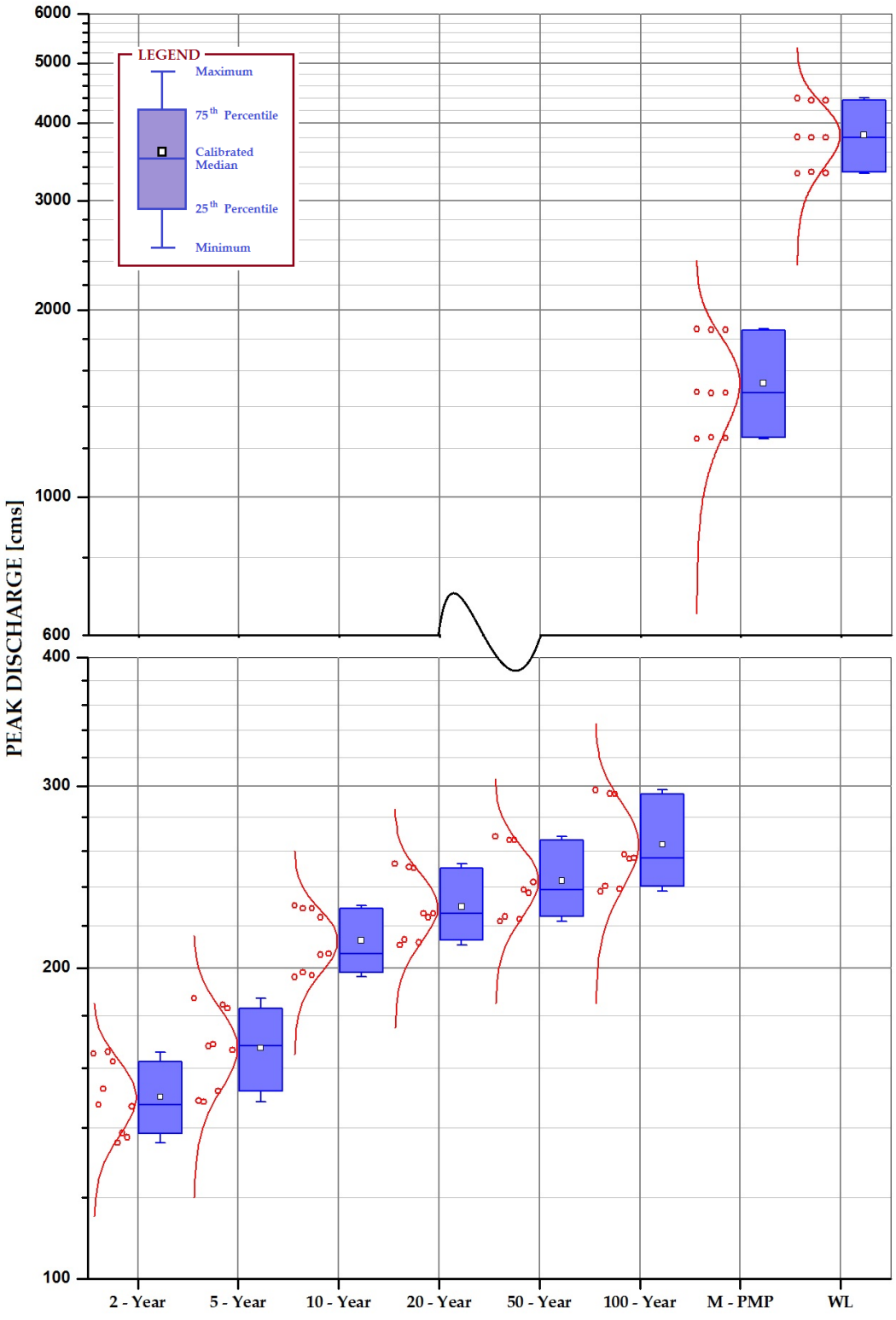

Figure 5.17 Box-plot for hydrological uncertainty at medium watershed (Semenyih)

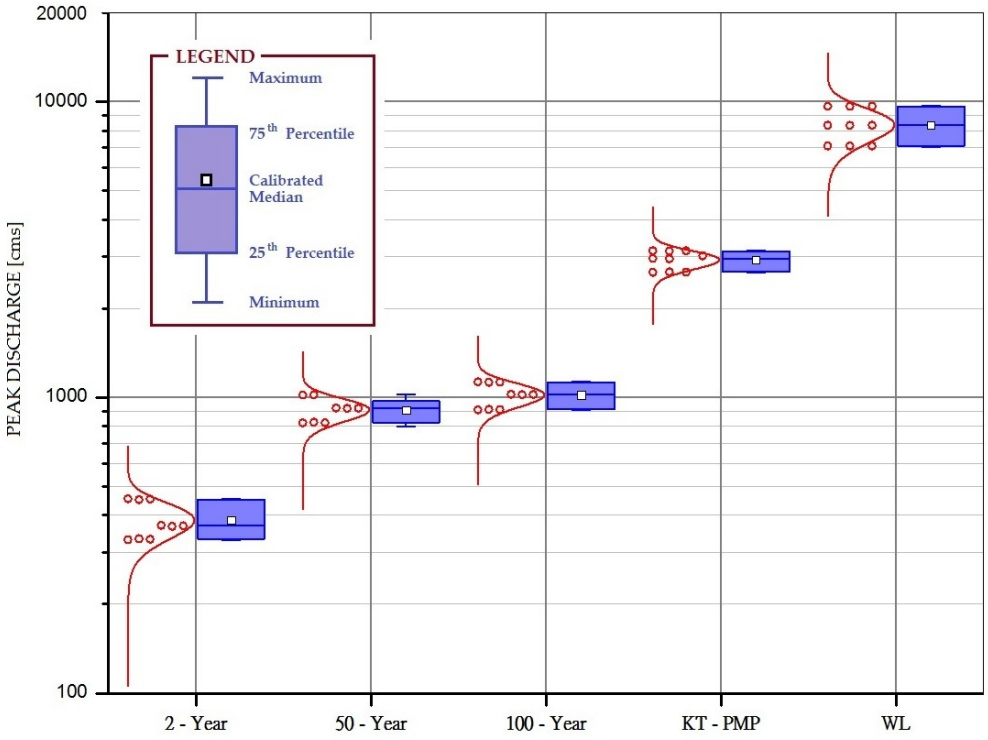

Figure 5.18 Box-plot for hydrological uncertainty at large watershed (Kota Tinggi)

the most uncertain parameter as compared to hydraulic conductivity, K_h. The maximum runoff coefficient for all watersheds calculated when the lower limit of *Manning's n* was applied. The trends of the C values were the same, as indicated by the uncertainty analysis conducted for peak discharges.

The uncertainty analysis on water depth distribution across small, medium and large watersheds based on these rainfall events was done. For a small watershed, during 100-year event, the main channel will be flooded (Figure H4 - Appendix H) with the uncertainty ranging between 86% and 91%. The uncertainty limit for this event is ±3%. It was estimated that 13% to 34% of the valley area will be flooded with water depths of more than 1.72 m during S-PMP event. Flooded areas at the valley increased between 77% and 85% during the world's largest

rainfall event. The valley area at medium watershed is safe from any water depth more than 4.49 m, except in the main channel during 100-year event. For this event, the DD zone in the main channel does not change, i.e., 55% (Figure H5 – Appendix H). During S-PMP event, 67% to 82% of the main channel will reach the DD zone. The valley area at a medium watershed is prone flooding, at the range between 85% and 96% during the world's largest rainfall event. The valley areas at a large watershed were flooded during 100-year, KT-PMP and world's largest rainfall events as shown in Figure H6 (Appendix H).

Figure 5.19 shows the uncertainty value of the peak specific-discharge as a function of watershed area. The upper (UP) and lower limits (LL) were obtained from the sensitivity analysis as discussed in the first paragraph of this section. The uncertainty of the 100-year flood at small watershed is ±20% from the estimation of calibrated/validated value; while medium and large watersheds give ±10% for the same comparison. However, the uncertainty of peak discharges for PMP event shows increasing bounds (i.e., lower and upper limit) at small and medium watersheds. The values are ±30% and ±22%, respectively. The uncertainty of the peak discharge at large watershed for PMP event is ±8%. For the world's largest rainfall event, the uncertainty of the peak discharge at small, medium and large watersheds is ±16%. The distribution of large, PMP and world's largest event, as shown in Figure 5.20 is classified by considering the data reported by Creager et al. (1945), USNRC (1980), Fontaine (1992), Eberle et al. (2002), REDAC (2006), England et al. (2007), and USACE (2008), Moussa and Bocquillon (2009) and Sharif et al. (2010).

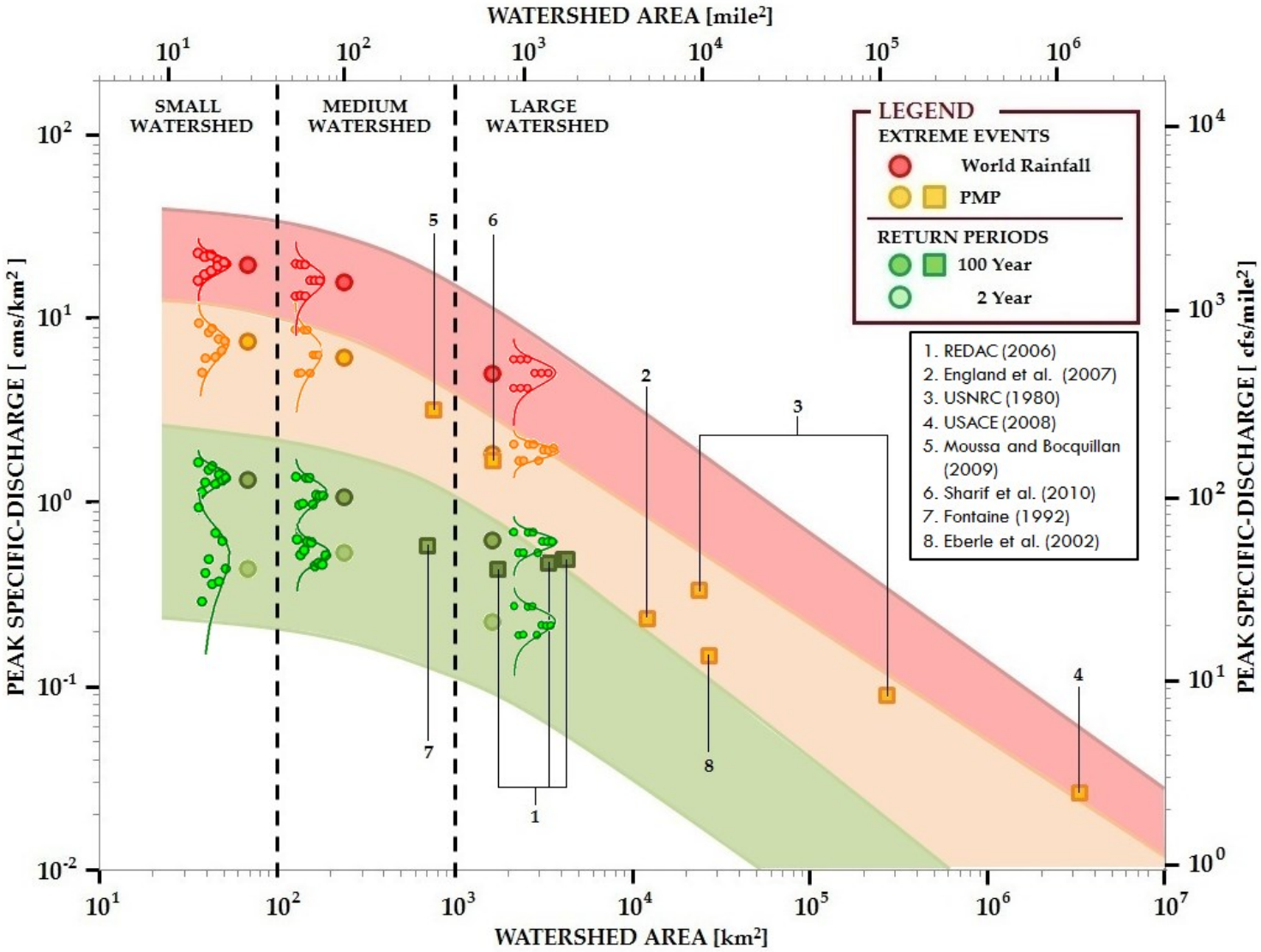

Figure 5.19 Uncertainty of the peak specific-discharge as a function of watershed areas

SUMMARY

The simulated results for 100-year return period (large event), PMP (including S-PMP (small and medium watersheds) and KT-PMP (large watershed)), and world's largest rainfall events were presented and discussed. For small and medium watersheds, the analyses and discussions were based on simulated discharges, whereas for the large watershed, simulated stage was used for analysis and discussion. The temporal and spatial distributions of water depths for all events at the three watersheds were visualized in 3D.

The highest MED values for the large event (100-year return period) at small and medium watersheds were 91 and 256 cms, respectively. The rainfall intensities for these watersheds were 38 and 15 mm/hr, respectively. Although the rainfall intensity at the small watershed was higher than at the medium watershed, the duration of rainfall that gave the highest MED value was the opposite. This means the duration of rainfall at the medium watershed was 12 hours to simulate the highest MED value, as compared to the small, which is 4 hours. For the large watershed, the intensity and duration of rainfall were 7.6 mm/hr and 168 hours, respectively. The intensity at this watershed was smallest when compared to the small and medium watersheds. However, a much longer duration of rainfall was required to simulate the highest MED value, which was 1,023 cms. Simulation of the 100-year return period showed the valley areas at the small and medium watersheds were not flooded except in main channel (Figures 5.2 and 5.4). However, for the same level event, most of the low land areas (along tributaries and channels) at the large watershed were estimated to have water depth more than 2.8 m (Figure 5.6b).

Extreme rainfall events, PMP and world's largest rainfall data, were simulated at these watersheds also. The rainfall and duration for small, medium and large were presented in

Table 2.6. The highest MED for the PMP event at small, medium and large watersheds was 520, 1,474 and 3,016 cms, respectively. These values were estimated at rainfall durations of 12 hours for small and medium watersheds and 168 hours (7 days) for the large watershed. The highest estimated MED values for small, medium and large watersheds using the world's largest rainfall are 1,358, 3,793 and 8,332 cms, respectively. The distributions of water depth above alert zone levels for all watersheds were not the same. The hydrological simulation indicates that all study areas were estimated to be flooded, except the S-PMP event at the medium watershed (Figure 5.9). For the small watershed, the flooded areas were estimated at the far-upstream and end-downstream of the valley (Figures 5.7 and 5.8). At the medium watershed, the whole valley area was flooded during the world's largest rainfall event (Figure 5.10). At large watershed, Figures 5.11 and 5.12 indicate that the low land areas (i.e., along the tributaries and channels) are more likely to be flooded.

The relationships between rainfall duration, peak specific discharge and watershed size were also discussed. From these analyses and discussions, it was concluded that rainfall intensity does not affect the estimation of the highest MED values for large and extreme events at the large watershed. Rainfall duration is the main factor that creates flooding. Instead of rainfall duration, the intensity of rainfall is the main factor that contributes to flooding at the small and medium watersheds. From the simulation results as shown in Figure 5.14, three regions were produced and shown in Figure 5.15. These regions are very useful in providing the first approximation for a hydrological modeler or any practitioner to estimate peak discharges. The uncertainty analysis was conducted to quantify the reliability of peak discharge and flooding area for large, PMP and world's largest rainfall events on these watersheds.

CHAPTER SIX

CONCLUSIONS

Lui (small – 68 km^2), Semenyih (medium – 236 km^2) and Kota Tinggi (large – 1,635 km^2) watersheds were used to simulate large and extreme rainfall events. Large rainfall events covered return periods from two to 100-year events. Extreme rainfall events included Selangor-PMP (S-PMP), Kota Tinggi PMP (KT-PMP) and the world's largest rainfall events. This study used the distributed two-dimensional TREX model for the simulation of infiltration, overland runoff, and channel flow during extreme rainfall events. Following the objectives outlined in the first chapter, these conclusions have been reached from conducting this study:

Objective 1: Calibrate the distributed hydrological model to simulate monsoon floods.

The model was calibrated and validated for the available period of record from 2009 to 2010 and from 2002 to 2009 for small and medium watersheds, respectively. The rainfall and discharge recorded in 2010 and the flood event in December 2006 to January 2007 were used to calibrate and validate the model parameters of the large watershed. The calibrated and validated model parameters were K_h and Manning's n. Two approaches were used to evaluate the model's performance, these were graphical and statistical (relative percentage difference (RPD), Nash-Sutcliffe Efficiency Coefficient (NSEC) and Percent BIAS (PBIAS)) methods. Generally, the graphical method showed that the observed and simulated hydrograph achieved good results for the small watershed and very good results for both medium and large watersheds. Overall, the PBIAS values showed that the model underestimated the volume of water with an average of 14% and 1.5% for small and large watersheds, respectively. For the medium watershed, the

PBIAS indicated that the model overestimated the volume of water with an average of 28%. The NSEC values indicate that the model performed differently. The NSEC value indicated *satisfactory* (0.4) for the small watershed, *good* (0.7) for the medium watershed, and *very good* (0.8) for the large watershed.

Objective 2: Determine the affected flooding area under different rainfall events.

The spatial and temporal runoff distributions overland and in the channel were successfully visualized in 3D. The valley areas at small and medium watersheds were not flooded by the large events, except in the main channel. Approximately 89% and 55% of the main channel at small and medium watersheds had water depths more than 1.72 m and 4.49 m, respectively. Runoff simulations using S-PMP and the world's largest events showed that the valleys were flooded. The water depths at both upstream and downstream of the valley for the small watershed were estimated to be more than 1.72 m. During S-PMP and the world's largest events, it was estimated that about 24% (±10%) and 83% (±5%), respectively, of the valleys were covered with water deeper than 1.72 m. At the medium watershed, the valley areas were covered with water more than 4.49 m during the world's largest events with uncertainty between 81% and 96%. During the S-PMP events, the valley area was safe from flooding. However, it was estimated that the main channel's water depth exceed 4.49 m over about 81% from the total length of the main channel. However, most of the low land areas (i.e., valley area along tributaries and main channel) of the large watershed were estimated to have water depth greater than 2.8 m, which was overtopping the river bank.

Objective 3: Examine the effect of rainfall duration on the magnitude of the peak flood discharge as a function of watershed size.

The highest maximum estimated discharge (MED) values for each large event were obtained between 3 and 5 hours of rainfall duration for the small watershed. However, for the medium watershed, the highest MED values were obtained at rainfall durations between 5 and 12 hours. The highest MED values for extreme rainfall events were estimated at rainfall duration between 10 and 12 hours for both watersheds. The large watershed required more time to reach the highest MED value for all events, which was 168 hours (7 days). The average magnitude for the PMP and the world's extreme rainfall events was 5 and 12 times bigger than the 100-year event, respectively.

Objective 4: Determine and produce graphs for the relationship between peak specific-discharge and watershed sizes.

The intensity of rainfall is the main factor in determining the flood magnitude of small and medium watersheds. The flooding events of large watersheds resulted from longer rainfall durations. The graph showing the relationship between peak specific discharges and watershed areas was plotted (Figures 5.14 and 5.15). From this graph, three main regions were produced to estimate the peak discharge for the three sizes of watersheds. These regions were established based on the rainfall events of large, PMP, and the world's largest rainfall events. The peak specific-discharge decreased slightly as the watershed size increased up to 1×10^3 km^2. However, beyond this watershed size, the value of peak specific-discharge decreased significantly. The graph is useful to estimate the peak discharge at first-order approximation to design any hydraulic and hydrology system before conducting further analysis.

REFERENCES

Ab. Ghani, A., Zakaria, N. A., and Falconer, R. A. (2009). "River modeling and flood mitigation; Malaysian perspective." *Proceedings of the Institute of Civil Engineers, Water Management*, 162, 1-2.

Abbott, M. B., Bathurst, J.C., Cunge, J.A., O'Connell, P.E., and Rasmussen, J. (1986a). "An introduction to the European Hydrological System—Système Hydrologique Europèen, SHE. 1: History and philosophy of a physically-based, distributed modelling system." *Journal of Hydrology*, 87(1-2), 45-59.

Abbott, M. B., Bathurst, J.C., Cunge, J.A., O'Connell, P.E., and Rasmussen, J. (1986b). "An introduction to the European Hydrological System—Système Hydrologique Europèen, SHE. 2: Structure of a physically-based, distributed modelling system." *Journal of Hydrology*, 87(1-2), 61-77.

Abbott, J. (1978). "Testing of several runoff models on an urban watershed." *U. S. Army Corps of Engineers*, Hydrologic Engineering Center Technical Paper No. 59.

Abdullah, M. (2011). "Kangar paling teruk dilanda banjir (The worst city flood-stricken is Kangar)." Utusan Melayu, Apr. 1, 2011 <http://www.utusan.com.my/utusan/info.asp?y=2011&dt=0401&pub=Utusan_Malaysia&sec=Dalam_Negeri&pg=dn_17.htm#ixzz2DODO1nyQ> [Accessed on Nov. 26, 2012]

Acevedo, W., and Masuoka, P. (1997). "Time-series animation techniques for visualizing urban growth." *Computers and Geosciences*, 23(4), 423-435

Ali, A. N. A., and Ariffin, J. (2011). "Model reliability assessment: A hydrodynamic modeling approach for flood simulation in Damansara catchment usinh InfoWorks RS." *Advanced Materials Research*, 250-253, 3769-3775

ASCE Task Committee on Definition of Criteria for Evaluation of Watershed Models of the Watershed Management Committee, Irrigation and Drainage Division, (1993). "Criteria for evaluation of watershed model." *Journal of Irrigation and Drainage Engineering*, 119(3), 429-442

Barnard, T. E., Kuch, A. W., Thompson, G. R., Mudaliar, S., and Phillips, B. C. (2007). "Evolution of an integrated 1D/2D modeling package for urban drainage." *Contemporary Modeling of Urban Water System*, Monograph 15., James, I. McBean, Pitt and Wright, eds., Guelph Ont.

Bates, P. D., and De Roo, A. P. J. (2000). "A simple raster-based model for flood inundation simulation." *Journal of Hydrology*, 236, 54-77

Bedient, P. B., and Huber, W. C. (2002). "CHAPTER 6: Urban Hydrology". *Hydrology and Floodplain Analysis*, Bedient, P. B. and W. C. Huber, (eds.), Prentice Hall, 3rd Edition.

Beven, K., Calver, A., and Morris, E. M. (1987). "The Institute of Hydrology Distributed Model.", *Wallingford, Institute of Hydrology*, 98, 33

Beven, K., and Binley, A. (1992). "The future of distributed models: Model calibration and uncertainty prediction." *Hydrological Processes*, 6, 279-298

Billa, L., Mansor, S., and Mahmud, A. R. (2004). "Spatial information technology in flood early warning systems: An overview of theory, application and latest developments in Malaysia." Disaster Prevention Management, 13(5), 356-363

Billa, L., Mansor, S., Mahmud, A. R., and Ghazali, A. (2006). "Hydro-meteorological modeling and GIS for operational flood forecasting and mapping." The 2nd International Conference on Water Resources and Arid Environment, 1-16

Bissonnais, Y. L., Cerdan, O., Lecomte, V., Benkhadra, H., Souchere, V., and Martin, P. (2005). "Variability of soil surface characteristics influencing runoff and interrill erosion." Catena, 62, 111-124

Bitew, M. M., and Gebremichael, M. (2011). "Assessment of satellite rainfall products for streamflow simulation in medium watersheds of the Ethiopian highlands." *Hydrology and Earth System Sciences*, 15, 1147-1155

Blöschl, G., Sivapalan, M., Gupta, V. K., and Beven, K. J., (1997). "Scale problems in hydrology." *Water Resources Research*, 33(12), 2881-2999

Bormann, H. (2006). "Impact of spatial data resolution on simulated catchment water balances and model performance of the multi-scale TOPLATS model." *Hydrology and Earth System Sciences*, 10, 165-179

Boston, T., Xia, J., and Zhu, Y. (2004). "Pre-processing rainfall data from multiple gages to improve TOPMODEL simulation results in a large semi-arid region." *Hydrological Processes*, 18, 2313-2325

Bras, R. L. (1990). *Hydrology, an introduction to hydrologic science*, Addison Wesley Publication

Calver, A. (1988). "Calibration, sensitivity and validation of a physically-based rainfall-runoff model." *Journal of Hydrology*, 103(1-2), 103-115

Calver, A., and Wood, W. L. (1995). "Chapter 17: The Institute of Hydrology Distributed Model, Computer models of watershed hydrology." *Computer Model of Watershed Hydrology*, V. P. Singh, ed., Water Resources Publications, 595-626

Calver, A., and Cammeraat, L. H. (1993). "Testing a physically-based runoff model against field observations on a Luxembourg hillslope." *Catena*, 20, 273-288

Camoens, A. and Wong, P. M. (2012). "Serdang, Kajang hit by floods." The Star, Sept. 5, 2012 <http://thestar.com.my/news/story.asp?file=/2012/9/5/nation/11970180&sec=nation> [Accessed on Nov. 28, 2012]

Carmona, C., and Vargas, H. (2008a). "Modeling the Tabasco floods. User case studies <http://www.innovyze.com/news/fullarticle.aspx?id=846> [Accessed on Nov. 24, 2011]

Carpenter, T. M., and Konstantine P. G. (2004). "Continuous Streamflow Simulation with the HRCDHM Distributed Hydrologic Model." *Journal of Hydrology*, 298, 61-79

Cartwright, W. (1997). "New media and their application to the production of map products." *Computers and Geosciences*, 23(4), 447-456

Chan, J. (2012). "Flyover users face pool hazard." The Star, Oct. 18, 2012 < http://thestar.com.my/news/story.asp?file=/2012/10/18/nation/12186165&sec=nation> [Accessed on Nov. 28, 2012]

Chan, Y., and Mori, M. (2011). "Web-served flood monitoring system using Google Earth and 3D GIS." *2011 IEEE International Geoscience and Remote Sensing Symposium*, 1902-1905

Chang, C. K., Ab-Ghani, A.,Abdullah, R., and Zakaria, N. A. (2008). "Sediment transport modeling for Kulim River - A case study." *Journal of Hydro-Environment Research*, 2(1), 47-59

Chapra, S. C., and Vanale, R P. (1985). *Numerical methods for engineers with Personel computer applications*, 1st Edition, McGraw-Hill, Inc., New York

Cheng, Q. W. (1987). "Analysis of the design storm time-intensity pattern for medium and small watersheds." *Journal of Hydrology*, 97, 305-317

Church, M. (2006). "Scales of process, modes of analysis: multiples scales in rivers." *Proceeding*, 6th International Gravel-Bed Rivers Conference.

Chow, V.T., Maidment, D., and Mays, L. W. (1988). *Applied hydrology*, McGraw Hill Publication

Cunge, J., Holly, F.M. and Verwey, A., (1980). "Practical aspects of computational river hydraulics." *Pitman Advanced Publishing Program*, London. 420 p.

COMET (2012) , Distributed Hydrologic Models for Flow Forecasts (Part 1), <http://www.meted.ucar.edu/hydro/DHM/dhm2/part1/print.htm#page_4.0.0> [Accessed on Jan. 1, 2012]

Creager, W. P., Justin, J. D., and Hinds, J. (1945). *Engineering for Dams: Volume 1 – General Design*, John Wiley and Sons, NY

Creager, W. P. (1939). "Possible and probable futures flood." *Civil Engineering (New York)*, 9(11), 668-670

Curran, J. C., Bryan, D., and Jennings, M. A. (2005). "Comparison of Modeled Flood Characteristics to Measurements of the 2002 Flood on the Guadalupe River, Texas." *Physical Geography*, 26(5), 396-408

Cui, M. R., Wen, B. D., Ze, Y. L., Lin, M., and Li, Y. (2011). "Evaluation of sustainable development of typical small watershed in mountain area – A case study of Puwa small watershed." *Advanced Material Research*, 183-185, 729-733

CWCB (Colorado Water Conservation Board) (2008). "CHAPTER 12: Unique hydraulic conditions." *Floodplain Stormwater and Criteria manual*, CWCB, WRC Engineering Inc., Denver, CO.

Daxikar, A., Hillier, T., Makarem, F., and Stone, S. (2008). "Application of GIS technology in coastal flood hazard mitigation." *Solution to Coastal Disaster Congress*, 396-409

Daluz Vieira, J.H. (1983). "Conditions governing the use of approximations for the Saint-Venant equations for shallow water flow." *Journal of Hydrology*, 60, 43–58.

Doe, W. W., and Harmon, R. S. (2001). "*Introduction to soil erosion and landscape evolution modeling.*" In *Landscape Erosion and Evolution Modeling*, Harmon R. S. and Doe, W. W. (eds). Kluwer Academic/Plenum: New York; 1–14

Dooge, S. A. (1977). "Problems and methods of runoff-rainfall modeling." *Mathematical Models for Surface Water Hydrology*, T. A. Cirinai, U. Maione and J. R. Wallis, (eds.), John Wiley & Sons, New York, NY.

Dorling, D. (1992). "Stretching space and splicing time: From cartographic animation to interactive visualization." *Cartography and Geographic Information System*, 29(4), 215-227

Donigian, A. S., Imhoff, J. C., and Bicknell, B. R. (1983). "Predicting Water Quality Resulting from Agricultural Nonpoint Source Pollution via Simulation – HSPF." *Agricultural Management and Water Quality*, Schaller, F.W. and Baily, G.W. (eds.), Iowa State University Press, Ames, IA, 209-249

Downer, C.W., Ogden, F.L., Martin, W.D. and Harmon, R.S. (2002). "Theory, development, and applicability of the surface water hydrologic model CASC2D." *Hydrological Processes*, 16, 255–275.

Dransch, D. (2000). "The use of different media in visualizing spatial data." *Computer and Geosciences*, 26, 5-9

Drogue, G., Pfister, L., Leviandier, T., Humbert, J., Hoffmann, L., Idrissi, A. E., and Iffly, J. –F. (2002). "Using 3D dynamic cartography and hydrological modelling for linear streamflow mapping." *Computers and Geosciences*, 28, 981-994

Dykes, J. A. (1997). "Exploring spatial data representation with dynamic graphics." *Computers and Geosciences*, 23(4), 345-370

Eberle, M.,Buiteveld, H., Beersma, J., Krahe, P. and K. Wilke, K. (2002). *Estimation of extreme floods in the river Rhine basin by combining precipitation-runoff modelling and a rainfall generator*, International Conference on Flood Estimation, M. Spreafico et al. (Ed), 2002, March 6-8, Berne, Switserland, CHR Report II-17, International Commission for the Hydrology of the Rhine basin (CHR), Lelystad, The Netherlands

El-Nasr, A. A., Jeffrey, G. A., Feyen, J., and Berlamont, J. (2005). "Modelling the hydrology of a catchment using a distributed and a semi-distributed model." *Hydrological Processes*, 19(3), 573-587

England, J. (2006). "Frequency analysis and two-dimensional simulations of extreme floods on a large watershed." Ph.D thesis, Department of Civil and Environmental Engineering, Colorado State University, CO

England, J., Velleux, M., and Julien, P. Y. (2007). "Two-dimensional simulations of extreme floods on a large watershed." *Journal of Hydrology*, 347(1), 229-241

ESRI (2012). What is raster data?, <http://webhelp.esri.com/arcgisdesktop/9.2/index.cfm?TopicName= What_is_raster_data%3F> [Accessed on Dec. 11, 2012]

Ewen, J., Parkin, G., and O'Connell, P.E. (2000). "SHETRAN: distributed river basin flow and transport modeling system." *Journal of Hydrologic Engineering*, 5(3), 250-258

Ewen, J., Bathurst, J.C., Parkin, G., O'Connell, E., Birkinshaw, S., Adams, R., Hiley, R., Kilsby, C., and Burton, A. (2002). "SHETRAN: physically-based distributed river basin modeling system." *Mathematical Modeling of Small Watershed Hydrology*, V.P. Singh, D.K. Frevert and S.P. Meyer, eds., Water Resources Publications, Englewood, Colorado, 43-68

Fedak, R. (1999). "Effect of spatial scale on hydrologic modeling in a headwater catchment." Msc. Thesis, Faculty of the Virginia Polytechnic Institute and State University (Unpublished)

Fernandez, G P., Chescheir, G. M., Skaggs, R. W., and Amatya, D. M. (2005). "Development and testing of watershed-scale models for poorly drained soils." *American Society of Agricultural Engineers*, 48(2), 639-652

Ferrick, M.G. (1985). "Analysis of river wave types." *Water Resources Research*, 21, 209–212.

Feyen, L., Vasquez, R., Christiaens, K., Sels, O., and Feyen, J. (2000). "Application of a distributed physically-based hydrological model to a medium size catchment." *Hydrology and Earth System Science*, 4(1), 47-63

Franchini, M., and Pacciani, M. (1991). "Comparative analysis of several conceptual rainfall-runoff models." *Journal of Hydrology*, 122, 161-219

Fontaine, T. A. (1992). "Rainfall-runoff model accuracy for an extreme flood." *Journal of Hydraulic Engineering*, 121(4), 365-374

Fread, D.L., 1985. Channel routing. In: Anderson, M.G., Burt, T.P. (Eds.), Hydrological Forecasting. Wiley, New York.

Frenette, M., and Julien, P. Y. (1987). "Computer modeling of soil and erosion and sediment yield from large watershed." *International Journal of Sediment Resources*, 1, 39-68

Ghazali, J. N., and Kamsin, A. (2008). "A real time simulation of flood hazard." *Fifth International Conference on Computer Graphics, Imaging and Visualization*, 393-397

Gersmehl, P. J. (1990). "Choosing tools: Nine metaphors of four-dimensional cartography." *Cartographic Perspective*, 19(4), 3-9

Grayson, R. B., and Blöschl, G. (2000). "CHAPTER 14: Summary of pattern comparison and concluding remarks." *Spatial Patterns in Catchment Hydrology: Observations and Modelling*, Grayson, R. B. and G. Blöschl, (eds.), Cambridge university Press: Cambridge, 355-367

Green, W.H., and Ampt, G.A. (1911). "Studies on soil physics, 1: the flow of air and water through soils." *Journal of Agricultural Sciences*, 4(1), 11-24

Green, I. R. A., and Stephenson, D. (1986). "Criteria for comparison of single event models." *Journal of Hydrological Sciences*, 31(3), 395-411

Grigg, N. S. (2003). "Surviving disasters: Learning from experience." *Journal of American Water Works Association*, 95(9), 64-75

Gupta, H. V., Sorooshian, S., and Yapo, P. O. (1999). "Status of automatic calibration for hydrologic models: Comparison with multilevel expert calibration." Journal of Hydrology Engineering, 4(2), 135-143

Gupta, S. G. (2001). *Hydrology and Hydraulic Systems*, Waveland Press. Inc., 2nd Edition

Güntner, A., and Bronstert, A. (2004). "Representation of landscape variability and lateral redistribution processes for large-scale hydrological modelling in semi-arid areas." *Journal of Hydrology*, 297, 136-161

Guo, X. C., Luo, D. G., Zou, S. L., Li, D. J., and Zheng, W. Q. (2009). "Developing the 3D flood model visualization system based on the ArcEngine." *2009 World Congress on Computer Science and Information Engineering*, 353-356

Hassan, A. J. (2011). "InfoWorks RS reveals the impact of flood mitigation works on the Damansara River in Malaysia." User case studies <http://www.innovyze.com/news/fullarticle.aspx?id=1358> [Accessed on Nov. 24, 2011]

Heeps, D. P., and Mein, R. G. (1974). "Independent comparison of the three urban runoff models." *ASCE Journal of the Hydraulic Division*, 100 (HY7), 995-1009

Hessel, R. (2005). "Effects of grid cell size and time step length on simulation results of the Limburg Soil Erosion Model (LISEM)." *Hydrological Processes*, 19, 3037-3049

Horritt, M.S., Bates, P.D. and Mattinson, M.J. (2006). "Effects of mesh resolution and topographic representation in 2D finite volume models of shallow water fluvial flow." *Journal of Hydrology*, 329, 306–314.

Hossain, A. K. M. A., Jia, Y., Ying, X., Zhang, Y., and Ting, T. Z. (2011). "Visualization of urban area flood simulation in realistic 3D environment." *World Environment and Water Resources Congress, Bearing Knowledge for Sustainability*, 1973-1980

Ismail, A. A. (2011). "1,400 dipindahkan akibat banjir di Tampin (Flood in Tampin – 1,400 people were evacuated)." Utusan Melayu, Jan. 31st, 2011 <http://www.utusan.com.my/utusan/info.asp?y=2011&dt=0131&pub=Utusan_Malaysia&sec=Terkini&pg=bt_11.htm#ixzz2DOGq3Ha6> [Accessed on Nov. 26, 2012]

Izham, M. Y., Md. Uznir, U., Alias, A. R., and Ayob, K. (2010). "Georeference, rainfall-runoff modeling and 3D dynamic simulation: Physical influence, integration and approaches, COM. Geo." *First International conference on computing for geospatial research and application*, Washington D. C., 1-8

Jaafar, O. (2007). "Kajian kesan perubahan guna tanah terhadap sumber air lembangan Sg. Langat melalui integrasi data penderiaan jauh satelit dan GIS serta permodelan hidrologi (The integration of satellite remote sensing data and the application of hydrodynamic model in water resources study of Langat River Basin)." Ph.D thesis, Department of Civil, Built and Environmental Engineering, National University, Malaysia

Jamaluddin, N., and Hassan N. M. (2012). "Banjir kilat terburuk Hulu Langat (The worst flash flood in Hulu Langat)." Utusan Melayu, March 9, 2012 <http://www.utusan.com.my/utusan/info.asp?y=2012&dt=0309&pub=Utusan_Malaysia&sec=Dalam_Negeri&pg=dn_10.htm#ixzz2DOa8odBd> [Accessed on Nov. 26, 2012]

James, W., and Kuch, A. W. (1998). "CHAPTER 9: Sensitivity-calibration decision-support tools for continuous SWMM modeling: A fuzzy-logic approach." *Modeling the Management of Stormwater Impacts*, W. James. (ed.), Monograph 6, Proceeding of

Conference on the Stormwater and Water Quality Management Modeling Conference, Toronto, 1997, Computational Hydraulics International, Guelph, Ontario.

Javier, J. R. N., Smith, J. A., England, J., Baeck, M. L., Steiner, M. and Ntelekos, A. A. (2007a). "Climatology of extreme rainfall and flooding from orographic thunderstorm systems in the upper Arkansas River Basin." *Water Resources Research*, 43, 1-13

Javier, J. R. N., Smith, J. A., Meierdiercks, K. L., Baeck, M. L., and Miller, A. J. (2007b). "Flash flood forecasting for small urban watersheds in the Baltimore Metropolitan region." *American Meteorological Society*, 22, 1331-1344

Jennings, A. H. (1950). "World's greatest observed point rainfalls." *Hydrometeorological Section*, U. S. Weather Bureau, Washington D. C., 4 – 5

Jiang, R., Xie, J., Li, J., and Chen, T. (2010). "Analysis and 3D visualization of flood inundation based on WebGIS." *2010 International Conference on E-Business and E-Government*, 1638-1641

Jinliang, H., Qingsheng, L., and Huasheng, H. (2009). "Primary study on response of water quality to land use pattern in a medium-sized watershed, southeast of China." *International Forum on Information Technology and Applications*, 225-229

Johnson, B.E., Julien, P.Y., Molnár, D.K., and Watson, C.C. (2000). "The two-dimensional upland erosion model CASC2D-SED." *Journal of the American Water Resources Association*, 36(1), 31-42.

Johnson, D. L., and Miller, A. C. (1997). "A spatially distributed hydrologic model utilizaing raster data structures." *Computer and Geoscinces*, 23(3), 267-272

Jorgeson, J. J. (1999). "Peak flow analysis using a two-dimensional watershed model with radar precipitation data." Ph.D. Thesis, Department of Civil and Environmental Engineering, Colorado State University, Fort Collins, Colorado.

Julien, P. Y. (2002). *River Mechanics*. Cambridge University Press, Cambridge, UK.

Julien, P. Y., and Rojas, R. (2002). "Upland erosion modeling with CASC2D-SED." *International. Journal of Sediment Research*, 17(4), 265-274

Julien, P. Y., Saghafian, B., and Ogden, F. L. (1995). "Raster-Based hydrologic modeling of spatially-varied surface runoff." *Water Resources Bulletin, AWRA*, 31(3), 523-536

Julien, P. Y. and Saghafian, B. (1991). "CASC2D User's Manual – A two-dimensional watershed rainfall-runoff model." *Center of Geoscience – Hydrologic Modeling Group*, Colorado State University (CER90-91PYJ-BS-12)

Juza, B., and Barad, M. F. (2000). "Dynamic and steady state modeling approaches to riverine hydraulic studies using 1-D, looped 1-D and 2-Dimensional topological discretization." *Conference Proceedings of Hydroinformatics*, Iowa City, Iowa

Kang, D. K. (2005). "Distributed snowmelt modeling with GIS and CAS2D at California Gulch, Colorado." M.S. thesis, Department of Civil and Environmental Engineering, Colorado State University, Fort Collins, Colorado.

Katopodes, N.D. (1982). "On zero-inertia and kinematic waves." *Journal of Hydraulic Engineering*, American Society of Civil Engineers 108 (HY11), 1380–1385.

Keckler, P. K. (1995). Surfer for windows, Golden Software Inc., Golden, CO.

Kelly, B. P., and Rydlund Jr., P. H. (2003). "Estimated Flood-Inundation Mapping for the Lower Blue River in Kansas City, Missouri." *USGS Scientific Investigations Report 2006-5089*

Knapp, H. V., Durgunoglu, A., and Ortel, T. W. (1991). *A review of rainfall-runoff modeling for stormwater management*. SWS contract report 516, U. S. Geological Survey, Illinois District

Knight, D.W. and Shiono, K. (1996). "River channel and floodplain hydraulics." In: Anderson, M.G., Walling, D.E., Bates, P.D. (Eds.), *Floodplain Processes*. Wiley, Chichester, pp. 139–182.

Knighton, D. (1998). *Fluvial forms and processes: A new perspective*, Hodder Education, United Kingdom

Krause, P., Boyle, D. P., and Base, F. (2005). "Comparison of different efficiency criteria for hydrological model assessment." *Advances in Geosciences*, 5, 89-97

Kuo, W. L., Steenhuis, T. S., McCulloch, C. E., Mohler, C. L., Weinstein, D. A., DeGloria, S. D., and Swaney, D. P. (1999). "Effect of grid size on runoff and soil moisture for a variable-source-area hydrology model." *Water Resources Research*, 35(11), 3419-3428

Lange, J., Leibundgut, C., Greenbaum, N., and Schick, A.P. (1999). "A non-calibrated rainfall-runoff model for large, arid catchments." *Water Resources Research*, 35(7), 2161-2172

Leavesley, G. H., Lichty, R. W., Troutman, B. M., and Saindon, L. G. (1983). "Precipitation-runoff modeling system: User's manual." *U. S. Geological Survey, Water Resources Investigation Report*, 83-4283, 207

Legate, D. R., and McCabe, G. J. (1999). "Evaluating the use of "goodness-of-fit" measures in hydrologic and hydroclimatic model validation." *Water Resources Research*, 35(1), 233-241

Leopardi, A., Oliveri, E., and Greco, M. (2002). "Two-dimensional modeling of floods to map risk-prone area." *Journal of Water Resources Planning and Management*, 128(3), 168-178.

Li, M., Li, Z., Yao, W., and Liu, P. (2009). "Estimating the erosion and deposition rates in a small watershed by the 137Cs tracing method." *Applied Radiation and Isotopes*, 67, 362-366

Li, R., Sun, T., and Li, G. (2011). "Application of three-dimensional GIS to water resources." *19th International Conference on Geoinformatics*, 1-4

Li, R.M., Stevens, M.A., and Simons, D.B. (1976). "Solutions to Green-Ampt infiltration equations." *Journal of Irrigation and Drainage Division, ASCE*, 239-248

Lim, S. P., and Cheok, H. S. (2009). "Two-dimensional flood modeling of the Damansara River." *Proceedings of the Institute Civil Engineers, Water management*, 162, 13-24

Linsley, R.K., Kohler, M.A., and Paulhus, J. L. H. (1982). *Hydrology for engineers*. McGraw-Hill Book Company, New York, New York, 3rd edition, 508

Liu, Y. B., De-Smedt, F. H., Hoffmann, F., and Pfister, L. (2004). "Parameterization using ArcView GIS in medium and large watershed modeling." *GIS and Remote Sensing in Hydrology, Water Resources and Environment, Proceedings*, 50-58

Loague, K. M., and Freeze, R. A. (1985). "A comparison of rainfall-runoff modeling techniques on small upland catchments." *Water Resources Research*, 21(2), 229-248

Ma, Z. (2008c). "Predicting water quantity and quality in the Taihu Basin." User case studies <http://www.innovyze.com/news/fullarticle.aspx?id=770> [Accessed on Nov. 24, 2011]

Mah, D. Y., Outuhena, F. J., and Said, S. (2007). "Use of Infoworks River Simulation (RS) in Sungai Sarawak Kanan modeling." *Journal of Institute of Engineers, Malaysia*, 68(1), 1-9

Mah, D. Y., Lai, S. H., Chan, R. B., and Putuhena, F. J. (2010). "Investigative modeling of the flood bypass channel in Kuching, Sarawak, by assessing its impact on the inundations of Kuching-Batu Kawa-Bau Expressway." *Structure and Infrastructure Engineering*, 1-10

Mah, D. Y. S.,Hii, C. P., Putuhena, F. J., and Lai, S. H. (2011). "River modeling to infer flood management framework." *Technical Note*

Mamillapalli, S., Srinivasan, R., Arnold, J. G., and Engel, B. A. (1996). "Spatial variability in basin scale hydrologic modeling." *Proceeding of the Third Conference / Workshop on 'Integrating GIS and Environmental Modeling'*, Santa Fe, Mexico

Marks, K. and Bates, P.D. (2000). "Integration of high-resolution topographic data with floodplain flow models." *Hydrological Processes*, 14, 2109–2122.

Marsalek, J., Dick, T. M., Wisner, P. E., and Clarke, W. G. (1975). "Comparative evaluation of three urban runoff models." *Water Resources Bulletin*, 11(2), 306-328

Maslih, K., Ismail, A. A., Yusof, M. F., and Mulup, A. (2011). "Banjir di 4 negeri semakin buruk (Flood at 4 states getting worst)." Utusan Melayu, Feb. 1st, 2011 <http://www.utusan.com.my/utusan/info.asp?y=2011&dt=0201&pub=Utusan_Malaysia &sec=Muka_Hadapan&pg=mh_01.htm#ixzz2DOEzm9T1> [Accessed on Nov. 26, 2012]

Maslih, K. (2012). "Keadaan seperti dilanda tsunami (The situation similar as Tsunami)." Utusan Melayu, March 13, 2012 <http://www.utusan.com.my/utusan/info.asp?y=2012&dt =0313&pub=utusan_malaysia&sec=Dalam_Negeri&pg=dn_09.htm#ixzz2DLYSYUOv> [Accessed on Nov. 26, 2012]

McPherson, M. B. (1978). *Urban Runoff Control Planning*, U. S. Environmental Protection Agency Report EPA-600/9-78-035

Md. Noor, A. (2011). "Banjir landa lebih 20 kanpung di Baling; 2,000 terjejas (More than 20 villages flood-stricken; 1,200 effected)." Utusan Melayu, Aug. 28, 2011 <http://www.utusan.com.my/utusan/info.asp?y=2011&dt=0828&pub=Utusan_Malaysia &sec=Terkini&pg=bt_22.htm#ixzz2DOELbBA2> [Accessed on Nov. 26, 2012]

Md. Noor, A. (2012). "600 rumah ditenggelami banjir (Flood submerged 600 houses)." Utusan Melayu Nov. 26, 2012 <http://www.utusan.com.my/utusan/Utara/20121126/wu_01/600-rumah-ditenggelami-banjir#ixzz2DLZPcPAm> [Accessed on Nov. 26, 2012]

Melching, C. S., Yen, B. C., and Wenzel, H. G. (1991). "Output reliability as guide for selection of rainfall-runoff models." *ASCE Journal of Water Resources Planning and Management*, 117(3), 383-398

Merwade, V., Cook, A., and Coonrod, J. (2008). "GIS techniques for creating river terrain models for hydrodynamic modeling and flood inundation mapping." *Environmental Modeling and Software*, 23, 1300-1311

Mishra, S. (2009). "Uncertainty and sensitivity analysis techniques for hydrologic modeling." *Journal of Hydroinformatics*, 11.3-4, 282-296

MMD (2007). "Extreme weather events." Malaysian Meteorological Department (MMD) and Ministry of Science, Technology and Innovation (MOSTI), 2007 Annual Report, p. 71-74

MMD (2008). "Extreme weather events." Malaysian Meteorological Department (MMD) and Ministry of Science, Technology and Innovation (MOSTI), 2008 Annual Report, p. 79-83

MMD (2009). "Extreme weather events." Malaysian Meteorological Department (MMD) and Ministry of Science, Technology and Innovation (MOSTI), 2009 Annual Report, p. 103-108

MMD (2010). "Extreme weather events." Malaysian Meteorological Department (MMD) and Ministry of Science, Technology and Innovation (MOSTI), 2010 Annual Report, p. 103-108

Mohd, H., and Perimbanayagam, K. (2011). "Flash flood in several areas in KL." New Straits Times, Dec. 3rd, 2011 <Flash flood in several areas in KL - New Straits Times http://www.nst.com.my/flash-flood-in-several-areas-in-kl-1.18803#ixzz2DRY4rjOG> [Accessed on Nov. 26, 2012]

Mohammed, T. A., Said, S., Bardaie, M. Z., and Basri, S. N. (2011). "Numerical simulation of flood levels for tropical rivers." *IOP Conference Series: Materials Science and Engineering*, 17, 1-10

Molnar, D. K. (1997). "Grid size selection for 2-D hydrologic modeling of large watersheds." Ph.D. thesis, Department of Civil Engineering, Colorado State Univ., Fort Collins, Colorado

Molnar, D. K., and Julien, P. Y. (2000). "Grid-size effects on surface runoff modeling." *Journal of Hydrology*, 5(1), 8-16

Moriasi, D. N., Arnold, J. G., Van-Liew, M., W., Bingner, R. L., Harmel, R. D. and Veith, T. L. (2007). "Model evaluation guidelines for systematic quantification of accuracy in watershed simulations." *American Society of Agricultural and Biological Engineers*, 50(3), 885-900

Morris, E. M. (1980). "Forecasting flood flows in grassy and forested basins using a deterministic distributed mathematical model." *Proceedings of the Oxford Symposium*, IAHS Publication, 129, 247-255

Morris, E.M., and Woolhiser, D.A., (1980). "Unsteady one-dimensional flow over a plane: partial equilibrium and recession hydrographs." *Water Resources Research,* 16, 355–360.

Mountz, T. W., and Crowley, J. (2009). "Comparison of HEC-RAS and InfoWorks RS: A case study in Grand Praire, Texas." *World Environmental and Water Resources Congress*, 2853-2862

Moussa, R. and Bocquillon, C. (1996). "Criteria for the choice of flood-routing methods in natural channels." *Journal of Hydrology*, 186 (1–4), 1–30.

Moussa, R. and Bocquillon, C. (2000). "Approximation zones of the Saint-Venant equations for flood routing with overbank flow." *Hydrology and Earth System Sciences*, 4(2), 251–261.

MSMA (2000). "Urban Stormwater Management Manual (MSMA Manual)." *Jabatan Pengairan dan Saliran Malaysia (DID – Department of Irrigation and Drainage, Malaysia)*, 13-3

Musser, J. W., and Dyar T. R. (2005). "Two-Dimensional Flood-Inundation Model of the Flint River at Albany, Georgia." *Proceedings of the 2005 Georgia Water Resources Conference*, University of Georgia, Athens, Georgia, April 25 – 27 2005

myMetro (2012). "Mangsa banjir di Selangor 1,820 orang setakat pagi ini (1,820 flood victims in Selangor)." myMetro, Nov. 7, 2012 < http://www.hmetro.com.my/articles/ MangsabanjirdiSelangor1_820orangsetakatpagiini/Article> [Accessed on Nov. 28, 2012]

NAHRIM (2008). "Technical guideline for estimating probable maximum precipitation for design floods in Malaysia." *NAHRIM Technical Research Publication No. 1 (TRP 1)*

Nash, J. E., and Sutcliffe, J. V. (1970). "River flow forecasting through conceptual models, Part 1 - A discussion of principles." *Journal of Hydrology*, 10(3), 282-290

Nathan, R. J., and Weinmann, P.E. (1999). "Estimation of Large to Extreme Floods: Book VI" in *Australian Rainfall and Runoff, A Guide to Flood Estimation*, The Institution of Engineers, Australia.

Ni, G. H., Liu, Z. Y., Lei, Z. D., Yang, D. W., and Wang, L. (2008). "Watershed of the Loess Plateau with distributed model." *Journal of Hydrologic Engineering*, 13(5), 392-399

Noh, M. H. (2008b). "Use of InfoWorks to tackle flooding in Malaysia." User case studies <http://www.innovyze.com/news/fullarticle.aspx?id=836> [Accessed on Nov. 24, 2011]

Nor, N. I. A., Harun, S., and Kassim, A. H. M. (2007). "Radial basis function modeling of hourly streamflow hydrograph." *Journal of Hydrologic Engineering*, 12(1), 113-123

Ogden, F.L. (1992). "Two-dimensional runoff modeling with weather radar data." Ph.D. Thesis, Department of Civil and Environmental Engineering, Colorado State University, Fort Collins, Colorado.

Ogden, F.L., and Julien, P.Y. (1993). "Runoff sensitivity to temporal and spatial rainfall variability at runoff plane and small basin scales." *Water Resources Research*, 29(8), 2589-2597.

Ogden, F.L., and Julien, P.Y. (1994). "Runoff model sensitivity to radar rainfall resolution." *Journal of Hydrology*, 158, 1-18.

Ogden, F.L., Sharif, H.O., Senarath, S.U.S., Smith, J.A., Baeck, M.L., and Richardson, J.R. (2000). "Hydrologic analysis of the Fort Collins, Colorado, flash flood of 1997." *Journal of Hydrology*, 228, 82-100.

Ogden, F.L., and Julien, P.Y. (2002). "CHAPTER 4: CASC2D: A Two-Dimensional, Physically-Based, Hortonian Hydrologic Model." *Mathematical Models of Small Watershed Hydrology and Applications*, Singh, V.P. and Frevert, D. (eds.), Water Resources Publications, Littleton, CO, pp. 69-112.

Ogden, F. L. (2000). "CASC2D Reference Manual, Version 2.0." *Department of Civil and Environmental Engineering*, University of Connecticut: Storrs, CT.

Overton, D. E., and Meadows, M. E. (1976). *Stormwater Modeling*, Academic Press, Inc.

Papadakis, C. N., and Preul, H. C. (1973). "Testing of methods for determination of urban runoff." *ASCE Journal of the Hydraulic Division*, 99 (HY9), 1319-1335

Papanicolaou, A. N., Elhakeem, M., and Wardman, B. (2009). "Calibration and verification of a 2D hydrodynamic model for simulating flow around emergent bendway weir structure." *Journal of Hydraulic Engineer*, 137(1), 75-89

Peterson, M. P. (ed.) (1995). *Interactive and animated cartography*. Englewood Cliffs, NJ, Prentice Hall

Poon, H. C., and Hwee, H. H. (2010). "Probable maximum precipitation derivation in Malaysia: Review and comparison." *International Journal of Hydro-Climate Engineering*, 37-73

Ponce, V. M. (1990). "Generalized diffusive wave equation with inertial effects." *Water Resources Research*, 26(5), 1099–1101.

Ponce, V. M., Li, R. M. and Simons, D. B. (1978). "Applicability of kinematic and diffusion models." *Journal of Hydraulic Division*, American Society of Civil Engineers 104 (HY3), 353–360.

Rahman, A. A., Pilouk, M., and Zlatanova, S. (2001). "The 3D GIS software development: Global efforts from researchers and vendors." *Geoinformation Science Journal, Universiti Teknologi Malaysia*, 1(13), 1-13

Rawls, W. J, Ahuja, L. R., Brakensiek, D. L., and Shirmohammadi, A. 1993. "Infiltration and Soil Movement." *Handbook of Hydrology*, Maidment, D.R., (ed). McGrawHill, Inc., New York, New York. pp 5.1-5.51.

Razi, M. A. M., Ariffin, J., Tahir, W., and Arish, N. A. M. (2010). "Flood estimation studies using hydrologic system (HEC-HMS) for Johor River, Malaysia." *Journal of Applied Sciences*, 10(11), 930-939

REDAC (2006). "Design option of the flood mitigation plan of Sg. Muda, Sungai Muda, Kedah." *Report*, REDAC-USM, September 2006

Refsgaard, J. C., and Storm, B. (1995). "Chapter 23: MIKE-SHE, Computer models of watershed hydrology." *Computer Model of Watershed Hydrology*, V. P. Singh, ed., Water Resources Publications, 809-846

Refsgaard, J. C. (1997). "Paramerization, calibration and validation of distributed hydrological models." *Journal of Hydrology*, 198, 69-97

Richardson, W. L., Smith, V. E., and Wethington, R. (1983). "Dynamic Mass Balance of PCB and Suspended Solids in Saginaw Bay – A Case Study." *Physical Behavior of PCBs in*

the Great Lakes, Mackay, D., Patterson, S. and Eisenreich, S. J. (eds.), Ann Arbor Science Publishers, Ann Arbor, Michigan, 329-366

Rogers, C. C. M., Beven, K., Morris, E. M., and Anderson, M. G. (1985). "Sensitivity analysis, calibration and predictive uncertainty of the Institute of Hydrology Distributed Model." *Journal of Hydrology*, 81, 179-191

Said, S., Mah, D. Y. S., Sumok, P., and Lai, S. H. (2009). "Water quality monitoring of Maong River, Malaysia." *Proceedings of the Institute Civil Engineers, Water management*, 162, 35-40

Sánchez, R. R. (2002). "GIS-based upland erosion modeling, geovisualization and grid size effects on erosion simulations with CASC2D-SED." Ph.D thesis, Department of Civil and Environmental Engineering, Colorado State University, CO

Saghafian, B. (1992). "Hydrologic analysis of watershed response to spatially varied infiltration." Ph.D thesis, Department of Civil and Environmental Engineering, Colorado State University, CO

Servat, E., and Dezetter, A. (1991). "Selection of calibration objective functions in the context of rainfall-runoff modeling in a Sudanese savannah area." *Journal of Hydrological Science*, 36(4), 307-330

Scoging, H., Parsons, A. J., and Abrahams, A. D. (1993). "Application of a dynamic overland-flow hydraulic model to a semi-arid hillslope, Walnut Gulch, Arizona." *Overland Flow: Hydraulics and Erosion Mechanics*, A. J. Parsons and A. D. Abrahams, eds., Chapman & Hall, New York, 1st Edition.

Schumann, G., Matgen, P., Cutler, M. E. J., Black, A., Hoffman, L., and Pfister, L. (2008). "Comparison of Remotely Sensed Water Stages from LiDAR, Topographic Contours and SRTM. *ISPRS Journal of Photogrammetry and Remote Sensing*, 63, 283-296

Shafie, A. (2009). "Extreme flood event: A case study on floods of 2006 and 2007 in Johor, Malaysia." Technical report, Department of Civil and Environmental Engineering, Colorado State University, Fort Collins, Colorado.

Sharif, H. O., Sparks, L., Hassan, A. A., Zeitler, J. and Xie, H. (2010). "Application of a distributed hydrologic model to the November 17, 2004, flood of Bull Creek watershed, Austin, Texas." *Journal of Hydrology Engineering*, 15(8), 651-657

Shaver, E., Horner, R., Skupien, J., May, C., and Ridley, G. (2007). "Fundamentals of urban runoff management." *Technical and Institutional Issues*, 15-41

Shah, S. M. S, O'Connell, P. E., and Hosking, J. R. M. (1996). "Modelling the effects of spatial variability in rainfall on catchment response. 1. Formulation and calibration of a stochastic rainfall field model." *Journal of Hydrology*, 175, 67-88

Shepard, D. (1968). "A two-dimensional interpolation function for irregularly-spaced data." *Proceedings of the 1968 ACM National Conference*, 517–524

Shrestha, R., Tachikawa, Y. and Takara, K. (2002). "Effect of forcing data resolution in river discharge simulation." *Annual Journal of Hydraulic Engineering JSCE*, 46, 139-144

Shrestha, R., Tachikawa, Y. and Takara, K. (2006). "Input data resolution analysis for distributed hydrological modeling." *Journal of Hydrology*, 319, 36-50

Shultz, M. J., and Robert J. C. (2006). " Development, Calibration, and Implementation of a Distributed Model for use in Real-Time River Forecasting." *Proceedings of the 3rd Federal Interagency Hydrologic Modeling Conference*, Reno, Nevada

Siang, L.C., Abdullah, R., Zakaria, N. A., Ghani, A. A., and Kiat, C. C. (2007). "Modelling urban river catchment: A case study of Berop River, Tanjong Malim, Perak." *2nd International conference on managing rivers in the 21st century: Solution towards sustainable rivers basin*, 165-171

Singh, V. P. (1995). *Computer models of watershed hydrology*, Water Resources Publication

Singh, V. P. (1989). *Hydrologic Systems*. Watershed Modeling. Volume II. Prentice Hall, Englewood Cliffs, New Jersey

Singh, J., Knapp, H. V., Arnold, J. G., and Demissie, M. (2005). "Hydrological modeling of the Iroquois river watershed using HSPF and SWAT." *Journal of The American Water Resources Association*, 41(2), 343 -360

Sinyang, A. (2012). "Banjir 'tsunami' Lembah Klang (Tsunami-flood in Lembah Klang)." Utusan Melayu, May 3rd, 2012 <http://www.utusan.com.my/utusan/Dalam_Negeri/20120503/dn_09/Banjir-%27tsunami%27--Lembah-Klang#ixzz2DLaSD9dB> [Accessed on Nov. 26, 2012]

Sivapalan, M., and Young, P. C. (2004). "134: Downward approach to hydrological model development." *Encyclopedia of Hydrological Sciences*, Anderson, M. G. (ed.), John Wiley & Sons, Ltd.

Skøien, J. O., Blöschl, G., and Western, G. (2003). "Characteristic space scales and timescales in hydrology." *Water Resources Research*, 39(10), 11-19

Sloan, A. (2009). "InfoWorks RS forms basis for flood map of Nothern Ireland." User case studies <http://www.innovyze.com/news/fullarticle.aspx?id=870> [Accessed on Nov. 24, 2011]

Smith, R. E., and Parlange, J. Y. (1978). "A parameter efficient hydrologic infiltrations model." *Water Resources Research*, 14(3), 533-538

Smith, M. B., Dong-Jun, S., Victor I. K., Seann, M. R., Ziya, Z., Qingyun, D., Fekadu, M., and Shuzheng, C. (2004a). "The Distributed Model Intercomparison Project (DMIP): Motivation and Experiment Design." *Journal of Hydrology*, 298, 4-26

Smith, M. B., and Konstantine P. G. (2004b). "The Distributed Model Intercomparison Project (DMIP) – preface." *Journal of Hydrology*, 298, 1-3

Smith, J. A., Baeck, M. L., Meierdiercks, K. L., Nelson, P. A., Miller, A. J., and Holland, E. J. (2005a). "Field studies of the storm event hydrologic response in an urbanizing watershed." *Water Resources Research*, 41, 1-15

Smith, J. A., Miller, A. J., Baeck, M. L., Nelson, P. A., Fisher, G. T., and Meierdiercks, K. L. (2005b). "Extraordinary flood response of a small urban watershed to short-duration convective rainfall." *American Meteorological Society*, 6, 599-617

Smith, J. A., Baeck, M. L., Meierdiercks, K. L., Miller, A. J., and Krajewski, W. F. (2007). "Radar rainfall estimation for flash flood forecasting in small urban watersheds." *Advanced in Water Resources*, 30, 2087-2097

Smith, J. A. (1993), "CHAPTER 3: Precipitation." *Handbook of Hydrology*, Maidment, D. R. (ed.), McGraw-Hill, Inc.,

Suhaila, J., and Jemain, A. A. (2008). "Fitting the Statistical Distribution for Daily Rainfall in Peninsular Malaysia Based on AIC Criterion." *Journal of Applied Sciences Research*, 4(12), 1846 – 1857

Suhaila, J., and Jemain, A. A. (2007). "Fitting the statistical distributions to the daily rainfall amount in Peninsular Malaysia." *Jurnal Teknologi, Universiti Teknologi Malaysia*, 46(C), 33-48

Sulaiman, M., El-Shafie, A., Karim, O., and Basri, H. (2011). "Improved water level forecasting performance by using optimal steepness coefficients in an artificial neural network." *Water Resources Management*, 25, 2525-2541

Syme, W. J. (2001). "TUFLOW – Two & one-dimensional unsteady flow software for rivers, estuaries and coastal waters." *Institute Engineer Australia*, Seminar, Sydney, Feb. 2001.

Taucan, R. D., Alaui, S. A., and Latib, M. S. A. (2011). "Banjir Kelantan makin teruk (Flood in Kelantan getting worst)." Utusan Melayu, Jan. 9, 2011 <http://www.utusan.com.my/utusan/info.asp?y=2011&dt=0109&pub=Utusan_Malaysia&sec=Dalam_Negeri&pg=dn_07.htm#ixzz2DOB71mnx> [Accessed on Nov. 26, 2012]

Tayefi, V., Lane, S. N., Hardy, R. J., and Yu, D. (2007). "A comparison of one- and two-dimensional approaches to modeling flood inundation over complex upland floodplains." *Hydrologic Processes*, 21(23), 3190 – 3202.

Teo, F. Y., Falconer, R. A., and Lin, B. (2009). "Modelling effects of mangroves on tsunamis." *Proceedings of the Institute Civil Engineers, Water management*, 162, 3-12

Toriman, M. E., Hassan, A. J., Gazim, M. B., Mokhtar, M., Sharifah-Mastura, S. A., Jaafar, O., Karim, O., and Abdul-Aziz, N. A. (2009). "Integration of 1-d hydrodynamic model and GIS approach in flood management study in Malaysia." *Research Journal of Earth Sciences*, 1(1), 22-27

USACE (2008). "The Mississippi River & Tributaries Project: Designing the Project Flood." *Information Paper – April 2008*, p.12

USNRC (1980). *Design Basis Floods for Nuclear Power Plants: Regulatory Guide 1.59*, 1.59-11 – 1.59-39.

Usul, N., and Pasaogullari, O. (2004). "Effect of map scale and grid size for hydrological modeling." *GIS and Remote Sensing in Hydrology, Water Resources and Environmental*, (Proceeding of ICGRHWE held at the Three Gorges Dam, China), IAHS Publication, 91-100

Utusan (2011a). "Banjir: Kelantan makin parah (Flood: Getting worst in Kelantan)." Utusan Melayu, Jan. 8, 2011 <http://www.utusan.com.my/utusan/info.asp?y=2011&dt=0108&pub=Utusan_Malaysia&sec=Terkini&pg=bt_04.htm#ixzz2DOSMvXwG> [Accessed on Nov. 26, 2012]

Utusan (2011b). "Terengganu banjir, hujan sejak malam semalam (Flood in Terengganu, whole night rain)." Utusan Melayu, March 29, 2011 <http://www.utusan.com.my/utusan/info.asp?y=2011&dt=0329&pub=Utusan_Malaysia&sec=Terkini&pg=bt_03.htm#ixzz2DODacWYI> [Accessed on Nov. 26, 2012]

Utusan (2011c). "Mangsa banjir di Kelantan meningkat (Flood victims in Kelantan is increasing)." Utusan Melayu, Nov. 25, 2011 <http://www.utusan.com.my/utusan/info.asp?y=2011&dt=1125&pub=Utusan_Malaysia&sec=Terkini&pg=bt_08.htm#ixzz2DORaEvd5> [Accessed on Nov. 26, 2012]

Utusan (2012a). "Beberapa kampong dilanda banjir kilat (Flash flood at several villages)." Utusan Melayu, Jan. 22nd, 2012 <http://www.utusan.com.my/utusan/info.asp?y=2012&dt=0122&pub=Utusan_Malaysia&sec=Timur&pg=wt_02.htm#ixzz2DOub4opA> [Accessed on Nov. 26, 2012]

Utusan (2012b). "Banjir kali ini paling teruk – Penduduk (The worst flood)." Utusan Melayu, Feb. 21st, 2012 <http://www.utusan.com.my/utusan/info.asp?y=2012&dt=0221&pub=Utusan_Malaysia&sec=Utara&pg=wu_02.htm#ixzz2DOCxZg5n> [Accessed on Nov. 26, 2012]

Utusan (2012c). "Mangsa cerita detik cemas rumah dilanda banjir (Experienced flood victims)." Utusan Melayu, Apr. 20, 2012 <http://www.utusan.com.my/utusan/Dalam_Negeri/20120420/dn_12/Mangsa-cerita-detik-cemas-rumah-dilanda-banjir#ixzz2DOlKJtRO> [Accessed on Nov. 26, 2012]

Utusan (2012d). "Bandar raya Georgetown dilanda banjir kilat (Georgetown city flooded)." Utsan Melayu, Aug. 6, 2012 <http://www.utusan.com.my/utusan/Dalam_Negeri/20120806/dn_29/Bandar-raya-Georgetown-dilanda-banjir-kilat#ixzz2DOmTVvuS> [Accessed on Nov. 26, 2012]

Utusan (2012e). "Banjir kilat landa Kampung Jalan Tengku Putra (Flood at Kg. Jalan Tengku Putra)." Utusan Melayu, Nov. 16, 2012 <http://www.utusan.com.my/utusan/Utara/20121116/wu_03/Banjir-kilat-landa-Kampung-Jalan-TengkuPutra#ixzz2DOlxRs3U> [Accessed on Nov. 26, 2012]

Valeo, C., and Moin, S. M. A. (2000). "Grid-resolution effects on a model for integrating urban and rural areas." *Hydrological Processes*, 14, 2505-2525

Vázquez, R. F., Feyen, L., Feyen, J., and Refgaard, J. C. (2002). "Effect of grid size on effective parameters and model performance of the MIKE-SHE code." *Hydrological Processes*, 16, 355-372

Vieux, B. E. (2001a). "Distributed Hydrologic Modeling Using GIS." *Kluwer Academic Publishers*, Norwell, Massachusetts, Water Science Technology Series, 38, 293

Vieux, B. E. (2001b). "Chapter 11: Radar Rainfall Applications in Hydrology". *Hydrology and Floodplain Analysis*, P. B. Bedient, and W.C. Huber, eds., Addison-Wesley Publishing Co., Reading, Massachusetts, 3rd Edition

Vieux, B. E., and Vieux, J. E. (2002). "Vflo™: A Real-time Distributed Hydrologic Model." *Proceedings of the 2nd Federal Interagency Hydrologic Modeling Conference*, Las Vegas, Nevada

Vieux, B.E., and Fekadu, G. M. (2003). "Ordered Physics-Based Parameter Adjustment of a Distributed Model." *Calibration of Watershed Models*, Vol. 6, p. 267-281

Vieux, B. E. (2004). "CHAPTER 2: Data Sources and Strudture." *Distributed Hydrologic Modeling Using GIS*, Vieux, B. E. (ed.), Water Science and Technology Library, 2nd Edition.

Velleux, M., Julien, P. Y., Rojas-Sanchez, R., Clements, W., and England, J. (2006). "Simulation of metals transport and toxicity at a mine-impacted watershed: California Gulch, Colorado." *Environmental Science and Technology*, 40(22), 6996-7004

Velleux, M., England, J., and Julien, P. Y. (2008). "TREX: spatially distributed model to assess watershed contaminant transport and fate." *Science of the Total Environment*, 404(1), 113-128

Velleux, M. (2005). "Spatially distributed model to assess watershed contaminant transport and fate." Ph.D thesis, Department of Civil and Environmental Engineering, Colorado State University, CO

Votteler, T. H. (2002). "Flood Texas Parks & Wildlife Magazine" March, 60(3), 38-53

Wagner, C. R., and Mueller, D. S. (2001). "Calibration and Validation of a Two-Dimensional Hydrodynamic Model of the Ohio River, Jefferson County, Kentucky." *Water Resources Investigations Report 01-4091*

Wan Alias, W. N. H. (2012). "Banjir landa Batang Kali (Flood-stricken Batang Kali)." Utusan Melayu, May 8, 2012 <http://www.utusan.com.my/utusan/Dalam_Negeri/20120508/dn_13/Banjir-landa-Batang-Kali#ixzz2DLWg1D8U> [Accessed on Nov. 26, 2012]

Wan-Zin, W. Z., Jemain, A. A., Ibrahim, K., Suhaila, J., and Sayang, M. D. (2009a). "A comparative study of extreme rainfall in Peninsular Malaysia: with reference to partial duration and annual extreme series." *Sains Malaysiana*, 38(5), 751-760

Wan-Zin, W. Z., Jemain, A. A., and Ibrahim, K. (2009b). "The best fitting distribution of annual maximum rainfall in Peninsular Malaysia based on methods of L-moment and LQ-moment." *Theory and Application in Climatology*, 96, 337-344

Wang, C., Wan, T. R., and Palmer, I. J. (2007). "A real-time dynamic simulation scheme for large-scale flood hazard using 3D real world data." *11th International Conference Information Visualization*, 607-612

Wardah, T., Bakar, S. H. A., Bardossy, A., and Maznorizan, M. (2008). "Use of geostationary meteorological satellite images in convective rain estimation for flash-flood forecasting." *Journal of Hydrology*, 356, 283-298

Watson, D. F. and Philip, G. M. (1985). "A refinement of inverse distance weighted interpolation." *Geo-Processing,* 2, 315-327.

Wilcox, B. P., Raels, W. J., Brakensiek, D. L., and Wight, J. R. (1990). "Predicting runoff from rangeland catchments: A comparison of two models." *Water Resources Research*, 26(10), 2401-2410

WMO (World Meteorological Organization) (1975). "Intercomparison of conceptual models used in operational hydrological forecasting." *WMO Operational Hydrology Report No. 7*, WMO – No. 429, Geneva, Switzerland.

Wood, E. F., Sivapalan, M., Beven, K., and Band, L. (1988). "Effects of spatial variability and scale with implications to hydrologic modeling." *Journal of Hydrology*, 102, 29-47

Woolhiser, D. A. (1996). "Search for Physically Based Runoff Model—A Hydrologic El Dorado?." *Journal of Hydraulic Engineering*, 122(3), 122-129.

Woolhiser, D. A. and Liggett, J. A. (1967). "Unsteady one-dimensional flow over a plane: The rising hydrograph." *Water Resources Research*, 3(3), 753–771.

Wu, S., Li, J., and Huang, G. H. (2007). "Modeling the effects of elevation data resolution on the performance of topography-based watershed runoff simulation." *Environmental Modelling and Software*, 22, 1250-1260Xevi, E., Christiaens, K., Espino, A., Sewnandan, W., Mallants, D., Sorensen, H., and Feyen, J. (1997). "Calibration, validation and sensitivity analysis of MIKE-SHE model using Neuenkirchen catchment as case study." *Water Resources Management*, 11, 219-242

Yaolin, L., and Zhijun, L. (2005). "A study on estimation of the amount of soil erosion in small watershed based on GIS: A case study in the Three Gorge area of China." *IEEE International Geoscience and Remote Sensing Symposium Proceedings*, Seoul, Korea

Yusop, Z., Chan, C. H., and Katimon, A. (2007). "Runoff characteristics and application of HEC-HMS for modeling stormflow hydrograph in oil palm catchment." *Water Science Technology*, 56(8), 41-48

Zakaria, N. A., Azamathulla, H. M., Chang, C. K., and Ab. Ghani, A. (2010). "Gene expression programming for total bed material load estimation – a case study." *Science of the Total Environment*, 408, 5078 – 5085

Zhang, W., and Montgomery, D. R. (1994). "Digital elevation model grid size, landscape representation, and hydrologic simulations." *Water Resources Research*, 30(4), 1019-1028

Zhao, G. J., Hörmann, G., Fohrer, N., and Gao, J. F. (2009). "Impacts of spatial data resolution on simulated discharge, a case study of Xitiaoxi catchment in South China." *Advances in Geosciences*, 21, 131-137

Zhou, Y., Wu, B., and Meng, J. (2005). "Design and implementation of small watershed management information system." *Geoscience and Remote Sensing Symposium, IGARSS Proceedings*, 590-592

APPENDIX A

TABLES AND GRAPHS FOR CALIBRATION/VALIDATION, LARGE AND EXTREME EVENTS

Table A1 Value of peak discharge, rainfall intensity (mm/hr) and total rainfall (depth in mm) at small watershed

FLOOD EVENTS		RAINFALL DURATION, T_{RD} (Hour)							
		1	**2**	**3**	**4**	**5**	**12**	**14**	**16**
2-years	Q_p	14	21	22	22	21	14	12	10
	i	54	35	26	21	18	8	7	6
	$i \times T_{RD}$	54	70	79	84	88	96	97	96
5-years	Q_p	22	32	42	45	46	28	23	18
	i	64	43	32	26	22	10	9	7
	$i \times T_{RD}$	64	85	97	105	110	120	119	118
10-years	Q_p	29	45	55	60	62	43	35	27
	i	72	48	37	30	25	11	10	8
	$i \times T_{RD}$	72	96	110	118	124	134	134	133
20-years	Q_p	35	54	66	72	74	57	51	42
	i	80	53	40	32	27	12	11	9
	$i \times T_{RD}$	80	106	120	129	136	149	150	149
50-years	Q_p	43	65	81	85	85	65	59	53
	i	88	58	44	36	30	14	12	10
	$i \times T_{RD}$	88	116	133	143	150	163	162	162
100-years	Q_p	50	76	89	91	90	71	65	59
	i	95	62	47	38	32	15	12	11
	$i \times T_{RD}$	95	125	141	152	160	174	174	173
		RAINFALL DURATION, T_{RD} (Hour)							
		1	**2**	**3**	**4**	**6**	**12**	**14**	**16**
S-PMP	Q_p	141	---	278	---	418	520	---	---
	i	188	---	100	---	65	43	---	---
	$i \times T_{RD}$	188	---	300	---	391	518	---	---
		RAINFALL DURATION, T_{RD} (Hour)							
		2	**4**	**6**	**8**	**10**	**12**	**14**	**16**
World's event	Q_p	493	888	1164	1321	1358	1275	1072	750
	i	187	133	110	95	86	78	73	68
	$i \times T_{RD}$	374	532	660	760	860	936	1019	1092

Note: Qp = Peak discharge in cms; i = rainfall intensity in mm/hr; i x T_{RD} = Total rainfall in mm

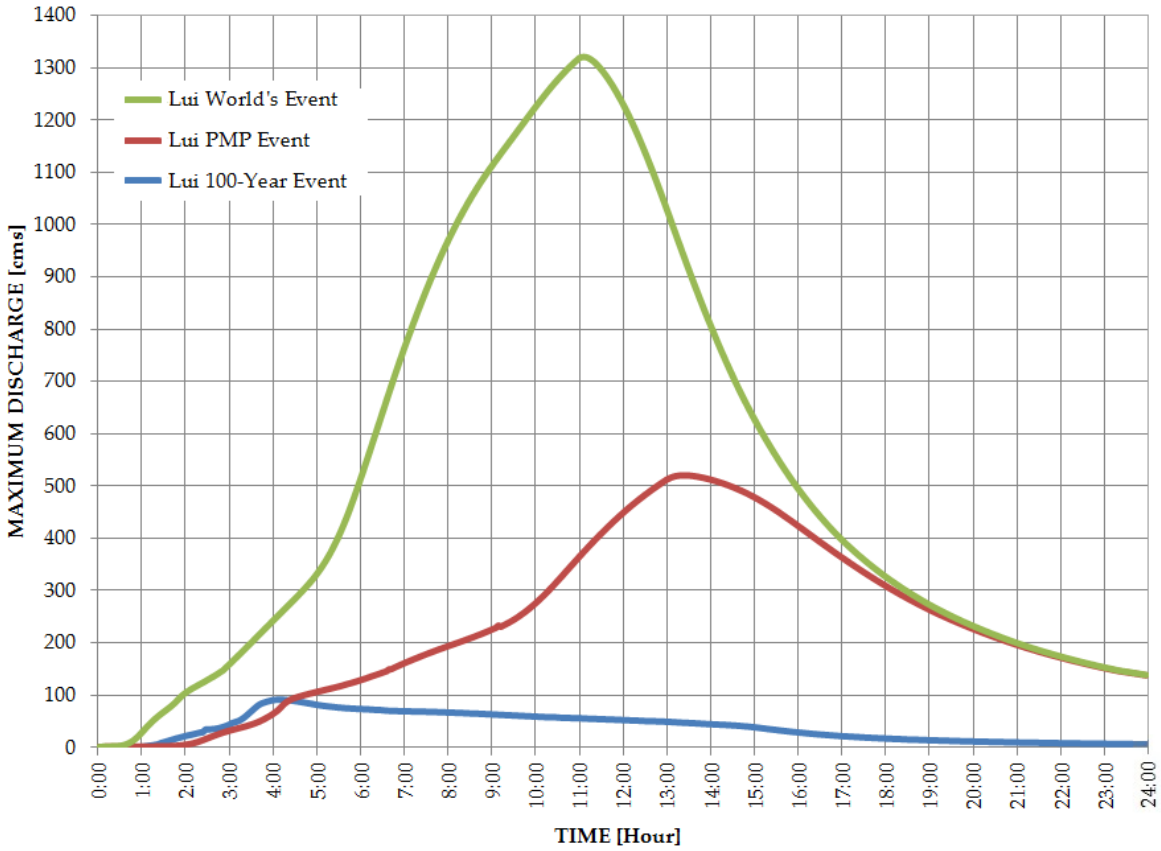

Figure A1 The hydrograph of the highest MED for 100-year return period, S-PMP and WL events at small watershed

Table A2 Value of peak discharge, rainfall intensity (mm/hr) and total rainfall (depth in mm) at medium watershed

FLOOD EVENTS		RAINFALL DURATION, T_{RD} (Hour)							
		1	**2**	**3**	**4**	**5**	**12**	**14**	**16**
2-years	Q_p	89	114	135	143	147	142	139	136
	i	54	35	26	21	18	8	7	6
	$i \times T_{RD}$	54	70	79	84	88	96	97	96
5-years	Q_p	106	130	150	160	164	167	163	157
	i	64	43	32	26	22	10	9	7
	$i \times T_{RD}$	64	85	97	105	110	120	119	118
10-years	Q_p	116	158	194	205	206	202	200	179
	i	72	48	37	30	25	11	10	8
	$i \times T_{RD}$	72	96	110	118	124	134	134	133
20-years	Q_p	124	180	205	214	219	226	224	210
	i	80	53	40	32	27	12	11	9
	$i \times T_{RD}$	80	106	120	129	136	149	150	149
50-years	Q_p	135	197	219	229	236	242	238	234
	i	88	58	44	36	30	14	12	10
	$i \times T_{RD}$	88	116	133	143	150	163	162	162
100-years	Q_p	148	209	227	240	249	256	251	246
	i	95	62	47	38	32	15	12	11
	$i \times T_{RD}$	95	125	141	152	160	174	174	173
		RAINFALL DURATION, T_{RD} (Hour)							
		1	**2**	**3**	**4**	**6**	**12**	**14**	**16**
S-PMP	Q_p	304	---	643	---	1023	1474	---	---
	i	188	---	100	---	65	43	---	---
	$i \times T_{RD}$	188	---	300	---	391	518	---	---
World's event	Q_p	501	---	1513	---	2717	3793	3774	3562
	i	261	---	153	---	110	78	73	68
	$i \times T_{RD}$	261	---	460	---	658	941	1019	1092

Note: Qp = Peak discharge in cms; i = rainfall intensity in mm/hr; i x T_{RD} = Total rainfall in mm

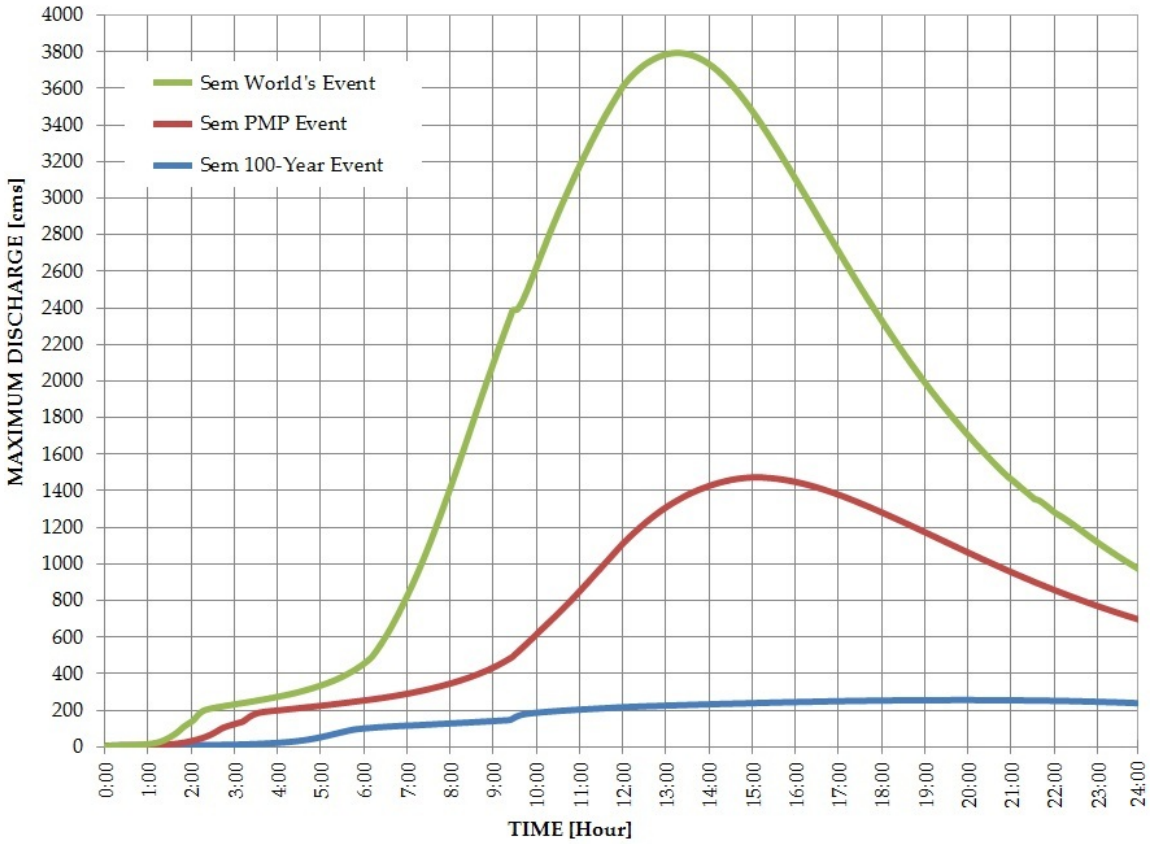

Figure A2 The hydrograph of the highest MED for 100-year return period, S-PMP and WL events at medium watershed

Table A3 Value of peak discharge, rainfall intensity (mm/hr) and total rainfall (depth in mm) at large watershed

FLOOD EVENTS		RAINFALL DURATION, T_{RD} (Hour)								
		1	**3**	**6**	**12**	**24**	**48**	**72**	**150**	**168**
2-years	Q_p	29	38	62	76	101	138	222	300	368
	h	1.08	1.28	1.71	1.93	2.30	2.69	3.07	3.46	3.47
	i	67	35	22	14	10	7	5	4	4
	$i \times T_{RD}$	67	104	133	172	228	312	389	660	672
50-years	Q_p	53	83	116	199	310	452	654	853	920
	h	1.56	2.04	2.45	2.93	3.51	3.75	4.34	4.84	5.00
	i	118	66	50	31	21	14	11	9	7
	$i \times T_{RD}$	118	199	300	367	497	677	814	1305	1226
100-years	Q_p	62	97	136	251	384	562	808	995	1023
	h	1.71	2.22	2.66	3.22	3.67	4.29	4.73	5.18	5.24
	i	130	73	50	34	23	16	12	9	8
	$i \times T_{RD}$	130	218	300	409	554	749	893	1380	1277
KT-PMP	Q_p	210	255	528	994	1304	2396	2721	2982	3016
	h	3.00	3.24	4.41	5.17	5.83	7.76	8.25	8.64	8.69
	i	186	74	59	44	27	19	15	11	9
	$i \times T_{RD}$	186	223	353	528	655	926	1066	1620	1529
World's event	Q_p	297	743	1224	2453	3996	6552	7680	8332	8010
	h	3.45	5.14	5.67	7.85	10.01	12.94	14.09	14.72	14.41
	i	261	153	110	78	56	40	33	26	22
	$i \times T_{RD}$	261	460	658	941	1346	1925	2376	3870	3679

Note: Qp = Peak discharge in cms; h = Stage in m; i = rainfall intensity in mm/hr; i x T_{RD} = Total rainfall in mm

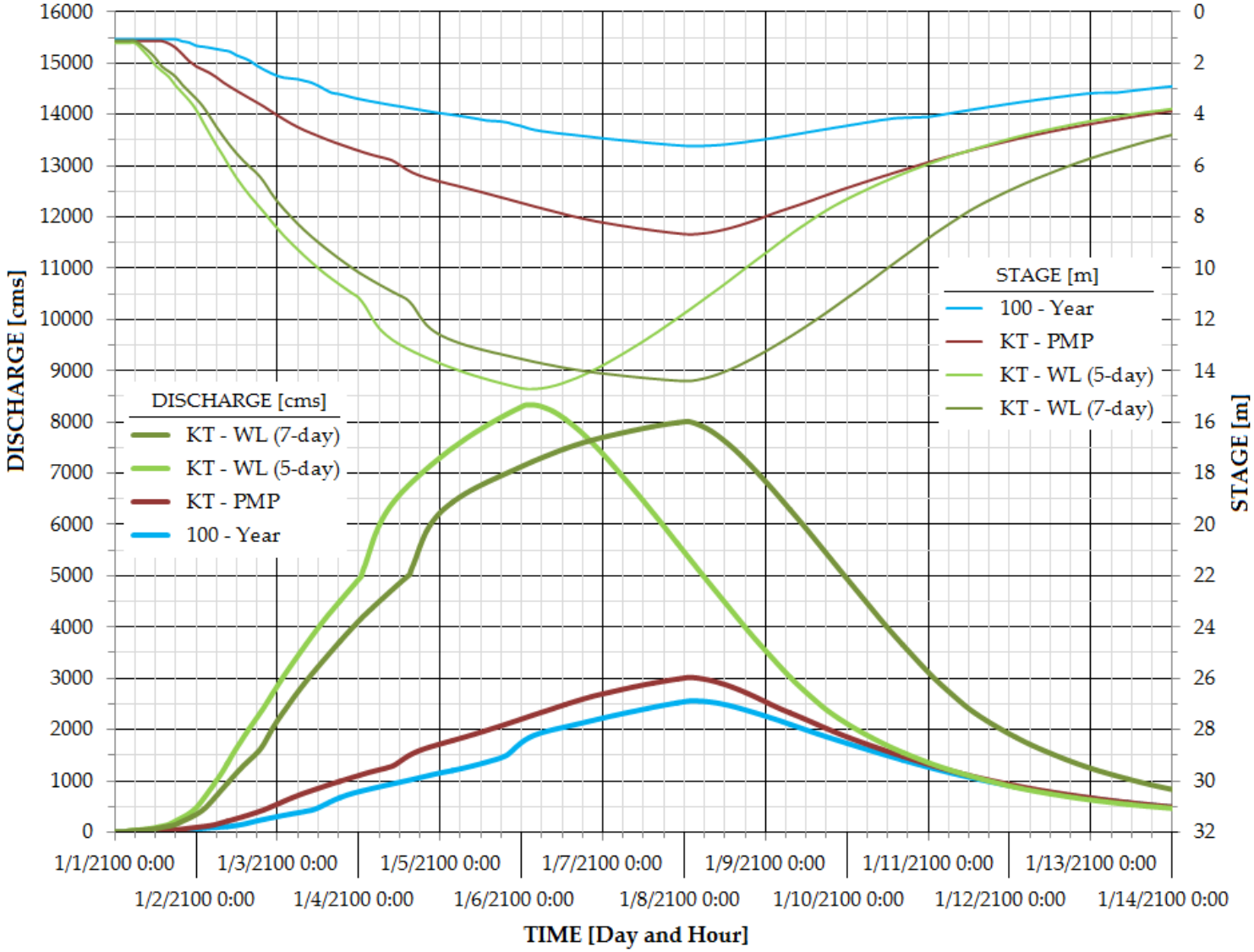

Figure A3 The hydrograph of the highest MED and MES for 100-year return period, KT-PMP and WL events at large watershed

APPENDIX B

SENSITIVITY ANALYSIS

A sensitivity analysis attempts to determine the change in model output values that results from the changes in the TREX model parameter values. This analysis is a valuable tool for identifying important model parameters. Table B1 shows the parameters that have been used to determine which are most sensitive when conducting a hydrological model using TREX. These values are calculated by subtracting and adding 50% from the calibrated / validated value to represent lower and upper values, respectively. The sensitivity analysis was conducted using the small (Lui) watershed. The results were assumed to be same for the medium (Semenyih) and large (Kota Tinggi) watershed. Additionally, the small watershed has a lot of advantages as compared to medium and large watershed for conducting sensitivity analysis (see Figure 2.3).

Figure B1 shows the results from the hydrologic parameters model sensitivity analysis. The hydraulic conductivity, K_h, and flow resistance (Manning's n) are the most sensitive parameters in the model (Figure B1a and B1b). Changing the K_h value by ±50% will affect the time to drain-out the water and also the peak discharge. However, the *n* values only control the peak discharge without affecting time to drain-out the water. The soil moisture deficit, θ_r, and capillary suction head, H_c (Figure B1c) and interception, V_i (Figure B1d) had minimal effect on discharge.

Table B1 Hydrological parameters for sensitivity analysis

PARAMETER	LOWER LIMIT	UPPER LIMIT	APPLICATION
Interception depth (m)	0.0	0.0	Urbanization
	1.0	3.0	Agricultural
	2.5	7.5	Forest
Soil moisture deficit (-)	0.145	0.435	Sandy loams Loams Mountain - limestone
Capillary suction head (m)	0.110	0.330	Sandy loams
	0.070	0.210	Loams
	0.085	0.255	Mountain - limestone
Hydraulic conductivity (m/s)	1.135×10^{-7}	3.405×10^{-7}	Sandy loams
	1.310×10^{-7}	3.930×10^{-7}	Loams
	4.335×10^{-7}	1.301×10^{-6}	Mountain - limestone
Manning's n	0.025	0.075	Urbanization
	0.085	0.255	Agricultural
	0.200	0.600	Forest

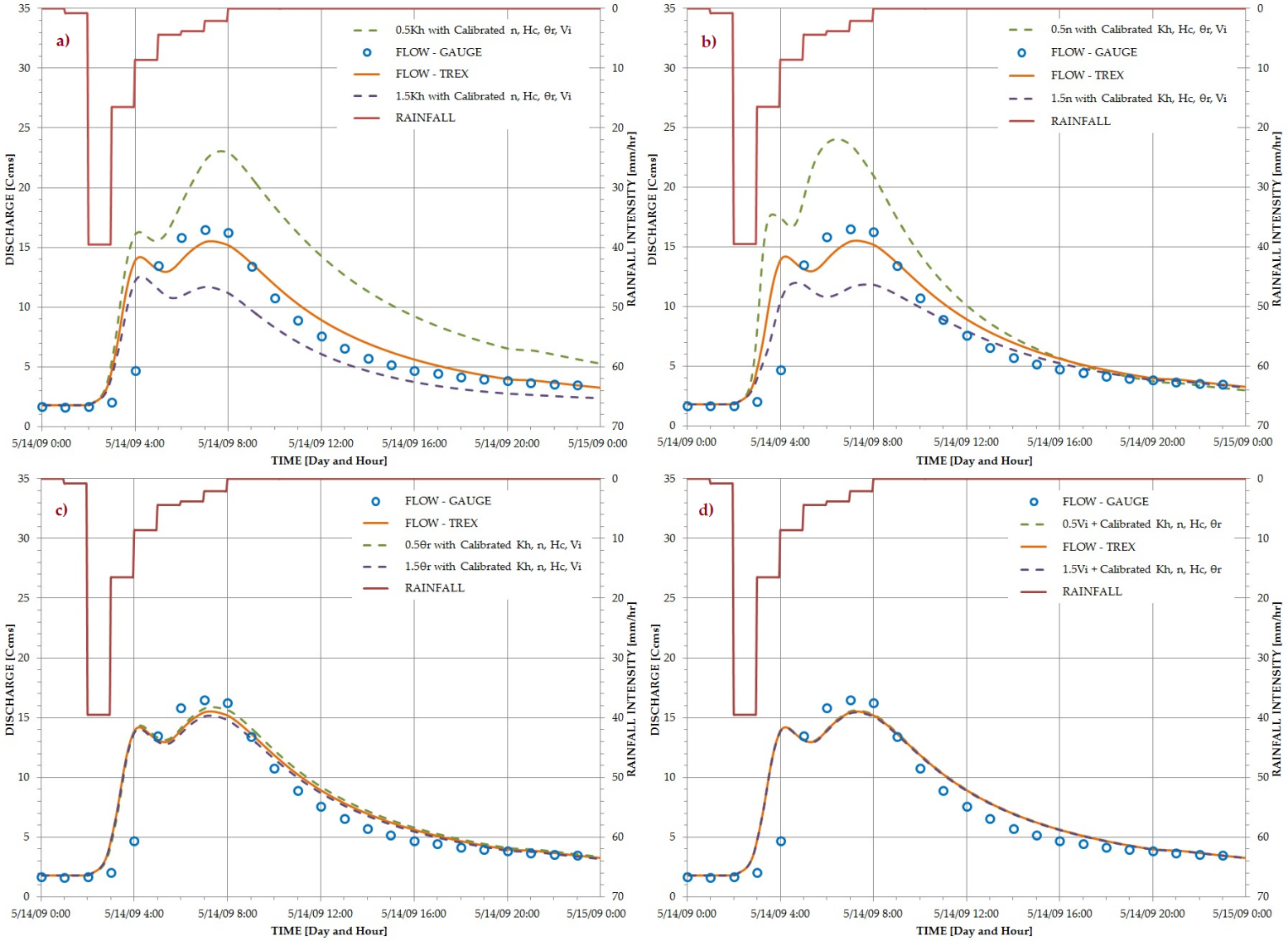

Figure B1 Hydrologic parameter model sensitivity analysis

APPENDIX C

FLOOD FREQUENCY ANALYSIS

Data were assumed to follow the Gumbel (1958) model distribution. This model distribution was used for fitting the frequency distribution of extreme natural events at study areas. This method is one of the most recommended to analyze the frequency of floods (Benson 1962; Reich and Jackson 1971; Reich 1972; Lettenmaier and Burges 1982). The moment method was used to estimate Gumbel's parameters as suggested by Lowery and Nash (1970), Landwehr et al. (1979), Lettenmaier and Burges (1982), and Raynal and Salas (1986).

$$F(x) = \exp\left\{-\exp\left[-\frac{(x - x_o)}{\alpha}\right]\right\} \qquad -\infty < x < \infty \qquad \text{[Equation C1]}$$

Where: x_o = the scale parameter ($x_o > 0$)

α = the location parameter

The scale and location parameter is calculated using Equations C2 and C3, respectively.

$$x_o = \mu - 0.5772\alpha \qquad \text{[Equation C2]}$$

$$\alpha = \sigma\frac{\sqrt{6}}{\pi} = 0.7797\sigma \qquad \text{[Equation C3]}$$

Where: μ = sample mean [Equation C4]

σ = sample standard deviation [Equation C5]

The sample mean and standard deviation value is calculated from Equations C4 and C2.

$$\mu = \frac{1}{N}\sum_{i=1}^{N} x_i \qquad \text{[Equation C4]}$$

$$\sigma = \left[\frac{1}{N-1}\sum_{i=1}^{N}(x_i - \mu)^2\right]^{1/2} \quad \text{where} \quad N = \text{sample size} \qquad \text{[Equation C5]}$$

The daily maximum discharges from flow gage stations were used in this analysis and shown in Tables C1, C2 and C3 and C4 for the small, medium and large watershed, respectively. This method was used to compare between calculated flood frequency event and TREX model results for large rainfall events (i.e. from two to one hundred years return periods). Peak discharge probabilities are calculated using Weibull (1939) as shows in Equation 4.6.

$$F(i) = \frac{i}{N+1} \qquad \text{[Equation C6]}$$

Where: i = rank (ordered sample either from smaller to the largest or vice versa)

N = sample size

Figures C1, C2, C3 and C4 were plotted in semi-log graph from the calculated values using Weibull (1939) and Gumbel (1958) equations for observed and fitted data, respectively. The 5% and 95% confidence limit were calculated and plotted as a lower and upper limit, respectively. These limits are useful to determine either the simulated discharge from the TREX model can be estimated between these limits. These graphs indicated that the model can be used to estimate the peak discharges for the large event (i.e., from two to one hundred years return periods) as well as the stochastic approach. However, there are several advantages to using the TREX model as compared to the stochastic approach. First, the simulated result can be extended to the map and animation created aided by using any animation software such as ArcGIS and GRASS to determine the distribution of the area that likely would be flooded.

Table C1 Maximum daily discharge in cms at small watershed

RANK	YEAR	Q_{MAX}	RANK	YEAR	Q_{MAX}	RANK	YEAR	Q_{MAX}	RANK	YEAR	Q_{MAX}
1	1971	121.33	12	2002	23.55	23	2004	14.52	34	1981	8.69
2	1977	111.49	13	1974	23.02	24	1982	12.98	35	1990	7.79
3	1978	40.85	14	2008	22.34	25	1987	12.77	36	2001	7.67
4	1996	40.82	15	1989	21.67	26	1973	11.47	37	2000	7.58
5	1997	27.48	16	2010	20.23	27	1986	11.43	38	1980	7.33
6	2009	26.98	17	1998	18.20	28	2007	11.22	39	1983	6.07
7	1979	26.76	18	1993	18.11	29	1995	10.46	40	1999	4.29
8	1991	26.49	19	1970	16.48	30	1994	9.78	41	2005	3.36
9	1976	25.91	20	1975	16.17	31	1984	8.90			
10	1972	24.52	21	2006	16.02	32	1988	8.90			
11	2003	24.34	22	1985	15.64	33	1992	8.72			

Table C2 Maximum daily discharge in cms at medium watershed

RANK	YEAR	DISCH.	RANK	YEAR	DISCH.	RANK	YEAR	DISCH.	RANK	YEAR	DISCH.
1	2009	244.90	10	1983	153.56	19	1991	142.05	28	1975	135.01
2	2008	242.61	11	1988	149.87	20	2007	141.48	29	1995	131.53
3	1982	237.50	12	1987	149.56	21	1986	139.53	30	2006	129.21
4	2010	167.89	13	1993	148.86	22	1979	138.66	31	1998	127.36
5	1989	165.67	14	1984	145.54	23	2002	137.71	32	2000	125.72
6	2004	165.46	15	1980	144.89	24	1978	136.64	33	1997	120.64
7	2003	157.99	16	1985	144.70	25	1994	136.33	34	1999	120.03
8	1992	157.58	17	1990	142.74	26	1976	135.96	35	2001	119.88
9	1981	155.73	18	2005	142.08	27	1977	135.44	36	1996	119.85

Table C3 Maximum daily discharge at large watershed (station no. 1836402)

RANK	YEAR	DISCH.	RANK	YEAR	DISCH.	RANK	YEAR	DISCH.	RANK	YEAR	DISCH.
1	2006	475.87	10	1987	135.94	19	1999	75.88	28	1997	53.60
2	1983	288.53	11	1995	133.33	20	2010	75.63	29	1981	52.36
3	2011	237.68	12	2005	111.28	21	1980	75.19	30	1993	50.30
4	1986	230.36	13	2007	109.91	22	1992	74.99	31	1994	50.29
5	1984	175.13	14	1996	105.51	23	1985	65.33	32	1989	41.96
6	2004	164.61	15	1982	101.53	24	1977	64.11	33	1991	40.69
7	2003	159.25	16	2008	88.00	25	2009	63.29			
8	1990	150.81	17	1978	85.00	26	1998	60.07			
9	2002	150.78	18	1979	83.57	27	2001	53.70			

Table C4 Maximum hourly discharge at large watershed (station no. 1737451)

RANK	YEAR	DISCH.	RANK	YEAR	DISCH.	RANK	YEAR	DISCH.	RANK	YEAR	DISCH.
1	1996	709.66	13	1981	273.98	25	1985	184.37	37	1998	100.30
2	1969	554.35	14	1971	273.60	26	1988	179.64	38	2000	98.67
3	1983	536.65	15	1978	256.31	27	1999	164.99	39	1968	97.95
4	2007	544.76	16	1995	254.32	28	1990	145.66	40	1965	97.12
5	1982	521.45	17	1992	235.19	29	1994	139.65	41	1997	95.03
6	1989	501.77	18	2001	226.11	30	2003	138.84	42	1970	92.45
7	1984	426.01	19	2005	223.34	31	2009	133.35	43	1993	88.07
8	2006	365.62	20	2004	213.54	32	1973	131.57	44	1966	84.40
9	1986	351.81	21	1991	203.51	33	1980	119.11	45	2010	81.81
10	1979	329.20	22	1977	202.20	34	2002	118.42	46	1972	80.09
11	2011	321.62	23	1987	199.97	35	1975	106.18	47	1974	79.52
12	1967	307.68	24	1976	190.76	36	2008	101.20			

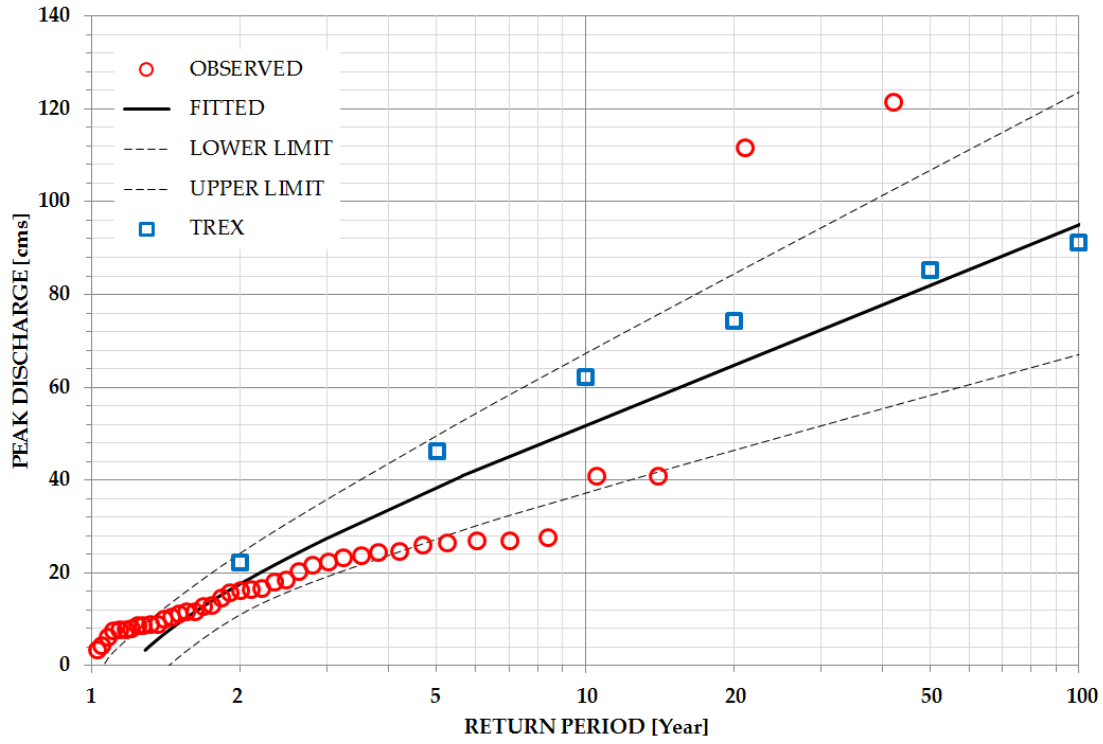

Figure C1 Comparison the daily maximum discharge between flood frequency analysis and TREX model at small watershed

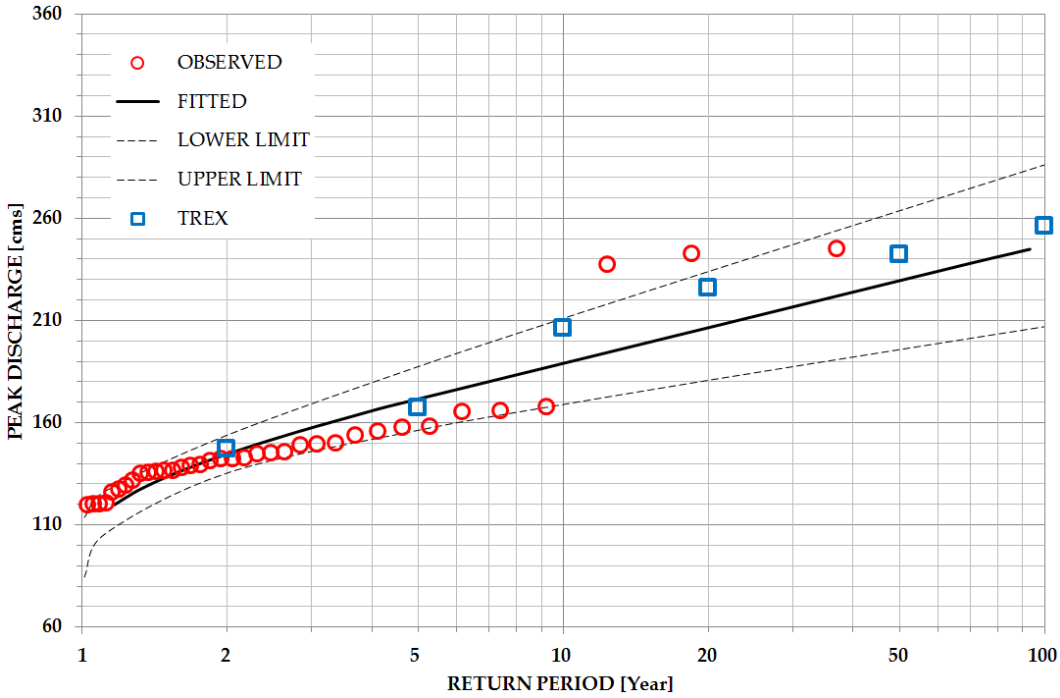

Figure C2 Comparison the daily maximum discharge between flood frequency analysis and TREX model at medium watershed

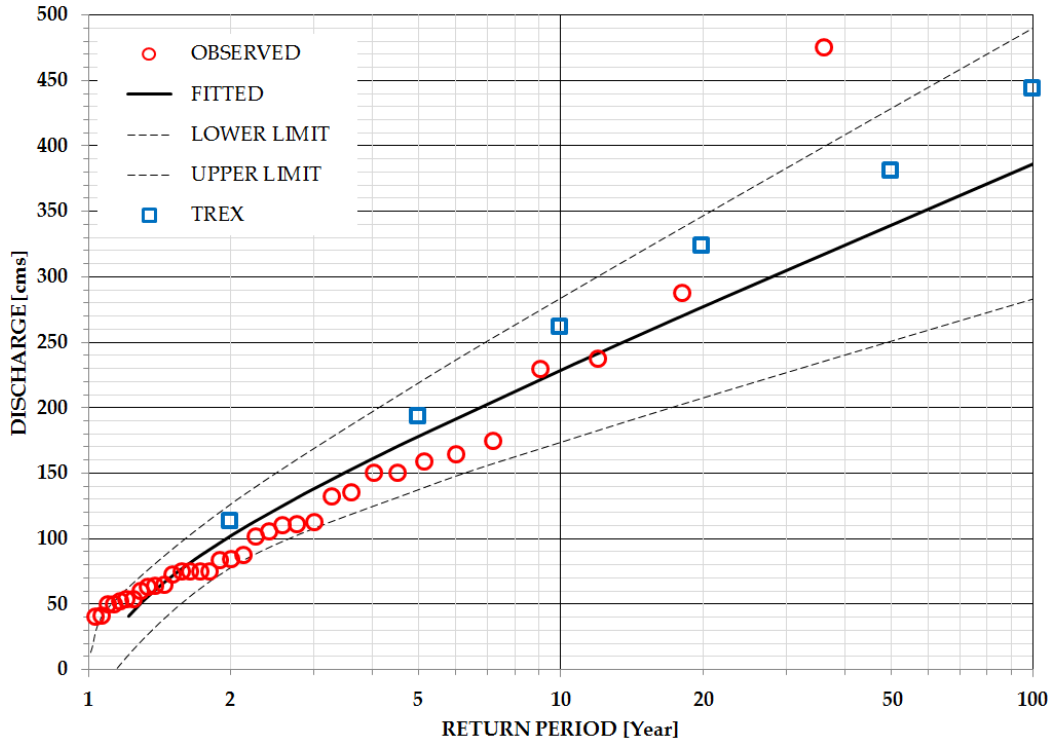

Figure C3 Comparison the daily maximum discharge between flood frequency analysis and TREX model at large watershed (1836402)

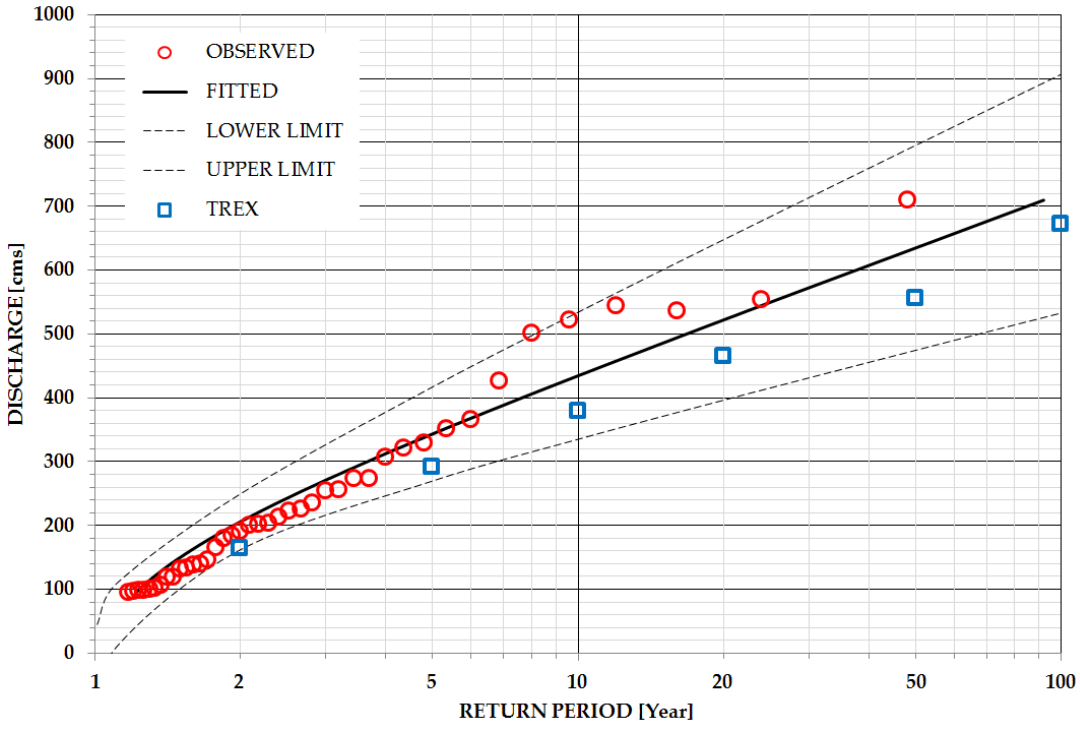

Figure C4 Comparison the daily maximum discharge between flood frequency analysis and TREX model at large watershed (1737451)

From this map and animation, the contingency plan can be managed to evacuate people from the flooded area. TREX model also is a 2D distributed model and has an advantage to give discharge estimates at any point in the watershed. This advantage is helpful to the authorities and rescue teams to evacuate and relocate the flood victims by knowing the distribution of water depth at any watershed spatially and temporally.

Secondly, the stochastic approach can only estimate the discharge for the year of $N+1$. This means, for instance from Figure C4, the maximum year is 48 (N = 47 years of sample data). When the TREX model has been calibrated and validated, the accuracy of the estimated peak discharge can be beyond what the stochastic approach can gives. Normally, the extrapolation method has been used to estimate the discharge beyond the plotted flood frequency graph plotted. The predicted peak discharge can be either high or low. This prediction also will affect the cost of any construction. For instance, to design a dam, the designs must factor for discharge from return periods longer than fifty years. If the stochastic approach cannot produce reliable results, the cost for this project would increase by over predicting the peak discharge. Conversely, under estimating peak discharge would make the main objective of the dam construction to fail. The peak discharge that is simulated using the TREX model take into account the physical topography such as the elevation, land use and soil type. The rainfall amount was applied from the recorded data. For these watersheds, the quality of the rainfall data is more reliable when compared to flow data. As a result, the estimated discharge by the model is more reliable.

The ability of the model to go beyond the stochastic approach provides the motivation for this study to go further by simulating the extreme events as described in section 2.5.2. There is a

need to have other methods that not only can estimate the discharge but also can show the most critical flooded area accurately and precisely.

APPENDIX D

GRID SIZE ANALYSIS

Different sizes of the grid have a significant impact on the simulation results (Blöschl et al. 1997). Therefore, an appropriate grid size should be considered carefully to reduce the difficulty in obtaining results (Grayson and Blöschl 2000; Wu et al. 2007) as describe in section 2.3.2. Grid sizes ranging from 30 to 330 m were used to analyze the performance of the TREX model in estimating the peak discharge, time to peak and total volume at a small (Lui) watershed. This grid size analysis at the small watershed is done by considering the time to prepare the input data, simulation time and post-processing the result. The analysis for this watershed was conducted by applying the calibrated and validated hydrologic parameters as shown in Table D1. This table shows the calibrated and validated values of hydraulic conductivity and Manning's n, respectively. The interception depth, soil moisture deficit and capillary suction head were same as shown in Table 4.1. The hydraulic conductivity and surface roughness were chosen because these values control the peak discharge, time to peak and volume of the water. The graphical and three statistical methods: NSEC, PBIAS and RPD, were used to classify the performance of the model.

Figure D1 shows the hydrographs of the observed and simulated discharge at different sizes of grid. This figure is used to evaluate the performance of the model graphically. The hydrograph reveals that the model performed *very good* in estimating the peak discharge, time to peak and rising and falling limbs grid size of 30 and 90 m and good for 150 m grid size. At a grid size more than 150 m, the simulation results changed obviously. Time to peak simulated by the model was clearly three hours earlier than observed. The estimated peak discharge and volume of water were larger than observed. The rising and falling limbs indicated that the model did not show at least the minimum level to be accepted.

Table D1 The evaluation of hydrologic model performance at difference grid sizes

Grid size (m)	Simulation time (seconds)	NSEC [-]	PBIAS [%]	RPD (Q_p) [%]	RPD (T_p) [%]
30	40,248 (11.2 hrs.)	0.9	- 8.1	- 2.2	0
90	780 (13 mins.)	0.8	- 11.3	- 4.3	0
150	49	0.6	- 15.7	- 9.0	- 43
210	19	0.6	- 22.1	16.1	- 43
270	9	0.3	- 41.6	25.7	- 43
330	6	0.1	- 50.0	32.6	- 43

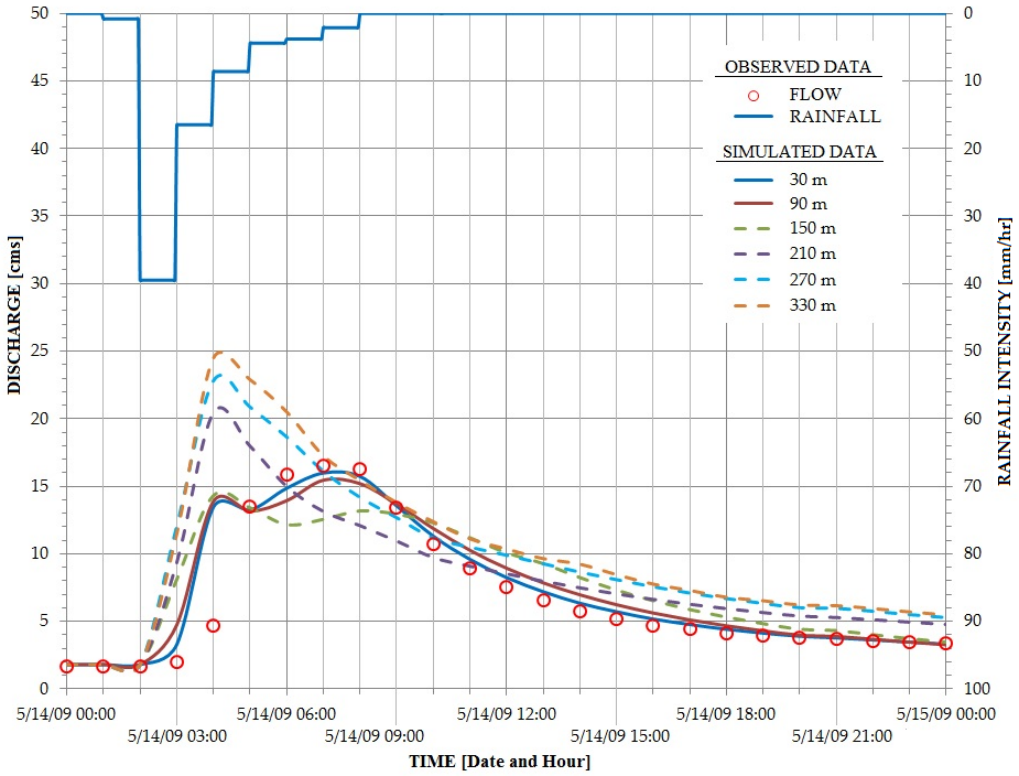

Figure D1 Comparison of discharge hydrograph at difference grid sizes

Three statistical methods were calculated and tabulated in Table D1. These data were plotted in Figure D2. The performance rating as classified in Table 4.2 was used. The performance of the model can be classified as very good, good and satisfactory when the statistical values are located in the green, orange and red regions, respectively. From Table D1,

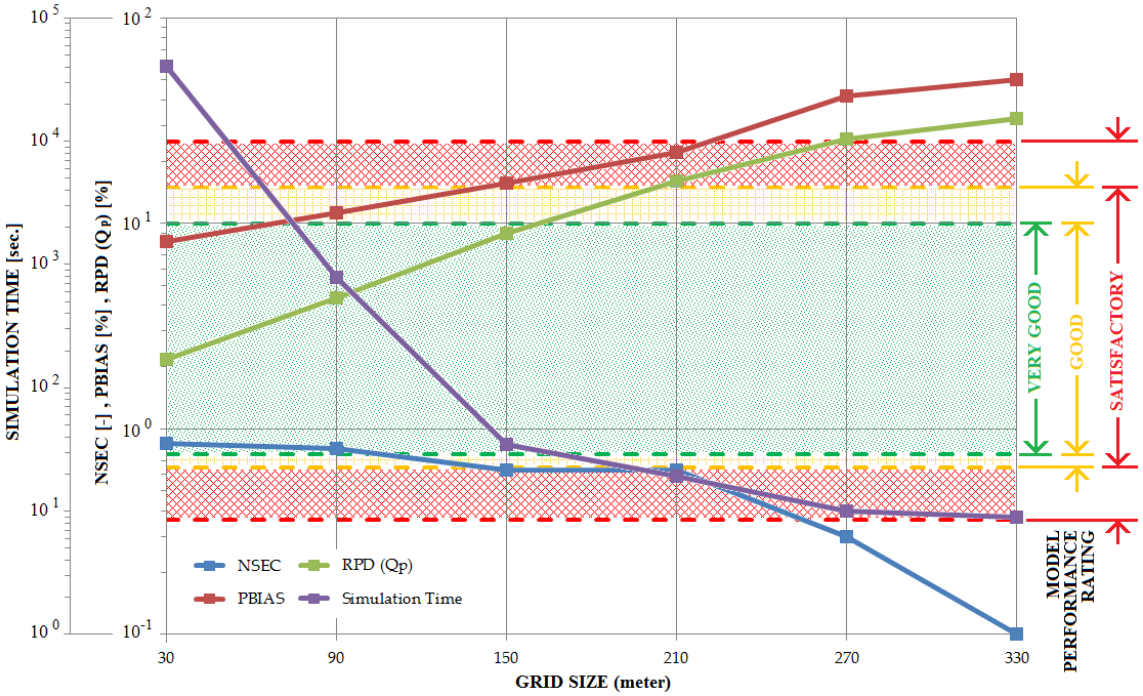

Figure D2 The model performance rating as a function of grid sizes at the small watershed (Lui)

all the calculated values described that the model simulated results are varied resulting from grid size changes. The calculated NSEC values for hourly discharges show that the model performance is very good for grid sizes of 30 and 90 m and good at grid sizes 150 and 210 m (Table D1 – third column and Figure D2 – blue line). However, by increasing the grid size from 210 to 330 m led to decreasing the NSEC values (unsatisfactory) as shown in Table D1. The performance of the model in estimating hourly volume was compared to observed data using the PBIAS method. The model had very good and good performance, as indicated in Table D1 (fourth column) and Figure D2 (red line), for grid sizes of 30 and 90 m and 150 m, respectively. The application of the model using different grid sizes than becomes less significant as the hourly volume estimated has not reached the minimum rating, i.e. satisfactory, for grid size coarser than 210 m. The estimated volume decreased as coarser grid sizes were applied. The

RPD method indicated that the estimation of the peak discharge (Figure D2 – grid line) and time to peak at grid sizes up to 90 m is very good. However, for grid size of more than 90 m, the discrepancies of simulated and observed time to peak increased from -9% to 33%.

The temporal and spatial distributions of water depth at various grid sizes were visualized in 3D as shown in Figure D3. From this figure, water depth distributions are uncertain for grid sizes larger than 150 m. Increasing the grid size from 30 to 330 m resulted in the inaccuracy of input data such as DEM, land use and soil type (Figure D4).

Based on two methods of performance evaluation, it can be said that as the grid size increases, the simulated results become less significant. Simulation time required by the TREX model decreased significantly when coarser grid size was used (Figure D2 – purple line). Simulation using coarser grid size resulted in high discrepancies values of the estimated peak discharge, time to peak and volume of water. Generally, coarser grid size makes the topography of this watershed become more flat. However, this watershed is surrounded by mountains, i.e., about 80%. This situation contributed to an earlier time to peak (about 3 hours) simulated using coarser grid size. Other than topography, changing the grid size from fine to coarse has oversimplified the model parameters. Figures D4 and D5 illustrate the simplified DEM, land use and soil type. Numerically, the model is stable and consistent during the simulations. The simulation converged to the observed data when finer grid sizes were used (Figure D1).

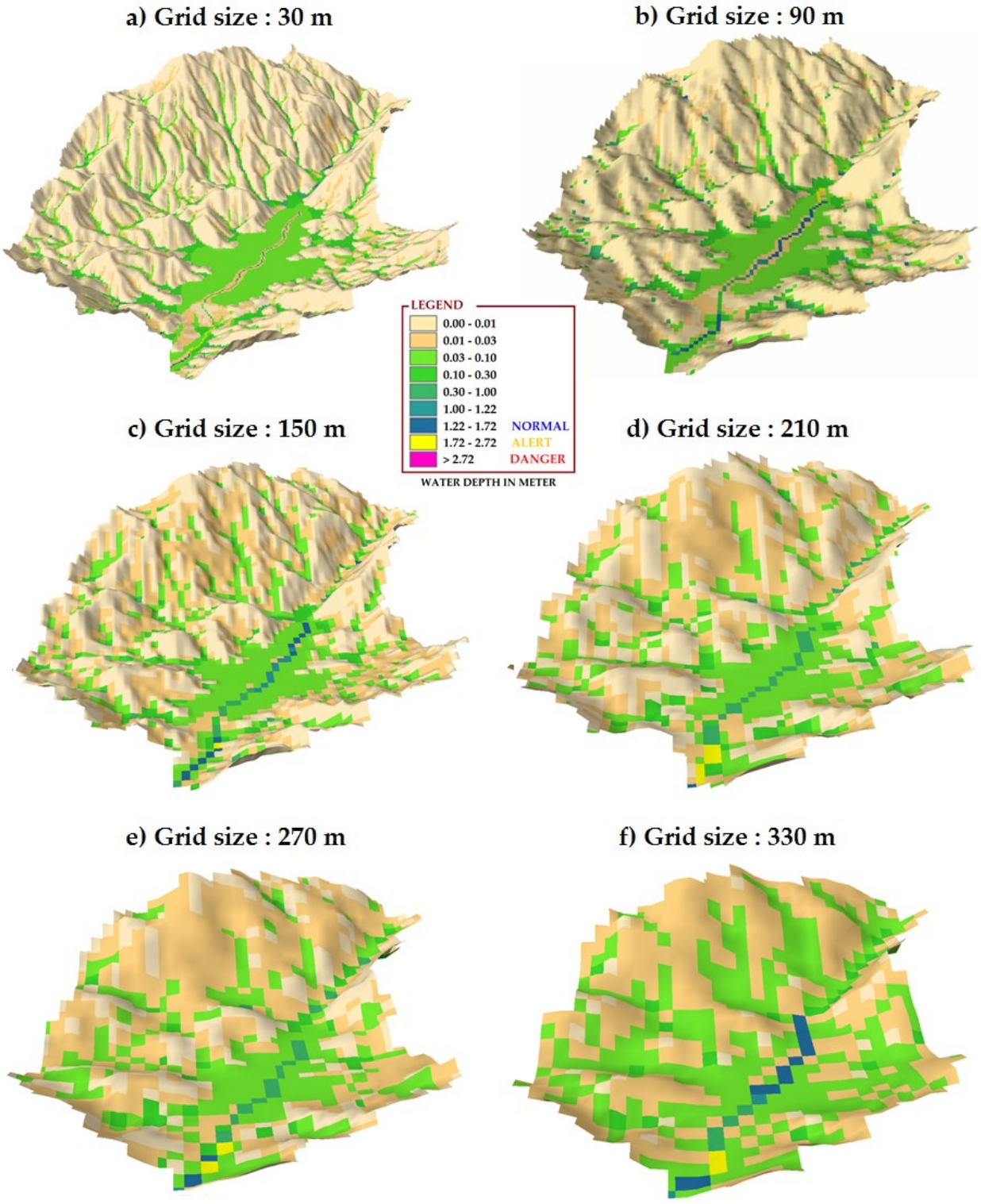

Figure D3 Comparison of the maximum water depth distribution for different grid sizes at the small watershed (Lui)

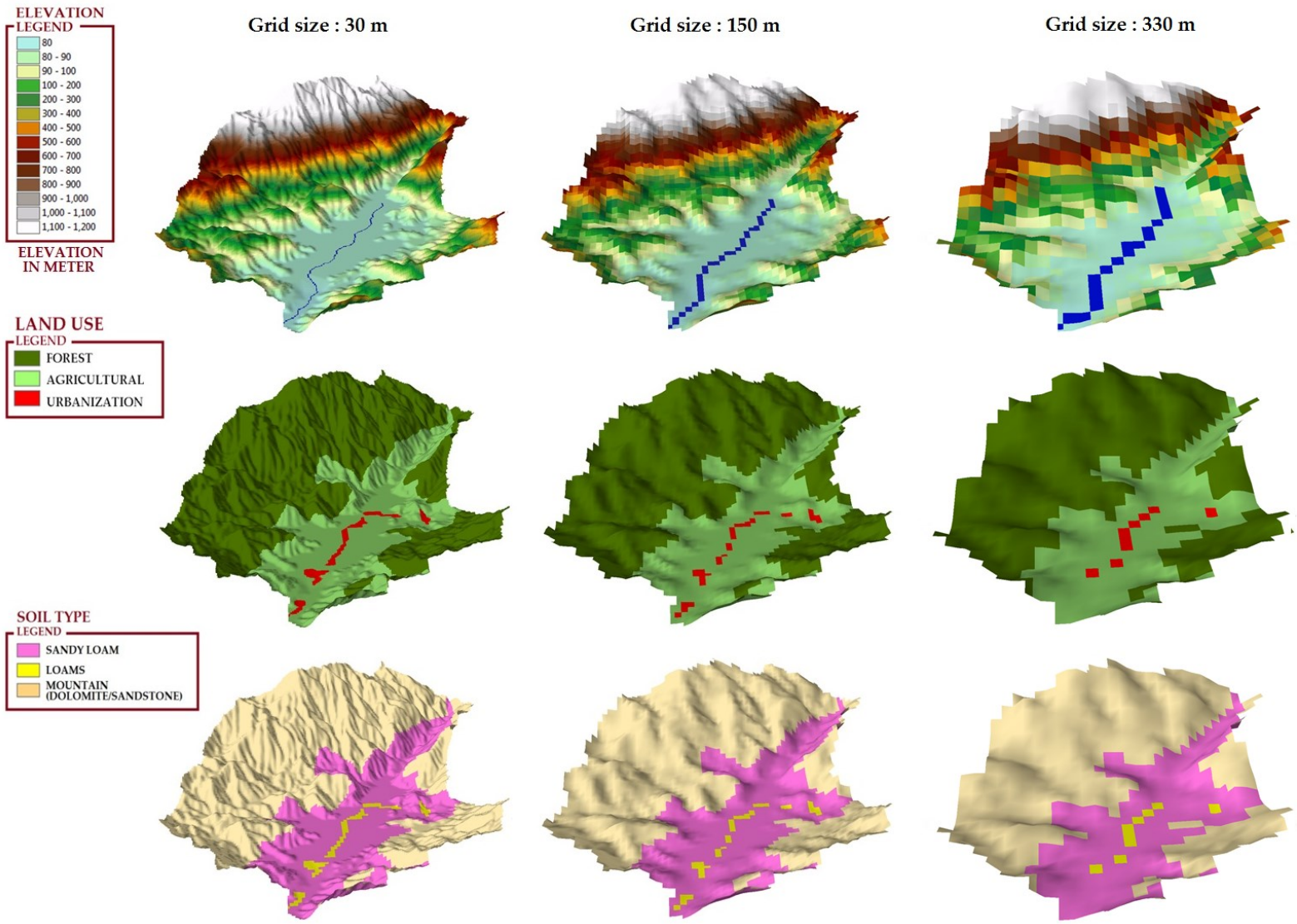

Figure D4 Comparison of the DEM, land use and soil type using different grid sizes

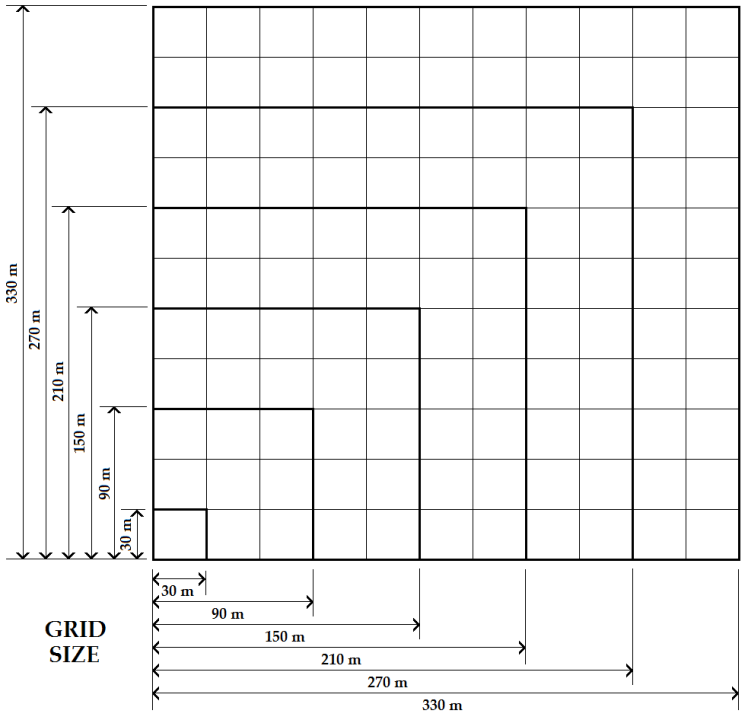

Figure D5 Various sizes of grid used to represent DEM, land use, soil type and other model parameters

APPENDIX E

COMPARISON BETWEEN 1D AND 2D HYDROLOGICAL MODELS

The comparison between 1D and 2D was made. The HEC-HMS was used to simulate 1D rainfall-runoff relationship. In Malaysia, there were several studies conducted to simulate rainfall-runoff and rainfall-water surface profile relationships. The most common software from HEC group was applied to this watershed, i.e., the HEC-HMS (Yusop et al. 2007; Razi et al. 2010) and HEC-2 (Mohammed et al. 2010). Both models are capable of simulating the rainfall-runoff relationship in Malaysia, based on the historical events. The HEC-HMS model gives the simulation results in terms of a hydrograph, while the HEC-2 model produced the water level of the study area. Since the TREX model is capable of producing a hydrograph of the study area, therefore HEC-HMS was chosen in this study because a more meaningful comparison between both models can be made.

Table E1 and Figures E1 and E2 show the estimated hydrographs for the 100-year, PMP and world greatest rainfall (WGR) events on the small and medium watersheds, respectively. The HEC-HMS model has the ability to estimate the peak discharge for the 100-year and PMP events on both watersheds. However, the peak discharges estimated by the HEC-HMS model for the WGR event are less than the TREX model for both watersheds. The difference between these two models on both watersheds is 25% and 15%, respectively. In this study, the estimated peak discharges from TREX model were assumed to be reliable because the model use grid to represent the land use, soil type and elevation of the watershed. In addition to that, the formulations to solve the hydrologic cycles are based on the physically-based model which includes the mass balance and momentum equations. Whereas the HEC-HMS is a lumped model which the properties of the watershed is presented as an average across the watershed. Another reason that the 1D model cannot estimate peak discharge for the WGR event is because the model assumed a linear relationship between Q_p and rainfall intensity, *i*. The 2D model performs

much better in simulating the nonlinear relationship between Q_p and i, as shown in Figures E1 and E2 and Table E1.

Table E1 Comparison of simulated peak discharges (cms), Q_p, between 1D (HEC-HMS) and 2D (TREX) models for different watershed sizes

Rainfall events	Watershed area							
	Small			Medium			Large	
	i	Q_p (cms)		i	Q_p (cms)		i	Q_p (cms)
		1D	2D		1D	2D		
100-year	38	101	91	15	222	256	8	1,023
PMP	43	421	520	43	1,508	1,474	9	3,016
WGR	86	1,027	1,358	78	3,195	3,793	26	8,332

Note: i = Rainfall intensity (mm/hr); Q_p = Highest peak discharge

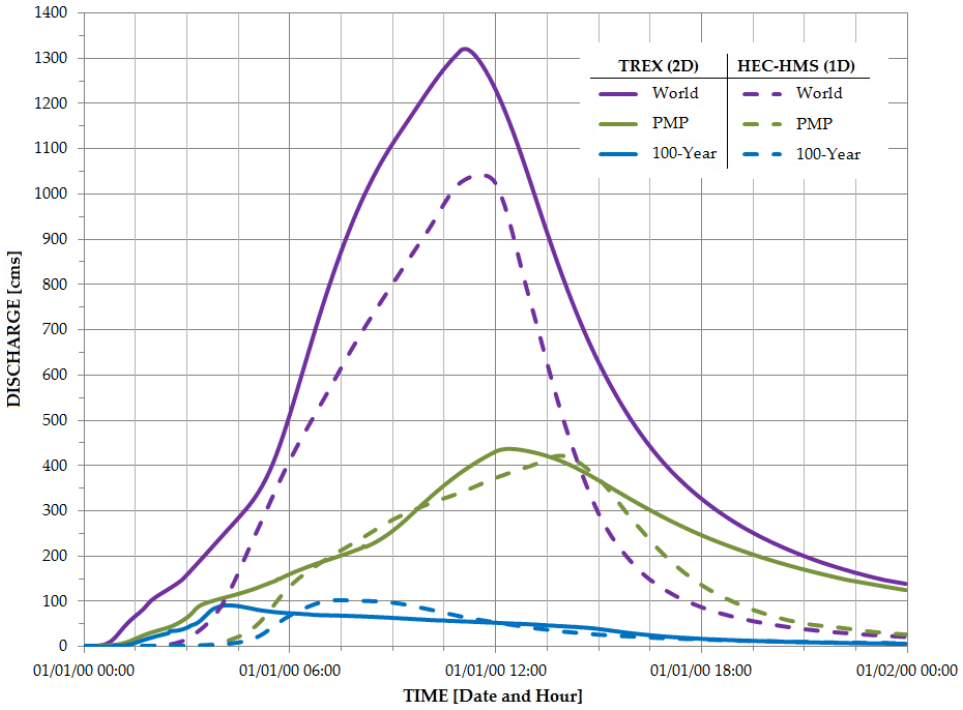

Figure E1 Discharge comparison between 1D (HEC-HMS) and 2D (TREX) models for 100-year, PMP and the world's largest rainfall on a small watershed

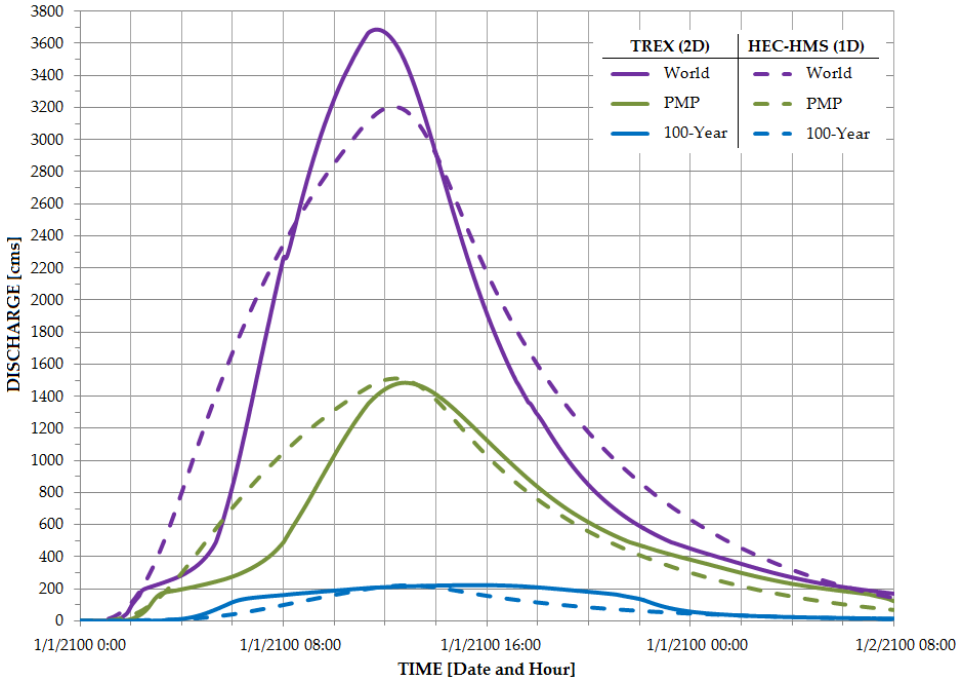

Figure E2 Discharge comparison between 1D (HEC-HMS) and 2D (TREX) models for 100-year, PMP and the world's largest rainfall on a medium watershed

Other significant topic that should be included when comparing the 1D and 2D models is the calibrated and validated model parameters. Both models use the Green and Ampt method to calculate infiltration. The 2D diffusive wave approximation is used to calculate the overland flow, while 1D diffusive wave approximation is used to estimate the channel flows in the 2D model. However, these flows are calculated using only the 1D kinematic wave approximations in the 1D model. The same storm events were used to calibrate and validate the model parameters (i.e., K_h and Manning's n). The storm event on May 14, 2009 (Figure E5) was chosen to compare between the TREX model, HEC-HMS model and observed flow gage measurement. The hydraulic conductivity values on both watersheds are higher than the suggested limit by Liong et al. (1989), as shown in Table E2 and Figure E3.The allowable upper and lower limits of the hydraulic conductivity and roughness were derived from the suggested values by Rawls et al. (1982 and 1993) and Maidment (1993). These values are 100 times higher and lower (as

suggested by Liong et al. 1989) for the upper and lower limits, respectively. The calibrated and validated roughness are within the acceptable limit for the small watershed but not for the medium watershed (see Table E3 and Figure E4). The calibrated and validated roughness for the medium watershed is higher than the values suggested by Chow (1969). Additionally, the 1D simulation is unable to estimate the flooding area as compared to the 2D model, especially on the flood plains. This is because the 1D model use 1D kinematic wave approximation which force the overland flow to be in one-direction, i.e., only flow in y-direction, by assuming that the channel flow is in x-direction from upstream to downstream.

Table E2 Calibrated and validated hydraulic conductivity, K_h, using 1D (HEC-HMS) and 2D (TREX) models at small and medium watersheds

SOIL TYPE	**SUGGESTED VALUE (Rawls et al (1982,1993); Maidment (1993))**		**2D (TREX)**		**1D (HEC-HMS)**	
	Lower	**Upper**	**Small**	**Medium**	**Small**	**Medium**
Sandy loams	1.81×10^{-8}	6.06×10^{-4}	1.14×10^{-7}	1.12×10^{-6}		
Loams	9.44×10^{-9}	3.67×10^{-4}	1.31×10^{-7}	4.00×10^{-7}		
Clay	8.33×10^{-10}	1.67×10^{-5}	---	1.27×10^{-8}	9.12×10^{-2}	6.12×10^{-3}
Mountain (Limestone)	3.20×10^{-11}	3.20×10^{-6}	4.34×10^{-7}	1.18×10^{-10}		

Table E3 Calibrated and validated roughness values (Manning's n) using 1D (HEC-HMS) and 2D (TREX) models at small and medium watersheds

LAND USE	**SUGGESTED VALUE (Chow (1969))**		**2D (TREX)**		**1D (HEC-HMS)**	
	Lower	**Upper**	**Small**	**Medium**	**Small**	**Medium**
Main channel *	0.02	0.08	0.04	0.03	0.04	0.45
Urbanization	0.01	0.08	0.05	0.045		
Agricultural	0.02	0.2	0.17	0.1		
Forest	0.11	0.4	0.4	0.2	0.04	0.47
Grassland	0.03	0.1	---	0.1		
Open area	0.03	0.1	---	0.1		

*Note: * Suggested value for roughness at main channel obtained from Zakaria et al. (2010)*

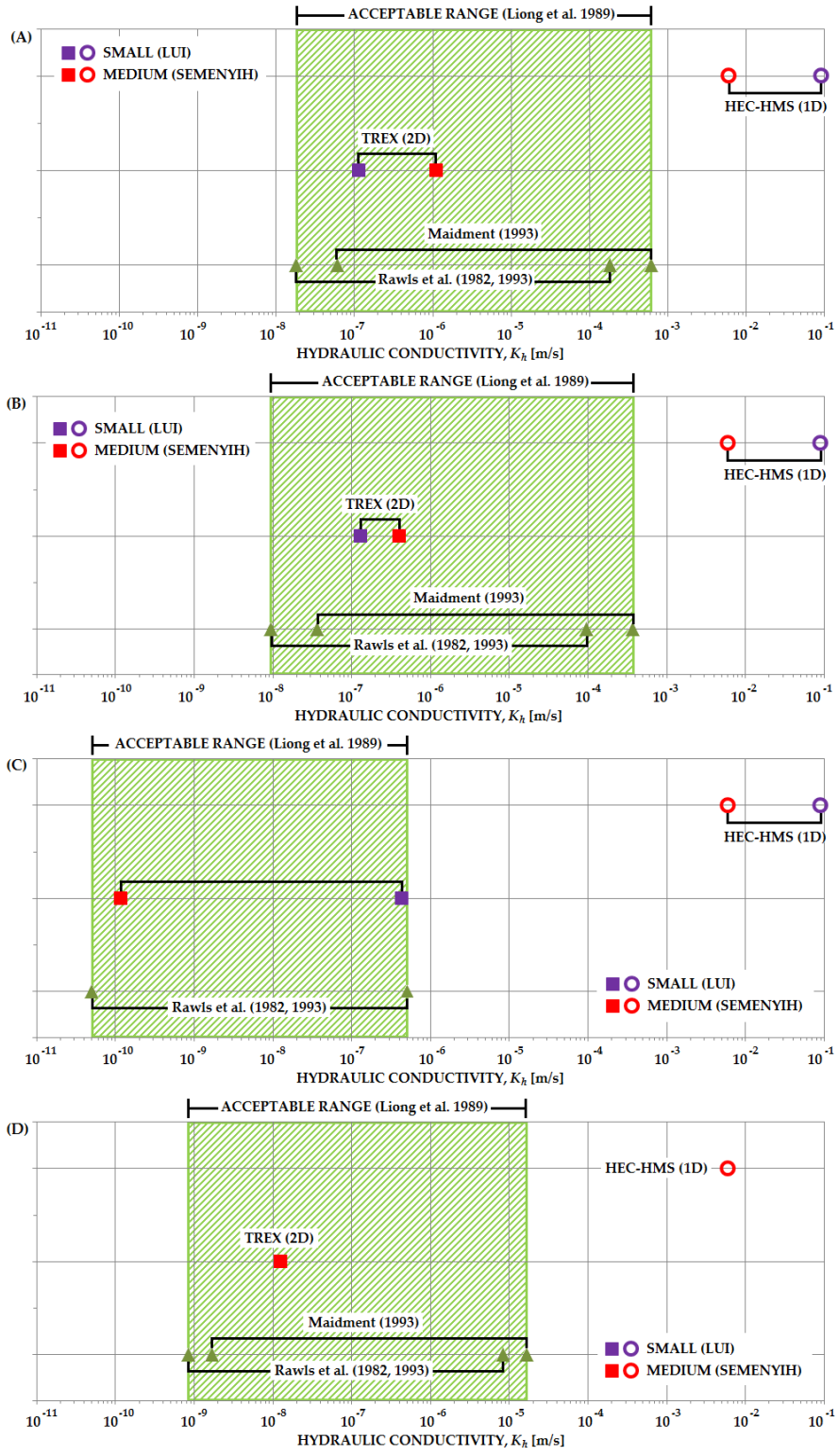

Figure E3 The calibrated and validated hydraulic conductivity using 1D (HEC-HMS) and 2D (TREX) models for different soil types: (a) sandy loam, (b) loam, (c) mountain (limestone) and (d) clay

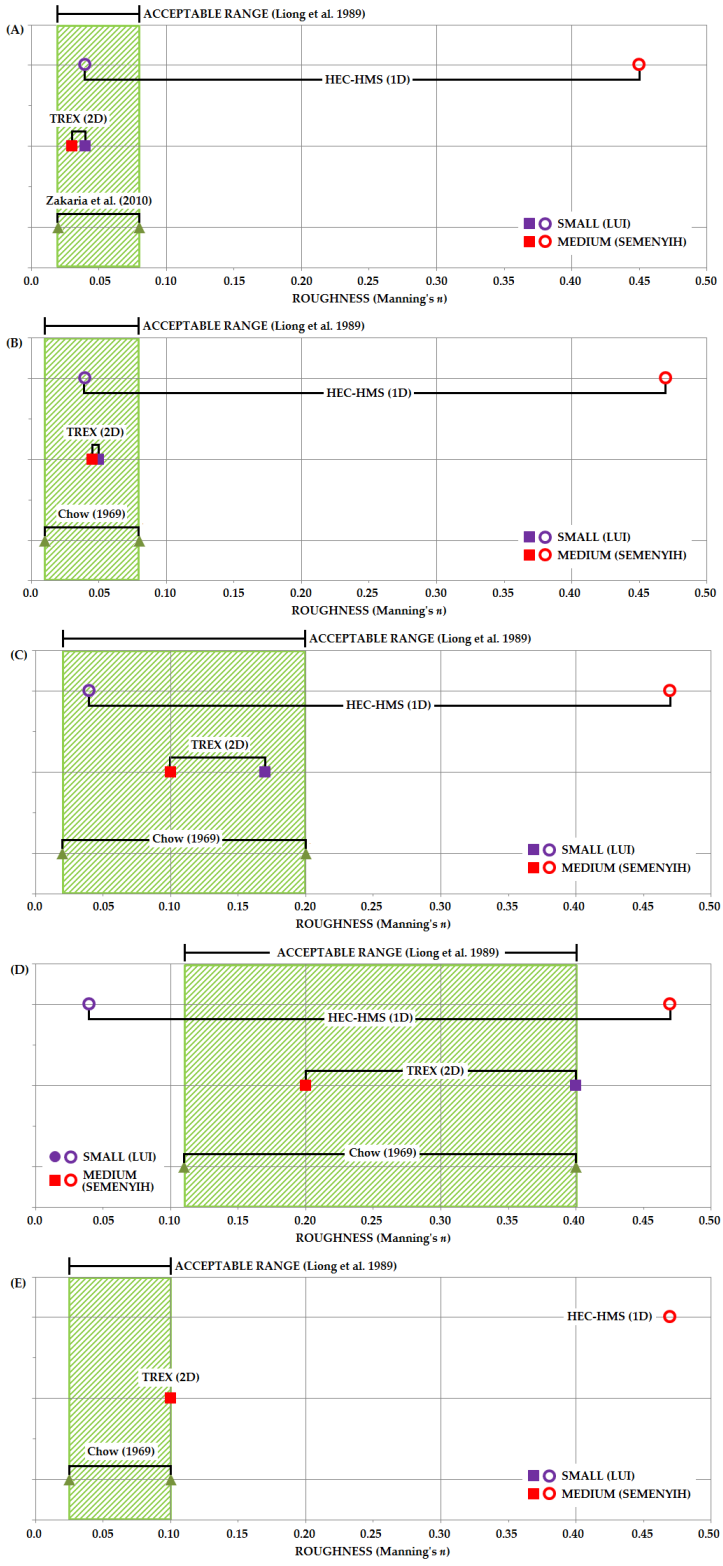

Figure E4 The calibrated and validated roughness values (Manning's n) using 1D (HEC-HMS) and 2D (TREX) models for different land use: (a) main channel, (b) urbanization, (c) agricultural, (d) forest and (e) grassland and open area

Figure E5 shows the comparison of the hydrograph produced by both 1D and 2D models. The hydrograph simulated using calibrated and validated model parameters for 1D (black) and 2D (purple – 30 m grid size and green – 90 m grid size) models are comparable to the observed data (red dots). However, the calibrated and validated model parameters are off from the acceptable limit for 1D model, as discussed in the previous paragraph. When the acceptable model parameters were applied to the 1D model, the peak discharge is 5 times larger than the observed data.

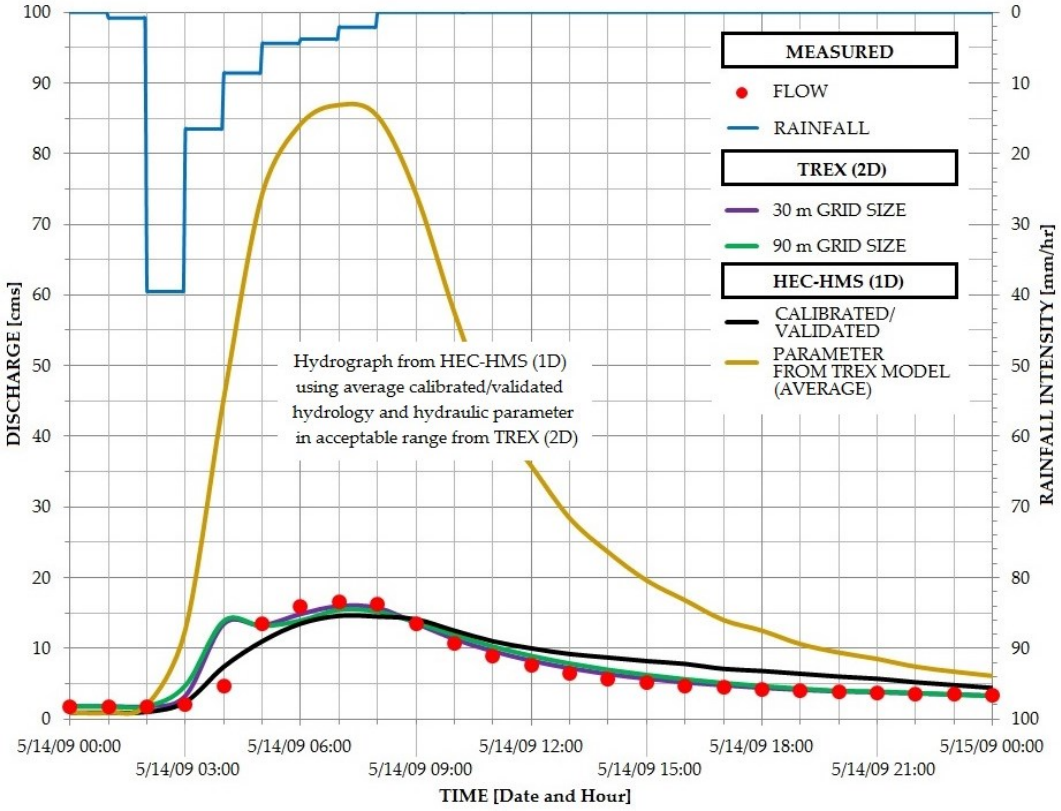

Figure E5 Comparison of the hydrograph produced by the 1D (HEC-HMS) and 2D (TREX) models

APPENDIX F

PICTURES OF LAND USE FOR THE STUDY AREAS

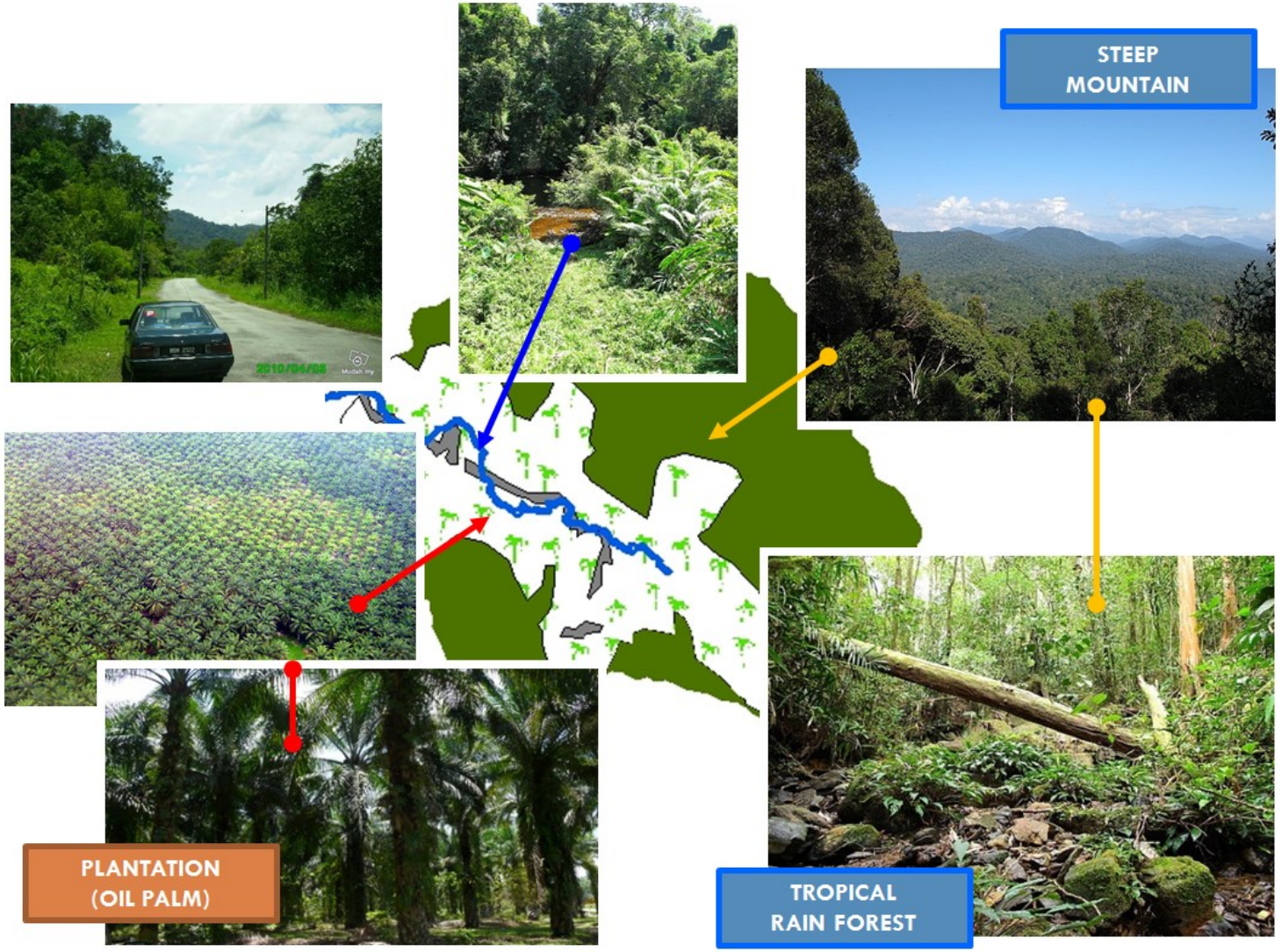

Figure F1 Picture of land use at small watershed (Lui)

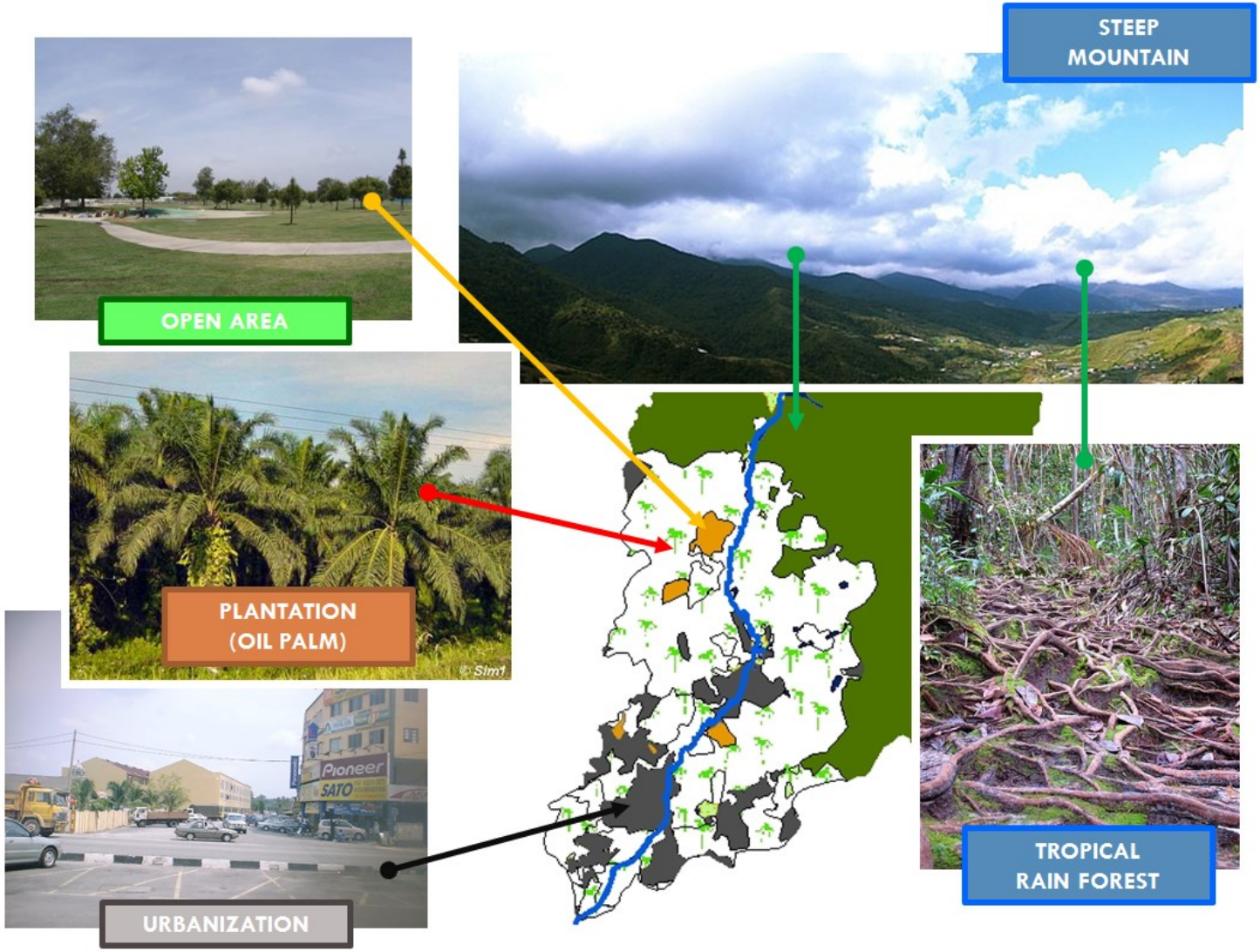

Figure F2 Picture of land use at medium watershed (Semenyih)

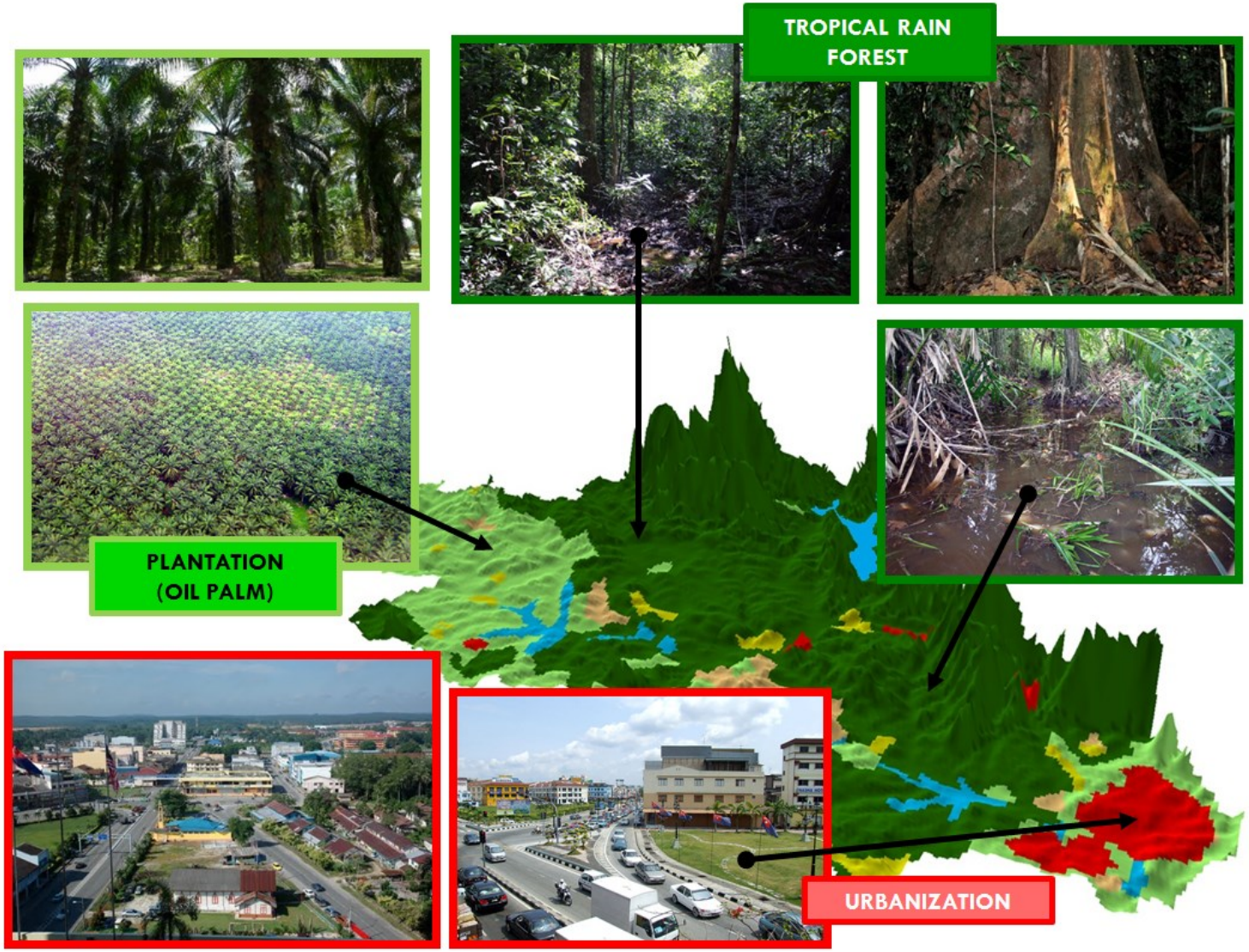

Figure F3 Picture of land use at large watershed (Kota Tinggi)

APPENDIX G

CREAGER'S DATA

Table G1(a) Data from Creager et al. (1945)

	Stream and location	Drainage area (km ^{2})	Flood (cms)	Date of Flood Month	Date	Year	Peak Specific-Discharge [cms/km ^{2}]	Authority
	ALABAMA							
1	Tennessee R., Florence	79771	12573	Mar.		1897	0.16	132
2	Tennessee R., Decatur	68116	8014				0.12	142
3	Alabama R., Selma	39886	4134	Jan.		1892	0.10	1
4	Coosa R., Childersburg	21730	425	July		1916	0.02	99
5	Black Worrior, Tuscaloosa	12510	6088	Apr.	18	1900	0.49	155
6	Tallapoosa, Milstead	9946	1982	Dec.		1901	0.20	72
7	Tallapoosa, Sturdevant	6475	1671	Mar.		1906	0.26	69
8	Elk, Rogersville	5439	1744				0.32	142
9	Black Worrior, Cordova	4921	1614	Mar.		1902	0.33	120
10	Elk R., Elkmont	4403	1467				0.33	142
11	Conecuh R., Brantley	1305	442	Aug.	19	1939	0.34	191
12	Choccolocco Cr., Jenifer	704	334				0.47	69
13	Camp Branch, Ensley	19	14			1909	0.75	11
14	Venison Branch, near Mulga	10	6				0.58	11
	ARIZONA							
15	Colorado R., below Gila Junction	582744	6683	Jan.		1916	0.01	119
16	Gila R., Yuma	145039	6230	Jan.		1916	0.04	75
17	Gila R., Florence	45972	3766	Feb.		1891	0.08	72
18	Salr R., below Phoenix	31080	8382	Feb.		1891	0.27	72
19	Salt R., McDowell	16213	3908	Mar.		1893	0.24	69
20	Verde R., McDowell	15540	4701			1893	0.30	72
21	Salt R., Roosevelt	14908	5862	Mar.		1893	0.39	72
22	San Pedro R., near Mammoth	9971	2549	Sept.	28	1926	0.26	167
23	San Pedro R., Charleston	3833	2775	Sept.	28	1926	0.72	167
24	Canyon Diablo, Leupp	1409	1263	Sept.		1923	0.90	74
25	Troxton Canyon, E. of Kingman	1165	1402			1894	1.20	2
26	Canyon Diablo, Arch Bridge	881	1002	Sept.		1923	1.14	74
27	Sonoita Cr., near Patagonia	544	566	Aug.		1934	1.04	167
28	Cave Cr., near Phoenix	518	708	Aug.		1921	1.37	92
29	Pinal Cr., Globe	78	374	Aug.		1904	4.81	92
30	Chase Cr., of Gila River	52	366	Dec.		1906	7.07	92
	ARKANSAS							
31	Mississippi R., above Arkansa Junction	2719474	68527			1912	0.03	89
32	Mississippi R., Helena	2589975	57766			1912	0.02	119
33	Arkansas R., Van Buren	389273	15631	Apr.	16	1927	0.04	132
34	Red R., Garland	133384	9260	Feb.	25	1938	0.07	195
35	White R, Clarendon	49210	9061			196	0.18	132
36	Ouachita R., Remmel Dam	3989	3964	May	16	1923	0.99	89
	CALIFIFORNIA							
37	Sacramento R.	58274	16282			1904	0.28	2
38	Sacramento R., Red Bluff	24087	8382	Dec.		1937	0.35	161
39	Feather R., Oroville	9394	5295	Mar.		1907	0.56	70
40	Eel R., Scotia	7951	8212	Feb.		1915	1.03	132
41	Feather R., N. Fk., Big Bend	5025	3087	Mar.		1907	0.61	8
42	American R., Fair Oaks	4975	5179	Mar.		1928	1.04	132
43	Yuba R., Smartville	3111	3398	Mar.	26	1928	1.09	171
44	Los Angelas R., Long Beach	2745	2265	Mar.	2	1938	0.83	162
45	Santa Ana R., Mentone	2189	2832	Mar.	2	1938	1.29	198
46	Putah Cr., Winters	1696	1699	Dec.		1913	1.00	70
47	American R., Middle Fk., near E. Auburn	1603	2832	Mar.	25	1928	1.77	171
48	Smith R., near Crescent City	1588	1747	Mar.	18	1932	1.10	171
49	McCloud R., near Gregory	1575	1521	Mar.		1904	0.97	69
50	San Luis Rey R., Oceanside	1463	2704	Jan.		1916	1.85	66
51	Los Angelas R., Dayton Ave.	1321	1926	Mar.	2	1938	1.46	180
52	San Luis Rey R., Bonsall	1204	3625	Feb.	23	1891	3.01	169
53	Calaveras R., Jenny Lind	1020	1968	Jan.		1911	1.93	70
54	San Diego R., Sante	971	1991	Jan.		1916	2.05	66
55	San Luis Rey R., near Pala	842	2124	Jan.		1916	2.52	70
56	San Dieguito R., Bernardo	774	2044	Jan.		1916	2.64	66
57	Bear R., Van Trent	679	2486	Feb.		1907	3.66	70
58	Sespe Cr., near Fillmore	658	1586	Mar.	2	1938	2.41	198
59	Mattole R., New Petrolia	645	1574				2.44	70
60	Smith R., at (Junction) Crescent City	588	1203	Nov.		1915	2.05	70
61	Sab Gabriel R., Azusa	575	1557	Mar.	2	1938	2.71	162
62	Santa Ynez R., near Santa Barbara	567	1081	Mar.	2	1938	1.91	198
63	San Luis Rey R., Mesa Grande	541	1657	Jan.		1916	3.06	66
64	San Gabriel R., Dam No. 1 - Inflow	528	2549	Mar.		1938	4.82	192
65	San Diego R., Lakeside	490	1076	Jan.		1916	2.20	66
66	Sweetwater R., Jamacha	445	1218	Jan.		1916	2.73	66
67	San Jacinto R., near San Jacinto	363	1274	Feb.	16	1927	3.51	171
68	Sweetwater R., near Dehesa	290	688	Jan.		1916	2.37	66
69	San Jacinto R., near San Jacinto	280	850	Jan.		1916	3.04	66
70	Otay R., Lower Otay Dam	255	1059	Jan.		1916	4.15	70
71	Putah Cr., near Guenoc	236	697	Mar.		1904	2.96	180
72	Loas Angelas R., Tujunga No. 1 Dam	211	963	Mar.	2	1938	4.57	99
73	Smith R., N. Fk., Crescent	210	799	Nov.		1915	3.81	66
74	Santa Ysabel Cr., Mesa Grande	138	597	Jan.		1916	4.32	198
75	Lytle Cr., near Fontana	124	714	Mar.	2	1938	5.75	164
76	San Gabriel R., San Gabriel Dam No. 2	105	674	Mar.	2	1938	6.44	198
77	Santa Paula Cr., Ventura County	103	382	Mar.	2	1938	3.71	148
78	Pine Tree Canyon, 12 mi N. of Mojave	91	1685	Aug.	12	1931	18.59	180
79	Little Tujunga Cr., Canyon Mouth, near Loas Angelas	50	242	Mar.	2	1938	4.84	198
80	Topanga Cr., near Topanga Beach	46	225	Mar.	2	1938	4.86	198
81	Arroyo Secco, 5.5 miles N. W. of Pasadena	42	244	Mar.	2	1938	5.75	200
82	San Gabriel R., Devil's Canyon above Dam No. 2	40	651	Mar.	2	1938	16.33	180
83	Santa Anita canyon, Santa Anita Dam	28	130	Mar.	2	1938	4.66	180
84	Sawpit Canyon, Los Angelas	19	115			1889	6.01	107
85	Cameron Cr., near Tehachapi	9.3	382	Sept.	30	1932	41.11	201
86	Fall Cr., near Mouth, near Los Angelas	5.7	119	Mar.	2	1938	20.87	180
87	Upper Willow Springs Canyon, near Mojave	2.1	139	Sept.	30	1932	66.14	210
	COLORADO							
88	Colorado (Grand) R., Fruita	44289	340	July		1884	0.01	99
89	Arkansas R., Pueblo	11914	2908	June		1921	0.24	68
90	Arkansas R., Pueblo	4507	2812	June		1921	0.62	91
91	Bijou Cr., at Mouth	3740	8014	May	31	1935	2.14	139
92	Repiblican R., Newton	3289	2917	May		1935	0.89	152
93	Arkansas R., Florence to Pueblo	2435	2129	June		121	0.87	106
94	Republican R., S. Fk., Newton	1733	2350	May	30	1935	1.36	139
95	Purgatoire Cr., Nine Mile Dam	1645	1818	Sept.	15	1934	1.11	139
96	St. Charles R., Pueblo	1248	2033	June		1921	1.63	68
97	W. Bijou Cr., Byers	725	4663	May	30	1935	6.43	139
98	Kiowa Cr., Bennett	689	2132	May	30	1935	3.10	139
99	Middle Bijou Cr., Peoria	596	4067	May	30	1935	6.83	139
100	Kiowa Cr., N. of Kiowa	492	3115	May	30	1935	6.33	139
101	Middle Bijou Cr., below Wilson Cr.	391	2018	May		1935	5.16	139
102	Cherry Cr., Castlewood, Dam	339	906	Aug.	2	1933	2.67	139
103	Monument Cr., Colorado Spring	337	1416	May	30	1935	4.21	139
104	W. Bijou Cr., Johnson's Bridge	306	970	May	30	1935	3.17	139
105	Horse Cr., near Holly	259	623	Aug.	28	1935	2.41	139

Table G1(b) Data from Creager et al. (1945) (continued)

	Stream and location	Drainage area (km^2)	Flood (cms)	Date of Flood Month	Date	Year	Peak Specific-Discharge [cms/km^2]	Authority
106	Dry Cr., near Pueblo	223	688	June		1921	3.09	68
107	Kiowa Cr., Elbert	155	1232	May	30	1935	7.93	139
108	Rock Cr., near Pueblo	153	1523	June		1921	9.97	68
109	Granda Cr., above Granada	104	878	July	11	1935	8.47	139
110	Peck's Cr., near Pueblo	89	549	June		1921	6.17	68
111	Burro Canyon, Madrid	75	702			1925	9.35	170
112	Boggs Cr., near Pueblo	67	428	June		1921	6.35	68
113	N. Arroyo, near Pueblo	40	274	June		1921	6.77	68
114	Osteen Arroyo, near Pueblo	20	256	June		1921	12.69	68
115	Cameron Arroyo, near Pueblo	19	394	June		1921	20.82	68
116	Templeton Gap, Colorado Springd	18	173	May		1922	9.42	76
117	Blue Ribbon Cr., Pueblo	17	258	June		1921	14.87	68
118	Hogan's Gulch, Eden	16	273	Aug.		1904	17.28	112
119	Misouri Canyon, near mouth, Sec. 26, T.6N R.70W	6.2	123	June	15	1923	19.82	135
120	S. Arroyo, near Pueblo	4.7	54	June		1921	11.60	68
121	Magpie Gulch, near Golden	3.9	54	July		1923	13.92	112
122	Skyrocket Cr., Ouray	2.6	57	July		1923	21.87	112
	CONNECTICUT							
123	Connecticut R., Thompsonville	24960	7985	Mar.	20	1936	0.32	153
124	Hoosatonic, Gaylordsville	2642	895				0.34	69
125	Farmington R.	1513	691				0.46	72
126	Scantic R., N. Br.	306	174				0.57	72
127	Hockanum R.	205	174				0.85	72
128	Farmington R., E. Br., West Hartford	123	190	Nov.		1927	1.55	158
129	Pequonnock, Bridgeport	65	111	July		1905	1.71	1
	DISTRICT of COLUMBIA							
130	Potomac R., near Washington	29940	13705	Mar.		1936	0.46	135
131	Rock Cr., Q St., N. W., Washington	201	277				1.38	140
132	Rock Cr., at Sherill Drive, Washington	161	126	Aug.		1911	0.78	172
	FLORIDA							
133	Yellow R., near Holt	3160	974	Aug.	19	1939	0.31	191
134	Alafia R.	870	850				0.98	182
	GEORGIA							
	Appalachicola R., Junction	44807	10789				0.24	74
135	Savannah R., Augusta	18917	9911	Oct.	3	1929	0.52	132
136	Ocmulgee R., Lumber City	13416	1240	Mar.	9	1939	0.09	191
137	Chattahoochee, West Point	8547	3936	Dec.		1919	0.46	99
138	Oconee Milledgeville	7356	3256	Jan.		1925	0.44	119
139	Rhine, Macon	6667	2727				0.41	69
140	Ocmulgee R., Macon	6281	2549	Jan.		1925	0.41	119
141	Flint R., Culloden	5180	2407	July		1916	0.46	99
142	Etowah R., Rome	4662	1682	Mar.		1906	0.36	69
143	Oconee R., Greensboro	2849	1931	Aug.		1908	0.68	119
144	Broad R., near Carlton	1974	1337	Aug.		1908	0.68	90
145	Tocca R., near Blueridge	598	345			1901	0.58	16
146	Soquee R., Demorest	409	251				0.61	69
	IDAHO							
147	Snake R., near Murphy	108520	1342	June		1918	0.01	103
148	Snake R., S. Fk., Minidoka	58533	1535	June		1896	0.03	69
149	Salmon R., Whitebird	34706	3398	June		1894	0.10	173
150	Snake R., S. Fk., Lyon	14193	1458	May		1904	0.10	69
151	Clearwater R., Kamiah	12561	2169	May		1913	0.17	72

	Stream and location	Drainage area (km^2)	Flood (cms)	Date of Flood Month	Date	Year	Peak Specific-Discharge [cms/km^2]	Authority
152	Payette R., Horshoe Bend	5776	626	June		1921	0.11	173
153	Weiser R., Weiser	4325	507	May		1896	0.12	99
154	Coeur d'Alene R., near Cataldo	3160	623	Mar.	1921		0.20	103
155	St. Joe R., Calder	2797	490	May		1922	0.18	103
156	Teton R., near St. Anthony	2486	215	June		1916	0.09	69
157	Clearwater R., S. Fk., Grangeville	2435	279	May		1921	0.11	103
158	Mooyie R., Snyder	1857	306	June		1916	0.16	103
159	Payette R., N. Fk., Van Wyck	1518	249	May		1921	0.16	103
160	St. maries R., Lotus	1088	250	Mar.		1921	0.23	103
161	Payette R., N. Fk., Lardo	339	119	June		1909	0.35	103
162	Hull's Gulch, Boise	13	142	July		1913	10.93	91
	ILLINOIS							
163	Mississippi R.,Cairo	2338489	56917			1912	0.02	89
164	Ohio R., Cairo	528096	55218	Feb.	3-4	1937	0.10	149
165	Wabash R., Mt. Carmel	74073	12120	Mar.	30	1913	0.16	132
166	Illinois R., at mouth	72297	3540	Apr.		1904	0.05	90
167	Illinois R., Peoria	34913	2268	Mar.		1904	0.06	72
168	Kankakee R., Peoria	12613	954	May	14	1933	0.08	157
169	Iroquois R., Chebanse	5491	765	May	13	1933	0.14	157
170	Spoon R., Seville	4144	1000	Aug.	22	1924	0.24	157
171	Pecatonica R., Freeport	3445	521	Mar.	16	1929	0.15	157
172	Mackinaw R., Green Valley	2849	617	May	19	1927	0.22	157
173	Vermilion R., Streator	2797	453	Jan.	21	1916	0.16	157
174	Big Muddy R., Plumfield	1950	462	Feb.	1	1916	0.24	157
175	Des Plaines R., Riverside	1632	371			1889	0.23	72
176	Sangamon R., S. Fk., Kincaid	1321	334	Mar.	16	1922	0.25	157
177	Spring Cr., Joliet	51	30	June	11	1926	0.59	157
	INDIANA							
178	White R., Hazleton	29267	6654	Mar.	29	1913	0.23	132
179	White R., E. Fk., Shoals	12794	3851	Mar.	28	1913	0.30	132
180	Wabash R., Logansport	9738	3285	Mar.	26	1913	0.34	132
181	Antietam Cr., Sharpsburg	764	192			1902	0.25	17
182	Gunpowder Falls, Glencoe	414	159				0.38	69
	IOWA							
183	Misouri R., Sioux City	837759	15036			1881	0.02	30
184	Mississippi R., Keokuk	308207	10194			1851	0.03	150
185	Mississippi R., Clayton	204712	5947			1880	0.03	30
186	Des Moines R., Keosauqua	36001	2747			1903	0.08	174
187	Cedar R., Cedar Rapids	16369	1611	Apr.		1917	0.10	90
188	Iowa R., Iowa City	8366	1025	June		1918	0.12	174
189	Devil's Cr., near Viele	370	2430	June		1905	6.56	9
190	Dry Run, Decorah	58	456	Mar.		1915	7.89	91
191	Little Devil's Cr.	49	300	June		1905	6.10	91
192	Panther Cr.	36	206	June		1905	5.69	91
	KANSAS							
193	Kansas R., Lawrence	154987	6456			1903	0.04	1
194	Kansas R., Junction City	116316	5069	day-June		1935	0.04	152
195	Republican R., Junction City	64646	4757	day-June		1935	0.07	152
196	Blue R., near Manhattan	16809	2452	May		1903	0.15	72
197	Neosha R., Iola	9505	2110	July		1904	0.22	2
198	Verdifris R., Liberty	7943	1424	July		1904	0.18	2
199	herryvale Cr., Cherryvale	5	53				10.17	31

Table G1(c) Data from Creager et al. (1945) (continued)

	Stream and location	Drainage area (km ^{2})	Flood (cms)	Date of Flood Month	Date	Year	Peak Specific-Discharge [cms/km^2]	Authority
	KENTUCKY							
200	Mississippi R., Columbus	2387698	70792	Feb.	27	1937	0.03	135
201	Ohio R., Paducah	524988	52386	Feb.		1913	0.10	135
202	Ohio R., Louisville	234652	31149	Jan.	27	1937	0.13	135
203	Ohio R., Ashland	156952	20954				0.13	165
204	Green R., Livermore	19425	5890	Jan.	27	1937	0.30	132
205	Kentucky R., Lockport	15980	2803	Jan.	24	1937	0.18	132
206	Cumberland R., Burnside	12665	4644				0.37	142
207	Licking R., Catawba	8599	2441	Jan.	23	1937	0.28	132
208	Big Sandy R., Levisa Fk., Paintsville	5568	1954	Jan.	29	1918	0.35	132
209	Cumberland R., Cumberland Falls	5206	1688				0.32	142
210	Cumberland R., S. Fk., Nevelsville	3263	4531	Mar.	23	1929	1.39	132
211	Cumberland R., Barbourville	2543	1136				0.45	142
212	Rock Castle R., Rock Castle Springs	1932	1031				0.53	142
	LUOISIANA							
213	Mississippi R., Carrollton	3625965	42475	May		1922	0.01	89
214	Mississippi R., Red River Landing	3218562	56634	Feb.	18	1937	0.02	135,132
215	Atchafalaya R., Krotz Springs	388496	12544	Feb.	28	1937	0.03	132
	MAINE							
216	St. John R., Van Buren	21419	3794	May	2	1923	0.18	175
217	Penobscot R., Bangor	19943	3256				0.16	10
218	St. John R., below Fish River at Fort Kent	14737	3426	May	5	1933	0.23	154
219	Penobscot R., West Enfield (Montague)	12147	4332	May	1	1923	0.36	99
220	Kennebec R., Waterville	7848	4446	Dec.	16	1901	0.57	99
221	Androscroggin R., Gulf Island	5853	4219	Mar.	19	1936	0.72	146
222	Sacao R., W. Buxton	4071	2265	Mar.	22	1936	0.56	146
223	Mattawaumkeag R., Mattawaumkeag	3885	1243	May	1	1923	0.32	175
224	Androscroggin R., Rumford	3232	1934	Apr.	15	1895	0.60	99
225	Piscataquis R., near Foxcroft	741	614	Sept.	29	1909	0.83	154
	MARYLAND							
226	Potomas R., Point of Rocks	25004	13592	Mar.		1936	0.54	135
227	Potomasc R., Cumberland	2266	2407	Mar.		1936	1.06	146
228	Monocacy R., Jag Bridge, near Frederick	2116	1832	Aug.	24	1933	0.87	99
229	Gunpowder R.	782	711			1889	0.91	69
230	Potomac R., Bloomington	743	2121	Mar.	23	1924	2.85	146
231	Wills Cr., Cumberland	640	1237	Mar.		1936	1.93	172
232	Octoraro Cr., near Rising Sun	495	719	Aug.	24	1933	1.45	166
233	Patapsco R., N. Br., near Marriottsville	427	552	Aug.	24	1933	1.29	99
234	Town Cr., near Oldtown	383	765	Mar.		1936	1.99	187
235	Deer Cr., Rocks	244	640	Aug.	23	1933	2.62	166
236	Lake Roland	101	254			1868	2.51	91
237	Little Gunpowder Falls, Laurel Branch	93	261	Aug.	23	1933	2.79	99
238	Anacostia R., N. W. Br., near Colesville	55	127	Aug.	23	1933	2.31	99
239	Owens Cr., Lantz	15	127	Dec.		1934	8.63	187
	MASSACHUSETTS							
240	Connecticut R., Montague City	20305	6683	Mar.	19	1936	0.33	153
241	Merrimack R., Lowell	11458	4899	Mar.	20	1936	0.43	153
242	Westfield R., near Westfield	1287	1572	Sept.	21	1938	1.22	183
243	Deerfield R., Charlemont	938	1586	Sept.	21	1938	1.69	183
244	Great R., Westfield	906	1495			1878	1.65	72
245	Westfield R., Knightville	420	954	Sept.	21	1938	2.27	183
246	Fomer R., above reservoir, Holyoke	34	80				2.39	69
247	Manhan R., Holyoke	34	67	Feb.		1900	1.99	91

	Stream and location	Drainage area (km ^{2})	Flood (cms)	Date of Flood Month	Date	Year	Peak Specific-Discharge [cms/km^2]	Authority
	MICHIGAN							
248	Grand R., Grand Rapids	12691	1402	June		1905	0.11	72
249	Tittabawassee R., Freeland	6374	1402	Mar.		1919	0.22	102
250	Escanaba R., Escanaba	2072	303				0.15	69
251	Dead R., Forestville	368	69				0.19	69
	MINNESOTA							
252	Mississippi R., St. Paul	95311	3030	Apr.	29	1881	0.03	132
253	Mississippi R., Anoka	44289	1390				0.03	25
254	Minnesota R., Mankota	37814	1240				0.03	25
255	Mississippi R., Sauk Rapids	32116	1441				0.04	69
256	St. Croix R., St. Croix Falls	15410	1011				0.07	72
257	Pine R., below Pine Reservoir	1171	513	June		1908	0.44	69
	MISSISSIPPI							
258	Mississippi R., Vicksburg	2964227	70651	May	4	1927	0.02	132
259	Yazoo R., Yazoo Mouth	35871	3936	Apr.		1874	0.11	72
260	Coldwater R., Coldwater	3626	1699	Jan.	21	1935	0.47	160
261	Tombigbee R., E. Fk., near Fulton	1683	685	Feb.	15	1939	0.41	191
262	Rocky Cr., near Ellisville	39	470	May		1882	12.10	91
	MISSOURI							
263	Mississippi R., St. Louis	1815573	36812	June	28	1844	0.02	132
264	Missouri R., St. Charles	1374785	16990	June	19	1844	0.01	30
265	Osage, Bagnell	36260	4248	June		1844	0.12	196
266	Meramec R., Eureka	9842	4955	Aug.	22	1915	0.50	132
267	Big R., Byrnesville	2310	2265	Aug.		1915	0.98	132
268	Castor R., Zalma	1023	1133	Jan.	14	1937	1.11	132
269	Rio des Perca, St. Luois	62	172	Aug.		1915	2.80	81
270	Rio des Perca, near St. Louis	40	181	Aug.		1915	4.49	81
	MONTANA							
271	Yellowstone R., Intake	173010	4502	June		1921	0.03	98
272	Clark Fk., near Plains	51541	3256	June		1913	0.06	98
273	Kootenai R., Libby	28490	3681	June		1916	0.13	98
274	Flathead R., near Polson	18156	2124	June		1913	0.12	98
275	Flathead R., Columbia Falls	11810	2492	June		1922	0.21	98
276	Flathead R., N. Fk., Belton	2331	1376	June		1916	0.59	98
277	Sun R., N. FK., Augusta	1554	917	June		1916	0.59	68
278	Beaver Cr., Wibeaux	805	934	June	7	1929	1.16	197
279	Custer Cr., N. E. of Miles City	401	595	June	19	1938	1.48	135
280	Le Noir Coulee, Malta	41	244	June		1906	5.88	120
	NEBRASKA							
281	Republican R., Cambridge	31857	7929	May		1935	0.25	152
282	Republican R., Max	15125	5380	May-June		1935	0.36	152
283	Republican R., below Benkelman	13297	5380	May-June		1935	0.40	169
284	North Loup, St. Paul	10412	2163	June		1899	0.21	120
285	Republican R., Kansas state line	6604	4248	May		1935	0.64	152
	NEVADA							
286	Humboldt R., Oreana	35742	86	May		1897	0.00	72
287	Meadow Valley Wash, near Moapa	5568	231	Jan.		1910	0.04	74
288	Truckee R., Reno	2771	212			1913	0.08	72
289	Carson R., E. Fk., Rodenbohs	1072	152				0.14	69
290	Carson R., E. Fk., State line	772	138	June		1911	0.18	70
291	Baker Cr., Baker	26	5			1914	0.19	72

Table G1(d) Data from Creager et al. (1945) (continued)

	Stream and location	Drainage area (km^2)	Flood (cms)	Date of Flood Month	Date	Year	Peak Specific-Discharge [cms/km^2]	Authority
	NEW HAMPSHIRE							
292	Connecticut R., Orford	8029	1625	Mar.		1913	0.20	99
293	Merrimac R., Franklin Junction	3903	2350	Mar.	19	1936	0.60	136
294	Merrimac R., Franklin Junction	2543	1574	Nov.		1927	0.62	99
295	Pemigewassett R., Plymouth	1611	1863	Mar.	19	1936	1.16	134
296	Saco R., near Contway	1000	1150	Mar.	19	1936	1.15	153
297	Bakers R., near Wentworth	135	425	Nov.		1927	3.15	99
298	Peabody R., near Gorham	104	281	Nov.		1927	2.71	99
299	Ellis R., above Wildcat Brook, Jackson	73	419	Nov.		1927	5.78	99
300	Peabody R., near Glen House	45	0	Nov.		1927	0.01	99
	NEW JERSEY							
301	Delaware R., Trenton	17601	8353	Oct.		1903	0.47	187
302	Delaware R., Belvidere	11764	6230	Oct.	10-11	1903	0.53	166
303	Raritan R., Bound Brook	2088	1869	Sept.		1882	0.90	1
304	Passaic R., Peterson	2033	1008	Oct.	10	1903	0.50	166
305	Pompton R., Two Bridges	984	668			1903	0.68	1
306	Raritan R., N. Br., Milltown	492	442	Sept.	15	1933	0.90	99
307	Ramapo R., Mahwah	306	354	Oct.		1903	1.16	120
308	Pequannock R., Macopin Dam	165	239	Oct.	9	1903	1.45	99
309	Raritan R., N. Br., near Far Hills	67	198	July	23	1919	2.94	166
	NEW MEXICO							
310	San Juan R., at Ship Rock	33152	4248	Oct.	6	1911	0.13	186
311	Canadian R., at Logan	29008	7872	Sept.	30	1904	0.27	186
312	S. Canadian R., near Tucumcari	18777	7929			1904	0.42	184
313	Canadian R., at Taylor Springs	7330	2580	Sept.		1904	0.35	186
314	Ute Cr., near Logan	5206	2832	May	1	1914	0.54	186
315	Canadian R., at French	3833	4417	Sept.		1904	1.15	186
316	Pecos R., near Anton Chico	2797	1141	June	1	1937	0.41	186
317	Couchas R., at Variadero	1787	1467	June	3	1937	0.82	186
318	Mora R., at Loma Parda	1515	977	June	11	1913	0.64	186
319	Mora R., Weber	761	782	Sept.		1904	1.03	68
320	Sapello Cr., at mouth, near Watrous	736	1781	Sept.	29	1904	2.42	186
321	Turquillo R., Mora Valley	414	453			1893	1.09	97
322	Mora R., below Mora	412	631	Sept.		1904	1.53	2
323	Gallinas R., at Montezuma	231	328	Sept.	30	1904	1.43	186
324	Palomas R., near Hermosa	135	246	July		1925	1.83	74
325	Tanner Draw, near Clapham	53	317	May-June		1937	6.03	186
326	Draw, near Clayton	6.9	72	May-June		1937	10.48	186
	NEW YORK							
327	St. Lawrence R., near Ogdensburg	772020	9033				0.01	105
328	Niagara R., Niagara	682303	8438				0.01	114
329	Niagara R. (Land Area Only)	453246	8467				0.02	114
330	Hudson R., Albany	20979	6230	Mar.	28	1913	0.30	141
331	Hudson R., Mechanicsville	11655	3398	Mar.	28	1913	0.29	166
332	Mohawk R., Cohoes	8951	3964	Mar.		1914	0.44	146
333	Delaware R., Port Jervis	7967	4389	Oct.	10	1903	0.55	166
334	Chemung R., Chemung	6553	2614				0.40	166
335	Susquehanna R., Conklin	5802	1758	Mar.	18	1936	0.30	146
336	Chemung R., below Big Flats	5568	2469	Mar.		1936	0.44	187
337	Chemung R., Elmira	5322	3908	June	1	1889	0.73	9
338	Chenango R., Chenango Forks	3864	2345	July		1935	0.61	154
339	Tioga R., near Erwins	3548	1693	Mar.	12	1936	0.48	146
340	Genesee R., St. Helena	2569	1235	May		1916	0.48	113
341	Schoharie Cr., Fort Hunter	2331	1405	Mar.		1901	0.60	37
342	Black R., Lyons Falls	2323	1169	Apr.		1869	0.50	72
343	Delaware R., E. Br., Hancock	2170	2599	Mar.	26	1904	1.20	99
344	Delaware R., E. Br., Fishs Eddy	2028	1509	Aug.	24	1933	0.74	166
345	Tioga R., Lindley	1994	1167	Mar.		1936	0.58	187
346	Tioughnioga R., Itaska	1904	1266	July	8	1935	0.66	166
347	Delaware R., W. Br., Hales Eddy	1536	1303	Oct.	10	1903	0.85	166
348	Cohocton R., near Campbell	1222	1286	July	8	1935	1.05	166
349	Cattaraugus Cr., Versailles	1210	847	Mar.		1918	0.70	104
350	Ausable R., Ausable Forks	1150	705	Mar.		1913	0.61	113
351	Esopus Cr., Saugerties	1080	1560	Dec.		1878	1.44	69
352	West Canada Cr., Hinckley	963	1107	Apr.		1869	1.15	37
353	Canisteo R., West Cameron	891	991	July		1935	1.11	99
354	Croton R., Croton Dam	878	719			1867	0.82	72
355	East Canada Cr., Dolgeville	684	566	Mar.	26	1913	0.83	99
356	Beaver Kill, Cook's Falls	624	538	Aug.		1933	0.86	187
357	Schoharie Cr., Prattsville	611	821	Sept.		1924	1.34	101
358	Neversink R., Oakland Valley	575	566	Aug.	24	1933	0.98	133
359	Catskill Cr., South Cairo	544	595	Spring		1901	1.09	27
360	Esopus Cr., Coldbrook	497	1557	Aug.	24	1933	3.13	166
361	Owego Cr., near Owego	482	665	July	8	1935	1.38	166
362	Canisteo R., Canisteo	479	708	July		1935	1.48	187
363	Fall Cr., Ithaca	321	731	July		1935	2.27	122
364	Ouleout Cr., East Sidney	262	473	July		1935	1.81	187
365	Rondout Cr., near Lackawack	259	756	Aug.	26	1928	2.92	166
366	Salmon Cr., Myers	231	524	July		1935	2.27	133
367	Bennett Cr., near Canisteo	185	351	July		1935	1.90	99
368	Canacadea Cr., Hornell	154	753	July		1935	4.90	99
369	Taughannock Cr., N. Halseyville	147	1192	July		1935	8.12	133
370	Canacadea Cr., Almond	129	623	July		1935	4.83	187
371	Meads Cr., E. Campbell	119	858	July		1935	7.19	133
372	Campbell Cr., near Kanona	93	396	July		1935	4.28	99
373	Dudley Cr., near Lisle	77	459	July		1935	5.98	133
374	Glen Cr., Watkins Glen	55	790	July		1935	14.32	133
375	Purdy Cr., near Canisteo	55	255	July		1935	4.64	99
376	Merill Cr., near Upper Lisle	54	428	July		1935	7.94	99
377	Stony Brook, Stony Brook Glen	47	164	July		1935	3.50	99
378	Fivemile Cr., Enfield	47	237			1935	5.09	133
379	Big Cr., near North Hornell	43	337	July		1935	7.89	99
380	Sawkill, near Bearsville	31	283	July		1935	9.02	99
381	Trumansburg Cr., Trumansburg	30	504	July		1935	16.92	133
382	Willet Cr., Marathon	28	182	July		1935	6.39	99
383	Sawkill, near Shady	25	260	July		1935	10.56	133
384	Stephens Cr., near Carson	18	190	July		1935	10.41	99
385	Strongs Br., near Smithville Flats	17	188	July		1935	11.34	99
386	Pine Cr., near Monterey	13	93	July		1935	7.15	187
387	Glen Cr., near Towsend	7.5	208	July		1935	27.54	133
388	Harrisburg Hollow, near Hickory Hill	6.4	80	July		1935	12.34	99
389	Brook, Bradford	4.4	55	July		1935	12.63	99
390	Mad Cr., Leroy	3.9	98	May		1916	25.15	71
391	Gilmore Br., near Preston	1.6	15	July		1935	9.13	99
392	Beacon Cr., near Fishkill	0.6	23	July		1935	34.99	27
	NORTH CAROLINA							
393	Roanoke R., Old Gaston	21626	7787	Nov.	26	1877	0.36	99
394	Pee Dee R., near Rockingham	17897	6003	Sept.	19	1928	0.34	155
395	Cape Fear R., Fayetteville	11111	3766	Aug.	29	1908	0.34	156
396	Yadkin R., High Rock	10179	5210	July		1916	0.51	99

Table G1(e) Data from Creager et al. (1945) (continued)

	Stream and location	Drainage area (km^2)	Flood (cms)	Date of Flood Month	Date	Year	Peak Specific-Discharge [cms/km^2]	Authority
397	Yadkin R., Donaha	4144	2265	July		1916	0.55	99
398	Haw R., near Pittsboro	3471	2775	Aug.		1908	0.80	156
399	French Broad R., Asheville	2458	2549	July		1916	1.04	99
400	Little Tennessee R., Jackson	1748	1628	Dec.		1901	0.93	21
401	Tuckasegee R., Bryson	1715	1093	Mar.		1889	0.64	72
402	Flat R., Bahama	388	385	Sept.	8	1934	0.99	176
403	Broad R., near Chimney Rock	251	580	Aug.	15	1928	2.31	176
404	Little Sugar Cr., near Charlotte	107	199	Aug.	16	1928	1.86	176
405	Morgan Cr., near Chapel Hill	70	850	Aug.	4	1924	12.15	196
406	Cane Cr., Bakersville	57	835	May		1901	14.66	34
407	Pigeon R., W. Fk., Spruce	32	467	Aug.		1940	14.79	194
408	Pigeon R., Middle Prong, Spruce	22	464	Aug.		1940	21.35	194
409	Big Cr., near Sunburst	4	464	Aug.	30	1940	106.10	189
410	Big Cr., near Sunburst	3	365	Aug.		1940	106.85	194
	NORTH DAKOTA							
411	Red R., Grand Forks	64749	1203			1897	0.02	25
412	Little Missouri, Medora	14970	541				0.04	69
413	Heart R., Richardton	3237	227				0.07	72
414	Grande, N. Br., Haley	1295	164			193	0.13	72
	OHIO							
415	Ohio R., Cincinnati	196320	26901	Jan.	26	1937	0.14	135
416	Muskingum R., McConnellsville	19192	7646				0.40	135
417	Miami R., Miami	10197	10930	Mar.		1913	1.07	107
418	Scioto R., Chillicothe	9971	7079	Mar.		1913	0.71	132
419	Miami R., Dayton	6501	7079	Mar.		1913	1.09	132
420	Scioto R., Columbus	4206	3908	Mar.	25	1913	0.93	147
421	Lower Scioto R., Columbus	4066	3143	Mar.		1913	0.77	71
422	Little Miami R., Milford	3095	2347	Mar.	19	1913	0.76	132
423	Miami R., Tadmor	2927	3596	Mar.		1913	1.23	107
424	Scioto R., Columbus	2712	2401	Mar.		1913	0.89	39
425	Mad R., Osborn	1681	2152	Mar.		1913	1.28	107
426	Stillwater R., Englewood	1673	2418	Mar.		1913	1.45	147
427	Olentangy R., Columbus	1331	1427	Mar.		1913	1.07	71
428	Stillwater R., Englewood	1160	1458	Mar.		1913	1.26	107
429	Tein Cr., Germantown	699	1866	Mar.		1913	2.67	107
430	Ludlow Cr., above Dayton	168	490	Mar.		1913	2.91	91
431	Lost Cr., above Dayton	135	841	Mar.		1913	6.24	91
432	Honey Cr., E. Fk., New Carlisle	31	428	July		1918	13.99	71
433	Honey Cr., E. Fk., New Carlisle	17	419	July		1918	24.15	71
434	Honey Cr., W. Fk., New Carlisle	9	99	July		1918	10.93	109
	OKLAHOMA							
435	Arkansas R., Muskogee	250710	6881	June	9	1935	0.03	132
436	W. Quartermaster Cr.	280	1954	Apr.		1934	6.99	169
437	W. Quartermaster Cr.	158	968	Apr.		1934	6.13	169
438	Ninemile Cr.	109	1022	Apr.		1934	9.40	169
439	E. Quartermaster Cr.	107	1552	Apr.		1934	14.44	169
440	Sergeant Major Cr.	96	1519	Apr.		1934	15.85	169
441	East Hay Cr. (Washita Basin)	10	181	Apr.		1934	17.49	169
	OREGON							
442	COLUMBIA R., Dalles	613824	39360	June		1894	0.06	72
443	Willamette R., Albany	12587	8580			1861	0.68	72
444	Willamatte R., Middle Fk., Jasper	3755	2633				0.70	69
445	Siletz R., Siletz	528	1155	Nov.	20	1921	2.19	177
446	Willow Cr., near Heppner	324	1019			1903	3.15	19
447	Willow Cr., near Heppner	52	1019	June	4	1903	19.68	19
	PENNSYLVANIA							
448	Susquehanna R., McCall's Ferry	69411	24636	Mar.	19	1936	0.35	135
449	Ohio R., Pittsburg	49484	18123	Mar.		1936	0.37	146
450	Susquehanna R., Sunbury	47397	15008	Mar.		1936	0.32	187
451	Susquehanna R., Danville	29060	7306	Mar.	18	1865	0.25	154
452	Allegheny R., Kittaning	23336	8637	Mar.		1913	0.37	90
453	Susquehanna R., Towanda	20194	5324	Mar.		1936	0.26	166
454	Allegheny R., Parkers Landing	19868	7079	Mar.		1865	0.36	187
455	Susquehanna R., W. Br., Watsonton	17083	8042	Mar.	18	1936	0.47	134
456	Allegheny R., Franklin	15493	5550	Mar.		1865	0.36	187
457	Susquehanna R., W. Br., Williamsport	14716	8863	Mar.		1936	0.60	146
458	Monongahela R., Lock No. 4	14064	5862	July	11	1888	0.42	1
459	Juniata R., Newport	9013	8269	Mar.		1902	0.92	90
460	Susquehanna R., W. Br., Renovo	7705	6683	Mar.	18	1936	0.87	135
461	Beaver R., Wampun	5789	2464	Mar.		1913	0.43	187
462	Schuylkill R., Philadelphia	4903	3596	Oct.		1869	0.73	187
463	Kiskiminetas R., Avonmore	4463	5663	Mar.		1936	1.27	134
464	Youghiogheny R., Sutersville	4442	2832	Mar.		1936	0.64	187
465	Youghiogheny R., Connellsville	3434	2619	Mar.		1936	0.76	187
466	Lehigh R., Bethlehem	3315	2662	Feb		1902	0.80	187
467	Youghiogheny R., Ohiopyle	2758	2407	Mar.		1936	0.87	187
468	Juniata R., Raystown Br., Hawn's Bridge	2455	2449	Mar.		1936	1.00	187
469	Schuylkill R., Reading	2331	2268			1850	0.97	107
470	Juniata R., Frankstown Br., Petersburg	2088	2265	Mar.		1936	1.09	187
471	Junaita R., Raystown Br., Saxton	1958	2280	Mar.		1936	1.16	187
472	Conemaugh R., New Florence	1937	2582				1.33	134
473	Juniata R., Raystown Br., Juniata Crossing	1422	1897	Mar.		1936	1.33	187
474	W. Conewago Cr., near Manchester	1321	1348	Aug.	24	1933	1.02	166
475	Stony Cr., Ferndale	1168	1659	Mar.		1936	1.42	187
476	Blacklick Cr., Blacklick	1010	1464	Mar.		1936	1.45	187
477	Clearfield Cr., Dimeling	961	1065	Mar.		1936	1.11	187
478	Swatara Cr., Harper Tavern	862	1501	June		1889	1.74	187
479	Juniata R., Frankstown Br., Williamsburg	754	1348	Mar.		1936	1.79	187
480	Perkiomen Cr., Grater's Ford	723	1167	July		1935	1.61	187
481	Loyalhanna Cr., New Alexandria	686	878	Mar.		1936	1.28	187
482	Codorus Cr., York	572	963	Aug.	23-24	1933	1.68	135
483	Neshaminy Cr., near Langhorne	544	850	Aug.		1933	1.56	187
484	Sherman Cr., Shermandale	518	1048	July		1927	2.02	187
485	Little Conemaugh R., Conemaugh	484	816	Mar.		1936	1.68	187
486	Pequea Cr., near Pequea	396	793	June		1938	2.00	187
487	Chester Cr., near Philadelphia	161	1756	Aug.		1843	10.93	77
488	Darby Cr., near Philadelphia	124	787	Aug.		1843	6.33	77
489	Crum Cr., near Philadelphia	57	255	Aug.		1843	4.48	77
490	Ridley Cr., near Philadelphia	52	425	Aug.		1843	8.20	77
491	Mill Cr., Erie	33	365	Aug.		1915	10.93	91
492	Gist Run, near Dunbar	18	109	July		1912	6.01	187
493	Canodochly Branch, East Prospect	5.7	102	July		1914	17.84	71
494	Canodochly Cr., near Long Level	5.7	70	July		1914	12.23	187
495	Indian Run, Letort	5.4	115				21.14	71
496	Green Branch, Bridgeville	4.4	77	July		1914	17.43	83
497	Mann's Run, Creswell Station	1.7	48	July		1914	27.74	71
498	Docker's Hollow, north Braddock	1.6	68	June		1917	43.73	71
499	Whictler's Run, near Long Level	1.6	13	July		1914	8.31	187
500	Shingle Run, Johnstown	1.6	8	Aug.		1931	5.39	187

Table G1(f) Data from Creager et al. (1945) (continued)

	Stream and location	Drainage area (km ^{2})	Flood (cms)	Date of Flood Month	Date	Year	Peak Specific-Discharge [cms/km ^{2}]	Authority
501	Bull's Run, Long Level	1.5	69	July		1914	45.62	71
	RHODE ISLAND							
502	Seekonk, Providence	492	306			1867	0.62	72
503	Flat River	158	207	Mar.		1843	1.31	72
	SOUTH CAROLINA							
504	Santee R., Ferguson	38332	10421	July	22	1916	0.27	176
505	Peedee R., Cheraw	23569	7730	Sept.		1908	0.33	74
506	Savannah R., Woodland	17094	5663	Aug.	26	1908	0.33	99
507	Broad R. of Carolina, Richtex	12432	6768	Oct.	3	1929	0.54	156
508	Broad R., Alston	11937	3710	May		1901	0.31	72
509	Catawba R., near Rock Hill	7899	4276	May	23	1901	0.54	99
510	Saluda R., near Silverstreet	4066	2373	Oct.	3	1901	0.58	176
511	Catawba R., Catawba	3976	3115	July		1916	0.78	118
512	Pacolet R., Spartansburg	1036	1008	June		1903	0.97	19
513	Enoree R., near Enoree	795	1014	Oct.	2	1929	1.27	176
514	Ready R., near Princeton	557	793	Aug.		1908	1.42	99
	SOUTH DAKOTA							
515	Cheyenne R., Hot Springs	22585	4248	May		1920	0.19	112
516	White R., near interior	10593	464			1905	0.04	72
517	Red Water R., Belle Fourche	2606	228			1904	0.09	72
	TENNESSEE							
518	Mississppi R., Memphis	2415929	50970	Jan.	29	1937	0.02	135
519	Tennessee R., Johnsville	99714	13026	Mar.	24	1897	0.13	132
520	Tennessee R., Chattanooga	55379	12997	Mar.	11	1867	0.23	135
521	Tennessee R., Breedenton	45221	11327	Mar.	11	1867	0.25	135,132
522	Cumberland R., Clarksville	41440	8212	Jan.	24	1937	0.20	132
523	Cumberland R., Nashville	33307	5748	Jan.	1	1927	0.17	132
524	Tennessee R., London	31857	10336	Mar.	11	1867	0.32	135,132
525	Cumberland R., Carthage	27816	5182	Dec.	30	1926	0.19	132
526	Tennessee R., Knoxville	23284	5522	Mar.	1	1902	0.24	142
527	Cumberland, Celina	18959	4332	Dec.	29	1926	0.23	132
528	French Broad R., Dandridge	11515	4389	May	21	1901	0.38	135,132
529	Clinch R., Rogersville	8003	2104			1862	0.26	142
530	Holston R., Rogersville	7925	2008	Jan.	29	1918	0.25	132
531	Little Tennessee R., McGhee	6397	3341	Apr.	2	1920	0.52	142
532	Hiwassee R., Charleston	5949	3497	Mar.	13	1886	0.59	132,142
533	Caney Fk., Silver Point	5439	5040	Mar.	23	1929	0.93	196
534	Hatchie R., Stantn	5025	1671	Jan.	22	1935	0.33	132
535	Obion R., Obion	4869	2818	Jan.	24	1937	0.58	132
536	Little Tennessee R., Calderwood	4843	1982				0.41	142
537	French Wood R., Newport	4817	1761	Apr.	8	1903	0.37	142
538	Caney Fork, Rock Island	4248	5947	Mar.	23	1929	1.40	142
539	Duck R., Columbia	3134	1240	Mar.	25	1929	0.40	142
540	Hiwassee R., Greenville	3056	1560	Nov		1906	0.51	69
541	Nolichucky R., Greenville	2953	2081				0.70	142
542	Elk R., Fayetteville	2220	1291				0.58	142
543	Nolichucky R., Embreeville	2059	1192	Mar.	26	1935	0.58	132
544	Emercy R., Harriman	2054	4276	Mar.	3	1929	2.08	196
545	Emery R., Oakdale	1979	1917	Jan.	2	1937	0.97	132
546	Watauga R., Elizabethton	1792	1133	July	16	1916	0.63	132
547	Little Tennessee R., Judson	1748	1628	Dec.		1901	0.93	69
548	Collins R., McMinnville	1616	2132	Mar.	23	1929	1.32	142
549	Stones R., Smyrna	1430	1274	Mar.	23	1929	0.89	132
550	Obey R., Byrdstown	1171	991	June	29	1928	0.85	142
551	Buffalo R., Flatwoods	1137	985				0.87	142
552	Little Pigeon R., Sevierville	914	906	June	29	1928	0.99	132
553	New R., New River	808	1982	Mar.	23	1929	2.45	142,196
554	Piney R., Spring City	251	467				1.86	142
555	Big Rock Cr., near Verona	204	748	June	18	1939	3.67	185
556	Daddy Cr., Grassy Cove	119	413	Mar.	23	1929	3.47	142
557	Robertson Fork, E. of Lynnville	32	173	June	18	1939	5.34	185
558	Big Rock Cr., above Lewisburg	31	275	June	18	1939	8.84	185
559	Fountain Cr., Culleoka	28	207	June	18	1939	7.46	185
560	Belfast Cr., above Farmington	26	113	June	18	1939	4.29	185
561	Fountain Cr., S. Fk., below Campbells Sta.	22	173	June	18	1939	7.94	185
562	Globe Cr., E. Fk., Mackenzie School	17	462	June	18	1939	27.00	185
563	Mooresville Cr., near Mooresville	11	195	June	18	1939	17.96	185
564	Bear cr., near Mooresville	8.3	93	June	18	1939	11.27	185
565	Little R., E. Fk., Pigeon	1.0	127	Aug.	30	1940	123.00	189
566	Murchison Farm, Jackson	0.4	9	Apr.		1918	20.77	116
	TEXAS							
567	Rio Grande, near Del Rio	319391	17120	Sept.	1	1932	0.05	126
568	Colorado R., Austin	68246	13620	June	15	1935	0.20	150
569	San Juan R., Sta. Rosalia	33670	9486				0.28	135
570	Colorado R., near Stacy	30199	10081	Sept.	18	1936	0.33	150
571	Little R., Cameron	18218	18321	Sept.	10	1921	1.01	150
572	Concho R., near Paint Rock	13615	8523	Sept.	17	1936	0.63	150
573	Little R., near Little River	13571	9373	Sept.	10	1921	0.69	150
574	Concho R., near San Angelo	10922	6966	Aug.	6	1906	0.64	150
575	Devils R., near Del Rio	10515	16905	Sept.	1	1932	1.61	150
576	Llano R., near Castell	9101	10987	June	14	1935	1.21	150
577	Frio R., near Derby	9047	6513	July	4	1932	0.72	150
578	San Jacinto R., Huffman	7229	7164	Nov.		1940	0.99	188
579	Devils R., near Juno	7078	10477	Sept.		1932	1.48	129
580	Nueces R., near Uvalde	4999	17443	June	14	1935	3.49	150
581	San Jacinto R., near Humble	4690	5295	Nov.		1940	1.13	188
582	Llano R., near Junction	4564	9033	June	15	1935	1.98	150
583	Lozier Cr., near Langtry	4475	5578	Sept.	4	1935	1.25	150
584	North Concho R., San Angelo	4338	5210	Sept.	17	1936	1.20	150
585	Pecan Bayou, near Brownwood	4180	6654	July	3	1932	1.59	150
586	Pedernales R., near Spicewood	3351	4389	May	28	1929	1.31	150
587	San Macros R., Ottine	3235	5720	May	29	1929	1.77	150
588	Guadalupe R., near Comfort	2372	5154	July	1	1932	2.17	150
589	W. Nueces R., near Cline	2279	15178	June	14	1935	6.66	150
590	Frio R., near Uvalde	2176	4191	July	3	1932	1.93	150
591	San Jacinto, Conroe	2155	3115	Nov.		1940	1.45	188
592	nueces R., Laguna	1979	6031	June	14	1935	3.05	150
593	Dry Devils R., near mouth	1937	3653	Sept.	1	1932	1.89	150
594	Jim Ned Cr., near Brownwood	1730	5295	July	3	1932	3.06	150
595	Guadalupe R., Kerrville	1476	5550	July	1	1932	3.76	129
596	S. Llano R., near Telegraph	1399	4531	June	14	1935	3.24	150
597	Sycamore Cr., near Del Rio	1357	6088	June	14	1935	4.49	150
598	Sandies Cr., near Westhoff	1277	2625	July	2	1936	2.06	150
599	Frio R., Concan	1256	4587	July	1	1932	3.65	131
600	South Concho R., Christoval	1124	2268	Sept.	17	1936	2.02	150
601	San Gabriel R., Georgetown	1116	4531	Sept.	10	1921	4.06	67
602	Blanco R., near San Marcos	1111	3936	May	28	1929	3.54	150
603	W. Nueces R., near Brackettville	1041	16424	June	14	1935	15.77	150
604	Hondo Cr., near hondo	1036	2118	July	2	1932	2.04	150

Table G1(g) Data from Creager et al. (1945) (continued)

	Stream and location	Drainage area (km ^{2})	Flood (cms)	Date of Flood Month	Date	Year	Peak Specific-Discharge [cms/km^2]	Authority
605	Blanco R., Wimberley	979	3200	May	28	1929	3.27	150
606	Teneha Cr., near Joaquin	969	3313	July	24	1933	3.42	150
607	Aquilla Cr., near Gholson	963	2393	Sept.	27	1936	2.48	150
608	Frio R., Rio Frio	961	3625	July	1	1932	3.77	150
609	Plum Cr., near Lulina	922	2223	July	1	1936	2.41	150
610	Onion Cr., near Delvalle	873	3908	Sept.	10	1921	4.48	150
611	Guadalupe R., near Ingram	870	5833	July	1	1932	6.70	150
612	James R., near Mason	870	2432	July	2	1932	2.80	150
613	Sabinal R., Sabinal	668	2030	July	1	1932	3.04	150
614	Pinto Cr., near Del Rio	593	1548	Aug.	31	1932	2.61	150
615	Paint Cr., near Telegraph	565	1962	June	14	1935	3.48	150
616	Seco Cr., near D'Hanis	396	6513	May	31	1935	16.44	150
617	Onion Cr., near Buda	391	1506	May	28	1929	3.85	150
618	Salado Cr., Salado	383	4049	Sept.	10	1921	10.56	67
619	Dry Frio R., near Reagan Wells	311	1832	June	14	1935	5.89	150
620	Copperas Cr., near Roosevelt	306	2801	Sept.	15-16	1936	9.16	150
621	Barton Cr., near Riley	295	1116	May	28	1929	3.78	150
622	Johnson Cr., near Ingram	287	3908	July	2	1932	13.59	150
623	N. Fk., Guadalupe R., near Hunt	285	3058	July	1	1932	10.73	150
624	Terrett Draw, near Ft. McKavett	267	1014	Sept.	16	1936	3.80	150
625	Sandies Cr., near Dewitt	246	1538	July	1	1936	6.25	150
626	Blanco R., near Blanco	239	1232	May	28	1929	5.16	150
627	San Antonio R., below San Pedro Creek	220	1201	Sept.	10	1921	5.46	150
628	W. Fk., Copperas Cr., near Roosevelt	210	1427	Sept.	16	1936	6.80	150
629	Pecan cr., near San Angelo	210	864	Sept.	15	1936	4.12	150
630	Childress Cr., near China Springs	205	1331	Sept.	26-27	1936	6.50	150
631	E. Fk., Frio R., near Leakey	194	2534	July	1	1932	13.05	150
632	Brushy Cr., Round Rock	193	977	Sept.	10	1921	5.05	67
633	Hamilton Cr., near Marble Falls	174	824	Sept.	15	1936	4.75	150
634	S. Fk., Guadalupe R., Victoria	169	2387	July	1	1932	14.11	150
635	San Felipe Cr., Del Rio	161	1274	June		1935	7.94	150
636	E. Fk., James R., Old Knoxville	157	2973	July	1	1932	18.88	150
637	Flat Fork Cr., near Center	150	1195	Sept.	17	1936	7.95	150
638	N. Fk. Of Medina R., Lima	140	1138	Sept.	9	1921	8.14	150
639	Grape Cr., near Carlsbad	137	900	July	2	1932	6.56	150
640	San Pedro Cr., below Apache Creek	120	919	Sept.		1921	7.63	150
641	Sabinal R., Vanderpool	118	1481	July	2	1932	12.51	150
642	San Antonio, San Antonio	89	671	Sept.		1921	7.55	67
643	E. Fk., Terrett Draw, below Coal Kiln Draw	85	530	Sept.	16	1936	6.20	150
644	E. Fk., Grape Cr., near Carlsbad	83	665	Sept.	17	1936	8.03	150
645	O'Neil Cr., near Leesville	78	850	July	1	1936	10.93	150
646	Olmos Cr., San Antonio	68	793	Sept.	9	1921	11.60	150
647	Boogs Cr., near Pueblo	67	428				6.35	71
648	Apache Cr., San Antonio	62	640	Sept.		1921	10.38	67
649	Atascosa R., near Benton City	55	733	June	22	1924	13.29	150
650	Martinez Cr., San Antonio	51	677				13.33	71
651	E. Fk., Terrett Cr., above Coal Kiln Draw	49	343	Sept.	16	1936	6.96	150
652	Alazan Cr., Ssan Antonio	45	946	Sept.		1921	20.99	165
653	W. Fk., Grape Cr., near Carlsbad	44	402	Sept.	17	1936	9.13	150
654	Dry Cr., near San Angelo	36	697	Sept.	17	1936	19.21	150
655	Bunton Branch, near Angelo	11	391	June	30	1936	36.80	150
656	Sevenmile Draw, Ames	6.2	146	Sept.	26	1936	23.42	150
657	Red Bank Cr., near San Angelo	2.0	71	Sept.	17	1936	35.82	150
	UTAH							
658	Green R., Blake	98937	1903	May		1897	0.02	120
659	Virgin R., Virgin City	2616	340			1912	0.13	72
660	Weber R., Oakley	422	116				0.27	69
661	Farmington Canyon, Farmington	18	69	Aug.		1923	3.83	74
662	North Canyon, near Centerville	10	51	Aug.		1923	4.92	74
663	China Wash, near Hurricane	3	16	Aug.		1916	5.47	74
	VERMONT							
664	Connecticut R., White River Junction	10536	3851	Nov.	4	1927	0.37	136
665	Winooski R., Montpelier	2771	3285	Nov.	4	1927	1.19	145
666	White R., West Hartford	1787	3398	Nov.	4	1927	1.90	136
667	Winooski R., Montpelier	1121	1614	Nov.	3	1927	1.44	136
	VIRGINIA							
668	James R., near Richmond	17500	4474	Mar.		1936	0.26	172
669	Stauton R., Randolph	7977	2124	Dec.		1901	0.27	120
670	Dan R., South Boston	7071	2294	Aug.	16	1940	0.32	135
671	New R., Radford	7058	4927			1900	0.70	21a
672	James R., Buchanan	5398	2611	Mar.	27	1913	0.48	172
673	Shenandoah R., S. Fk., near Front Royal	4242	3200	Mar.	18	1936	0.75	172
674	Rappahannock, near Fredericksburg	4141	1869	May	13	1924	0.45	154
675	James R., N. Fk., Glasgow	2152	1053			1896	0.49	71
676	Roanoke R., Roanoke	1005	793	Aug.	14	1940	0.79	135
677	Craig Cr., Parr	857	609	Jan.	23	1935	0.71	176
678	Powell R., Pennington	787	818				1.04	142
679	Blackwater R., near Union Hall	539	558	Aug.	14	1940	1.04	135
	WASHINGTON							
680	Columbia, Grand Coulee	181298	13932				0.08	150
681	Clark Fk., Newport	62677	6145	June		1894	0.10	69
682	Yakima R., Kiona	14297	1798	Nov.		1906	0.13	72
683	Yakima R., Union Gap	9194	1809	Nov.		1906	0.20	99
684	Yakima R., Umtanum	4196	1161	Nov.		1906	0.28	178
685	Cowlitz R., Mossy Rock	3030	1441	Nov.		1906	0.48	72
686	Yakima R., Cle Elum	1295	725	Nov.		1906	0.56	178
687	Cle Elum Lake, Roslyn	523	530	Nov.		1906	1.01	178
688	Baker R., near Anderson Cr.,	477	1042	Dec.		1917	2.19	119
689	Cedar R., Landsberg	352	385	Nov.	19	1911	1.09	178
690	Wynoochee R., near Montesano	272	708	Feb.	11	1924	2.60	99
	WEST VIRGINIA							
691	Ohio R., Parkersburg	98290	18406	Mar.	30	1913	0.19	165
692	Ohio R., Wheeling	61641	14357	Feb.		1884	0.23	99
693	Kanawha, Kanawha Falls	21694	7646	Sept.	14	1878	0.35	172
694	Potomac R., Shepherdstown	15374	9486	Mar.	19	1936	0.62	135
695	Shenandoah R., Millville	7874	4248	Mar.		1936	0.54	172
696	Monongahela R., Hoult	6294	2591	Jan.		1919	0.41	187
697	Potomac R., S. Br., near Springfield	3810	4049	Mar.		1936	1.06	172
698	Cheat R., Morgantown	3574	4531	July		1888	1.27	187
699	Greenbriar R., Alderson	3481	1773	Mar.		1913	0.51	69
700	Tygart R., Fetterman	3377	2104	July		1912	0.62	187
701	Big Shady R., Tug Fk., Kermit	3069	1982	Mar.	29	1913	0.65	132
702	Elk R., Queen Shoals	2966	2585	July	5	1932	0.87	132
703	Cheat R., Rowlesburg	2517	1846	Feb.		1932	0.73	187
704	Monongahela, W. Fk., Enterprise	1966	1982	July	10	1888	1.01	132
705	Cheat R., near Parsons	1862	2407	July		1888	1.29	187
706	Gauley R., Summerville	1777	2605	July	4	1932	1.47	144
707	Cacapon R., near Great Cacapon	1735	2917	Mar.		1936	1.68	172
708	Middle Island Cr., Little	1186	1274	Aug.		1875	1.07	132

Table G1(h) Data from Creager et al. (1945) (continued)

	Stream and location	Drainage area (km ^{2})	Flood (cms)	Date of Flood			Peak Specific-Discharge [cms/km ^{2}]	Authority
				Month	Date	Year		
709	Coal R., Ashford	1018	1152	Aug.	9	1916	1.13	132
710	Potomac R., S. Fk. Of S. Br., near Moorefield	702	1218	Mar.		1936	1.73	99
711	Shavers Fork, Parsons	596	708	July		1907	1.19	187
712	Big Shady Cr., Rockville	518	850	July		1907	1.64	187
713	Shavers Fk., Cheat Bridge	149	311	July		1896	2.09	187
714	Elkhorn Cr., Keystone	114	1699	June		1901	14.91	34
	WISCONSIN							
715	Mississippi R., Prescott	116549	3794	Apr.	30	1881	0.03	132
716	Wisconsin R., Muscoda	26677	2288	Sept.	16	1938	0.09	132
717	Wisconsin R., Killburn	20720	2265				0.11	90
718	Chippewa R., Eau Claire	17456	1719	June		1905	0.10	1
719	Wisconsin R., Necedah	15022	2645	June		1905	0.18	120
720	Chippewa R., Chippewa Falls	14504	2209	Mar.	27	1920	0.15	132
721	Wisconsin R., near Merrill	7200	1274	July	24	1912	0.18	132
722	Black R., Neillsville	1748	654				0.37	69
	WYOMING							
723	Big Horn R., Hardin	53612	1155			1908	0.02	72
724	Big Horn, Thermopolis	20927	844	July	24	1923	0.04	125
725	Powder R., Arvada	15669	2690	Sept.		1923	0.17	112
726	Salt Cr., below Reservoir	2056	1371	Sept.		1923	0.67	112
727	Salt Cr., Sec. 36 T.41N, R.79W	1347	906	Sept.	27	1923	0.67	196
728	Laramie Reservoir Outlet, Laramie	186	198	Mar.		1913	1.06	38
	FOREIGN							
729	Amazon R., at mouth, Brazil	6133061	201333				0.03	96
730	Amazon R., Obidos, Brazil	5037502	192838				0.04	96
731	Yangtze Kiang R., China	2848973	84951				0.03	92
732	Ganges R., India	953033	50970				0.05	93
733	Irrawaddy R, India	387978	53802				0.14	93
734	Rhine, Germany-Dutch border	224344	12997				0.06	181
735	Rhine, Emmerich, Germany	160578	12035				0.07	165
736	Fitsroy R., Austria	150219	17358	Feb.		1896	0.12	85
737	Danube, Vienna, Austri	102045	14017			1501	0.14	107
738	Cagayan R., Luzon, Philippine Island	10619	27751	Dec.	4	1936	2.61	135
739	San Juan R., China	8702	7079				0.81	138
740	Chagres R., near Gatun, Panama	3419	3511	Dec.	28	1909	1.03	32
741	Musi R., Hyderabad, India	2233	12035			1908	5.39	107
742	Ardeche R., at Junction with Rhones, France	2152	9005			1827	4.18	63
743	Towbrapoorny R., India	1520	5409				3.56	107
744	Santa Catarine R., Monterey, Mexico	1409	6654	Aug.	27	1909	4.72	91
745	Krishna R., India	894	3341				3.74	93
746	Irrity R., India	870	4248				4.88	107
747	Ardeche R., Aubenas, France	461	3497			1890	7.59	63
748	Orba R., at reservoir, Italy	150	2265	Aug.		1935	15.08	130
749	Tansa R., India	136	991				7.29	93
750	Orba R., Valle Orbicella, Italy	109	1546	Aug.		1935	14.21	128
751	Wailua, near Lihue, Kauai, Hawaii	60	1274	Jan.		1921	21.39	78
752	Elbe R., headwaters, Germany	52	991	July	9	1927	19.13	165
753	Orba R., Martina, Italy	47	968	Aug.		1935	20.43	128
754	Orbicella R., Italy	26	569	Aug.		1935	21.98	128
755	Kaneohe, Oahu, Hawaii	14	311	Jan.		1921	22.69	78

APPENDIX H

TABLE FOR THE UNCERTAINTY ANALYSIS

Table H1 *Small watershed*: The hydrologic parameter combination, discharge and runoff coefficient

HYDROLOGIC PARAMETERS				RAINFALL EVENTS													
				LARGE EVENTS										EXTREME EVENTS			
				2-year		5-year		10-year		20-year		50-year		100-year		S-PMP		World	
				Q_p	C	Q_p	C	Q_p	C	Q_p	C	Q_p	C	Q_p	C	Q_p	C	Q_p	C
Hydraulic conductivity	LL	Manning's n	LL	48	0.1	77	0.2	88	0.2	95	0.2	106	0.3	111	0.3	661	0.8	1516	0.9
	UP		UP	14	0.0	25	0.1	41	0.1	55	0.1	67	0.2	76	0.2	342	0.4	1092	0.7
	LL		UP	20	0.1	49	0.1	62	0.1	71	0.2	80	0.2	86	0.2	413	0.5	1174	0.7
	UP		LL	25	0.1	57	0.1	72	0.2	84	0.2	95	0.2	101	0.3	583	0.7	1449	0.9
	CV		LL	18	0.0	65	0.2	81	0.2	89	0.2	100	0.3	106	0.3	615	0.8	1481	0.9
	CV		UP	34	0.1	37	0.1	54	0.1	65	0.2	76	0.2	84	0.2	421	0.5	1223	0.8
	LL		CV	18	0.0	58	0.1	72	0.2	81	0.2	90	0.2	95	0.2	534	0.7	1385	0.9
	UP		CV	31	0.1	35	0.1	53	0.1	66	0.2	80	0.2	88	0.2	459	0.6	1299	0.8
CV				22	0.1	46	0.1	62	0.1	74	0.2	85	0.2	91	0.2	520	0.6	1358	0.8

Note: LL = Lower Limit Value; UP = Upper Limit Value; CV = Calibrated / Validated Value; Q_p = Peak discharge in cms;
C = *Runoff-coefficient*

Table H2 *Medium watershed*: The hydrologic parameter combination, discharge and runoff coefficient

HYDROLOGIC PARAMETERS			RAINFALL EVENTS															
			LARGE EVENTS												EXTREME EVENTS			
			2-year		5-year		10-year		20-year		50-year		100-year		S-PMP		World	
			Q_p	C	Q_p	C	Q_p	C	Q_p	C	Q_p	C	Q_p	C	Q_p	C	Q_p	C
Hydraulic conductivity	LL	Manning's n LL	166	0.1	187	0.2	230	0.2	253	0.2	268	0.3	298	0.3	1866	0.7	4389	0.9
	UP	UP	147	0.1	149	0.1	196	0.2	211	0.2	222	0.2	237	0.2	1242	0.5	3321	0.7
	LL	UP	153	0.1	148	0.1	198	0.2	213	0.2	224	0.2	240	0.2	1249	0.5	3341	0.7
	UP	LL	163	0.1	168	0.1	228	0.2	251	0.2	266	0.3	295	0.3	1860	0.7	4355	0.9
	CV	LL	162	0.1	169	0.1	228	0.2	250	0.2	266	0.3	295	0.3	1860	0.7	4355	0.9
	CV	UP	135	0.1	152	0.1	197	0.2	212	0.2	223	0.2	239	0.2	1245	0.5	3324	0.7
	LL	CV	138	0.1	184	0.2	224	0.2	226	0.2	238	0.3	258	0.3	1476	0.6	3797	0.8
	UP	CV	137	0.1	183	0.2	206	0.2	224	0.2	237	0.3	255	0.3	1472	0.6	3796	0.8
CV			147	0.1	167	0.1	206	0.2	226	0.2	242	0.3	256	0.3	1474	0.6	3793	0.8

Note: LL = Lower Limit Value; UP = Upper Limit Value; CV = Calibrated / Validated Value; Q_p = Peak discharge in cms;
C = *Runoff-coefficient*

Table H3 *Large watershed*: The hydrologic parameter combination, discharge and runoff coefficient

HYDROLOGIC PARAMETERS		RAINFALL EVENTS									
		LARGE EVENTS						EXTREME EVENTS			
		2-year		50-year		100-year		S-PMP		World	
		Q_p	C	Q_p	C	Q_p	C	Q_p	C	Q_p	C
Hydraulic conductivity: LL	Manning's n: LL	455	0.3	1022	0.3	1128	0.3	3135	0.8	9664	0.9
UP	UP	331	0.2	821	0.2	909	0.3	2653	0.6	7095	0.6
LL	UP	333	0.2	824	0.2	911	0.3	2660	0.6	7101	0.6
UP	LL	452	0.2	1019	0.3	1126	0.3	3130	0.8	9656	0.9
CV	LL	453	0.2	1021	0.3	1127	0.3	3132	0.8	9659	0.9
CV	UP	332	0.2	822	0.2	910	0.3	2656	0.6	7096	0.6
LL	CV	369	0.2	922	0.3	1025	0.3	2952	0.7	8333	0.8
UP	CV	367	0.2	919	0.3	1022	0.3	2945	0.7	8327	0.8
CV		368	0.2	920	0.3	1023	0.3	3016	0.7	8332	0.8

Note: LL = Lower Limit Value; UP = Upper Limit Value; CV = Calibrated / Validated Value; Q_p = Peak discharge in cms;
C = *Runoff-coefficient*

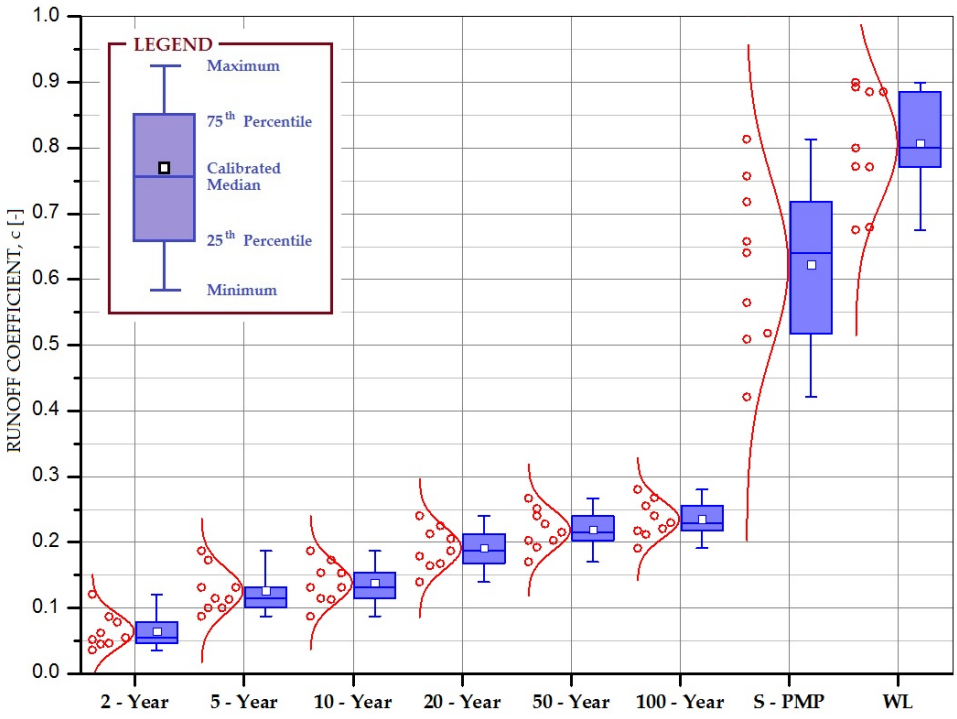

Figure H1 Box-plot the uncertainty for runoff coefficient at small watershed (Lui)

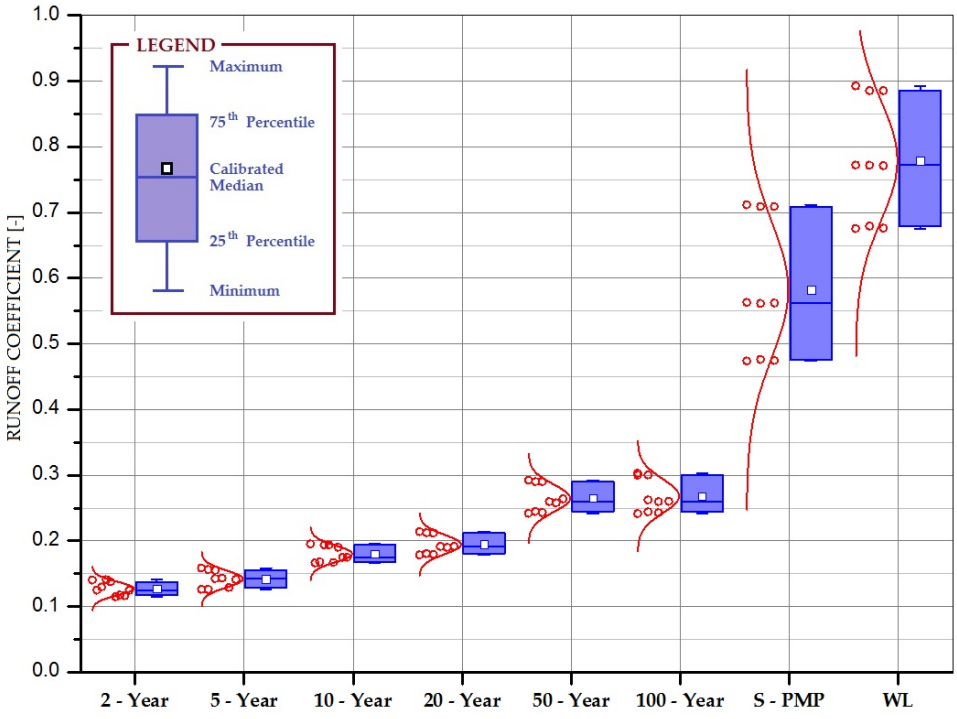

Figure H2 Box-plot the uncertainty for runoff coefficient at medium watershed (Semenyih)

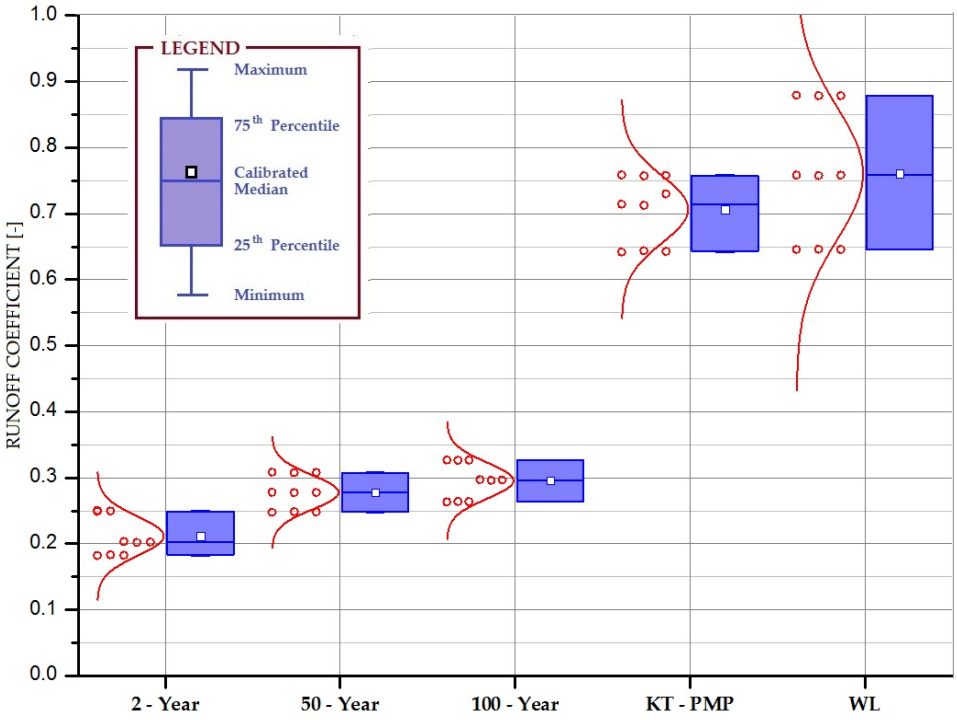

Figure H3 Box-plot the uncertainty for runoff coefficient at large watershed (Kota Tinggi)

Table H4 The variation coefficient of the maximum estimated discharge (MED) on a small, medium and large watershed

Rainfall events		**Coefficient of variation (C_v) [%]**		
		Small watershed (68 km^2)	**Medium watershed (263 km^2)**	**Large watershed (1,635 km^2)**
Large events	2-year	41	8	14
	5-year	32	9	---
	10-year	23	7	---
	20-year	17	8	---
	50-year	14	8	10
	100-year	12	10	10
Extreme events	PMP	21	18	8
	WGR	11	12	14
Note: The coefficient of variation (C_v) = standard deviation (σ) / mean (μ)				

The coefficient of variation C_v is significantly decreased from 2-year event to WGR event for the small watershed (Table H4). Conversely trend was found for the medium watershed and approximately same for the large watershed as shown in Table H4.

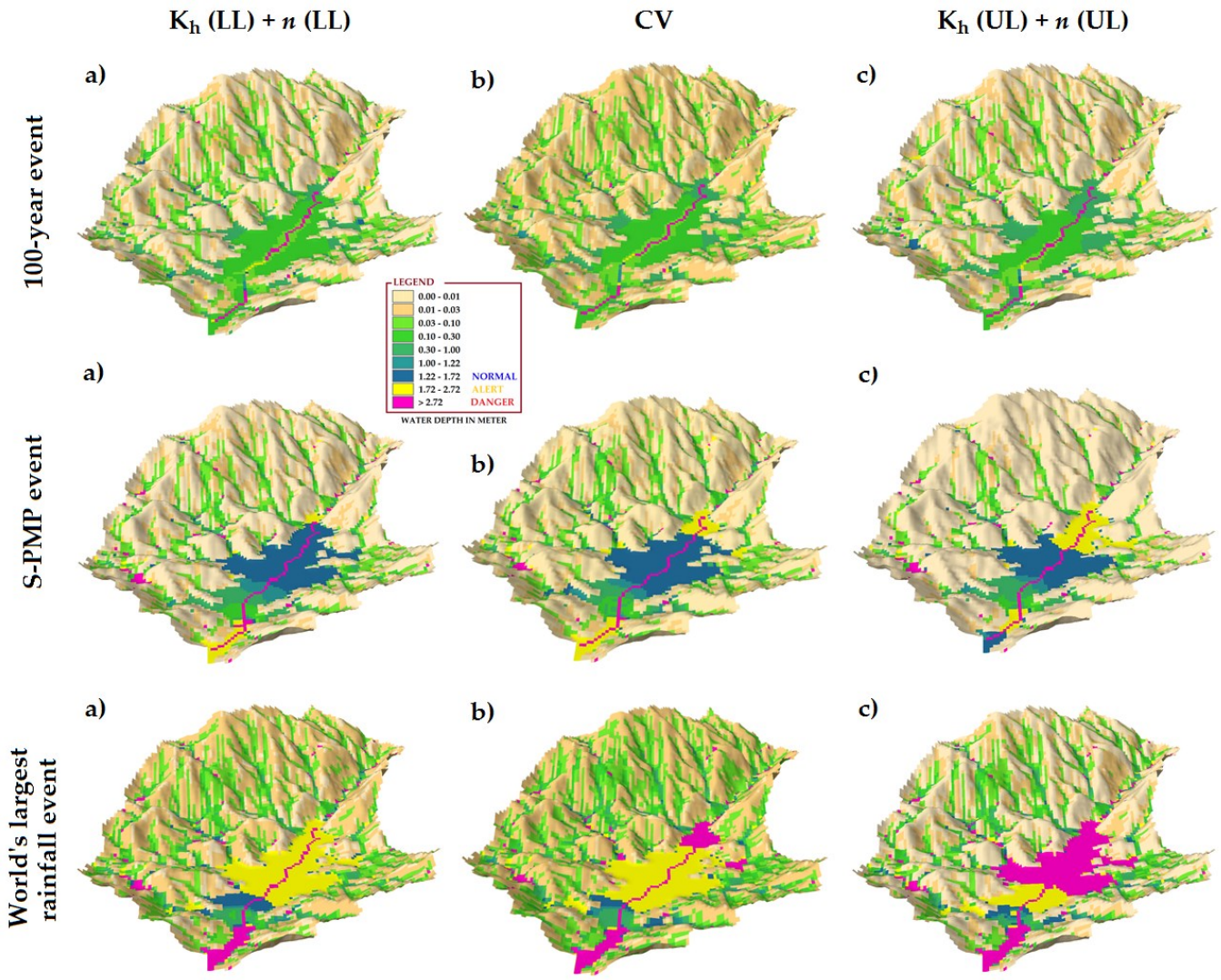

Figure H4 Uncertainty of water depth distribution for (a) Lower limit of K_h and n, (b) Calibration/Validation of K_h and n, and (c) Upper limit of K_h and n, at small watershed during 100-year, S-PMP and world's largest rainfall events

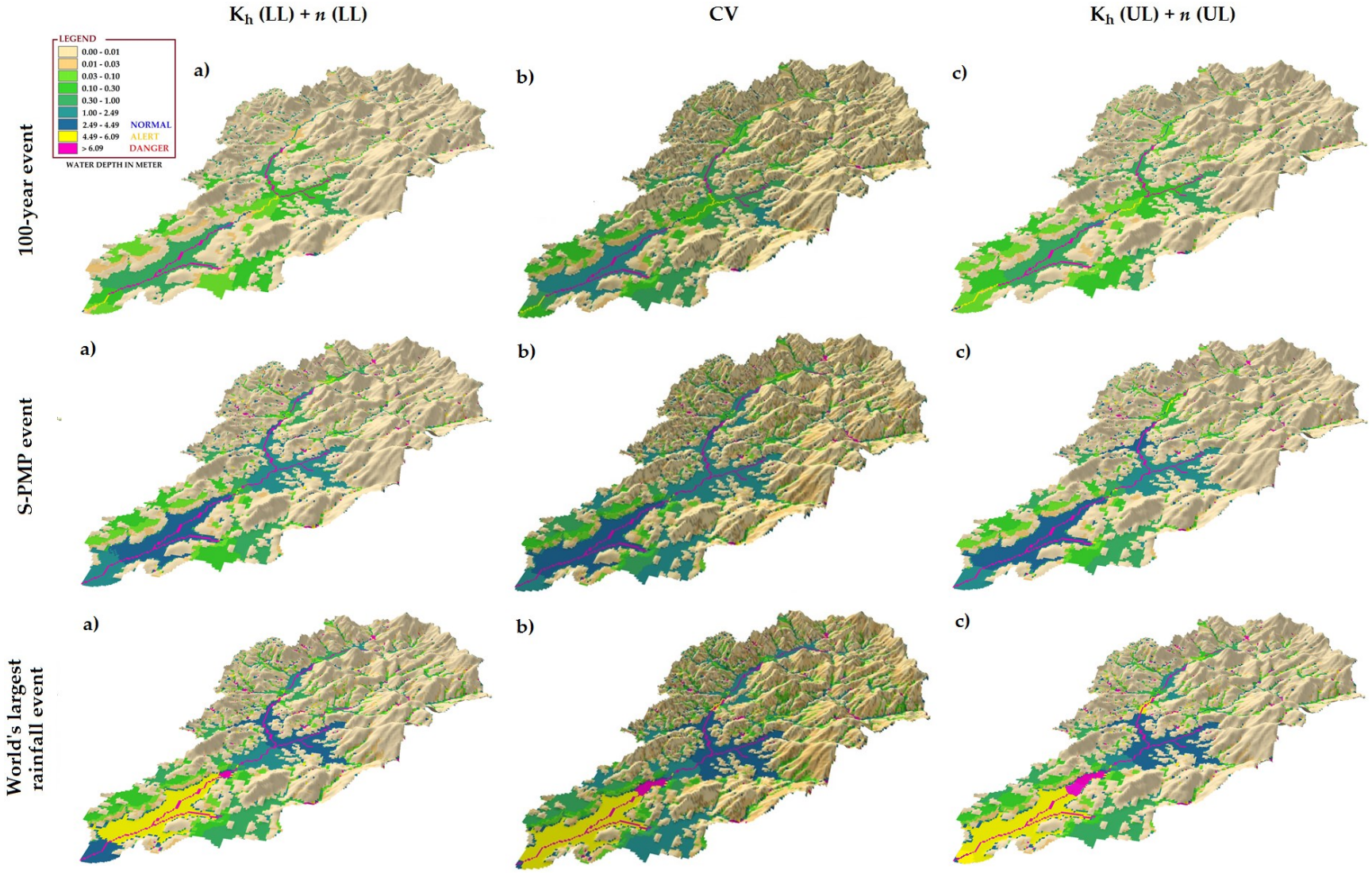

Figure H5 Uncertainty of water depth distribution for (a) Lower limit of K_h and n, (b) Calibration/Validation of K_h and n, and (c) Upper limit of K_h and n, at medium watershed during 100-year, S-PMP and world's largest rainfall events

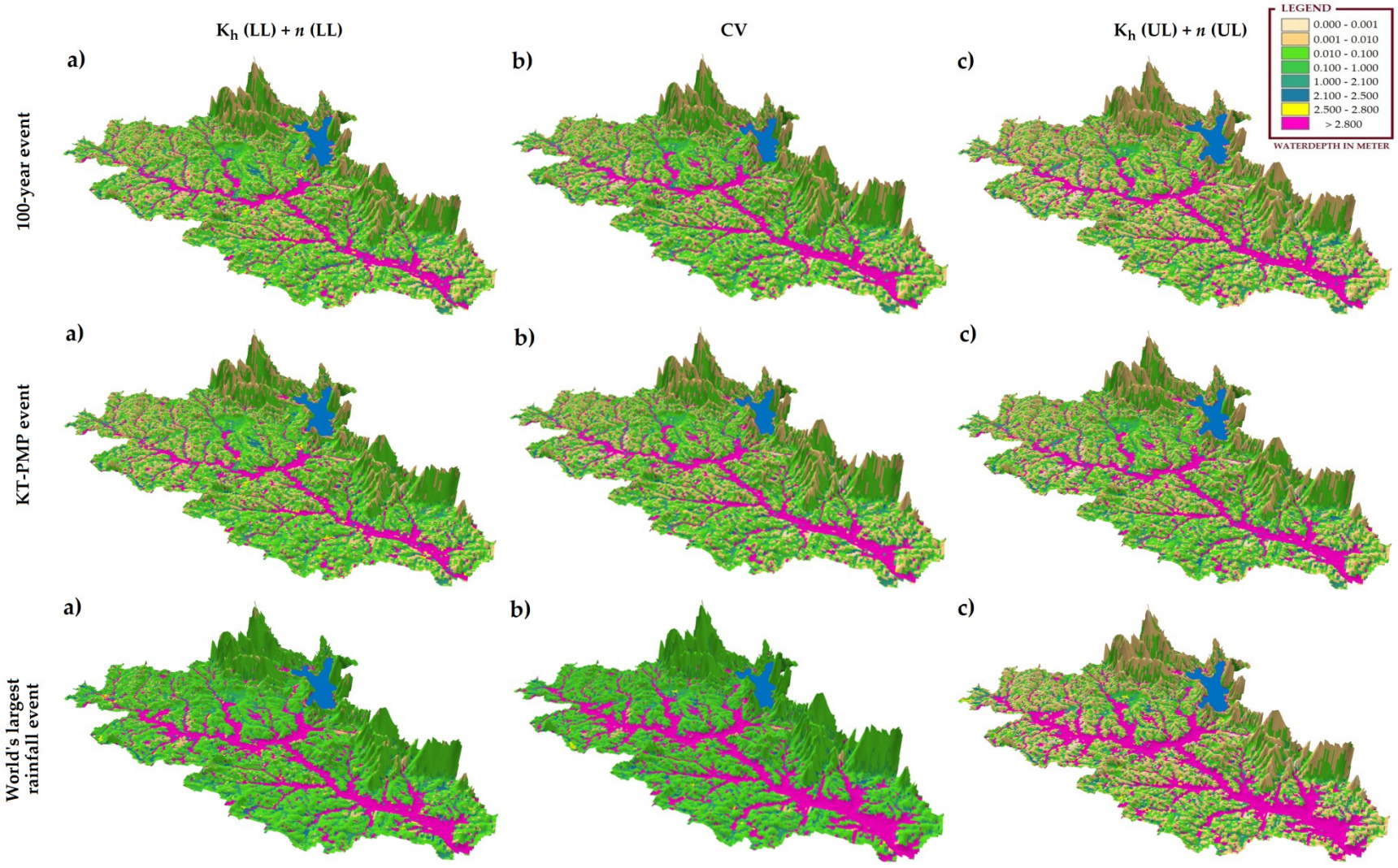

Figure H6 Uncertainty of water depth distribution for (a) Lower limit of K_h and n, (b) Calibration/Validation of K_h and n, and (c) Upper limit of K_h and n, at large watershed during 100-year, KT-PMP and world's largest rainfall events

REFERENCES

Benson, A. M. (1962). "Factors influencing the occurrence of floods in a humid region of diverse terrain." *U.S. Geological Survey, Water Supply Paper*, 1580-B

Blöschl, G., Sivapalan, M., Gupta, V. K., and Beven, K. J., (1997). "Scale problems in hydrology." *Water Resources Research*, 33(12), 2881-2999

Grayson, R. B., and Blöschl, G. (2000). "CHAPTER 14: Summary of pattern comparison and concluding remarks." *Spatial Patterns in Catchment Hydrology: Observations and Modelling*, Grayson, R. B. and G. Blöschl, (eds.), Cambridge university Press: Cambridge, 355-367

Gumbel, E. J. (Ed.) (1958). "Statistic of extreme", *Columbia University Press*, New York, p. 375

Landwehr, J. M., Matalas, N. C. and Wallis, J. R. (1979). "Probability weighted moments compared with some traditional techniques in estimating Gumberl parameters and quantiles." *Water Resources Research*, 15(5), 1055-1064

Lettenmaier, D. P. and Burges, S. J. (1982). "Gumbel's extreme value I distribution: A new look." *Journal of Hydrology Division ASCE*, 108(HY4), 502-514

Liong, S. Y., Selvalingam, S. and Brady, D. K. (1989). "Roughness values for overland flow in subcatchments." *Journal of Irrigation and Drainage Engineering*, 115(2), 203-214

Lowery, M. D. and Nash, J. E. (1970). "A comparison of methods of fitting the double exponential distribution." *Journal of Hydrology*, 10, 259-275

Maidment, D. R. (1993). *Handbook of hydrology*, Mc-Graw Hill, 1424

Rawls, W. J., Brakensiek, D. L. and Logsdon, S. D. (1993). "Predicting saturated hydraulic conductivity utilizing fractal principles." *Journal of Soil Science Society of America*, 57, 1193-1197

Rawls, W. J., Brakensiek, D. L. and Saxton, K. E. (1982). "Estimation of soil water properties." *Soil and Water Division of ASAE*, 81-2510, 1316-1328

Raynal, J. A. and Salas, J. D. (1986). "Estimation procedures for the type-I extreme value distribution." *Journal of Hydrology*, 87, 315-336

Reich, B. M. (1972). "Log-Pearson type III and Gumbel analysis of floods." *Proceedings of the Second International Symposium in Hydrology, Fort Collins, CO, USA*, 291-303

Reich, B. M. and Jackson, D. R. (1971). "Flood prediction methods for Pennsylvania highway crossings". Report prepared for the Pennsylvania Department of Transportation, The Civil Engineer Department, Pennsylvania State University, University Park, Pennsylvania.

Weibull, W. (1939). "A statistical theory of the strength of materials." Ingeniörsvetenskapsakademiens Handlingar Nr 151, 1939, Generalstabens Litografiska Anstalts Förlag, Stockholm (in English)

Wu, S., Li, J., and Huang, G. H. (2007). "Modeling the effects of elevation data resolution on the performance of topography-based watershed runoff simulation." *Environmental Modelling and Software*, 22, 1250-1260Xevi, E., Christiaens, K., Espino, A., Sewnandan, W., Mallants, D., Sorensen, H., and Feyen, J. (1997). "Calibration, validation and sensitivity analysis of MIKE-SHE model using Neuenkirchen catchment as case study." *Water Resources Management*, 11, 219-242

Zakaria, N. A., Azamathulla, H. M., Chang, C. K., and Gnahi, A. A. (2010). "Gene expression programming for total bed material load estimation – a case study." *Science of the Total Environment*, 408, 5078 – 5085

LIST OF ABBREVIATIONS

Abbreviations

DID	Department of Irrigation and Drainage
DEM	Digital Elevation Model
DMM	Department of Meteorology Malaysia
DSMM	Department of Surveying and Mapping Malaysia
KT-PMP	Kota Tinggi Probable Maximum Precipitation
MED	Maximum Estimated Discharge
MES	Maximum Estimated Stage
NSEC	Nash-Sutcliffe Efficiency Coefficient
ND/NS, AD/AS, DD/DS	Normal Discharge/Stage, Alert Discharge/Stage, Danger Discharge/Stage
PBIAS	Percent BIAS
RPD	Relative Percentage Difference
S-PMP	Selangor Probable Maximum Precipitation

Symbols

A_s	surface area over which precipitation occurs [L^2]
A_c	cross sectional area of flow [L^2]
a to *d*	fitting constants dependent on ARI (Table 2.1)
B_x, B_y	flow width in x- or y-direction [L]
C	runoff coefficient [-]
E	evaporation rate [LT^{-1}]
F	cumulative infiltrated water depth [L]
f	infiltration rate [LT^{-1}]
H_c	capillary pressure (suction) head at the wetting front [L]
H_w	hydrostatic pressure head (depth of water in channel) [L]
h	surface water depth [L]
I_t^R	the average rainfall intensity (mm/hr) for ARI and duration t
i_e	excess precipitation [LT^{-1}]
i_g	gross precipitation rate [LT^{-1}]
K_h	effective hydraulic conductivity [LT^{-1}]
N	number of data for simulated / observed [-]
n	Manning roughness coefficient [$TL^{-1/3}$]
P	wetted perimeter of channel flow [L]

Q	total discharge [L^3T^{-1}]
Q_x, Q_y	flow in x- or y-direction [L^3T^{-1}]
q_l	lateral flow into or out of the channel [L^2T^{-1}]
q^{mean}	mean value from observed data [L^3T^{-1}]
q_x, q_y	unit discharge in the x- or y-direction = Q_x/B_x , Q_y/B_y [L^2T^{-1}]
$q_{obs.}$, $q_i^{obs.}$	observed value
$q_{sim.}$, q_i^{sim}	simulated value
R	average return interval (years)
R_h	hydraulic radius of flow $(= A_c/P)$ [L]
S_e	effective soil saturation [-]
S_{fx} , S_{fy}	friction slope (energy grade line) in the x- or y-direction [-]
S_i	interception capacity of projected canopy per unit area [L^3L^{-2}]
S_{ox} , S_{oy}	ground surface slope in the x- or y-direction [-]
T	cumulative depth of water transported by transmission loss [L]
t	time [T]
t_d	duration (minutes or hours)
t_l	transmission loss rate [LT^{-1}]
t_R	precipitation event duration [T]
V_g	gross precipitation [L^3]
V_i	interception volume [L^3]
V_n	net precipitation volume reaching the surface [L^3]
$\dot{W}$	discharge from / to a point source / sink [LT^{-1}]
$\widehat{W}$	unit discharge from / to a point sink / source [L^2T^{-1}]

Greek Symbols

α_x , α_y	resistance coefficient for flow in the x- or y-direction [$L^{1/3}T^{-1}$]
β	resistance exponent $(= 5/3)$ [-]
θ_e	effective soil porosity $(\varphi - \theta_r)$ [-]
θ_r	residual soil moisture content [-]
φ	total soil porosity [-]